"Around here, however, we don't look backwards for very long. We keep moving forward, opening up new doors and doing new things, because we're curious...and curiosity keeps leading us down new paths."

…… Walt Disney

"Live as if you were to die tomorrow. Learn as if you were to live forever."

……Mahatma Gandhi

SYNTHESIS OF "CLIKABLE" POLYPEPTIDE BY NCA POLYMERIZATION AND THEIR APPLICATION AS BIOMATERIAS

A DISSERTATION SUBMITTED TO THE

UNIVERSITY OF PUNE

FOR THE DEGREE OF

DOCTOR OF PHYLOSOPHY

IN

CHEMISTRY

By

MRITYUNJOY KAR

RESEARCH SUPERVISOR

DR. SAYAM SEN GUPTA

CHEMICAL ENGINEERING DIVISION

NATIONAL CHEMICAL LABORATORY

PUNE-411008

INDIA

NOVEMBER 2012

राष्ट्रीय रासायनिक प्रयोगशाला
(वैज्ञानिक तथा औद्योगिक अनुसंधान परिषद)
डॉ. होमी भाभा रोड, पुणे - 411 008. भारत
NATIONAL CHEMICAL LABORATORY
(Council of Scientific & Industrial Research)
Dr. Homi Bhabha Road, Pune - 411008. India

CERTIFICATE

This is to certify that the work incorporated in the thesis entitled **"synthesis of "clickable" polypeptide by NCA polymerization and their application as biomaterials"**, submitted by Mrityunjoy Kar for the degree of ***Doctor of Philosophy*** to the University of Pune, has been carried out by him under my supervision at Chemical Engineering Division, National Chemical laboratory, Pune-411008, India. All the materials from the other sources have been duly acknowledge in the Thesis.

Research supervisor
(Dr. Sayam Sen Gupta)

Communications Channels ☎ +91 20 25902000 +91 20 25893300 +91 20 25893400 Fax +91 20 25902601 (Director) +91 20 25902660 (Admin.) +91 20 25902639 (Business Development) URL : www.ncl-india.org

DECLARATION

I hereby declare that the thesis entitled **“synthesis of “clickable” polypeptide by NCA polymerization and their application as biomaterials”**, submitted for the degree of ***Doctor of Philosophy*** to the University of Pune, has been carried out by me at National Chemical laboratory, Pune-411008, india, under the supervision of Dr. Sayam Sen Gupta. The work is original and has not been submitted in part or full by me for any other degree or diploma to this or any other University.

Mrityunjoy Kar

Dedication

This dissertation is dedicated to

My beloved parents

Who give me warmest love, encouragement, endless support and happiness

Acknowledgement

"At times our own light goes out and is rekindled by a spark from another person. Each of us has cause to think with deep gratitude of those who have lighted the flame within us."

..... Albert Schweitzer

"Let us be grateful to people who make us happy; they are the charming gardeners who make our souls blossom."

….. Marcel Proust

Studying at National Chemical Laboratory (NCL) has been one of the most memorable experiences. I am very grateful to have had the opportunity to study chemistry here and meet many great, nice and friendly people.

First and foremost, it is my great pleasure to express my utmost gratitude to my research supervisor, Dr. Sayam Sen Gupta. I feel very lucky and honoured that I have conducted my doctoral study under his supervision. His invaluable guidance, constant support, numerous discussion and constructive suggestions for not only in science but also to be a sensible and responsible human being nourished throughout my doctoral study. I especially appreciate his support of creating a new research area in his group and allowing me to explore science in my way. His continuous support and encouragements enlighten the path to pursue my future career goal in academia. His wide knowledge, logical way of thinking and understanding has provided me a good basis for the present thesis. I am also really thankful to him to give me the opportunity to demonstrate fun sciences to school children, which has really entertained me throughout my stay in NCL. I salute his supporting attitude that has always led me to think and work independently and do something constructive for the science and the society. My deepest regards and reverence are always due for his wonderful and charming personality; I always enjoyed his presence in all the meetings and lectures. I sincerely thank for his care and affection that I received from him and his family in the entire period.

I would like to thank the Council of Scientific and Industrial Research for award of research fellowship. I am thankful to Dr. S. Sivaram, Ex-Director, Dr. B. D. Kulkarni, Ex-Deputy Director, Dr. S. Pal, Director and Dr. V. V.Ranade, Deputy Director, National Chemical Laboratory to carry out my research work and extending all possible infrastructural facilities for completion of my research work. I would like to express my heartfelt thanks to all the scientific members of our CEPD Division, especially, Dr. A. Kulkarni, Dr. V.

Panchagnula, and Dr. Kelkar for their helping hands and fruitful discussions. I need to express my thanks to the support group (Patane kaka, Kamble kaka, Subbi, Ravi & Radha) and all the staff members of our division, especially Mr. Raheja for his valuable cooperation and help to do all the official work.

I am especially thankful to Dr. B. L. V. Prasad, Dr. Guruswamy Kumaraswamy and Dr. (Mrs.) M. Gadgil from NCL for their help and scientific discussions. My special thanks to Prof. Mayurika Lahiri from IISER, Pune for letting me start working with her group. I am very thankful to prof. Mayurika Lahiri's group; Mitali, Payel, Abhinav, Surojit, Arijita and Swaroopa, it was my pleasure to work with them and explore biology. I am thankful to Mrs. D. Dhoble, Mrs. P. Purohit and Mr. S. Jha for help regarding FT-IR and TGA analysis. I would like to thank Dr. S. Bhatt and his research group for help with DLS and zeta potential measurements. I acknowledge to Dr. Ajithkumar and his research group from NMR division and Mr. R. Gholap, Mr. Ketan, Mr. Naren, Mr. Anuj, Mr. Pandiraj and Mr. Pankaj from Centre for Materials characterization for their help in characterizations with NMR, SEM and TEM. I am also very thankful to Vijay from IISER for helping me to image biological samples. I would like to acknowledge the director of NCCS and Prof. Limaye for giving me the permission to use FACS facilities. I am very thankful to Aswini, Vikash and Amit for helping me to conduct FACS analysis.

I am very lucky to work with all the talented and great people in the Sayam's group. I have learned so much from all of you, not only in science but every little aspect of life. I would like to thank all my colleagues and lab mates (past and present) for their helpful hand and cheerful attitude that had made my work very easy and enjoyable. I should mention my seniors Bibhas Da, Shashi, and Amit for their support and help. I specially thank all the present lab mates Malvi, Anal, Debasis, Chaka, Sushma, Munmun, Soumen, Neha, Vinita, Kundan, Santanu and Basabda (CSIR pool officer) for their presence in all aspects of my Ph.D. career. I would like to thank Iti, Pauline, Serin T.K., Anindita, Suyana, Rajeesh, Vinita and Neha for their help and support during my doctoral study. It has been a great and enjoyable experience to mentor undergraduates and work with graduate student colleagues. I truly believe they will be very successful in the future.

I am very thankful to Dr. Ashis Lele and Dr. Rahul Banerjee for letting me conduct tree plantation around the PAML building. I would like to acknowledge Dr. Jana and all the

people from NCL horticulture division to make the tree plantation event very successful. I am now very happy to see all the trees are growing very well around the campus.

I would like to thank all the exciting science group members, especially Bhakti for her support and help; I have enjoyed so many successful fun chemistry demonstrations to the school children.

I would like to thanks Dr. Neelanjana Sengupta, Dr. Kumar Vanka and Dr. Guruswamy Kumaraswamy. I had long chats with them about various global issues, movies, origin of 'life' and many more other subjects during my stay in NCL. I will miss those times spent with them.

I would like to acknowledge Debabrata Bhattashali, who gave me support when first time I came to NCL for the PhD interview here in NCL. I am thankful to him for his support and friendship. I would like to acknowledge Bibhas da, Roopa di, Prabhas da, Soumitra da, Alam da, Pradip da, Himadri da, Debashis da, Sujitda, Anal, Debasis, Munmun, Partha, Sumanta, Ajeet, Anand, Ankush, Deepika, Nivedita, Asif, Roshan, Dev, Mohan, Latif, Ajay, JP, Kapil, Sanjeev, the entire bengali group at GJ Hostel and many more in NCL for their support and friendship throughout my staying in NCL. It gives me great pleasure to thank my old roommate Abhasaheb, from whom I received great support and encouragement during first few years of my doctoral studies.

I want to acknowledge especially my higher secondary chemistry teachers, Mr. Prabhat Senapati, without his encouragement I could not able to be here to PhD in chemistry. I also would like to thank Prof. Rupendranath Banerjee (Jadavpur University), Prof. Tapan Mondal (Principal of Panskura Banamali College), Prof. Pulakesh Bera (Panskura Banamali College) and all other professor from my B.Sc. and M.Sc. study, who really nourished my interest in Chemistry.

Finally, I owe an enormous debt of gratitude to my parents and my brother for their love, support, tremendous patience, trust and encouragement. Love you all.

Place: NCL, Pune

Mrityunjoy Kar

Table of Contents

List of Figures

List of schemes

List of Tables

List of Abbreviations

AM	Activated Monomer
AzPTES	3-Azidopropyl Triethoxysilane
BET	Braunauer-Emmett-Teller
BJH	Barrett-Joyner-Halenda
COD	Cyclooctadiene
CP-MAS	Cross-Polarization Magic Angle Spinning
CPP	Cell Penetrating Peptide
CTAB	Cetyltrimethyl ammonium bromide
CuAAC	Cu (I) catalyzed azide-alkyne cycloaddition
DLS	Dynamic Light Scattering
FTIR	Fourier Transform Infrared
GPC	Gel Permeation Chromatography
GTP	Group Transfer Polymerization
HMDS	Hexamethyldisilazane
HRTEM	High Resolution Transmission Electron Microscopy
MALDI-TOF	Matrix Assisted Laser Desorption/Ionitiation Time of Flight
MCM	Mobil's Composition Material
MSN	Mesoporous Silica Nanoparticle
MWD	Molecular Weight Distribution
NA	Normal Amine
NCA	N-Carboxyanhydride
NMR	Nuclear Magnetic Resonance
ORMOSIL	Organically Modified Silica
PDI	Polydispersity Index
PLArg	Poly-L-Arginine
PLGA	Poly-L-Glutamic acid
PLL	Poly-L-Leucine
PLLeu	Poly-L-Lysine
PTD	Protein Transduction Domain
ROP	Ring Opening Polymerization
SBA	Santa Barbara Amorphous
SEC	Size Exclusion Chromatography
SEM	Scanning Electron Microscopy
TEOS	Tetraethyl orthosilicate
TEM	Transmission Electron Microscopy
TEOS	Tetraethyl orthosilicate
TGA	Thermogravimatric Anlysis
TMS	Trimethyl Silyl
XRD	X-Ray Diffraction

Abstract of the Thesis

Polypeptides and proteins are the nature's most important and abundant polymers. The tremendous ability of polypeptides to modulate biological function has encouraged the scientific community to develop synthetic routes for their preparation, study their properties and above all to understand their structure-function relationship. This would then lead to various biomedical applications such as in biotechnology (artificial tissues and implants), bio-mineralisation (resilient, lightweight and ordered inorganic composites) and bio-analytics (biosensors and medical diagnostics). Unlike conventional synthetic polymers, polypeptides have significant advantages since they are expected to be biocompatible. Further, polypeptides are highly intriguing building blocks for macromolecules to organize into progressively more complex, higher-order structures due to their various unique three-dimensional stable ordered conformations like secondary structures (helices, sheets, turns), tertiary structures (β-strand-helix-β-strand unit found in β-barrels) and quaternary assemblies (collagen microfibrils).

Polypeptide polymer grafted silica nanoparticles are of considerable interest because they combine the biological property of polypeptides and the structural properties of silica nanoparticles.[33] For example, silica nanoparticles have been extensively used in drug delivery since they are known to enter most of mammalian cells efficiently. Grafting of functional polypeptides on the surface of silica nanoparticles would allow then to interact very strongly with the cell surface and perhaps increase the efficiency of cellular uptake in comparison to bare nanoparticles which only has silanol groups on its surface. In addition to this, the presence of a wide range of side chains (such as amines, thiols and carboxylic acid) in the polypeptides make them responsive to external stimuli such as pH, temperature, solvent and electrolytes. Therefore, polypeptide grafted silica particles can possibly have various applications in coatings, catalysis, gene delivery, among other things.

For us to explore possible applications for polypeptide-silica conjugate first requires development of a practical methodology which allows facile synthesis of polypeptide silica nanoconjugates in high yield. Since polypeptides contain several reactive functional groups like amines, thiols and carboxylic acid, a methodology that was very efficient and bioorthogonal had to be envisaged. We therefore used a combination of NCA polymerization of α-amino acids for the synthesis of polypeptides followed by attachment of these polypeptides by "click chemistry" to silica nanoparticles having organoazides on their

surface. The discovery of the Cu(I)-catalyzed 1,3-dipolar cycloaddition of organic azides to alkynes (CuAAC) has provided the most powerful "click chemistry" tool for conjugation between appropriately functionalized binding partners via an 1,2,3-triazole linkage. We have synthesized several alkyne terminated polypeptides with different molecular weight and grafted them successfully onto various organoazide containing silica materials using CuAAC reaction. The hybrid silica nanomaterials synthesized by this methodology was used for various applications such as antimicrobial agents, as gene delivery carrier and as building blocks for the synthesis of 3D macroporous scaffolds. The dissertation is presented in five chapters; a brief summary of each chapter is given below.

Chapter 1 provides a brief review on the synthesis of amino acid NCA's and their ring opening polymerization for the synthesis of polypeptides. This chapter also discusses the importance of the surface modification of various conventional materials in biological context as well as the synthesis, surface modification and application of organic-inorganic hybrid nanomaterials. A brief introduction to Cu(I) catalyzed azide-alkyne click chemistry (CuAAC) is discussed. Finally, the motivation for the development of polypeptide grafted core-shell silica nanoparticles that would combine the biological property of polypeptides and the structural properties of silica nanoparticles is discussed.

Chapter 2 describes the synthesis of alkyne terminated various homo and block co-polypeptides. All the synthetic methodologies developed for the preparation of the various amino acid NCA monomers were high yielding and easy to handle. NCA ring opening polymerization was used to synthesize alkyne terminated homo- and block co- polypeptides using propargylamine TMS as the initiator. Use of N-TMS propargylamine as the initiator allows the synthesis of polypeptides with very low polydispersity and precise molecular weights. It also leads to the incorporation of a C- terminal alkyne at the polypeptide end which can be further modified by using Cu(I) catalyzed azide alkyne cycloaddition reaction. All synthesized polypeptides were characterized by FT-IR, GPC and NMR.

Chapter 3 describes the synthesis of homo and block co-polypeptides grafted silica nanoconjugates and their application as biomaterials. "Grafting to" methodology was used for the synthesis of all the silica polypeptide nanoconjugates via CuAAC. This methodology developed by us is general and can be extended for grafting any natural and unnatural polypeptide. For example, uniform poly-L-lysine (PLL), poly-L-glutamic acid (PLGA) and poly-L-arginine (PLArg) coated silica nanoparticle was synthesized using this methodology.

The grafting density was characterized by using thermogravimetric analysis (TGA). Solid state CP MAS NMR was used to structurally characterize the silica polypeptide nanoconjugates and to investigate the secondary conformations of the polypeptides that were grafted onto the surface of the silica nanoparticles. The silica polypeptide nanoconjugates exhibited interesting aggregation properties. For example, although silica-poly-L-lysine (silica-PLL) nanoconjugates containing very high grafting density of charged poly-L-lysine onto the silica surface was highly cationic, yet the nanoconjugates are very prone to aggregation in water. On the other hand, positively charged silica-poly-L-arginine (silica-PLArg) nanoconjugates showed much less partial aggregation in water while negatively charged silica-poly-L-glutamic acid (silica-PLGA) nanoconjugates showed no aggregation in water. Application of all these synthesized polypeptide silica nanoconjugates was explored. Silica-PLL and silica-PLL-*b*-PLLeu conjugates displayed excellent antimicrobial properties at concentrations of 250 μg/mL against both Gram positive and Gram negative bacteria. PLGA functionalized silica nanoparticles were used to generate well defined, aligned three dimensional macroporous structures using ice templating with directional freezing. Thus, these macroporous materials are comprised of a biocompatible polymer shell covalently attached to rigid inorganic cores. Since the synthetic scheme of the nanoparticle developed by us allows the polymer and inorganic components to be individually tailored, scaffolds having a wide range of physical properties can be synthesized. Finally, highly water dispersible silica-PLArg nanoconjugate having very high surface positive charge has been successfully synthesized. Since silica-PLArgs have very high positive surface charge they bind very efficiently with the nucleic acids. The inherent cell penetrating property of surface poly-L-arginine renders the silica-PLArg nanoconjugates very efficient for entering mammalian cells. From FACS analysis, 90% cellular uptake efficiency was observed. However, these nanoparticles were not efficient as a carrier for the transfection of protein of interest. However, the transfection can be affected in presence of 100 μM chloroquine.

Chapter 4 describes the synthesis of poly-L-lysine grafted SBA-15 with reasonable grafting density by using CuAAC via the "grafting to" methodology. Alkyne terminated poly-L-lysine containing both 20 and 10 repeating units were successfully grafted onto azide grafted SBA-15 material. The resultant materials were characterized by NMR, FT-IR and nitrogen adsorption desorption studies. The materials retain their porosity after conjugation with PLL and this is in contrast to the lack of porosity observed in the SBA-PLL-conjugate material synthesized by the "grafting from" method.

The above methodology was modified to graft poly-L-arginine specifically onto the surface of the mesoporous silica thus keeping the pores empty. The low cytotoxicity together with the very high ability to penetrate cancer cells like HeLa and A549 make MSN-PLArg excellent delivery vehicles for nucleic acid. The poly-L-arginine grafted MSNs were used effectively to deliver mCherry DNA plasmid into cells leading to expression of the protein mCherry inside the cells. The observed transfection efficiencies with MSN-PLArg were 48% and 60% for HeLa and A549 cells respectively. The biocompatibility of poly-L-arginine and its cell penetrating ability will make these MSN conjugates more exciting over synthetic cationic polymer like PEI whose long term toxicity is unknown.

Chapter 5 presents an overall summary of the work done and describes the major findings of the studies. Future directions based on the work reported in this thesis are also discussed.

Chapter 1

Introduction and Literature Survey

1.1 Introduction: Polypeptides

Polypeptides are polymers of amino acid monomers that are conjugated by peptide bonds. The modern development of polypeptide chemistry started long back in 1901 by Noble laureate German organic chemist Emil Fischer, who first discovered in collaboration with Ernest Fourneau, the synthesis of dipeptide glycylglycine.[1] In 1902 at the 14th meeting of the German scientists and physicians, Fischer first introduced the name peptides (from pepsis = digestion or peptones = digestion products of proteins). 'Peptides' denote relatively small compounds which resemble proteins that are built up of amino acid residues. The shortest peptide is a dipeptide which consists of two amino acids linked by a single peptide bond. Similarly, by attaching two or more amino acids via the peptide bond, higher peptides such as tripeptides and tetrapeptides can be generated. Polypeptides are composed of many (poly) amino acids that are linked together via the peptide bond.[2] Polypeptides are typically distinguished from proteins on the basis of their size. Macromolecules that have 50 or more amino acids joined together by peptide bonds are regarded as proteins while those containing fewer amino acids are denoted as polypeptides. Therefore, the chemical synthesis of peptides, as envisaged by Emil Fischer, involves the reproduction or perhaps recreation of Nature's molecules.[2]

Proteins that are synthesized by biological system have the ability to fold into complex yet highly ordered structure to perform their desired function.[3] Biological systems display remarkable control over the properties of the proteins by precisely controlling the sequences and compositions of the constituent amino acid monomers. Biologically active peptides, that range from small molecules that contain only two or three amino acids to large molecules (polypeptides and proteins) containing several tens of amino acids display a wide range of chemical, physical and physiological properties in living organism. These include neuropeptides,[4] hypothalamic hormones (releasing and release-inhibiting hormones),[5] proteohormones of the pituitary,[6] enzymes to catalyse and regulate biological reactions,[7] thyroid hormones,[8] gastrointestinal peptides,[9] muramyl peptides,[10] peptides of immunological significance, peptide vaccines,[11] atrial natriuretic peptides,[12] peptide antibiotics,[13] peptide antimicrobial,[14] peptide toxins,[15] peptide insecticides and herbicides,[16] peptide flavour[17] among others. The tremendous ability of these polypeptides to modulate biological function has encouraged the scientific community to develop synthetic routes for their preparation, study their properties[18] and above all to understand their structure-function relationship.[19, 20] This would

then lead to various biomedical applications such as in biotechnology (artificial tissues, implants), bio-mineralisation (resilient, lightweight, ordered inorganic composites) and bio-analytics (biosensors, medical diagnostics).[21, 22]

1.2 Synthesis of polypeptides

The synthesis of polypeptides using naturally occurring or modified amino acids which can fold into various non-natural ordered supramolecular secondary structures (α-helix, β-sheet) is a challenge for polymer chemists. To synthesize the complex polypeptide sequences with controlled molecular weight various chemical methods have developed with the aim that these synthesized polypeptides would display novel properties for application in bionanotechnology.

1.2.1 Solid phase synthesis of polypeptides

A process by which chemical reaction can be carried out on solid support in order to prepare a wide range of synthetic compounds is called solid phase synthesis. This idea to synthesize polypeptide in stepwise on a solid support[23] was first developed by Bruce Merrifield for which he was awarded the Nobel Prize in1984. Solid phase synthesis of polypeptides was carried out on resins in which the C-terminal of first protected amino acid fragment was chemically anchored to the resin surface followed by coupling reaction with the second amino acid of interest.[23-25] Solid phase synthesis has many advantages over conventional solution methods[26] in terms of efficiency due to its convenient work-up and purification procedures. In solution phase peptide synthesis, particularly for longer sequences, the repetition of coupling and deprotection cycles can become very tedious since it requires the isolation and purification of all peptide intermediates. However solid phase synthesis is also not ideally suited for the synthesis of very long chain polypeptides (more than 50 mers) due to the side reactions that occur in each coupling step on the resin.

1.2.2 N-carboxyanhydride (NCA) ring opening polymerization

The most efficient, economical, expedient and straightforward process to synthesize the polypeptides is by the polymerization of α-amino acid N-carboxyanhydride's (NCA).[27, 28] This method is less time consuming, involves simple reagents and afford good yields without any

racemization at the amino acid chiral centers. The living nature of NCA polymerization is ideal for synthesis of precisely controlled and predictable high molecular weight polypeptides.

Herman Leuches, PhD student of Noble laureate Emil Fischer, published three consecutive papers[29-31] between 1906-1908 describing the synthesis and properties of α-amino acid N-carboxyanhydrides and their corresponding polypeptides. Herman Leuches discovered amino acid N-carboxyanhydride accidently while he was trying to purify N-ethoxy carbonyl or N-methoxy carbonyl amino acid chlorides by distillation for the purpose of peptide synthesis (Scheme 1.1). This versatile and attractive method for the synthesis of NCAs is called Leuches methods and the NCAs are denoted as Leuches anhydrides. After the publication of these three historic reports, [29-31] Herman Leuches abandoned his work on amino acid NCAs and continued his work on peptide chemistry since it was the major research area of his former supervisor Emil Fischer. It should also be noted that at that time the field of polymer science was not in existence and many distinguished scientists including Emil Fischer disagreed on the existence of molecules having molecular weight more that 5000 Da. This might have discouraged Herman Leuches to pursue his trysts with amino acid NCAs.

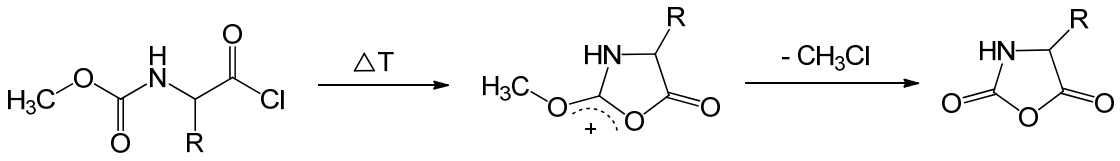

Scheme 1.1: NCA synthesis from N-methoxy carbonyl amino acid chloride

It was only later that amino acid NCA polymerization was revisited and advancements were made on understanding of the mechanism of NCA polymerization. Subsequently, scientists argued that study of NCA polymerization can shed light into the origin of life since the fast kinetics during polymerization without racemization of the amino acid constituents is ideal for peptide synthesis at prebiotic conditions.[32] The free energy of the hydrolysis of NCA was calculated to be -60 kJ mol^{-1}; this value is less negative than other proposed synthesis of peptides under prebiotic conditions. Out of the several proposed mechanisms for the formation of amino acid NCA under prebiotic conditions, COS mediated activation of α-amino acids to form NCAs (Scheme 1.2) are most likely as COS is one of the most abandoned compounds found in volcanic eruption. [33]

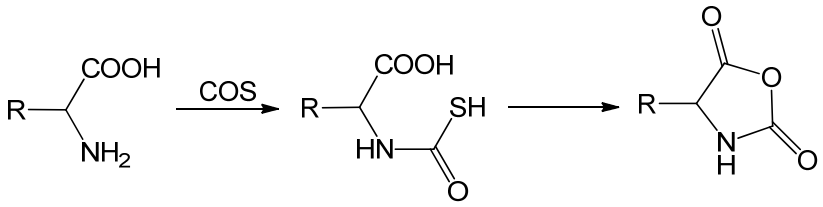

Scheme 1.2: COS mediated NCA synthesis

1.2.2.1 Synthesis of α-Amino acid NCAs

Although Herman Leuches had first serendipitously synthesized NCA from N-ethoxycarbonyl or N-methoxycarbonyl amino acid chlorides at high temperature, this method could not be generalized for the synthesis of all amino acid NCAs since several of them were unstable under these synthetic conditions. Thus several methodologies have been reported by various research groups to improve the synthesis of α-amino acid NCAs in last few decades. Initially thionyl chloride was used to make the acid chloride of α-amino acids by Leuches since byproduct formed would be gaseous and could be easily removed to purify the product. In 1935 Bergmann et al. used phosphorus pentachloride, which is much more reactive than thionyl chloride and this led to the successful synthesis of N-alkoxy carbonyl or N-benzyl carbonyl amino acid NCAs at lower temperature. However, phosphorus oxide trichloride is formed as a byproduct and that affects further purification of the amino acid NCA which is typically carried out by multiple crystallizations. [34] Subsequently, dichloromethyl methylether was used to make high purity NCAs as it is easy to purify solid NCAs by crystallization from the liquid byproducts.[35] Several other methodologies have been developed to synthesize amino acid NCAs. These include treatment of N-benzyloxycarbonyl amino acids with phosgene in presence of triethylamine leading to the formation of aziridine derivatives which on hydrogenation yields NCAs.[36] NCAs prepared from N-alkoxy carbonyl or N-benzyl carbonyl amino acids by reaction with phosphorus tribromide are also very convenient since the acylbromide cyclizes more readily than the corresponding acid chlorides. The rate of cyclization (Scheme 1.3) is dependent on the N-alkoxy/N-aryloxy substituent and follows the trend of ethyl<methyl<allyl<benzyl.[29-31, 37, 38]

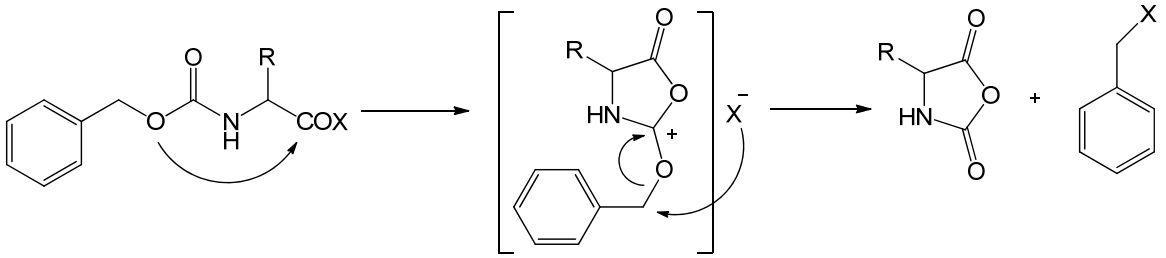

Scheme 1.3: Cyclization mechanism during NCA synthesis from N-benzyloxy carbonyl amino acid halides

Preparation of NCAs of α-amino acids that contain functional groups in their side chain, such as lysine, ornithine, arginine, glutamine and asparagines, require protection of the side chain functional group such that it can neither act as an initiator for subsequent polymerization nor interfere with the synthesis of NCA. For the preparation of these amino acid NCAs containing functional groups such as N-benzyloxy carbonyl-Lysine NCA,[39] N-benzyloxycarbonyl-Ornithine-NCA,[40] di-benzyloxycarbonyl-arginine-NCA,[41] arginine-NCA hydrobromide,[42] glutamine- and aspargine-NCA[42, 43] or NCAs with nucleobases in their side chains, [44, 45] the Leuches method still remains the most optimum and straightforward procedure.

The simplest and most widely used method to prepare α- NCAs directly from free α-amino acids is known as *Fuchs-Farthing method*.[46-48] In 1922, Fuchs first reported the synthesis of α-NCAs using phosgene gas directly from α-amino acids.[46, 49, 50] The proposed reaction mechanism involves formation of N-chloroformyl amino acids as an intermediate followed by cyclization with concomitant release of hydrochloric acid.(Scheme 1.4) The concentration of HCl released as the byproduct is very crucial during the reaction since at higher concentration HCl can cleave the NCA ring. Further, in presence of excess HCl and phosgene, amino acid can also form isocyanato acid chloride as the main product.[51] For successful completion of the reaction, inert, anhydrous and low boiling solvents (like tetrahydrofurun (THF) and dioxane) are widely used. To prepare large quantity of NCAs it is always best to use a mixture of THF (or dioxane) and methylenechloride (1:1) to solubilize the hydrochloric acid byproduct.[51] The conventional procedure to prepare NCAs by phosgenation of an amino acid involves passing gaseous phosgene through a suspension of the amino acid in a dry solvent such as dioxane or tetrahydrofuran until a clear solution is obtained. [48, 49] Goodman *et. al.*[52] have established a method that uses a stock solution of phosgene in anhydrous benzene for the preparation of the

NCAs. This reduces some of the potential danger of using a large amount of gaseous phosgene which is highly toxic.

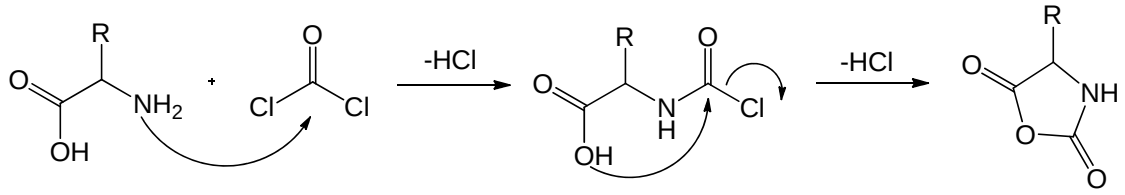

Scheme 1.4: NCA synthesis using phosgene gas

The danger of using phosgene was improved upon by using diphosgene and triphosgene. Unlike phosgene, trichloromethyl chloroformate (diphosgene) has an advantage that it can be easily added in stoichiometric amounts.[53] However, it also requires carbon black to catalyze the dissociation process for efficient cyclization which leads to the synthesis of NCAs.[54] In 1988, Daly *et. al.* first reported the use of bis(trichloromethyl) carbonate (triphosgene) to synthesize NCAs from several α-amino acids.[55] Triphosgene is a crystalline product, easy to handle and requires no catalyst for completion the reactions. In a typical reaction, amino acids suspended in anhydrous THF with 1/3 equivalent of triphosgene at a temperature 40-50ºC leads to formation of their corresponding NCAs in three hours.[55] All the above methods that use phosgene and their higher analogs generate hydrochloric acid as the by-product. This in turn interferes with the polymerization reaction by either quenching the nucleophilic initiator or by itself acting as an initiator. To overcome this problem, stoichiometric amounts of α-pinine or limonene is added to the reaction media during NCA preparation to trap the HCl byproduct. The amino acid NCAs thus obtained after several rounds of crystallization are mostly free of Cl^- ions.[56] It should be noted that all the phosgenes are lethally toxic to handle. Koga *et al.* first reported an effective alternative of phosgene for amino acid NCAs synthesis which is far less toxic, easily available, easy to store and handle. Bis(2,4-dinitrophenyl)carbonate (BDNPC) is one of such useful and effective phosgene alternative that allows synthesis of NCAs from various α-amino acids under mild condition with good yields[57](Scheme 1.5).

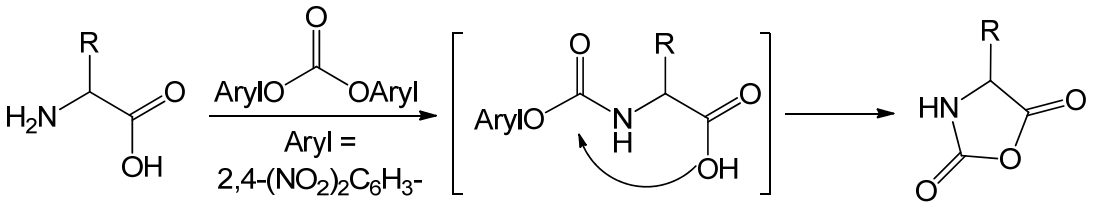

Scheme 1.5: NCA synthesis using BDNPC

With the scope to investigate the origin of life, amino acid NCA synthesis was attempted using reagents (NO and O_2) that mimicked prebiotic conditions as shown below (Scheme 1.6).[58]

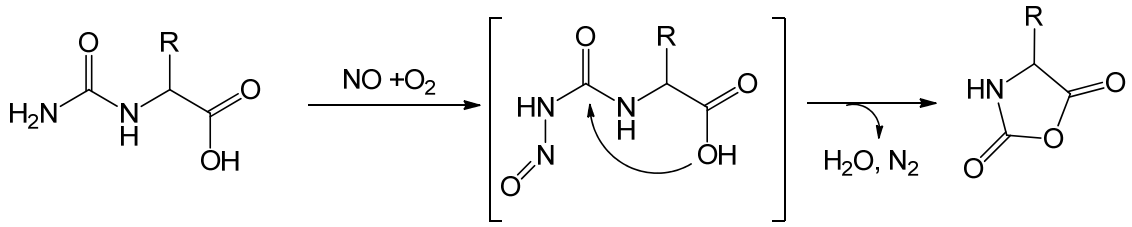

Scheme 1.6: NCA synthesis in presence of NO and O_2

1.2.2.2 Purification of NCAs

The purity of NCAs is extremely important for the successful synthesis of polypeptides having high molecular weight and low polydispersity using the ring opening polymerization. The impurities or contaminations present in the amino acid NCAs depend on the method of synthesis of NCAs. Over the last few decades, various NCA preparation methods and purification steps have been developed to obtain amino acid NCAs with very high purity. The most widely used method to synthesize NCAs, Leuches method, using thionyl chloride, phosphorus pentachloride, and phosphorus tribromide generates benzyl halogenides, phosphoryl trihalogenides and HCl as the common impurities (Scheme 1.7). Whereas, in *Fuchs-Farthing* method and all other modified phosgenation procedure that directly synthesizes amino acid NCAs from α-amino acids produce HCl as a common contamination along with N-chloro formyl amino acid chlorides and isocyanato acid chloride (Scheme 1.7). As most of these impurities are electrophile in nature, they may interfere with the NCA polymerization process either by deactivating the basic or nucleophilic initiator which are typically primary and secondary amines. Finally, the counter anions (Cl^-, Br^-) are known to be very effective towards initiating the amino acid NCA polymerization in DMF and that could lead to unpredictable changes in the molar mass and molar mass distribution of the resulting polypeptide. To purify the NCAs from impurities various

methodologies have been developed in the past decades. However, it has also been noticed that a small amount of acid chloride is required for the storage of amino acid NCAs as it protects the NCAs from attack by traces of moisture.

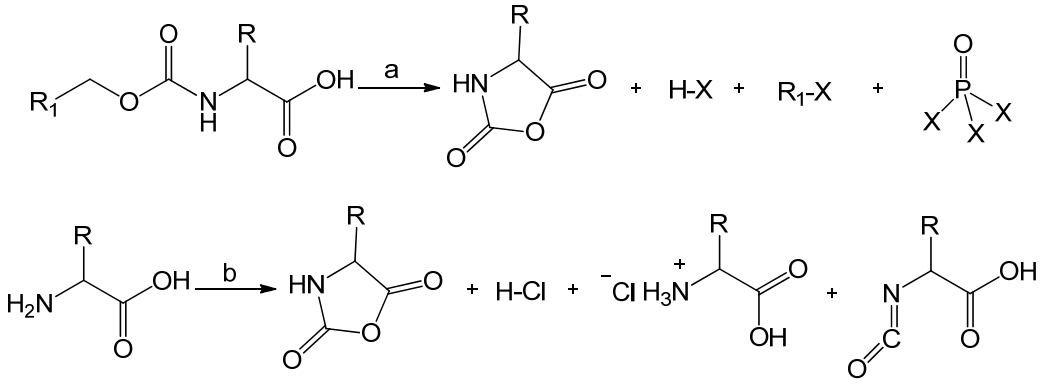

Scheme 1.7: Synthesis of NCA and their byproducts (a) phosgene and (b) various halogenating reagents ($SOCl_2$, PBr_3, PCl_3, PCl_5, etc)

Crystallization technique under anhydrous condition is widely used to purify the NCAs, as most conventional NCAs are crystalizable compounds in contrast to the impurities present.[59] According to most established protocols, the NCAs are treated through a series of three or more crystallizations from a suitable mixture of solvents and non-solvents. Ethyl acetate and petroleum ether/hexane/cyclohexane combinations are most widely used to purify the NCAs since most of the NCAs are generally soluble in ethyl acetate. For NCAs that are insoluble in ethyl acetate, like glycine and alanine NCA, a combination of hot THF or dioxane with toluene or carbon tetrachloride is used for crystallization. Kricheldorf has advocated the use of a mixture of solvents such dichloromethane with THF or dioxane as it is more likely to remove HCl and other byproducts since these impurities are less soluble in the pure solvents.[28] Crystallization is the most effective method to purify the amino acid NCAs that is solid in nature. For amino acid NCAs that are semi-solid or liquid, removal of contamination (like residual phosgene, HCl) remains much more challenging.

According to earlier reports, a treatment of NCAs with carefully dried activated charcoal is also very effective to purify the NCAs from HCl impurities in large quantities.[60] Several research groups[61, 62] also reported the purification of NCAs by sublimation methods in high vacuum. However, this can be only applied for thermally stable NCAs though this process does not exclusively yield purified NCAs. Several patents have described for the purification of NCAs by

using various 'active column' like, zeolites and urea with or without Ag_2O as a chloride scavenger. In 1992, Dormann *et. al.* first reported re-phosgenating the synthesized amino acid NCAs to remove the persistent small quantity of amino acid HCl salts. This additional phosgenation step yielded pure amino acid NCAs that upon polymerization resulted in formation of polypeptides with controlled molecular weights.[63]

In the year 1999, Poche *et. al.* first reported the purification methodology of liquid NCAs by washing with 0.5% aqueous bicarbonate solution that was pre-cooled to 0ºC.[64] The protocol involved first dissolving the amino acid NCA in water insoluble organic solvent that was pre-cooled to 0ºC followed by aqueous wash at 0ºC (to get rid of phosgene) and 0.5% sodium bicarbonate solution wash at 0ºC (to get rid of excess HCl). This extensive washing protocol is required to purify the NCAs from HCl, amino acid HCl salts and unreacted phosgene. However, it is very difficult to purify some long chain γ-alkyl glutamate NCAs by this method due to emulsion formation and over time the water present can initiate the polymerization leading to premature polypeptide synthesis. The use of silica gel chromatography to purify α-amino acid NCA was first reported by Hirchsmann et al. in the year 1971.[42] In recent report, Deming *et. al.* has reported to use silica column to purify various NCAs from all possible contaminations.[65]

1.2.2.3 Characterization of NCAs

The best possible way to characterize the NCAs is by Fourier Transform InfraRed (FT-IR) spectroscopy and Nuclear Magnetic Resonance (NMR) spectroscopy. FT-IR is the oldest and most well established method for the characterization of amino acid NCAs. However, FT-IR data is unable to give the information about the purity of the synthesized NCAs. NMR (^1H and ^{13}C) on the other hand gives information on both the structure and purity of the NCA monomers. NCA monomer has also been characterized by their characteristic melting point as well as by determining their crystallographic structure.

1.2.2.3.1 IR spectroscopy

With the help of oldest spectroscopic method, Fourier Transform InfraRed (FT-IR) spectroscopy, NCA monomers are characterized by their resonances at 1855±5 cm^{-1} and 1780±5 cm^{-1}, which are considered to be characteristic of the stretching modes of the two carbonyl groups in the anhydride ring. These resonances are typically unique and distinct from similar

compounds like N-protected amino acids, cyclodipeptides, polypeptides and hydantonic acids.[66] Two different stretching frequencies are observed for two carbonyl groups of NCA due to the unsymmetrical structure of the anhydride ring. Since the lone pair of nitrogen (NH) is delocalized through adjacent anhydride C-2 carbonyl (CO) group, the stretching frequency of this carbonyl group is observed at lower values that of the adjacent C-5 carbonyl group.[67]

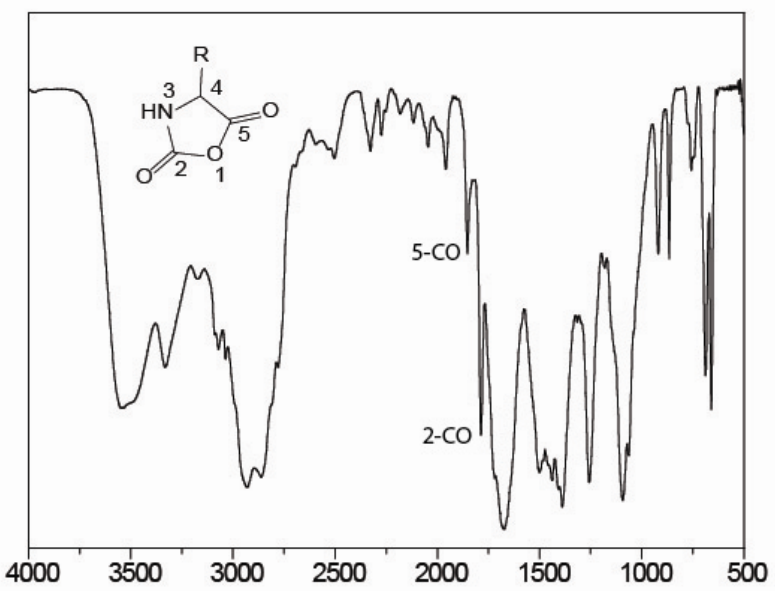

Figure 1.1: FT-IR spectrum of NCA

1.2.2.3.2 NMR spectroscopy

NMR spectroscopy (^{1}H and ^{13}C) is the most powerful analytical tool to elucidate chemical structures in organic chemistry. Over few decades, both ^{1}H and ^{13}C NMR has been routinely used to characterize amino acid NCAs. ^{13}C NMR is very useful for the determination of the structure of amino acid NCAs due to the presence of the two anhydride carbonyl signals.[68] It is generally general observed that the value for the carbonyl ^{13}C signal for carbamic acid derivatives lie in the range of 150-160 ppm while that for the corresponding amide and ester group the signal falls in the range of 168-180 ppm.[69] Since the ^{13}C signal of C-5 carbonyl carbon of NCAs falls in the range characteristic of amide and ester groups, the unique C-2 carbonyl ^{13}C signals allows the detection of NCAs. The two chemical shifts of the two carbonyl groups of a given NCA differ by ~15 ppm.

^{1}H NMR, in addition to being a very important tool for the characterization of amino acid NCAs, also allows the determination for the presence of impurities like solvents and salts which may hinder the polymerization reaction. The α-amino acid NCA ring (other than glycine) contains only two protons; one linked to the nitrogen and another to the chiral α-carbon of the amino acid (C_α-proton). The two β-protons neighboring the chiral center (α-carbon) of amino acid NCAs such as in leucine, cystine, serine or phenylalanine are magnetically nonequivalent and this leads to different proton signals at higher frequency (>100MHz) in ^{1}H NMR. The C_α-proton is normally observed as a triplet in low field NMR but this gets split into a doublet of doublets in high field NMR due to its coupling with two adjacent non-equivalent β-protons.

1.2.2.4 Polymerization of NCAs: Chemical aspect

Amino acid NCAs are polymerized to their corresponding polypeptides by ring opening polymerization (ROP). The polymerization is initiated by a wide range of nucleophilic initiators. These include, water, alcohols, primary/secondary/tertiary amines, phosphines, mercaptans, carbanions and alkoxides, zero valent transition metal complexes and silazane derivatives. Among all these types of initiators, polymerization initiated by primary, secondary and tertiary amines have been studied extensively by various research groups.[59] The ring opening polymerizations (ROP) of amino acid NCAs by amines are known to proceed through two different pathways and are known as the 'normal amine' (NA) and 'activated monomer' (AM) mechanisms.[28, 59, 70] Normal Amine (NA) mechanism is generally applied for polymerizations that are initiated by non-ionic initiator having one mobile hydrogen atom such as primary amines, secondary amines, alcohols and water (Scheme 1.8). For polymerizations initiated by mines, the reaction mainly depends on the nucleophilicity/ basicity of the amines, the NCA/ amine ratio, solvents and temperature. The proposed NA mechanism involves first the nucleophilic attack of the initiator amine onto the NCA ring at the carbonyl (C-5) position leading to the formation of the amide bond. This is followed by decarboxylation[71] and resulting amino acid amide attacks another NCA monomer leading to the propagation of the polymerization reaction.

Initiation:

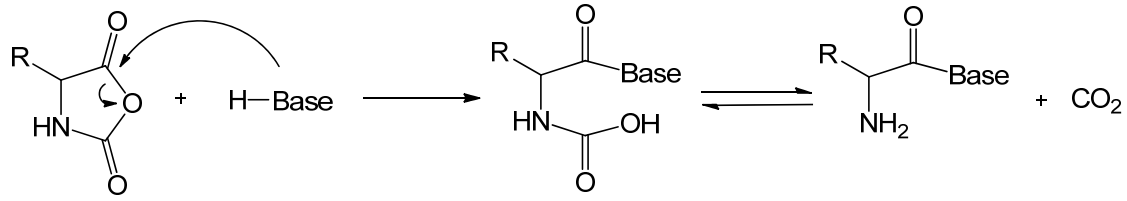

Propagation:

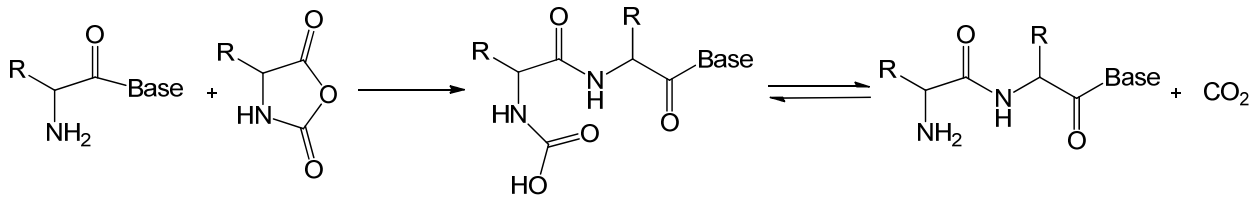

Scheme 1.8: Normal Amine (NA) mechanism pathway of NCA polymerization

Peggion *et. al.*[72] and Goodman *et. al.*[73] have demonstrated independently that best results concerning the agreement between the experimentally observed and the stoichiometric molecular weights was observed when primary amine was used as the initiator. Since primary amines are more nucleophilic than the ω-amino groups of the propagating chains, the initiation rate is faster than propagation leading to polypeptides with low polydispersity indices (PDI; M_w/M_n). As the nucleophilicity and basicity of amines depends on both the electron density at the nitrogen atom and the steric requirements, the incorporation ratio varies with the structure of the initiators.[74, 75] According to earlier reports, if primary alkyl amine with unbranched alkyl chains are used as initiators, 100% incorporation of the initiator occurs. In contrast, only 10% incorporation of initiator occurs if secondary amines, such as diisopropyl amine, are used as the initiator. This indicates that when secondary amine is used as the initiator, the NCA polymerization occurs by a different pathway known as the activated monomer (AM) pathway.[73, 76] The NCA ring opening polymerization process is generally called 'living polymerization' since its reactive end group remains alive throughout the course of the polymerization with 100% monomer conversion and the molecular weight distribution (MWD) is very narrow with polydispersity index (PDI) below 1.1. However, during the polymerization process, various factors like carbamic acid-CO_2 equilibrium,[77] solvents,[62,78] presence of impurities in the NCAs[79 80, 81]cause deviation from its 'living' nature.[82] Solvents play an important role in NCA polymerization. For example, in presence of nitrobenzene the polymerization of sarcosine NCA using primary amine initiator led

to the formation of salt between carbamic acid and amino group which in turn catalyzed the propagation of the polymerization reaction. Thus, kinetic studies showed the reaction to be higher than first order. In dimethylformamide (DMF), simple first order kinetics was observed as the basicity of the amine groups was shielded by the acidic DMF.[77]

The activated monomer (AM) mechanism was first proposed by Ballard *et. al*. to explain the polymerization of DL-phenylalanine NCA using tertiary amine as an initiator.[83, 84] (Scheme 1.9) Basic salt initiated polymerization of NCA also follow the AM mechanism.[85] It is believed that co-existence of both the NA and AM mechanism in the polymerization of NCAs using secondary, tertiary amines and alkali halides as an initiator.

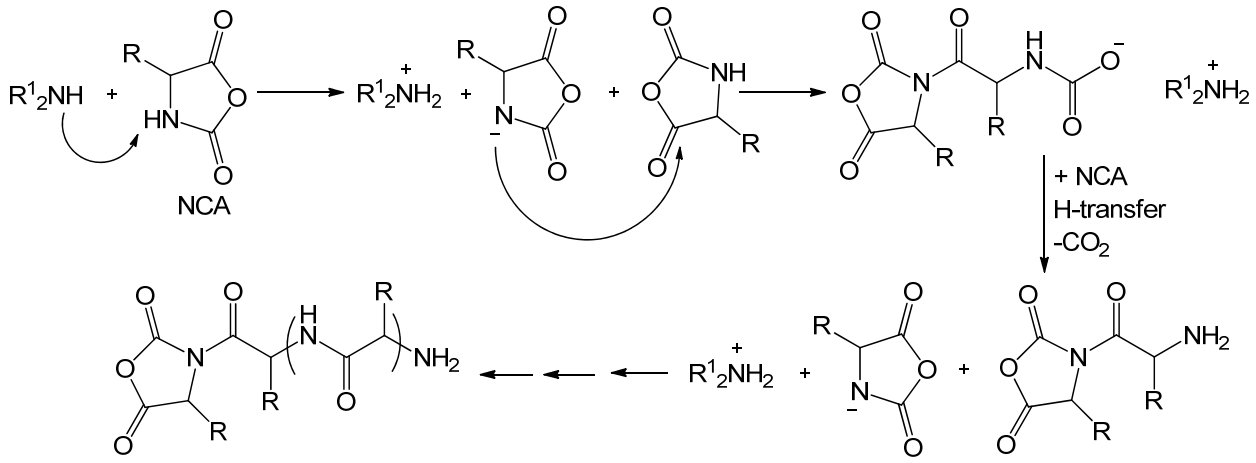

Scheme 1.9: Activated monomer mechanism pathway of NCA polymerization

In AM mechanism, the added initiator acts as a catalyst rather than a chain initiating precursor due to its high basicity. At the beginning of the NCA polymerization, the initiator acts as a base to abstract the proton from N-3 of the NCA ring and generate an anion. This generated anion on the NCA ring acts as an initiator and attacks the 5-CO of another NCA to give a tadpole dimer having an active anion at the end that was formed by releasing CO_2. In the propagation step, the tadpole dimer anion can attack another NCA monomer followed by CO_2 release leading to the synthesis of polypeptides with broad molecular weight distribution.

Bamford group has published several reports on the detailed study of the 'activated monomer' (AM) mechanism. The steric factor plays an important role in amino acid NCA polymerization by the AM mechanism. For example, sarcosine NCA was almost unreactive

when diisopropylamine was used as an initiator but under the same conditions the polymerization of γ-ethyl-glutamate NCA was faster in comparison to polymerization initiated with primary amine initiator.[76] The proline NCA (absence of 3-N hydrogen) polymerization in DMF using tri-*n*-butyl amine initiator induced very slow polymerization compared to γ-ethyl-glutamate NCA polymerization under the same conditions. But the presence of water impurity in the reaction mixture accelerated the polymerization of proline NCA.[86] The monomer and solvent purity is also very crucial for the polymerization by AM mechanism. Even the presence of trace salt like lithium chloride (LiCl) is detrimental since it can act as a very effective initiator for the polymerization of NCA in DMF because of the highly basic nature of the chloride anion.[84] The molecular weight of the polypeptide and PDI of the polypeptide obtained for amino acid NCA polymerized via AM mechanism is higher than that by the corresponding NA mechanism since the anionic intermediate involved in the propagation step of AM mechanism leads to higher propagation rates.[87]

In 2004, Vayaboury *et. al.* studied ε-trifluoroacetyl-L-lysine NCA (TFA-Lys NCA) polymerization in DMF with *n*-hexylamine initiator as a function of temperature.[88] In 2010, Habraken *et. al.* studied the effect of temperature on homo-, block- and graft co polymerization of various amino acid NCAs.[89] These authors observed that by lowering the temperature, the amount of 'living' chain increased and this lead to polypeptides with higher molecular weights having low molecular weight distribution (PDI). The percentage of 'living' chain increased from 22 to 99% when temperature was decreased from 20º to 0ºC. The authors concluded that at 0°C the activation energy barrier for chain propagation reduces and this in turn makes the chain propagation rates much higher than the deleterious side reactions such as end-group termination.[88, 89]

In 1997, Deming first introduced a new class of NCA-initiators based on zero valent organonickel compounds to polymerize various NCAs very effectively without termination of the end group ('living' in nature).[90] Highly efficient zero valent nickel and cobalt complex initiators (i.e. bipyNi(COD), $(PMe_3)_4Co$ (bipy- 2,2′-bipyridyl, COD- 1,5-cyclooctadiene) was used to allow the living polymerization of NCAs into controlled broad range of molecular weight ($500<M_n<500000$) with low polydispersity polypeptides ($M_w/M_n<1.2$)[90-93] (Scheme 1.10).

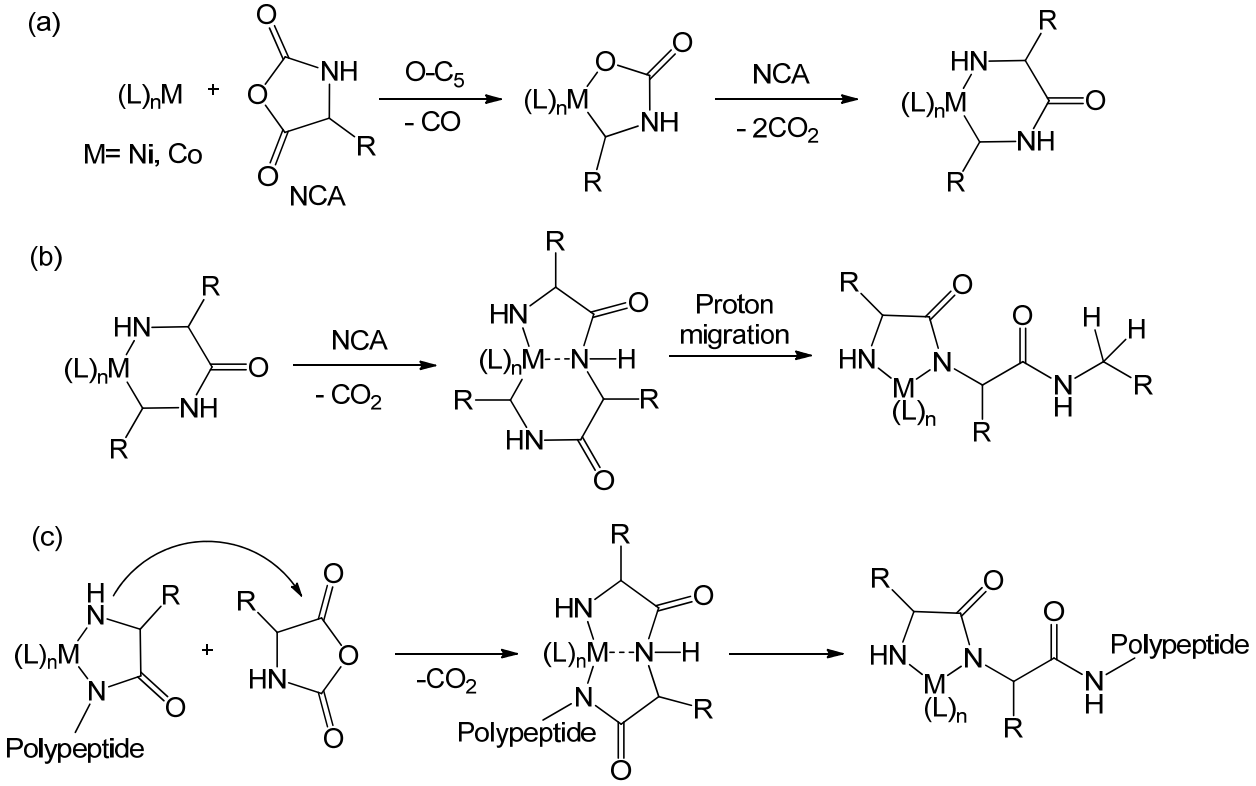

Scheme 1.10: Zero valent transition metal mediated NCA ring opening polymerization

In 2007, hexamethyldisilazane (HMDS) and its derivatives were introduced as effective initiator for NCA ring opening polymerization (Scheme 1.11) by the Cheng group.[94] They obtained polypeptides with controlled molecular weight (less than 22% deviation from the expected molecular weights) with very narrow polydispersity in very high yield (almost 100%).

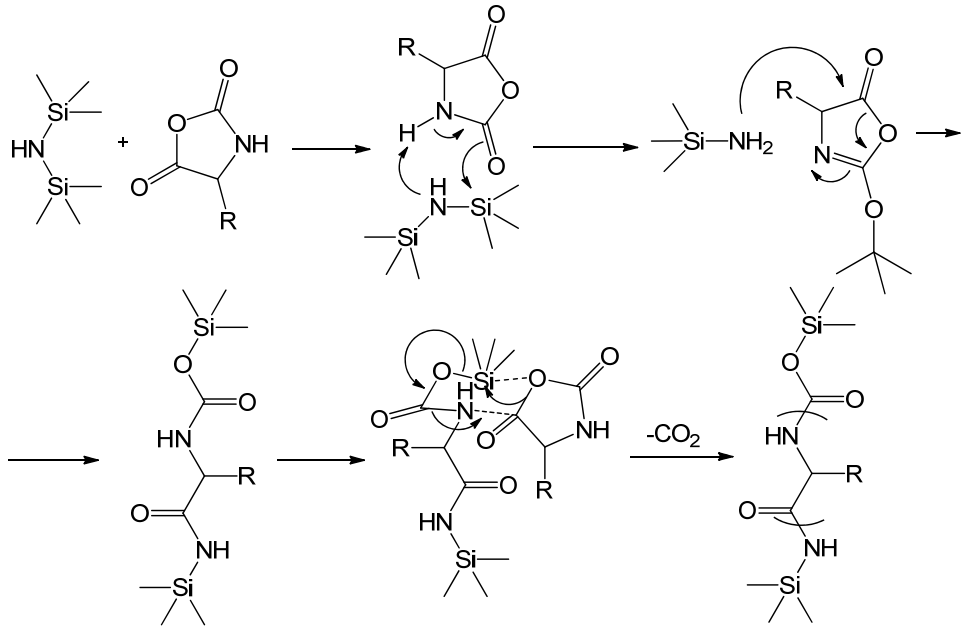

Scheme 1.11: Hexamethyldisilazane initiated NCA ring opening polymerization

Since HMDS is a secondary amine, it was expected to act either as a nucleophile to open the NCA ring at 5-C (NA mechanism) or act as a base to deprotonate the 3-N position (AM mechanism). According to the mechanism proposed by the authors, the secondary amine with two bulky trimethylsilyl groups in HDMS deprotonates the 3-N in the first step (AM mechanism) to form Me_3SiNH_2 (TMS amine) while the other TMS group gets attached to the carboxylic acid (Scheme 1.11). The generated TMS amine then subsequently attacks the 5-C (NA mechanism) to yield a TMS carbamate (TMS-CBM). In the propagation step, TMS group migrates from the terminal TMS-CBM to the incoming monomer to form a new TMS-CBM terminal. These HMDS initiated NCA polymerizations are similar to the group transfer polymerizations (GTP) of acrylic monomers initiated by similar organosilicon compounds.[95] Unlike GTPs, which typically require either Lewis acid or nucleophilic catalysts to facilitate polymerizations,[96] HMDS initiated NCA polymerizations do not require any additional catalyst as activators. The authors reported that it is unclear whether the TMS group transfers through an anionic process as GTP or through a proposed concerted process. HMDS initiator is also effective for the synthesis of block copolypeptides of defined sequence and composition like poly (*γ*-benzyl-L-glutamate)- *b*-poly(*ε*-carbobenzyloxy-L-lysine) (PBLG-*b*- PZLL).[94, 97] The authors have also demonstrated that their method allows facile functionalization of the C-terminal chain end of polypeptides with various functional groups when alkyl/aryl N-TMS amines derivatives are used as initiators. [98] These initiators may contain functional groups that can be further derivatized using "click" chemistry or ring-opening metathesis polymerization.[97, 98] NCA polymerization reaction initiated by HMDS and N-TMS amines usually takes 24 h for completion at ambient temperature. This is slower than metal complex mediated polymerization(Ni^0 or Co^0 initiators require about 30–60 min at ambient temperature) [90, 92, 93] but are much faster than those initiated by amines.[99]

1.2.2.5 Polymerization of NCAs: Physical aspect

Various analytical tools are used to characterize the synthesized polypeptides. These include determination of molecular weight, molecular weight distribution and end group analysis of the synthesized polypeptides. Though viscosity measurement is the oldest technique in polymer chemistry to determine molecular weight of the polymers, but for polypeptides this technique is not widely used due to the low solubility of polypeptides in various common

organic solvents. In the last two decades, gel permeation chromatography (GPC), NMR spectroscopy, light scattering and MALDI-TOF are extensively used to determine molecular weight and polydispersity index (PDI) of the synthesized polypeptides.

GPC analysis of polypeptides is performed by using 0.1M DMF as eluent at 60°C using RI or UV detector. Lithium bromide (LiBr) is used to denature the secondary structure of the solvated polypeptides and at 60°C the viscosity of the 0.1 M DMF is suitable for maintaining an optimal pressure inside the separating column. Separations of the polypeptides are effected by a guard column followed by series of 10^5, 10^3 and 10^2Å columns with constant eluent flow rate of 1 mL/min. The elution of polypeptides is usually monitored by observing changes in UV absorption or refractive index (RI) or light scattering. The molecular weight and the weight distribution of the polypeptides are determined from the GPC by comparing the values with known standard polystyrene or PMMA polymers. Using the above mentioned series of column, molecular weight from 5000 to 1000000 can be separated effectively.

^{1}H NMR is also very useful to determine the number average molecular weight and end group analysis of the polypeptides contains less than 50 repeating units. Above 50 repeating units, the ratio of end group protons to the other protons present in polypeptide chain is very low and accurate determination of molecular weight cannot be carried out.

Matrix assisted laser desorption/ionitiation time of flight (MALDI-TOF) mass spectroscopy analysis is also used to determine the absolute molecular weight of polypeptides and the polydispersity index. For polypeptides, 2,5-dihydroxy benzene (DHB) and α-cyano-4-hydroxy cinnamic acid (CHCA) are used as common matrix materials. Potassium trifluoroacetic acid (KTFA) is added as cationic ionization agent. Hexafluoro isopropanol (HFIP), trifluoro acetic acid (TFA) and dimethyl formamide (DMF) solvents are used to dissolve the polypeptides sample for MALDI-TOF.

1.3 Biomedical applications of synthetic polypeptides

After successful development of methodology that allows synthesis of well defined homo and block polypeptide, current efforts by several research groups is now focused towards application of these materials for biomedical research[100] Polypeptides offer several advantages over synthetic polymers due to their biocompatibility, biodegradability and very low

cytotoxicity. They also posses stable secondary structures (such as α-helix or β-sheet) that can be modulated by the application of external stimuli such as pH.[101] Therefore, polypeptide based biomaterials currently hold a great deal of interest in several biomedical research areas such as drug delivery, gene delivery and mimicking the extracellular matrix scaffold for tissue engineering. Over the last decade, several reports have been published on the synthesis of various polypeptide based stimuli responsive materials, their assembly and their biomedical applications.[101] For example, since it is well known that positively charged polymers can penetrate cell membrane very easily,[102] several studies have been reported on the use of various types of positively charged synthetic polymers, polypeptides and their assembled structure as a drug and gene delivery vehicle.[103-109] There are two familiar class of cationic polypeptides that are known to enter most of the mammalian cells very effectively through plasma membrane. These are the "protein transduction domain" (PTD) and "cell penetrating peptides" (CPPs) both of which are consists of positively charged amino acids (< 20 amino acids).[110, 111] The earliest report on synthetic polypeptides for biomedical uses focused on the easy synthesis of water soluble homo polypeptides as a drug delivery vehicle.[112]

Further, polypeptide based hydrogels have shown significant promises in microfluidics[113], drug delivery[114] and as tissue engineering scaffolds by mimicking the natural extracellular matrices of cells.[115, 116] Particularly, hydrogels based on synthetic polypeptides[100] are very important since the structural features and biofunctionalities of the gel network can be manipulated as desired by engineering the peptide sequences.[117]

1.4 Surface modification by polymers for biomedical applications

It is the surface of a biomaterial which first comes into contact with the living body when the biomaterial is implanted in the body. The initial response from the living body entirely depends on the surface properties of the foreign biomaterials. A very strong or very low response interaction of the biomaterial with the living body can severely hamper its functions. For instance, the haemodialyser will not function well if the blood clots on its surface and the contact lens can damage the surface of the cornea unless it is wetted with tears. Poor adhesion between a percutaneous device and the skin tissue probably causes infection because of the dead space present in between.[118] Surfaces play a vital role in almost all biological processes like cell

signaling, cell proliferation, cell migration, transportation and biomineralization since they depend entirely on ECM/cells, hydrated tissue/air and mineral/protein (bone) interactions.

Most conventional man-made synthetic bulk materials do not have the biofunctionality to elicit a proper response towards biological systems as is expected of a biomaterial. A poorly biocompatible surface in direct contact with the living body would evoke strong foreign body reactions that would severely limit its usage. Therefore, the surface of these man-made bulk materials need to be modified to make them biofunctional and biocompatible for biomedical applications. In recent decades, the materials scientists have been engaged in designing biomaterials which should have excellent bulk and surface properties that provide proper response towards biological systems. With the advent of various techniques in advanced surface engineering, surfaces can be easily modified with polymers with controlled chemical composition, topography, roughness and hydrophilic/hydrophobic balance so that it is suitable for biomedical applications.[119]

1.5 Organic-inorganic silica nanocomposite

Materials that consist of various phases with different composition but having at least one constituent phase with one dimension less than 100 nm is called "nanocomposite".[120] Organic/inorganic nanocomposites are generally a combination of organic molecules/polymers with nano sized inorganic materials and these materials have very novel properties. The combination of properties that are characteristic of the inorganic part like rigidity, thermal and structural stability with that that are characteristic of the organic part such softness, flexibility, ductility and processability result in properties that makes these materials unique. The high surface area of nanomaterials in the nanocomposites creates a significant volume fraction of interfacial surface area even at very small quantities leading to dramatic changes in properties than that is observed in the bulk. [121-123]

Silicon is the second most abundant element in the Earth's crust (about 28% by mass) after oxygen and over 83.77% earth' crust is composed of silicate minerals. Silicon oxide, popularly known as silica, is most commonly found in nature as sand or quartz.[124] Primitive life forms on earth such as diatoms and siliceous sponge used silica to build their structures. From the early days of human civilization, silica is being used as a hardening material. Modern chemistry discovered silica as comparatively inert, robust and thermally stable material due to the dπ-pπ

back bonding between silica and oxygen atom. But the use of pure silica is limited due to lack of surface functionality. The development of silicon surface chemistry together with various easy 'bottom up' approaches for control synthesis of silica nano materials[125] as well as silica mesoporous materials[126] from molecular silica precursor have made silica very attractive as a functional material. The large surface area and multimodality have made silica nano and mesoporous materials attractive for various industrial applications such as fillers in the manufacture of paints, rubber products, plastic binders,[127] catalysts, and coatings among others. The biocompatibility combined with low cytotoxicity has rendered silica materials very interesting for potential application in bio-imaging, diagnosis, drug delivery and gene delivery.

Surface modifications have greatly extended the utility of silica nanoparticles towards various industrial and biomedical applications. Silica particles coated with organic modifiers are used in various industrial and engineering applications such as stationary phase in chromatography,[128] heterogeneous supported catalysts,[129] and in the automotive, electronics, consumer goods,[130] aerospace and sensor industries.[131] The rich and versatile chemistry of organically modified silica (ORMOSIL) nanoparticles provide the ideal bio-nanotechnology platform for the fabrication of multimodal imaging probes, combining a wide variety of contrast agents that are suitable for large number of different imaging applications such as fluorescence (optical) imaging, magnetic resonance imaging (MRI), positron emission tomography (PET), optical coherence tomography (OCT) etc.[132-136] The tunable properties like hydrophobic core, tunable mesoporosity, optical transparency and well developed rich surface chemistry have made ORMOSIL nanoparticles very suitable for multimodal imaging, nanoprobes for biomedical applications such as drug delivery carrier, photodynamic therapy, and gene therapy.[137-142] Other beneficial features like ability to release drug in a controlled manner, low toxicity and systematic clearance from the body have made these nanoparticles very promising for practical biomedical applications.[143-145]

1.5.1 Polymer/silica nanocomposites

Surface modification of silica nano materials using polymers is very important and interesting as polymers alter the surface properties very drastically. The mechanical and thermal properties of the hybrid materials depend on the size and shape of the silica core. These polymer surface modified silica hybrids exhibit improved wet-ability, lubricity and superior dispersion.

These hybrids models are very much similar to the spherical brushes in which polymer chains are extended from the silica core to minimize the steric crowding.[146, 147] These hybrid materials often find a wide range of applications in optics, sensors, electronics, etc and in biomedical research.[148, 149]

Typically, the surface of the inorganic materials are modified by two methods, i) physically: through physisorption, blending and sol-gel process, ii) chemically: through covalent polymer grafting on the surface by various techniques and *in situ* or surface initiated polymerizations.[120]

1.5.1.1 Modification by physical interaction

Surface modification based on physical interaction is obtained by non-covalent interaction between adsorbed polymers or surfactant onto the surface of silica particle. The surfactant is usually used to reduce the agglomeration of the silica nanoparticles and it can also be easily incorporated into the polymer matrix. The most traditional and simple process to synthesize silica nanocomposite by physical interaction is known as 'blending'. The blending process involves simply direct mixing of silica nanoparticle into the polymers. The mixing can generally be done by either melt blending or solution blending.[120] Since physisorption involves association of the nanoparticle and polymer by non-covalent interaction; the composites suffer from leaching, sedimentation and agglomeration which make this technique unfavorable for the preparation of silica nanocomposites.

1.5.1.2 Modification by chemical interaction

There are several methodologies established to prepare silica/polymer nano composites, like sol-gel process, in-situ polymerization, photopolymerization and covalently surface grafting of polymers. All these methodologies have their own advantages and disadvantages for the preparation of polymer nanocomposites. The key challenge is to construct a nanocomposite system that has an improved specific interaction at the interface of the organic and inorganic component. Therefore, the development of the various grafting methodologies on the silica surface is of great current interest. It is also believed that the covalent grafting techniques are preferred since unlike grafting using physical interactions phase separation of the polymer and inorganic materials during synthesis of the nanocomposite is not possible. Two general methods

have been used to graft polymers onto silica surfaces i) 'grafting from' and ii) 'grafting to' methodology.

1.5.1.2.1 'Grafting from' methodology

The 'grafting from' methodology is also called surface initiated polymerization, like polymerization initiated in situ with monomers from the previously immobilized initiator onto the silica surface leading to the formation of polymer chain growing directly from the surface (polymer brushes or hairy nanoparticles) (Figure 1.2). This methodology appears to be very effective and promising to prepare silica nanocomposites with very high grafting density. Large varieties of polymerization techniques have been applied to synthesize the polymer/silica nanocomposites such as conventional radical polymerizations,[150, 151] control radical polymerizations,[152, 153] living anionic polymerizations,[154] living cationic polymerizations,[155] ring opening polymerization,[156] ring opening metathesis polymerization.[157]Among them control radical polymerization using ATRP, [158, 159]NMP[160, 161]and RAFT[162, 163] has been widely used. All these techniques are very useful to obtain polymers with controlled molecular weight and narrow polydispersity.

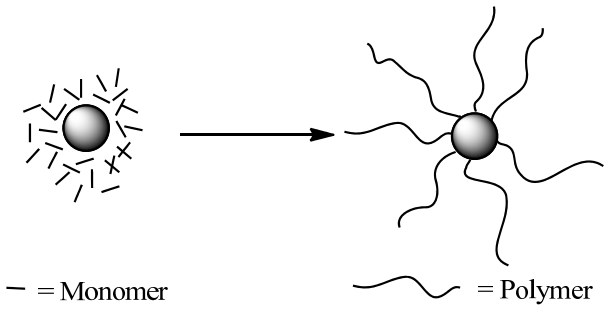

Figure 1.2: Schematic presentation of 'grafting from' methodology

The main advantage of this process is that the synthesis can be performed in one-pot and high grafting density of the polymer chains are obtained on the nanoparticle since single monomers that participate to propagate the polymerization onto the surface offer minimal steric hindrance to the growing chain. The disadvantage of 'grafting from' methodology is the difficulty in characterizing the polymers formed since they are covalently bound to the surface of the silica nanoparticles.

1.5.1.2.2 'Grafting to' methodology

The 'grafting to' methodology consists of a two step process. The first step involves the preparation of the well defined polymers and then subsequently in the second step the polymer is covalently grafted onto surface of interest by various chemical reactions (Figure 1.3). Unlike 'grafting from' methodology, the grafting density of the polymer chain is lower for 'grafting to' methodology because of the steric crowding of reactive sites by previously attached polymers. However, this process offers the post synthesis of well defined and well characterized polymers leading to well defined polymer surface onto the silica nanocomposites. Out of the several chemical methodologies that have been developed to graft polymers covalently onto the surface of nanoparticle, the recently developed Cu(I) mediated alkyne-azide cycloaddition reaction, known commonly as 'click chemistry', has become very popular in attaching end functionalized polymers onto the surface of nanoparticles. [164]

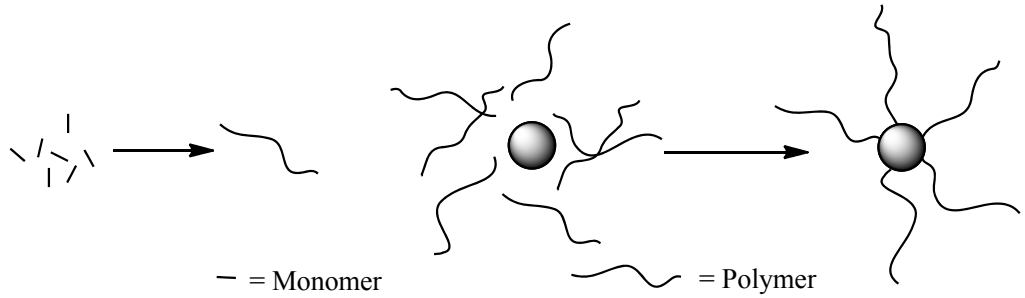

Figure 1.3: Schematic presentation of 'grafting to' methodology

1.5.1.2.2.1 Click chemistry

In 2001, Kolb, Finn and Sharpless published a landmark review describing the development of a set of powerful, highly reliable, and selective reactions for the rapid synthesis of useful new compounds in organic chemistry.[165] The authors have termed this approach as 'click chemistry'. A reaction has to meet a set of stringent criteria to be called as 'click chemistry'. This has been defined as "*reaction must be modular, wide in scope, give very high yields, generate only inoffensive byproducts that can be removed by non-chromatographic methods, and be stereospecific (but not necessarily enantio- selective).*" This process should have other characteristics like *"simple reaction conditions (ideally, the process should be insensitive to oxygen and water), readily available starting materials and reagents, the use of no*

solvent or a solvent that is benign (such as water) or easily removed, and simple product isolation." [165] Based on these defined characteristics several reported organic reactions are classified as 'click' reaction. The category of the 'click' chemistry reactions are 1) cycloaddition reactions of unsaturated species, such as 1,3-dipolar cycloaddition reactions, and hetero Diels - Alder reactions; 2) nucleophilic substitution chemistry, particularly ring-opening reactions of strained heterocyclic systems such as epoxides, aziridines, aziridinium ions, and episulfonium ions; 3) carbonyl chemistry of the "non-aldol" type; such as formation of ureas, thioureas, aromatic heterocycles, oxime ethers, hydrazones, and amides and 5) additions to carbon - carbon multiple bonds, especially oxidative reactions such as epoxidation, dihydroxylation, aziridination, and sulfenyl halide addition, but also Michael additions of Nu-H reactants. Although several identified reactions meet the requirements to be 'click' reaction, the Huisgen 1,3 dipolar cycloaddition of alkyne and azides to yield substituted 1,2,3-triazoles has been widely studied and used as a 'click' reaction. The beneficial effect of using water as a reaction medium, high efficiency, selectivity (regio- and chemo-) and the tolerance with a broad repertoire of organic functional groups place the Cu(I)-catalyzed azide alkyne cycloaddition (CuAAC) reaction at the centre stage of 'click' chemistry.[164, 166] The CuAAC has found application in various fields of research as diverse as organic synthesis, polymer,[167] and material science[167, 168] medicinal chemistry, molecular biology and biotechnology. The formation of a robust linker such as the 1,4-disubstituted 1,2,3-triazole ring which displays biological and pharmacological activities of its own, is an added advantage of the synthetic utility of the CuAAC reaction in the discovery of novel drugs.

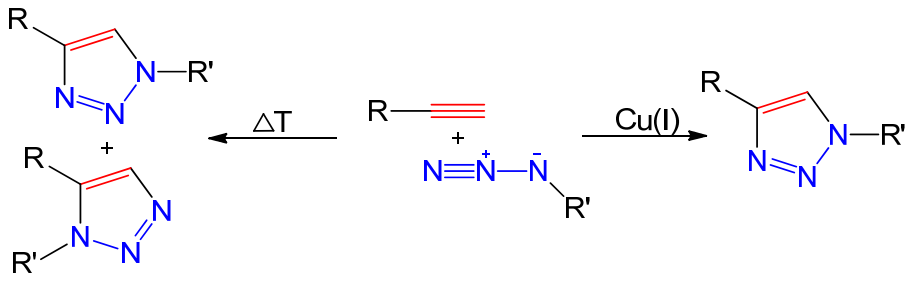

Scheme 1.12: Huisgen 1, 3 dipolar cycloaddition reaction

1.5.1.3 Applications of surface modified silica

Since, polymer/silica nanocomposites have unique properties along with improved physical properties such as mechanical and thermal properties; they have attracted strong interest in many industrial[120] and biomedical applications.[169] In industrial aspects, many potential and practical applications have been reported using polymer/silica nanocomposites such as coatings,[170, 171] flame retardant material,[172] optical devices,[173] electronics and optical packing materials,[174] photoresist materials,[175] photoluminescent conducting film,[176] pervaporation membrane,[177] ultrapermeable reverse selective membrane,[178] proton exchange membrane,[179, 180] grouting materials,[181] sensors, [182, 183] material for metal uptake,[184] etc. In biomedical research, these hybrid materials are used as stimuli-responsive drug delivery systems, nanocarrier for targeting of cancer cells[185] and gene transfection agent.[149] In stimuli responsive drug delivery systems, there are several triggers such as pH,[186] temperature,[187] magnetism,[188] chemicals, redox,[189] light or ultrasound,[190] which can activate the release of the cargos from the nanocarrier.

1.6 Physico-chemical Characterization

1.6.1 Fourier Transform Infra Red Spectroscopy (FT-IR)

FT-IR stands for Fourier Transform InfraRed spectroscopy, the invaluable tool in organic structure determination and verification involves the class of electromagnetic (EM) radiation with frequencies between 4000 and 400 cm^{-1} (wave numbers). In infrared spectroscopy, IR radiation is passed through a sample that is absorbed by interatomic bonds in organic compounds. Chemical bonds in different environments will absorb varying intensities and at varying frequencies. Thus IR spectroscopy involves collecting absorption information and analyzing it in the form of a spectrum. The resulting spectrum represents the molecular absorption and transmission, creating a molecular fingerprint of the sample. Like a fingerprint no two unique molecular structures produce the same infrared spectrum. This makes infrared spectroscopy useful for several types of analysis.

Over time organic chemists have recorded and catalogued the types and locations of IR absorptions produced by a wide variety of chemical bonds in various chemical environments. These data can be quickly referenced through tables of IR absorption ranges and compared to the spectrum under consideration. As a general rule, the most important factors determining where a chemical bond will absorb are the bond order and the types of atoms joined by the bond. Conjugation and nearby atoms shift the frequency to a lesser degree. Therefore, the same or

similar functional groups in different molecules will typically absorb within the same, specific frequency ranges. Today, FT-IR spectrometers have moved out of the laboratory and are being used extensively to characterize for a wide range of samples, including polymers, organic-inorganic hybrid materials, etc.

1.6.2 Gel Permeation Chromatography (GPC)

Gel permeation chromatography is a method to determine molecular weight and molecular weight distribution of polymers. Therefore a polymer solution is injected into a column containing porous beads with pores having the dimension of the polymer. The accessible volume of the pores depends on the hydrodynamic radius of the sample and the elution time or volume of the polymer is thus a function of its hydrodynamic radius. Polymers with a hydrodynamic volume exceeding the pore volume elute after a certain volume, the so called exclusion volume. The number of accessible conformations of a macromolecule within a pore is limited which lowers its entropy as compared to the interstitial volume ($\Delta S < 0$ J/K). This is counterbalanced by a concentration gradient driving diffusion into the pores.

This process is thought to be in a thermodynamic equilibrium and can thus be described by a distribution coefficient K:

$$K = \exp(-\Delta H^0/RT)\exp(\Delta S^0/R)$$

with the gas constant R and the temperature T. In contrast to high performance liquid chromatography (HPLC), which is based on interactions of the solute with the column material. These interactions are to be avoided in GPC mode to assure separation based on the hydrodynamic volume ($\Delta H = 0$ J).

$$K_{GPC} = \exp(\Delta S^0/R)$$

For a freely diffusing molecule, there is no entropy difference ΔS between both phases. However, when the hydrodynamic volume of the macromolecule reaches the dimensions of the pore diameter, a negative entropy change depends on the hydrodynamic volume of the molecule. The elution of polymers is usually monitored by observing changes in UV absorption or refractive index (RI). The width form of the elution peak contains information about the molecular weight distribution of the polymer. For block copolymers with block responding differently to UV and RI detectors, compositional heterogeneities may be visible and can even be

quantitatively evaluated. As mentioned before, a disadvantage of GPC is separation by hydrodynamic volume and not by molecular weight, which becomes evident when comparing the elution volume of branched and linear polymers of the same molecular weight. The molecular weight distribution of a certain polymer is only accessible after calibration with well defined standards of polymers of the same type, whose molecular weight has been determined by absolute methods such as light scattering or osmometry. Only few polymer standards are commercially available, thus GPC often serves only as relative method. Using a viscosity detector the molecular weight distribution of almost any polymer is accessible by means of universal calibration.

1.6.3 Thermogravimetric analysis (TGA)

Thermogravimetric Analysis is a technique in which the mass of a substance is monitored as a function of temperature or time as the sample specimen is subjected to a controlled temperature program in a controlled atmosphere. A TGA consists of a sample pan that is supported by a high sensitive precision balance. That pan resides in a furnace and is heated or cooled during the experiment in controlled atmosphere. The mass of the sample is monitored during the experiment. A sample purge gas controls the sample environment. This gas may be inert or a reactive gas that flows over the sample and exits through an exhaust.

Thermogravimetric techniques have a very wide field of application. TGA provides quantitative measurement of mass change in materials associated with transition and thermal degradation. The technique can be used in the examination of Inorganic organic hybrid materials, absorptive surfaces, together with the nature and processes involved in thermal decomposition and oxidation processes. The results from thermogravimetric analysis are usually reported in the form of curves relating the mass lost from the sample against temperature. In this form, the temperature at which certain processes begin and are completed are graphically demonstrated. An example of a Thermogravimetric analysis curve obtained from heating a sample of silica gel from 30°C to 700°C is shown in Figure 1.4.

The graft density of the grafted moiety on the silica surface was determined by thermogravimetric analysis (TGA) using following equation as described.

$$\text{Graft density } (\mu\text{mol/m}^2) = \frac{\frac{W_{grafted(30-600)}}{100-W_{grafted(30-600)}} \times 100 - W_{unmodified(30-600)}}{M \times S \times 100} \times 10^6$$

Where $W_{30\text{-}600}$ is the weight loss between 30 and 600 °C corresponding to the decomposition of the grafted material corrected from the thermal degradation**,** and M is the molecular weight of the grafted silane. *S* represents the specific surface area of the material while $M_{\text{unmodified}}$ represents the determined weight loss of the material before grafting.

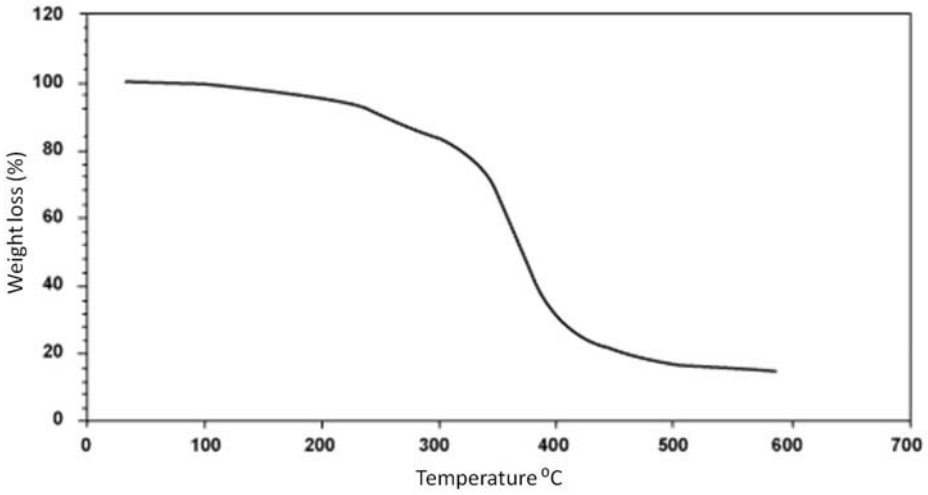

Figure 1.4: TGA graph in percentage (%) of weight loss respect to the temperature

1.6.4 Nuclear magnetic resonance (NMR) spectroscopy

Nuclear magnetic resonance (NMR) is a physical phenomenon in which magnetic nuclei in a magnetic field absorb and re-emit electromagnetic radiation. This energy is at a specific resonance frequency which depends on the strength of the magnetic field and the magnetic properties of the isotope of the atoms; in practical applications, the frequency is similar to VHF and UHF television broadcasts (60-1000 MHz). NMR allows the observation of specific quantum mechanical magnetic properties of the atomic nucleus. All isotopes that contain an odd number of protons and/or of neutrons have an intrinsic magnetic moment and angular momentum, in other words a nonzero spin, while all nucleus with even numbers of both have a total spin of zero. The most commonly studied nucleus are ^{1}H and ^{13}C, although nuclei from isotopes of many other elements (e.g. ^{2}H, ^{6}Li, ^{10}B, ^{11}B, ^{14}N, ^{15}N, ^{17}O, ^{19}F, ^{23}Na, ^{29}Si, ^{31}P, ^{35}Cl, ^{113}Cd, ^{129}Xe, ^{195}Pt) have been studied by high-field NMR spectroscopy as well.

A key feature of NMR is that the resonance frequency of a particular substance is directly proportional to the strength of the applied magnetic field. It is this feature that is exploited in imaging techniques; if a sample is placed in a non-uniform magnetic field then the resonance

frequencies of the sample's nuclei depend on where in the field they are located. Since the resolution of the imaging technique depends on the magnitude of magnetic field gradient, many efforts are made to develop increased field strength, often using superconductors. The effectiveness of NMR can also be improved using hyperpolarization, and/or using two-dimensional, three-dimensional and higher-dimensional multi-frequency techniques. Over time with improved NMR technology, millions of NMR spectra are recorded, analysed and summarised. This is the most reliable technique used extensively to determine the structure of the organic molecule.

1.6.5 Electron microscopy

The electron microscope is a type of microscope that uses a beam of electrons to create an image of the specimen. It is capable of much higher magnifications and has a greater resolving power than a light microscope, allowing it to see much smaller objects in finer detail. Electron microscopes are built with electromagnetic lenses to control the path of electrons. The electron beam passes through the centre of such solenoids on its way down the column of the electron microscope towards the sample. Electrons are very sensitive to magnetic fields and can therefore be controlled by changing the current through the lenses. The resolving power of a microscope is directly related to the wavelength of the irradiation used to form an image. Reducing wavelength increases resolution. Therefore, the resolution of the microscope is increased if the accelerating voltage of the electron beam is increased. There are mainly two types of electron microscope, transmission electron microscopy and scanning electron microscopy.

1.6.5.1 Transmission electron microscopy (TEM)

The transmission electron microscope (TEM) operates on the same basic principles as the light microscope but uses electrons instead of light. In transmission electron microscopy, a high voltage beam of electrons is transmitted through an ultra thin sample specimen. An image is formed by the transmitted electrons, which interacted with the sample specimen while passing through. The image is magnified and focused onto an imaging device, such as a fluorescent screen, or to be detected by a sensor such as a charge-coupled device (CCD) camera. TEMs are capable of imaging at a significantly higher resolution (~1000 times) with finer details than light

microscopes, owing to the smaller wavelength of electrons. TEM forms a major analysis method in a range of scientific fields, in physical, material and biological sciences.

1.6.5.2 Scanning electron microscopy (SEM)

Unlike TEM, scanning electron microscope (SEM) is used for inspecting topographies of materials with a magnification range that encompasses that of optical microscopy and extends it to the nanoscale. SEM can scan the surface of a sample with a finely focused electron beam to produce an image from the beam-specimen interactions detected by a wide array of detectors. A variety of detectors are available, from secondary electron detectors to provide surface information, to backscattered detectors for compositional information in both high and low vacuum modes.

The scanning electron microscope has many advantages over traditional microscopes. The SEM has a large depth of field, which allows more of a specimen to be in focus at one time. The SEM also has much higher resolution, so closely spaced specimens can be magnified at much higher levels. Since the SEM uses electromagnets rather than lenses, has much more control in the degree of magnification. All of these advantages, as well as the actual strikingly clear images, make the scanning electron microscope one of the most useful instruments in research today to get the information about the topography (surface features of an object), morphology (shape and size of the particles making up the object) of various samples.

1.6.6 Dynamic Light Scattering (DLS)

Dynamic light scattering (DLS) is one of the most popular light scattering techniques to determine particle size down to 1 nm. Typical applications are emulsions, micelles, polymers, proteins, nanoparticles or colloids. The basic principle is simple: The sample is illuminated by a laser beam and the fluctuations of the scattered light are detected at a known scattering angle θ by a fast photon detector. Simple DLS instruments that measure at a fixed angle can determine the mean particle size in a limited size range. More elaborated multi-angle instruments can determine the full particle size distribution.

From a microscopic point of view the scattering light from the particles imprint information about their motion. Analysis of the fluctuation of the scattered light thus yields information about the particles. Experimentally one characterizes intensity fluctuations by

computing the intensity correlation function $g_2(t)$, whose analysis provides the diffusion coefficient of the particles (also known as diffusion constant).

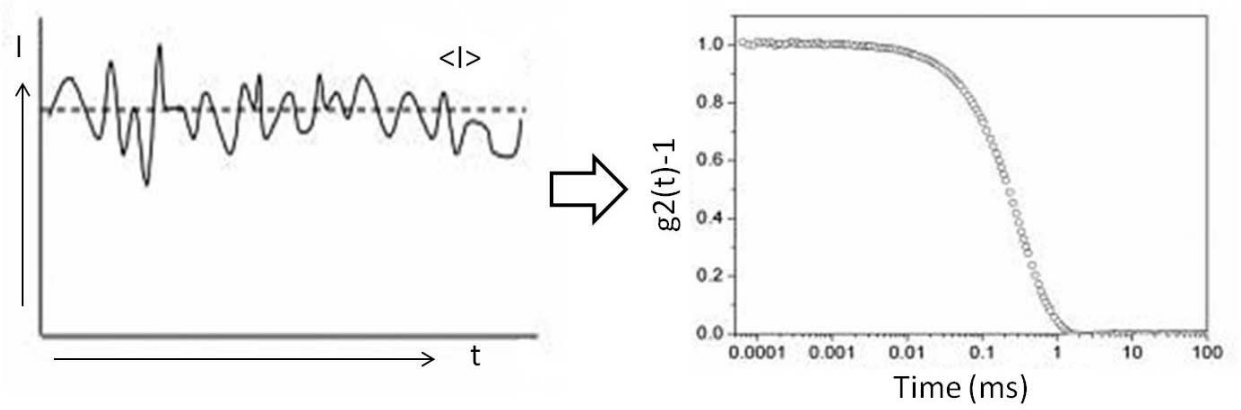

Figure 1.5: DLS analysis from the intensity fluctuations by computing the intensity correlation function $g_2(t)$

The diffusion coefficient *D* is then related to the radius *R* of the particles by means of the Stokes-

Einstein Equation: $D = kT/6\pi R\eta$

Where *k* is the Boltzmann constant, T the temperature and η the viscosity. The correlation of the intensity can be performed by electronic hardware or software analysis of the photon statistics.

To obtain the diffusion coefficient the intensity correlation function is analyzed by standard Cumulant method. By fitting a polynomial of third degree to the logarithm of the intensity correlation function, the decay rate $\boldsymbol{\Gamma}$ is obtained ($\boldsymbol{\Gamma} = q^2 D$), where decay rate is directly related to the diffusion coefficient *D* and *q* is the wave vector, which is dependent of the scattering angle. The Cumulant analysis can only determine the particle size distribution of a Gaussian distribution on mean particle size. For more a bi- or higher modal particle size distribution more complex analysis methods such as the Contin method are required.

The decay rate depends on the wave vector and thus the scattering angle. Different particles sizes scatter with different intensity in dependence of the scattering angle. Thus there is an optimum angle (90º) of detection for each particle size. A high quality analysis should always be performed at several scattering angles (multiangle DLS).

1.6.7 Zeta potential

Zeta potential is the charge that develops at the interface between a solid surface and its liquid medium. This potential, which is measured in MilliVolts (mV), may arise by any of several mechanisms. Among these are the dissociation of ionogenic groups in the particle surface and the differential adsorption of solution ions into the surface region. The net charge at the particle surface affects the ion distribution in the nearby region, increasing the concentration of counterions close to the surface. Thus, an electrical double layer is formed in the region of the particle-liquid interface.

This double layer (Figure 1.6) consists of two parts: an inner region that includes ions bound relatively tightly to the surface, and an outer region where a balance of electrostatic forces and random thermal motion determines the ion distribution. The potential in this region, therefore, decays with increasing distance from the surface until, at sufficient distance; it reaches the bulk solution value, conventionally taken to be zero. This decay is the indication is given that the zeta potential is the value at the surface of shear.

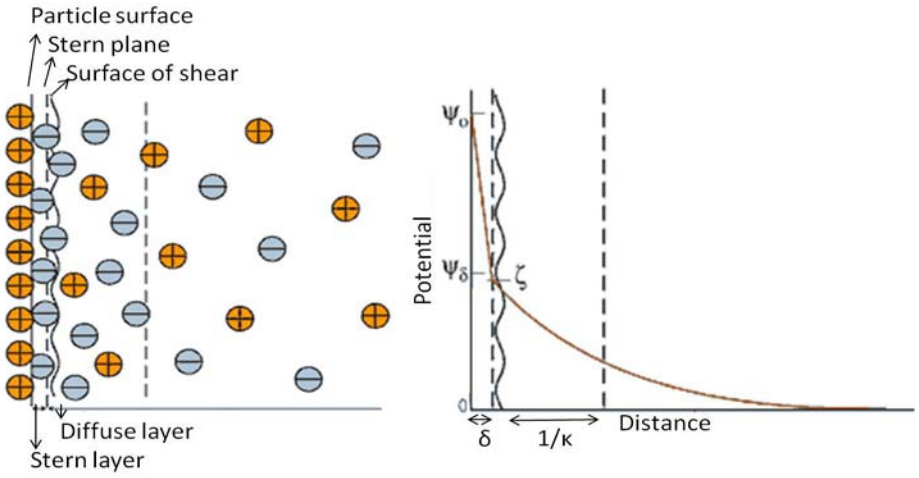

Figure 1.6: Schematic diagram of the surface ion double layer and zeta potential distribution

In an electric field, as in microelectrophoresis, each particle and its most closely associated ions move through the solution as a unit, and the potential at the surface of shear between this unit and the surrounding medium is known as the zeta potential. When a layer of macromolecules is adsorbed on the particle's surface, it shifts the shear plane further from the surface and alters the zeta potential.

Zeta potential is therefore a function of the surface charge of the particle, any adsorbed layer at the interface, and the nature and composition of the surrounding suspension medium. It can be experimentally determined and, because it reflects the effective charge on the particles and is therefore related to the electrostatic repulsion between them, the zeta potential has proven to be extremely relevant to the practical study and control of colloidal stability and flocculation processes.

The Smoluchowski's formula to determine Zeta Potential (ζ):

$$\zeta = \frac{4\pi\eta}{\varepsilon} \times U \times 300 \times 300 \times 1000$$

Where, η is viscosity of the solution, ε is the dielectric constant, U is the electrophoretic mobility ($= \frac{\nu}{V/L}$), ν is the speed of particle (cm/sec), V is the voltage(V) and L is the distance of electrode.

1.7 Motivation and Objectives of the present work

Organic inorganic nanocomposite materials combine the properties of a supportive inorganic core and surface grafted organic moiety to exhibit unique properties that make them very promising for a wide variety of practical application in industry and biomedical engineering.[123, 191] Typically, the inorganic core renders the structural properties of these nanomaterials while the organic surface gives the functionality. For example, ORMOSIL represents a very interesting class of organic-inorganic silica hybrid nanomaterial in which the organic component, typically a small organic molecule, is chemically bonded to the silica matrix. The chemical and mechanical properties of ORMOSIL can be modified by simple changing the nature and concentration of the inorganic core and organic component in the nanomaterial. For example, ORMOSIL that have organoamines attached to the surface of silica nanoparticles, have been very successfully used to deliver nucleic acids into cells. The amino groups on the surface renders positive charge onto the nanoparticle for binding the nucleic acids effectively while the silica nanoparticle makes this carrier enter effectively into cells. In another report, ORMOSIL that exhibits hardness that is about ten times that of the hardest organic polymer have been developed by addition of small amounts of polydimethylsiloxane (PDMS) into the silica precursor TEOS during its synthesis. In nano scale, small changes in concentrations of grafted organic groups in ORMOSIL have enormous effect on their properties since the local concentration of the organic groups in the nanoscale is very high. This enables synthesis of novel

organic-inorganic nanomaterials with tailored properties that can have both industrial and biomedical applications.

We therefore envisioned that synthesis of polypeptide grafted core-shell silica particles would lead to a very interesting class of nanomaterials as it would combine the biological property of polypeptides and the structural properties of silica nanoparticles.[192] In addition, the presence of a wide range of amino acid side chains in the polypeptides, such as, for example, amines, thiols and carboxylic acid, render the polymer-nanoparticle hybrids responsive to external stimuli such as pH, temperature, solvent and electrolytes, leads to wide range of potential and practical applications such as coatings, catalysis, gene delivery, among other things.[190] There have been recent reports in which polypeptides have been grafted to inorganic surfaces such as quartz planar surfaces,[193-197] colloidal silica particles,[198, 199] colloidal silica crystals[200] and ordered mesoporous materials.[201] In most of these reports, the polypeptide has been incorporated by surface initiated ring opening polymerization of the N-carboxyanhydrides of their corresponding amino acids onto an inorganic surface functionalized by a primary amine ('grafting from' methodology). In a recent approach, 'grafting to' methodology have been used to prepare organo soluble silica polypeptide conjugates using 'click chemistry' of alkyne terminated α-helical polypeptide onto azido-silica nanoparticles.[202] Although the synthesis, characterizations and studies related to physical properties of the silica-polypeptide conjugates have been reported, the potential and practical application of these hybrid nanocomposites are yet to be explored.

For us to explore possible applications for polypeptide-silica conjugate first requires development of a practical methodology which allows facile synthesis of polypeptide silica nanoconjugates in high yield. Since polypeptides contain several reactive functional groups like amines, thiols and carboxylic acid, a methodology that was very efficient and bio-orthogonal had to be envisaged. We therefore decided to use a combination of NCA polymerization of α-amino acids for the synthesis of polypeptides followed by attachment of these polypeptides by "click chemistry" to silica nanoparticles having organoazides on their surface.[59] The discovery of the Cu(I)-catalyzed 1,3-dipolar cycloaddition of organic azides to alkynes (CuAAC) has provided the most powerful "click chemistry" tool for conjugation between appropriately functionalized binding partners via an 1,2,3-triazole linkage.[165, 168] The present thesis describes the synthesis of

alkyne terminated various polypeptides with different molecular weight and their successful grafting onto various organoazide containing silica materials using CuAAC reaction. The application of these polypeptide silica hybrid nanomaterials for biomedical applications is also explored in this thesis. By keeping the above objectives in mind, the following specific work was selected for the present thesis:

1. Synthesis and characterization of various alkyne terminated polypeptides of various molecular weights by NCA polymerization.
2. Synthesis of silica-polypeptide nanoconjugates by using CuAAC reaction and study their properties and applications.
3. Synthesis of silica mesoporous-polypeptide conjugates by using CuAAC reaction and their applications as biomaterials.

1.8 Outline of the thesis

This dissertation includes synthesis of alkyne terminated homo-polypeptides, block co-polypeptides. Synthesized alkyne terminated polypeptides were grafted onto various silica substrates bearing azide functionality using CuAAC reaction. The physical properties of these various polypeptide silica nanoconjugates were studied in detail and the application of these hybrid nanomaterials towards various biomedical applications were explored. The thesis is divided into five chapters with proper references at the end of each chapter. A very brief outline of all five chapters is given bellow.

Chapter 1: A comprehensive review of literature on NCA ring opening polymerization: method of synthesis, purification and characterization. This chapter also discusses the importance of the surface modification of various conventional materials in biological context as well as the synthesis, surface modification and application of organic-inorganic hybrid nanomaterials. A brief introduction to Cu(I) catalyzed azide-alkyne click chemistry (CuAAC) is discussed.

Chapter 2: This chapter discusses synthesis and characterization of alkyne terminated various co- and block co- polypeptides, such as poly-L-lysine, poly-L-lysine-block-poly-L-leucine, poly-L-benzyl glutamate, poly-L-glutamic acid and poly-L-arginine with various molecular weights.

Chapter 3: This chapter discusses the synthesis of poly-L-lysine, poly-L-lysine-block-poly-L-leucine, poly-L-benzyl glutamate, poly-L-glutamic acid and poly-L-arginine grafted silica nanoparticle based hybrid materials using CuAAC reactions. These hybrid nanomaterials were characterized by several physical techniques including s FT-IR, ^{13}C and ^{29}Si solid state NMR spectroscopy, TGA, TEM, DLS and zeta potential. This chapter also discusses interesting reversible and irreversible aggregation properties of these silica-polypeptides nanoconjugates. Finally, the application of these hybrid nanomaterials as antimicrobial agents, as gene delivery agents and as building blocks for the synthesis of three dimensional macroporous structures is discussed.

Chapter 4: This chapter describes the synthesis of poly-L-lysine and poly-L-arginine grafted mesoporous silica hybrid material (SBA-15 and MSN) by using CuAAC reaction. These materials were fully characterized using several physical methods like ^{13}C and ^{29}Si CP MAS NMR, XRD, FT-IR, N_2 adsorption desorption and thermogravimetry. Poly-L-arginine, known to facilitate cellular uptake, was attached to selectively to the outer surface of mesoporous silica nanoparticles (MSN) having diameter 70 to 100 nm, by using click chemistry. The cytotoxicity of these poly-L-arginine grafted mesoporous silica nanoparticles and their enhanced cellular uptake is also discussed in this chapter.

Chapter 5: This chapter presents an overall summary of the work done and describes major findings of the studies. Future directions based on the work reported in the thesis are also discussed.

1.8 References

1. Fischer, E.; Fourneau, E., Ueber einige Derivate des Glykocolls. *Berichte der deutschen chemischen Gesellschaft* **1901,** 34, (2), 2868-2877.
2. Fischer, E., Synthese von Polypeptiden. XVII. *Berichte der deutschen chemischen Gesellschaft* **1907,** 40, (2), 1754-1767.
3. Branden, C.; Tooze, J., Introduction to Protein Structure. *Garland, New York* **1991**.
4. Hokfelt, T.; Broberger, C.; Xu, Z.-Q. D.; Sergeyev, V.; Ubink, R.; Diez, M., Neuropeptides - an overview. *Neuropharmacology* **2000,** 39, (8), 1337-1356.
5. Besser, G. M.; Mortimer, C. H., Hypothalamic regulatory hormones: a review. *Journal of Clinical Pathology* **1974,** 27, (3), 173-184.
6. Kelley, K. W.; Weigent, D. A.; Kooijman, R., Protein hormones and immunity. *Brain, Behavior, and Immunity* **2007,** 21, (4), 384-392.
7. Lopez, D. A., Enzymes: the fountain of life. *Neville Press* **1994**.
8. Cheng, S.-Y.; Leonard, J. L.; Davis, P. J., Molecular Aspects of Thyroid Hormone Actions. *Endocrine Reviews* **2010,** 31, (2), 139-170.
9. Wisser, A.-S.; Habbel, P.; Wiedenmann, B.; Klapp, B. F.; nnikes, H.; Kobelt, P., Interactions of Gastrointestinal Peptides: Ghrelin and Its Anorexigenic Antagonists. *International Journal of Peptides* **2010,** 2010.
10. Krueger, J. M.; Pappenheimer, J. R.; Karnovsky, M. L., Sleep-promoting effects of muramyl peptides. *Proceedings of the National Academy of Sciences* **1982,** 79, (19), 6102-6106.
11. Moisa, A.; Kolesanova, E., Synthetic peptide vaccines. *Biochemistry (Moscow) Supplemental Series B: Biomedical Chemistry* **2010,** 4, (4), 321-332.
12. Baxter, J. D.; Lewicki, J. A.; Gardner, D. G., Atrial Natriuretic Peptide. *Nat Biotech* **1988,** 6, (5), 529-546.
13. Odell, E. W., Peptide Antibiotics. Discovery, Modes of Action and Applications. *Journal of Antimicrobial Chemotherapy* **2002,** 50, (1), 149.
14. Jenssen, H. v.; Hamill, P.; Hancock, R. E. W., Peptide Antimicrobial Agents. *Clinical Microbiology Reviews* **2006,** 19, (3), 491-511.
15. Higashijima, T.; Uzu, S.; Nakajima, T.; Ross, E. M., Mastoparan, a peptide toxin from wasp venom, mimics receptors by activating GTP-binding regulatory proteins (G proteins). *Journal of Biological Chemistry* **1988,** 263, (14), 6491-6494.
16. Berry, J.; Gantar, M.; Perez, M.; Berry, G.; Noriega, F., Cyanobacterial Toxins as Allelochemicals with Potential Applications as Algaecides, Herbicides and Insecticides. *Marine Drugs* **2008,** 6, (2), 117-146.
17. Temussi, P. A., The good taste of peptides. *Journal of Peptide Science* **2012,** 18, (2), 73-82.
18. Goldstein, G.; Scheid, M.; Hammerling, U.; Schlesinger, D. H.; Niall, H. D.; Boyse, E. A., Isolation of a polypeptide that has lymphocyte-differentiating properties and is probably

represented universally in living cells. *Proceedings of the National Academy of Sciences* **1975,** 72, (1), 11-15.

19. Zhang, W.; Laursen, R. A., Structure-Function Relationships in a Type I Antifreeze Polypeptide. *Journal of Biological Chemistry* **1998,** 273, (52), 34806-34812.

20. Norton, R. S., Structure and structure-function relationships of sea anemone proteins that interact with the sodium channel. *Toxicon* **1991,** 29, (9), 1051-1084.

21. Cha, J. N.; Stucky, G. D.; Morse, D. E.; Deming, T. J., Biomimetic synthesis of ordered silica structures mediated by block copolypeptides. *Nature* **2000,** 403, (6767), 289-292.

22. van Hest, J. C. M.; Tirrell, D. A., Protein-based materials, toward a new level of structural control. *Chemical Communications* **2001**, (19), 1897-1904.

23. Merrifield, R. B., Solid Phase Peptide Synthesis. I. The Synthesis of a Tetrapeptide. *Journal of the American Chemical Society* **1963,** 85, (14), 2149-2154.

24. Merrifield, R. B., Solid Phase Peptide Synthesis. II. The Synthesis of Bradykinin. *Journal of the American Chemical Society* **1964,** 86, (2), 304-305.

25. Merrifield, R. B., Solid-Phase Peptide Synthesis. III. An Improved Synthesis of Bradykinin. *Biochemistry* **1964,** 3, (9), 1385-1390.

26. Fasman, G. D., *Proteins . 3rd Edition*. Crc Press: 1976.

27. Penczek, S., *Models of Biopolymers By Ring-Opening Poylmerization*. Taylor & Francis: 1989.

28. Kricheldorf, H. R., *a-aminoacid-N-carboxy-anhydrides and related heterocycles: syntheses, properties, peptide synthesis, polymerization*. Springer-Verlag: 1987.

29. Leuchs, H.; Geiger, W., Über die Anhydride von α-Amino-N-carbonsäuren und die von α-Aminosäuren. *Berichte der deutschen chemischen Gesellschaft* **1908,** 41, (2), 1721-1726.

30. Leuchs, H.; Manasse, W., Über die Isomerie der Carbäthoxyl-glycyl glycinester. *Berichte der deutschen chemischen Gesellschaft* **1907,** 40, (3), 3235-3249.

31. Leuchs, H., Ueber die Glycin-carbonsäure. *Berichte der deutschen chemischen Gesellschaft* **1906,** 39, (1), 857-861.

32. Pascal, R.; Boiteau, L.; Commeyras, A.; Walde, P., From the Prebiotic Synthesis of α-Amino Acids Towards a Primitive Translation Apparatus for the Synthesis of Peptides
Prebiotic Chemistry. In Springer Berlin / Heidelberg: 2005; Vol. 259, pp 84-84.

33. Leman, L.; Orgel, L.; Ghadiri, M. R., Carbonyl Sulfide-Mediated Prebiotic Formation of Peptides. *Science* **2004,** 306, (5694), 283-286.

34. Bergmann, M.; Zervas, L.; Ross, W. F., On proteolytic enzymes. *Journal of Biological Chemistry* **1935,** 111, (1), 245-260.

35. Poduska, K.; Gross, H., Über α-Halogenäther, VII: Reaktionen von Dichlormethyl-alkyl-äthern mit Aminosäurederivaten. *Chemische Berichte* **1961,** 94, (2), 527-537.

36. Miyoshi, M., Peptide Synthesis N-Acylated Aziridinone. II. The Reaction of N-Acylated Aziridinone and Its Use in Peptide Synthesis. *Bulletin of the Chemical Society of Japan* **1973,** 46, (5), 1489-1496.

37. Green, M.; Stahmann, M. A., Synthesis and enzymatic hydrolysis of glutamic acid polypeptides. *Journal of Biological Chemistry* **1952,** 197, (2), 771-782.
38. Ben-Ishai, D.; Katchalski, E., Synthesis of N-Carboxy-a-amino Acid Anhydrides from N-Carbalkoxy-a-amino Acids by the Use of Phosphorus Tribromide. *Journal of the American Chemical Society* **1952,** 74, (14), 3688-3689.
39. Katchalski, E.; Grossfeld, I.; Frankel, M., Poly-condensation of a-Amino Acid Derivatives. III. Poly-lysine. *Journal of the American Chemical Society* **1948,** 70, (6), 2094-2101.
40. Katchalski, E.; Spitnik, P., Ornithine Anhydride. *Journal of the American Chemical Society* **1951,** 73, (6), 2946-2947.
41. Hayakawa, T.; Kondo, Y.; Yamamoto, H.; Murakami, Y., The Synthesis of Poly-L-arginine Hydrobromide and Copolymers of L-Arginine and Other Amino Acids. *Bulletin of the Chemical Society of Japan* **1969,** 42, (2), 479-482.
42. Hirschmann, R.; Schwam, H.; Strachan, R. G.; Schoenewaldt, E. F.; Barkemeyer, H.; Miller, S. M.; Conn, J. B.; Garsky, V.; Veber, D. F.; Denkewalter, R. G., Controlled synthesis of peptides in aqueous medium. VIII. Preparation and use of novel .alpha.-amino acid N-carboxyanhydrides. *Journal of the American Chemical Society* **1971,** 93, (11), 2746-2754.
43. Ariely, S.; Fridkin, M.; Patchornik, A., Synthesis of poly-L-asparagine and poly-L-glutamine. *Biopolymers* **1969,** 7, (3), 417-422.
44. Kricheldorf, H. R.; Fehrle, M., New polymer syntheses. IV. Polypeptides of lysine and ornithine with pending pyrimidine bases. *Biopolymers* **1982,** 21, (11), 2097-2122.
45. Ishikawa, T.; Inaki, Y.; Takemoto, K., Synthesis of nucleic acid base substituted poly-L-lysine. *Polymer Bulletin* **1978,** 1, (2), 85-89.
46. Fuchs, F., Über N-Carbonsäure-anhydride. *Berichte der deutschen chemischen Gesellschaft (A and B Series)* **1922,** 55, (9), 2943-2943.
47. Brown, C. J.; Coleman, D.; Farthing, A. C., Further Studies in Synthetic Polypeptides. *Nature* **1949,** 163, 834-835.
48. Farthing, A. C.; Reynolds, R. J. W., Anhydro-N-Carboxy-DL-b-Phenylalanine. *Nature* **1950,** 165, (4199), 647-647.
49. Farthing, A. C., Synthetic polypeptides. Part I. Synthesis of oxazolid-2 : 5-diones and a new reaction of glycine. *Journal of the Chemical Society (Resumed)* **1950**, 3213-3217.
50. Levy, A. L., Anhydro-N-Carboxy-DL-b-Phenylalanine. *Nature* **1950,** 165, (4187), 152-152.
51. Iwakura, Y.; Uno, K.; Kang, S., The Synthesis and Reactions of 2-Isocyanatoacyl Chlorides. *The Journal of Organic Chemistry* **1965,** 30, (4), 1158-1161.
52. Fuller, W. D.; Verlander, M. S.; Goodman, M., A procedure for the facile syntheis of amino-acid N-carboxyanhydrides. *Biopolymers* **1976,** 15, (9), 1869-1871.
53. Oya, M.; Katakai, R.; Nakai, H.; Iwakura, Y., A novel synthesis of N-carboxy-a-amino acid anhydride. *Chemistry Letters* **1973,** 2, (11), 1143-1144.

54. Katakai, R.; Iizuka, Y., An improved rapid method for the synthesis of N-carboxy .alpha.-amino acid anhydrides using trichloromethyl chloroformate. *The Journal of Organic Chemistry* **1985,** 50, (5), 715-716.
55. Daly, W. H.; Poche, D., The preparation of N-carboxyanhydrides of a-amino acids using bis(trichloromethyl)carbonate. *Tetrahedron Letters* **1988,** 29, (46), 5859-5862.
56. Smeets, N. M. B.; van der Weide, P. L. J.; Meuldijk, J.; Vekemans, J. A. J. M.; Hulshof, L. A., A Scalable Synthesis of l-Leucine-N-carboxyanhydride. *Organic Process Research & Development* **2005,** 9, (6), 757-763.
57. Koga, K.; Sudo, A.; Nishida, H.; Endo, T., Convenient and useful synthesis of N-carboxyanhydride monomers through selective cyclization of urethane derivatives of α-amino acids. *Journal of Polymer Science Part A: Polymer Chemistry* **2009,** 47, (15), 3839-3844.
58. Lagrille, O.; Danger, G.; Boiteau, L.; Rossi, J.-C.; Taillades, J., Process improvement in amino acid N-carboxyanhydride synthesis by N-carbamoyl amino acid nitrosation. *Amino Acids* **2009,** 36, (2), 341-347.
59. Hadjichristidis, N.; Iatrou, H.; Pitsikalis, M.; Sakellariou, G., Synthesis of Well-Defined Polypeptide-Based Materials via the Ring-Opening Polymerization of a-Amino Acid N-Carboxyanhydrides. *Chemical Reviews* **2009,** 109, (11), 5528-5578.
60. Noguchi, J.; Tokura, S.; Nishi, N., Poly-α-amino acid fibres. *Die Angewandte Makromolekulare Chemie* **1972,** 22, (1), 107-131.
61. Waley, S. G.; Watson, J., The Kinetics of the Polymerization of Sarcosine Carbonic Anhydride. *Proceedings of the Royal Society of London. Series A. Mathematical and Physical Sciences* **1949,** 199, (1059), 499-517.
62. Ballard, D. G. H.; Bamford, C. H., Studies in Polymerization. VII. The Polymerization of N-carboxy-a-amino Acid Anhydrides. *Proceedings of the Royal Society of London. Series A. Mathematical and Physical Sciences* **1954,** 223, (1155), 495-520.
63. Dorman, L. C.; Shiang, W. R.; Meyers, P. A., Purification of γ-Benzyl and g-Methyl L-Glutamate N-Carboxyanhydrides by Rephosgenation. *Synthetic Communications* **1992,** 22, (22), 3257-3262.
64. Poche, D. S.; Moore, M. J.; Bowles, J. L., An Unconventional Method for Purifying the N-carboxyanhydride Derivatives of γ-alkyl-L-glutamates. *Synthetic Communications* **1999,** 29, (5), 843-854.
65. Kramer, J. R.; Deming, T. J., General Method for Purification of a-Amino acid-N-carboxyanhydrides Using Flash Chromatography. *Biomacromolecules* **2010,** 11, (12), 3668-3672.
66. Sekiguchi, H.; Froyerd□, G., Anionic polymerization mechanism of n-carboxy-α-amino acid anhydrides. *Journal of Polymer Science: Polymer Symposia* **1975,** 52, (1), 157-171.
67. Bellamy, L. J., *The infrared spectra of complex molecules: advances in infrared group frequencies. vol. two*. Chapman and Hall: 1980.
68. Breitmaier, E.; Voelter, W., *13C NMR spectroscopy: methods and applications*. Verlag Chemie: 1974.

69. Veber, D. F.; Pfister, K.; Hirschmann, R., Synthesis of a-Methyl-DL-glutathione. *Journal of Medicinal Chemistry* **1967,** 10, (5), 968-969.
70. Kricheldorf, H. R., Polypeptides and 100 Years of Chemistry of α-Amino Acid N-Carboxyanhydrides. *Angewandte Chemie International Edition* **2006,** 45, (35), 5752-5784.
71. Frankel, M.; Katchalski, E., Derivatives of N-Carboxy-a-amino Acid Esters. *Journal of the American Chemical Society* **1943,** 65, (9), 1670-1674.
72. Peggion, E.; Terbojevich, M.; Cosani, A.; Colombini, C., Mechanism of N-Carboxyanhydride (NCA) Polymerization in Dioxane. Initiation by Carbon-14-Labeled Amines1. *Journal of the American Chemical Society* **1966,** 88, (15), 3630-3632.
73. Goodman, M.; Hutchison, J., The Mechanisms of Polymerization of N-Unsubstituted N-Carboxyanhydrides1. *Journal of the American Chemical Society* **1966,** 88, (15), 3627-3630.
74. Cosani, A.; D'Este, G.; Peggion, E.; Scoefone, E., Solvent effects in N-carboxyanhydride (NCA) polymerization initiated by strong base type initiators. *Biopolymers* **1966,** 4, (5), 595-599.
75. Imanishi, Y.; Aoyama, A.; Hashimoto, Y.; Higashimura, T., Polymerization of N-carboxyanhydrides of various α-amino acids using secondary amines as initiator. *Biopolymers* **1977,** 16, (1), 187-197.
76. Bamford, C. H.; Block, H., The initiation step in the polymerization of N-carboxy-α-amino-acid anhydrides. Part II. Effects related to the structure of amine initiators. *Journal of the Chemical Society (Resumed)* **1961**, 4992-4995.
77. Thunig, D.; Semen, J.; Elias, H.-G., Carbon dioxide influence on NCA polymerizations. *Die Makromolekulare Chemie* **1977,** 178, (2), 603-607.
78. Ballard, D. G. H.; Bamford, C. H.; Weymouth, F. J., Studies in Polymerization. VIII. Reactions of N-Carboxy-α-Amino Acid Anhydrides Initiated by Metal Cations. *Proceedings of the Royal Society of London. Series A. Mathematical and Physical Sciences* **1955,** 227, (1169), 155-183.
79. Ballard, D. G. H.; Bamford, C. H., The polymerization of γ-benzyl-L-glutamate N-carboxy anhydride. *Journal of the American Chemical Society* **1957,** 79, (9), 2336-2338.
80. Bartlett, P. D.; Dittmer, D. C., A Kinetic Study of the Leuchs Anhydrides in Aqueous Solution. II. *Journal of the American Chemical Society* **1957,** 79, (9), 2159-2160.
81. Wessely, F.; Sigmund, F., Untersuchungen über α-Amino-N-Caxbonsäureanhydride. III. In *Hoppe-Seyler´s Zeitschrift für Physiologische Chemie*, 1926; Vol. 159, p 102.
82. Rinaudo, M.; Domard, A., Kinetics of γ-benzyl-L-glutamate NCAs polymerizations and molecular-weight distributions on corresponding polymers. *Biopolymers* **1976,** 15, (11), 2185-2199.
83. Ballard, D. G. H.; Bamford, C. H., 77. Reactions of N-carboxy-α-amino-acid anhydrides catalysed by tertiary bases. *Journal of the Chemical Society (Resumed)* **1956**, 381-387.
84. Bamford, C. H.; Block, H., The initiation step in the polymerization of N-carboxy-α-amino-acid anhydrides. Part I. Catalysis by tertiary bases. *Journal of the Chemical Society (Resumed)* **1961**, 4989-4991.

85. Szwarc, M., Thermodynamics of polymerization with special emphasis on living polymers. In Springer Berlin / Heidelberg: 1967; Vol. 4, pp 457-495.
86. Bamford, C. H.; Block, H.; Pugh, A. C. P., The polymerization of 3-substituted oxazolidine-2,5-diones. *Journal of the Chemical Society (Resumed)* **1961**, 2057-2063.
87. Peggion, E.; Cosani, A.; Mattucci, A. M.; Scoffone, E., Polymerization of γ-ethyl-L-glutamate-N-carboxyanhydride initiated by di-n-butyl and di-isopropyl amine. *Biopolymers* **1964,** 2, (1), 69-78.
88. Vayaboury, W.; Giani, O.; Cottet, H.; Deratani, A.; Schué, F., Living Polymerization of α-Amino Acid N-Carboxyanhydrides (NCA) upon Decreasing the Reaction Temperature. *Macromolecular Rapid Communications* **2004,** 25, (13), 1221-1224.
89. Habraken, G. J. M.; Peeters, M.; Dietz, C. H. J. T.; Koning, C. E.; Heise, A., How controlled and versatile is N-carboxy anhydride (NCA) polymerization at 0^{o}C? Effect of temperature on homo-, block- and graft (co)polymerization. *Polymer Chemistry* **2010,** 1, (4), 514-524.
90. Deming, T. J., Facile synthesis of block copolypeptides of defined architecture. *Nature* **1997,** 390, (6658), 386-389.
91. Deming, T. J.; Curtin, S. A., Chain Initiation Efficiency in Cobalt- and Nickel-Mediated Polypeptide Synthesis. *Journal of the American Chemical Society* **2000,** 122, (24), 5710-5717.
92. Deming, T. J., Cobalt and Iron Initiators for the Controlled Polymerization of α-Amino Acid-N-Carboxyanhydrides. *Macromolecules* **1999,** 32, (13), 4500-4502.
93. Deming, T. J., Amino Acid Derived Nickelacycles: Intermediates in Nickel-Mediated Polypeptide Synthesis. *Journal of the American Chemical Society* **1998,** 120, (17), 4240-4241.
94. Lu, H.; Cheng, J., Hexamethyldisilazane-Mediated Controlled Polymerization of α-Amino Acid N-Carboxyanhydrides. *Journal of the American Chemical Society* **2007,** 129, (46), 14114-14115.
95. Webster, O. W.; Hertler, W. R.; Sogah, D. Y.; Farnham, W. B.; RajanBabu, T. V., Group-transfer polymerization. 1. A new concept for addition polymerization with organosilicon initiators. *Journal of the American Chemical Society* **1983,** 105, (17), 5706-5708.
96. Webster, O., Group Transfer Polymerization: A Critical Review of Its Mechanism and Comparison with Other Methods for Controlled Polymerization of Acrylic Monomers
New Synthetic Methods. In Springer Berlin / Heidelberg: 2004; Vol. 167, pp 257-266.
97. Cheng, J.; Deming, T., Synthesis of Polypeptides by Ring-Opening Polymerization of α-Amino Acid N-Carboxyanhydrides
Peptide-Based Materials. In Springer Berlin / Heidelberg: 2011; Vol. 310, pp 1-26.
98. Lu, H.; Wang, J.; Lin, Y.; Cheng, J., One-Pot Synthesis of Brush-Like Polymers via Integrated Ring-Opening Metathesis Polymerization and Polymerization of Amino Acid N-Carboxyanhydrides. *Journal of the American Chemical Society* **2009,** 131, (38), 13582-13583.
99. Dimitrov, I.; Schlaad, H., Synthesis of nearly monodisperse polystyrene-polypeptide block copolymers via polymerisation of N-carboxyanhydrides. *Chemical Communications* **2003**, (23), 2944-2945.

100. Deming, T. J., Synthetic polypeptides for biomedical applications. *Progress in Polymer Science* **2007,** 32, (89), 858-875.
101. Mart, R. J.; Osborne, R. D.; Stevens, M. M.; Ulijn, R. V., Peptide-based stimuli-responsive biomaterials. *Soft Matter* **2006,** 2, (10), 822-835.
102. Ryser, H. J. P.; Hancock, R., Histones and Basic Polyamino Acids Stimulate the Uptake of Albumin by Tumor Cells in Culture. *Science* **1965,** 150, (3695), 501-503.
103. Snyder, E.; Dowdy, S., Cell Penetrating Peptides in Drug Delivery. *Pharmaceutical Research* **2004,** 21, (3), 389-393.
104. De Smedt, S. C.; Demeester, J.; Hennink, W. E., Cationic Polymer Based Gene Delivery Systems. *Pharmaceutical Research* **2000,** 17, (2), 113-126.
105. Pack, D. W.; Hoffman, A. S.; Pun, S.; Stayton, P. S., Design and development of polymers for gene delivery. *Nat Rev Drug Discov* **2005,** 4, (7), 581-593.
106. Osada, K.; Kataoka, K.; Klok, H.-A.; Schlaad, H., Drug and Gene Delivery Based on Supramolecular Assembly of PEG-Polypeptide Hybrid Block Copolymers
Peptide Hybrid Polymers. In Springer Berlin / Heidelberg: 2006; Vol. 202, pp 113-153.
107. Torchilin, V. P., Cell penetrating peptide-modified pharmaceutical nanocarriers for intracellular drug and gene delivery. *Peptide Science* **2008,** 90, (5), 604-610.
108. Mahato, R. I., Non-Viral Peptide-Based Approaches to Gene Delivery. *Journal of Drug Targeting* **1999,** 7, (4), 249-268.
109. Ogris, M.; Wagner, E., Targeting tumors with non-viral gene delivery systems. *Drug Discovery Today* **2002,** 7, (8), 479-485.
110. Lindsay, M. A., Peptide-mediated cell delivery: application in protein target validation. *Current Opinion in Pharmacology* **2002,** 2, (5), 587-594.
111. Fischer, P. M.; Krausz, E.; Lane, D. P., Cellular Delivery of Impermeable Effector Molecules in the Form of Conjugates with Peptides Capable of Mediating Membrane Translocation. *Bioconjugate Chemistry* **2001,** 12, (6), 825-841.
112. Pratesi, G.; Savi, G.; Pezzoni, G.; Bellini, O.; Penco, S.; Tinelli, S.; Zunino, F., Poly-L-aspartic acid as a carrier for doxorubicin: A comparative in vivo study of free and polymer-bound drug. *Br J Cancer* **1985,** 52, (6), 841-848.
113. Eddington, D. T.; Beebe, D. J., Flow control with hydrogels. *Advanced Drug Delivery Reviews* **2004,** 56, (2), 199-210.
114. Hoffman, A. S., Hydrogels for biomedical applications. *Advanced Drug Delivery Reviews* **2002,** 54, (1), 3-12.
115. Lutolf, M. P.; Hubbell, J. A., Synthetic biomaterials as instructive extracellular microenvironments for morphogenesis in tissue engineering. *Nat Biotech* **2005,** 23, (1), 47-55.
116. Lee, K. Y.; Mooney, D. J., Hydrogels for Tissue Engineering. *Chemical Reviews* **2001,** 101, (7), 1869-1880.
117. Yan, C.; Pochan, D. J., Rheological properties of peptide-based hydrogels for biomedical and other applications. *Chemical Society Reviews* **2010,** 39, (9), 3528-3540.

118. Ikada, Y., Surface modification of polymers for medical applications. *Biomaterials* **1994,** 15, (10), 725-736.
119. Vladkova, T. G., Surface Engineered Polymeric Biomaterials with Improved Biocontact Properties. *International Journal of Polymer Science* **2010,** 2010.
120. Zou, H.; Wu, S.; Shen, J., Polymer/Silica Nanocomposites: Preparation, Characterization, Properties, and Applications. *Chemical Reviews* **2008,** 108, (9), 3893-3957.
121. Schaefer, D. W.; Justice, R. S., How Nano Are Nanocomposites? *Macromolecules* **2007,** 40, (24), 8501-8517.
122. Krishnamoorti, R.; Vaia, R. A., Polymer nanocomposites. *Journal of Polymer Science Part B: Polymer Physics* **2007,** 45, (24), 3252-3256.
123. Balazs, A. C.; Emrick, T.; Russell, T. P., Nanoparticle Polymer Composites: Where Two Small Worlds Meet. *Science* **2006,** 314, (5802), 1107-1110.
124. Heaney, P. J.; Prewitt, C. T.; Gibbs, G. V.; Mineralogical Society of, A., *Silica: Physical Behavior, Geochemistry and Materials Applications*. Mineralogical Society of America: 1994.
125. Stober, W.; Fink, A.; Bohn, E., Controlled growth of monodisperse silica spheres in the micron size range. *Journal of Colloid and Interface Science* **1968,** 26, (1), 62-69.
126. Kresge, C. T.; Leonowicz, M. E.; Roth, W. J.; Vartuli, J. C.; Beck, J. S., Ordered mesoporous molecular sieves synthesized by a liquid-crystal template mechanism. *Nature* **1992,** 359, (6397), 710-712.
127. Hommel, H.; Touhami, A.; Legrand, A. P.; Balard, H.; Papirer, E., Segmental mobility of model compounds for rubber reinforcement. *Die Makromolekulare Chemie* **1993,** 194, (3), 879-889.
128. Wei, Y.; Fan, L.; Chen, L., Effect of different pore diameter silica based polymer-bonded phases and mobile phase on separation of proteins. *Chromatographia* **1997,** 46, (11), 637-640.
129. Mathew, J. P.; Srinivasan, M., Silica-supported polymer-palladium complexes as catalysts for the reduction of nitro and azo groups. *Polymer International* **1992,** 29, (3), 179-184.
130. Mizutani, Y.; Nagō, S., Microporous polypropylene films containing ultrafine silica particles. *Journal of Applied Polymer Science* **1999,** 72, (11), 1489-1494.
131. Mittal, K. L., *Adhesion aspects of polymeric coatings*. VSP: 2003.
132. Prasad, P. N., *Nanophotonics*. John Wiley & Sons: 2004.
133. Whitesides, G. M., The 'right' size in nanobiotechnology. *Nat Biotech* **2003,** 21, (10), 1161-1165.
134. Jain, T. K.; Roy, I.; De, T. K.; Maitra, A., Nanometer Silica Particles Encapsulating Active Compounds: A Novel Ceramic Drug Carrier. *Journal of the American Chemical Society* **1998,** 120, (43), 11092-11095.
135. Alexis, F.; Pridgen, E. M.; Langer, R.; Farokhzad, O. C.; Schäfer-Korting, M., Nanoparticle Technologies for Cancer Therapy Drug Delivery. In Springer Berlin Heidelberg: 2010; Vol. 197, pp 55-86.

136. Yong, K.-T.; Roy, I.; Swihart, M. T.; Prasad, P. N., Multifunctional nanoparticles as biocompatible targeted probes for human cancer diagnosis and therapy. *Journal of Materials Chemistry* **2009,** 19, (27), 4655-4672.
137. Liu, Y.; Lou, C.; Yang, H.; Shi, M.; Miyoshi, H., Silica Nanoparticles as Promising Drug/Gene Delivery Carriers and Fluorescent Nano-Probes: Recent Advances. *Current Cancer Drug Targets* **2011,** 11, (2), 156-163.
138. Rosenholm, J. M.; Sahlgren, C.; Linden, M., Towards multifunctional, targeted drug delivery systems using mesoporous silica nanoparticles - opportunities & challenges. *Nanoscale* **2010,** 2, (10), 1870-1883.
139. Roy, I.; Ohulchanskyy, T. Y.; Pudavar, H. E.; Bergey, E. J.; Oseroff, A. R.; Morgan, J.; Dougherty, T. J.; Prasad, P. N., Ceramic-Based Nanoparticles Entrapping Water-Insoluble Photosensitizing Anticancer Drugs: A Novel Drug Carrier System for Photodynamic Therapy. *Journal of the American Chemical Society* **2003,** 125, (26), 7860-7865.
140. Roy, I.; Ohulchanskyy, T. Y.; Bharali, D. J.; Pudavar, H. E.; Mistretta, R. A.; Kaur, N.; Prasad, P. N., Optical tracking of organically modified silica nanoparticles as DNA carriers: A nonviral, nanomedicine approach for gene delivery. *Proceedings of the National Academy of Sciences of the United States of America* **2005,** 102, (2), 279-284.
141. He, W.-T.; Xue, Y.-N.; Peng, N.; Liu, W.-M.; Zhuo, R.-X.; Huang, S.-W., One-pot preparation of polyethylenimine-silica nanoparticles as serum-resistant gene delivery vectors: Intracellular trafficking and transfection. *Journal of Materials Chemistry* **2011,** 21, (28), 10496-10503.
142. Kneuer, C.; Sameti, M.; Bakowsky, U.; Schiestel, T.; Schirra, H.; Schmidt, H.; Lehr, C.-M., A Nonviral DNA Delivery System Based on Surface Modified Silica-Nanoparticles Can Efficiently Transfect Cells in Vitro. *Bioconjugate Chemistry* **2000,** 11, (6), 926-932.
143. Roy, I.; Stachowiak, M. K.; Bergey, E. J., Nonviral gene transfection nanoparticles: function and applications in the brain. *Nanomedicine: Nanotechnology, Biology and Medicine* **2008,** 4, (2), 89-97.
144. Kumar, R.; Roy, I.; Ohulchanskky, T. Y.; Vathy, L. A.; Bergey, E. J.; Sajjad, M.; Prasad, P. N., In Vivo Biodistribution and Clearance Studies Using Multimodal Organically Modified Silica Nanoparticles. *ACS Nano* **2010,** 4, (2), 699-708.
145. Vivero-Escoto, J. L.; Slowing, I. I.; Trewyn, B. G.; Lin, V. S. Y., Mesoporous Silica Nanoparticles for Intracellular Controlled Drug Delivery. *Small* **2010,** 6, (18), 1952-1967.
146. Savin, D. A.; Pyun, J.; Patterson, G. D.; Kowalewski, T.; Matyjaszewski, K., Synthesis and characterization of silica-graft-polystyrene hybrid nanoparticles: Effect of constraint on the glass-transition temperature of spherical polymer brushes. *Journal of Polymer Science Part B: Polymer Physics* **2002,** 40, (23), 2667-2676.
147. Radhakrishnan, B.; Ranjan, R.; Brittain, W. J., Surface initiated polymerizations from silica nanoparticles. *Soft Matter* **2006,** 2, (5), 386-396.
148. Garcia, M.; van Zyl, W. E.; ten Cate, M. G. J.; Stouwdam, J. W.; Verweij, H.; Pimplapure, M. S.; Weickert, G., Novel Preparation of Hybrid Polypropylene/Silica

Nanocomposites in a Slurry-Phase Polymerization Reactor. *Industrial & Engineering Chemistry Research* **2003,** 42, (16), 3750-3757.

149. Radu, D. R.; Lai, C.-Y.; Jeftinija, K.; Rowe, E. W.; Jeftinija, S.; Lin, V. S. Y., A Polyamidoamine Dendrimer-Capped Mesoporous Silica Nanosphere-Based Gene Transfection Reagent. *Journal of the American Chemical Society* **2004,** 126, (41), 13216-13217.

150. Hayashi, S.; Takeuchi, Y.; Eguchi, M.; Iida, T.; Tsubokawa, N., Graft polymerization of vinyl monomers initiated by peroxycarbonate groups introduced onto silica surface by Michael addition. *Journal of Applied Polymer Science* **1999,** 71, (9), 1491-1497.

151. Sulitzky, C.; Rckert, B.; Hall, A. J.; Lanza, F.; Unger, K.; Sellergren, B. r., Grafting of Molecularly Imprinted Polymer Films on Silica Supports Containing Surface-Bound Free Radical Initiators. *Macromolecules* **2001,** 35, (1), 79-91.

152. von Werne, T.; Patten, T. E., Preparation of Structurally Well-Defined Polymer-Nanoparticle Hybrids with Controlled/Living Radical Polymerizations. *Journal of the American Chemical Society* **1999,** 121, (32), 7409-7410.

153. von Werne, T.; Patten, T. E., Atom Transfer Radical Polymerization from Nanoparticles: A Tool for the Preparation of Well-Defined Hybrid Nanostructures and for Understanding the Chemistry of Controlled/Living Radical Polymerizations from Surfaces. *Journal of the American Chemical Society* **2001,** 123, (31), 7497-7505.

154. Zhou, Q.; Wang, S.; Fan, X.; Advincula, R.; Mays, J., Living Anionic Surface-Initiated Polymerization (LASIP) of a Polymer on Silica Nanoparticles. *Langmuir* **2002,** 18, (8), 3324-3331.

155. Eismann, U.; Spange, S., Cationic Initiation of Vinyl Ether Polymerization Induced by (4-R1C6H4)(4-R2C6H4)R3CX in Conjunction with Silica: Producing Highly Head Group Functionalized Polymers. *Macromolecules* **1997,** 30, (12), 3439-3446.

156. Carrot, G.; Rutot-Houze, D.; Pottier, A.; Degee, P.; Hilborn, J.; Dubois, P., Surface-Initiated Ring-Opening Polymerization: A Versatile Method for Nanoparticle Ordering. *Macromolecules* **2002,** 35, (22), 8400-8404.

157. Mingotaud, A.-F.; Reculusa, S.; Mingotaud, C.; Keller, P.; Sykes, C.; Duguet, E.; Ravaine, S., Ring-opening metathesis polymerization on well defined silica nanoparticles leading to hybrid core-shell particles. *Journal of Materials Chemistry* **2003,** 13, (8), 1920-1925.

158. Pyun, J.; Jia, S.; Kowalewski, T.; Patterson, G. D.; Matyjaszewski, K., Synthesis and Characterization of Organic/Inorganic Hybrid Nanoparticles: Kinetics of Surface-Initiated Atom Transfer Radical Polymerization and Morphology of Hybrid Nanoparticle Ultrathin Films. *Macromolecules* **2003,** 36, (14), 5094-5104.

159. Bombalski, L.; Min, K.; Dong, H.; Tang, C.; Matyjaszewski, K., Preparation of Well-Defined Hybrid Materials by ATRP in Miniemulsion. *Macromolecules* **2007,** 40, (21), 7429-7432.

160. Sonnenberg, L.; Parvole, J.; Borisov, O.; Billon, L.; Gaub, H. E.; Seitz, M., AFM-Based Single Molecule Force Spectroscopy of End-Grafted Poly(acrylic acid) Monolayers. *Macromolecules* **2005,** 39, (1), 281-288.

161. Blomberg, S.; Ostberg, S.; Harth, E.; Bosman, A. W.; Van Horn, B.; Hawker, C. J., Production of crosslinked, hollow nanoparticles by surface-initiated living free-radical polymerization. *Journal of Polymer Science Part A: Polymer Chemistry* **2002,** 40, (9), 1309-1320.
162. Tsujii, Y.; Ejaz, M.; Sato, K.; Goto, A.; Fukuda, T., Mechanism and Kinetics of RAFT-Mediated Graft Polymerization of Styrene on a Solid Surface. 1. Experimental Evidence of Surface Radical Migration. *Macromolecules* **2001,** 34, (26), 8872-8878.
163. Li, C.; Benicewicz, B. C., Synthesis of Well-Defined Polymer Brushes Grafted onto Silica Nanoparticles via Surface Reversible Addition Fragmentation Chain Transfer Polymerization. *Macromolecules* **2005,** 38, (14), 5929-5936.
164. Rostovtsev, V. V.; Green, L. G.; Fokin, V. V.; Sharpless, K. B., A Stepwise Huisgen Cycloaddition Process: Copper(I)-Catalyzed Regioselective "Ligation" of Azides and Terminal Alkynes. *Angewandte Chemie International Edition* **2002,** 41, (14), 2596-2599.
165. Kolb, H. C.; Finn, M. G.; Sharpless, K. B., Click Chemistry: Diverse Chemical Function from a Few Good Reactions. *Angewandte Chemie International Edition* **2001,** 40, (11), 2004-2021.
166. Tornoe, C. W.; Christensen, C.; Meldal, M., Peptidotriazoles on Solid Phase:[1,2,3]-Triazoles by Regiospecific Copper(I)-Catalyzed 1,3-Dipolar Cycloadditions of Terminal Alkynes to Azides. *The Journal of Organic Chemistry* **2002,** 67, (9), 3057-3064.
167. Binder, W. H.; Sachsenhofer, R., 'Click' Chemistry in Polymer and Material Science: An Update. *Macromolecular Rapid Communications* **2008,** 29, (12-13), 952-981.
168. Nandivada, H.; Jiang, X.; Lahann, J., Click Chemistry: Versatility and Control in the Hands of Materials Scientists. *Advanced Materials* **2007,** 19, (17), 2197-2208.
169. Vallet-Regi, M.; Colilla, M.; Gonzalez, B., Medical applications of organic-inorganic hybrid materials within the field of silica-based bioceramics. *Chemical Society Reviews* **2011,** 40, (2), 596-607.
170. Bauer, F.; Sauerland, V.; Gläsel, H.-J.; Ernst, H.; Findeisen, M.; Hartmann, E.; Langguth, H.; Marquardt, B.; Mehnert, R., Preparation of Scratch and Abrasion Resistant Polymeric Nanocomposites by Monomer Grafting onto Nanoparticles, 3. Effect of Filler Particles and Grafting Agents. *Macromolecular Materials and Engineering* **2002,** 287, (8), 546-552.
171. Bauer, F.; Flyunt, R.; Czihal, K.; Buchmeiser, M. R.; Langguth, H.; Mehnert, R., Nano/Micro Particle Hybrid Composites for Scratch and Abrasion Resistant Polyacrylate Coatings. *Macromolecular Materials and Engineering* **2006,** 291, (5), 493-498.
172. Kashiwagi, T.; Morgan, A. B.; Antonucci, J. M.; VanLandingham, M. R.; Harris, R. H.; Awad, W. H.; Shields, J. R., Thermal and flammability properties of a silica–poly(methylmethacrylate) nanocomposite. *Journal of Applied Polymer Science* **2003,** 89, (8), 2072-2078.
173. Yu, Y.-Y.; Chen, C.-Y.; Chen, W.-C., Synthesis and characterization of organic-inorganic hybrid thin films from poly(acrylic) and monodispersed colloidal silica. *Polymer* **2003,** 44, (3), 593-601.

174. Sun, Y.; Zhang, Z.; Wong, C. P., Influence of interphase and moisture on the dielectric spectroscopy of epoxy/silica composites. *Polymer* **2005,** 46, (7), 2297-2305.
175. Sondi, I.; Fedynyshyn, T. H.; Sinta, R.; Matijevi, E., Encapsulation of Nanosized Silica by in Situ Polymerization of tert-Butyl Acrylate Monomerâ€ *Langmuir* **2000,** 16, (23), 9031-9034.
176. Li, X.; Li, X.; Wang, G., Conducting poly-N-[5-(8-quinolinol)ylmethyl]aniline/nano-SiO2 composite with fluorescence. *Materials Letters* **2006,** 60, (28), 3342-3345.
177. Khayet, M.; Villaluenga, J. P. G.; Valentin, J. L.; Lapez-Manchado, M. A.; Mengual, J. I.; Seoane, B., Filled poly(2,6-dimethyl-1,4-phenylene oxide) dense membranes by silica and silane modified silica nanoparticles: characterization and application in pervaporation. *Polymer* **2005,** 46, (23), 9881-9891.
178. Merkel, T. C.; Freeman, B. D.; Spontak, R. J.; He, Z.; Pinnau, I.; Meakin, P.; Hill, A. J., Sorption, Transport, and Structural Evidence for Enhanced Free Volume in Poly(4-methyl-2-pentyne)/Fumed Silica Nanocomposite Membranes. *Chemistry of Materials* **2002,** 15, (1), 109-123.
179. Saxena, A.; Tripathi, B. P.; Shahi, V. K., Sulfonated Poly(styrene-co-maleic anhydride)-Poly(ethylene glycol)-Silica Nanocomposite Polyelectrolyte Membranes for Fuel Cell Applications. *The Journal of Physical Chemistry B* **2007,** 111, (43), 12454-12461.
180. Chuang, S.-W.; Hsu, S. L.-C.; Liu, Y.-H., Synthesis and properties of fluorine-containing polybenzimidazole/silica nanocomposite membranes for proton exchange membrane fuel cells. *Journal of Membrane Science* **2007,** 305, (12), 353-363.
181. Xiang, X. J.; Qian, J. W.; Yang, W. Y.; Fang, M. H.; Qian, X. Q., Synthesis and properties of nanosilica-reinforced polyurethane for grouting. *Journal of Applied Polymer Science* **2006,** 100, (6), 4333-4337.
182. Su, Y.-l., Preparation of polydiacetylene/silica nanocomposite for use as a chemosensor. *Reactive and Functional Polymers* **2006,** 66, (9), 967-973.
183. Jang, J.; Ha, J.; Lim, B., Synthesis and characterization of monodisperse silica-polyaniline core-shell nanoparticles. *Chemical Communications* **2006**, (15), 1622-1624.
184. Neoh, K. G.; Tan, K. K.; Goh, P. L.; Huang, S. W.; Kang, E. T.; Tan, K. L., Electroactive polymer-SiO2 nanocomposites for metal uptake. *Polymer* **1999,** 40, (4), 887-893.
185. Allen, T. M., Ligand-targeted therapeutics in anticancer therapy. *Nat Rev Cancer* **2002,** 2, (10), 750-763.
186. Yang, Q.; Wang, S.; Fan, P.; Wang, L.; Di, Y.; Lin, K.; Xiao, F.-S., pH-Responsive Carrier System Based on Carboxylic Acid Modified Mesoporous Silica and Polyelectrolyte for Drug Delivery. *Chemistry of Materials* **2005,** 17, (24), 5999-6003.
187. Chang, J. H.; Shim, C. H.; Kim, B. J.; Shin, Y.; Exarhos, G. J.; Kim, K. J., Bicontinuous, Thermoresponsive, L3-Phase Silica Nanocomposites and Their Smart Drug-Delivery Applications. *Advanced Materials* **2005,** 17, (5), 634-637.

188. Giri, S.; Trewyn, B. G.; Stellmaker, M. P.; Lin, V. S. Y., Stimuli-Responsive Controlled-Release Delivery System Based on Mesoporous Silica Nanorods Capped with Magnetic Nanoparticles. *Angewandte Chemie International Edition* **2005,** 44, (32), 5038-5044.
189. Hernandez, R.; Tseng, H.-R.; Wong, J. W.; Stoddart, J. F.; Zink, J. I., An Operational Supramolecular Nanovalve. *Journal of the American Chemical Society* **2004,** 126, (11), 3370-3371.
190. Kim, H. J.; Matsuda, H.; Zhou, H.; Honma, I., Ultrasound-Triggered Smart Drug Release from a Poly(dimethylsiloxane)– Mesoporous Silica Composite. *Advanced Materials* **2006,** 18, (23), 3083-3088.
191. Binder, W. H.; Sachsenhofer, R., 'Click' Chemistry in Polymer and Materials Science. *Macromolecular Rapid Communications* **2007,** 28, (1), 15-54.
192. Ulijn, R. V.; Smith, A. M., Designing peptide based nanomaterials. *Chemical Society Reviews* **2008,** 37, (4), 664-675.
193. Wang, Y.; Chang, Y. C., Patterning of Polypeptide Thin Films by the Combination of Surface-Initiated Vapor-Deposition Polymerization and Photolithography. *Advanced Materials* **2003,** 15, (4), 290-293.
194. Wieringa, R. H.; Siesling, E. A.; Werkman, P. J.; Angerman, H. J.; Vorenkamp, E. J.; Schouten, A. J., Surface Grafting of Poly(l-glutamates). 2. Helix Orientation. *Langmuir* **2001,** 17, (21), 6485-6490.
195. Wieringa, R. H.; Siesling, E. A.; Geurts, P. F. M.; Werkman, P. J.; Vorenkamp, E. J.; Erb, V.; Stamm, M.; Schouten, A. J., Surface Grafting of Poly(l-glutamates). 1. Synthesis and Characterization. *Langmuir* **2001,** 17, (21), 6477-6484.
196. Chang, Y.-C.; Frank, C. W., Vapor Deposition Polymerization of a-Amino Acid N-Carboxy Anhydride on the Silicon(100) Native Oxide Surface. *Langmuir* **1998,** 14, (2), 326-334.
197. Chang, Y.-C.; Frank, C. W., Grafting of Poly(g-benzyl-l-glutamate) on Chemically Modified Silicon Oxide Surfaces. *Langmuir* **1996,** 12, (24), 5824-5829.
198. Fong, B.; Turksen, S.; Russo, P. S.; Stryjewski, W., Colloidal Crystals of Silica Homopolypeptide Composite Particles. *Langmuir* **2004,** 20, (1), 266-269.
199. Fong, B.; Russo, P. S., Organophilic Colloidal Particles with a Synthetic Polypeptide Coating. *Langmuir* **1999,** 15, (13), 4421-4426.
200. Abelow, A. E.; Zharov, I., Poly(l-alanine)-modified nanoporous colloidal films. *Soft Matter* **2009,** 5, (2), 457-462.
201. Lunn, J. D.; Shantz, D. F., Peptide Brush Ordered Mesoporous Silica Nanocomposite Materials. *Chemistry of Materials* **2009,** 21, (15), 3638-3648.
202. Balamurugan, S. S.; Soto-Cantu, E.; Cueto, R.; Russo, P. S., Preparation of Organosoluble Silica-Polypeptide Particles by "Click" Chemistry. *Macromolecules* **2009,** 43, (1), 62-70.

Chapter 2

Synthesis and Characterization of "Clickable" Polypeptides by NCA Polymerization

This chapter was adapted from

1) Synthesis and Characterization of Poly-**L**-lysine-Grafted Silica Nanoparticles Synthesized via NCA Polymerization and Click Chemistry
Mrityunjoy Kar, P. S. Vijayakumar, B. L. V. Prasad and Sayam Sen Gupta
Langmuir, **2010**, *26* (8), pp 5772–5781

2) Synthesis of Poly-L-glutamic Acid Grafted Silica Nanoparticles and Their Assembly into Macroporous Structures
Mrityunjoy Kar, Minois Pauline, Kamendra Sharma, Guruswamy Kumaraswamy, and Sayam Sen Gupta
Langmuir, **2011**, 27 (19), pp 12124–12133

2.1 Introduction

Amino acids are the building blocks of peptides. Nature produces polypeptides or proteins as highly refined and monodisperse polymers with precisely controlled primary sequence of amino acids. The controlled sequence of amino acid allows them to fold into stable secondary order conformations (α-helix, β-sheet, coils and turns) and hierarchical three dimensional structures (tertiary and quaternary structures) so that they can perform biological functions such as catalysis, signaling and cell proliferation among others.[1] Synthetic polypeptides are a class of attractive bio-mimetic materials that have mainly been exploited to mimic the structural and biological properties of proteins. They have also been successfully applied to a wide variety of practical biomedical applications.[2] They have a distinct advantage over synthetic polymers as they are expected to be biocompatible. For example, most synthetic cationic polymers like PAMAM and PEI that have been used for many biological applications such as gene transfection need long term studies to ascertain their biocompatibility. On the other hand, polypeptides that are synthesized from naturally occurring amino acids have ability to perform an appropriate host response in specific biological applications and are also expected to degrade into their constituent amino acids by various protease enzymes after completion of their desired biological function. The success of the synthetic polypeptides lies in the fact that a wide range of compositions and architectures can be easily synthesized which allows complete control over their properties.[3] Hence, synthetic polypeptides can self-assemble to form various hierarchical structures[4, 5] and these assemblies have found application in drug delivery,[6] tissue engineering,[7] biomineralization.

Various methods have been developed to prepare well defined synthetic polypeptides. However, all these techniques are having their own advantages and disadvantages. Conventional solid phase synthesis of polypeptides offers control over sequences of amino acids but it is neither useful nor practical to use solid-phase synthesis for the preparation of large polypeptides (>100 residues) due to technical difficulties. The most economical, convenient and established process for the preparation of long polypeptide chains is the ring opening polymerization of α-amino acid-N-carboxy anhydrides (NCAs). This method takes short time and involves simple reagents. The 'living' nature of the NCA ring opening polymerization allows proper control over molecular weight of polypeptides and polydispersity. This method also offers good yield of the polypeptide without racemization at the chiral centre of amino acids. There are considerable varieties of polypeptides (> 200) that

have been synthesized by using NCAs polymerization. These structural and functional properties of these polypeptides have also been studied in details.

This chapter describe the synthesis of various homo and block co- polypeptides. Poly-L-lysine, poly-L-benzylglutamate, poly-L-lysine-block-poly-L-leucine, poly-L-glutamic acid and poly-L-arginine were synthesized by using NCA-ring opening polymerisation.

2.2 Approach and strategy for selecting alkyne terminated polypeptides

Ring opening polymerization of amino acid NCA's allow incorporation of the functionality of interest at the C-terminating end group of the polypeptides. The incorporation is facilitated by using various modified nucleophilic initiator. Primary amine derivatives are commonly used to incorporate functionality into the C-terminating end group of the polypeptides. To incorporate the functionality at the end group of the ring opening polymerization reaction should proceed via the normal amine (NA) mechanism (Scheme 2.1). Normally, if the NCA ring opening polymerization proceeds through activated monomer mechanism the initiator will not be incorporated into the C-terminal end of the polypeptides (scheme 2.2). Hexylamine is very commonly used initiator and the incorporation of the hexylamine at the C-terminal end is nearly 100%. For facile attachment into surfaces we wanted to have a chain end with a functional group which can only react with its partner and would be orthogonal to other functional groups. To achieve this we decided to have a propargyl group at the chain end so that it can be easily attached to an azide modified surface though Cu(I) catalyzed azide-alkyne "click" reaction. The introduction of propargyl group at the chain end requires using propargyl group as the initiator. NCA polymerization initiated with propargyl amine suffers from mainly two difficulties, 1) the reaction takes more time to completion and 2) due to the high basicity of propargylamine, it can abstract the N-H acidic proton from NCA anhydride ring and the polymerization will proceed through the activated monomer mechanism. The activated monomer mechanism would not allow introduction of the propargyl group at the chain end.

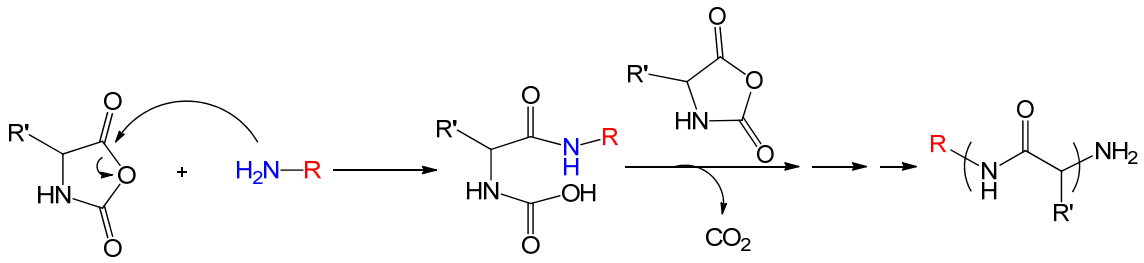

Scheme 2.1: Normal Amine (NA) mechanism of NCA ring opening polymerization by using primary amine initiator (Where R is any aliphatic or benzylic group)

To have 100% incorporation of propargyl group and short reaction times, N-TMS derivative of propargylamine initiated ring opening polymerization was used as has been developed by the Cheng group.[8] Reaction with N-TMS alkyl is much faster compared to normal amine and the polymerization is more 'living' in nature. N-TMS propargylamine also successfully incorporates the propargyl functionality at the C-terminating end group. The ring opening polymerization initiated with propargylamine N-TMS derivative starts with activated monomer mechanism to yield the primary amine and subsequently that primary amine leads to normal amine mechanism by incorporating the primary amine into the C-terminating end group. The alkyl group incorporated in the C-terminal of the polypeptides can be attached to surfaces having organoazide group using Cu(I) catalyzed 'click' reaction. The obtained polypeptides from the NCA polymerization also contains amino group at the N-terminating end and this can also be used for labeling the polypeptides with dyes and markers.

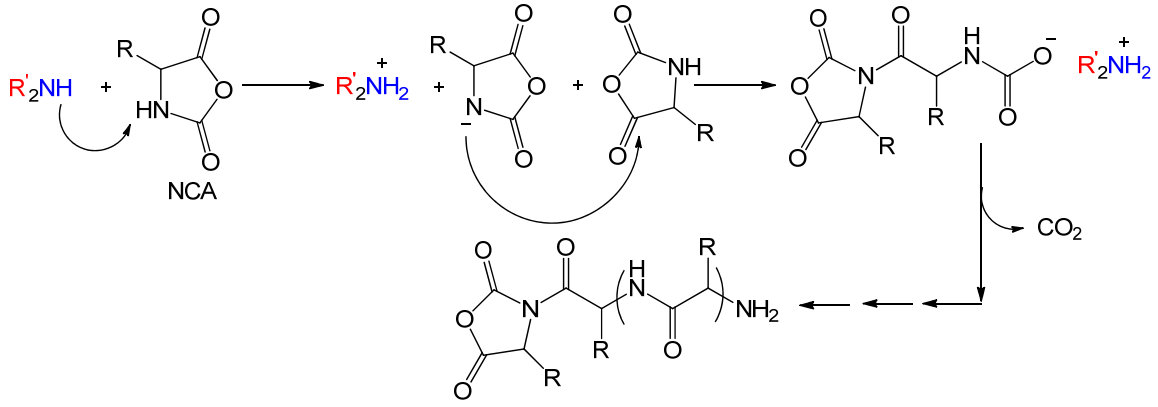

Scheme 2.2: Activated monomer (AM) mechanism of NCA ring opening polymerization

2.3 Experimental section

2.3.1 Materials

L-Lysine hydrochloride (puriss for biochemistry CHR), L-leucine (puriss for biochemistry CHR), L-glutamic acid (puriss for biochemistry CHR), L-arginine (puriss for biochemistry CHR) phthalic anhydride, phenyl hydrazine, tributylamine, pyridine, benzylchloroformate (50% toluene solution) were obtained from Spectrochem, India. L-δ-benzyl glutamate obtained from SRL, India. HBr (33% solution on acetic acid) was obtained from Loba Chemie, India. Benzene, ethyl methyl ketone, diethyl ether, petroleum ether (20-80), and ethylacetate were obtained from Merck, India. Diethyl ether, petroleum ether (20-80), ethylacetate used for NCA synthesis was dried, deoxygenated and stored in the glove box. DMF (99.99% dry) obtained from Merck (Germany) was used for polymerization inside the glove box. N-TMS propargylamine was synthesized according to the earlier report. DMF

(99.99% dry) obtained from Merck Germany was used for polymerization inside the glove box.

2.3.2 Synthesis

2.3.2.1 Synthesis of alkyne terminated poly-L-lysine

2.3.2.1.1 Synthesis of α,ε-dicarbobenzoxy-L-lysine (1)

This compound was synthesized according to earlier report.[9] 6 g (0.0328 mol) of L-lysine dihydrochloride was dissolved in 42 mL 2(N) NaOH, was taken into a 250 mL jacketed two necked flask and cooled to 0ºC. 28.8 g (0.0846 mol) of carbobenzoxy chloride (50% toluene solution) containing 34 ml (4)N NaOH was taken into a dropping funnel and added dropwise into the two necked flask at 0ºC with stirring. After 12 hrs the resulting mixture was washed with diethyl ether (20mL x 2). The reaction mixture was acidified with aqueous potassium bisulfate and extracted with diethyl ether. For further purification aqueous potassium bicarbonate solution was added to the ether extract. Aqueous layer was taken and acidified with potassium bisulfate and the product was extracted with fresh diethyl ether. The combined organic layer was dried with anhydrous sodium sulfate and concentrated under reduced pressure to obtain *α,ε*-dicarbobenzoxy-L-lysine as a colorless syrup. Yield: 12g

2.3.2.1.2 Synthesis of ε-carbobenzoxy- α -carboxyl-L-lysine anhydride (2)

According to the previous report,[9] 7 g (16.9 mmol) of crude *α,ε*-dicarbobenzoxy-L-lysine was dissolved in 30 mL of dry diethyl ether, was taken into a 50 ml flame dried schlenk flask and cooled to 0°C. Then 4.22 g (20.28 mmol) of powdered phosphorus pentachloride was added in it and stirred for about 30-45 min until dissolution of the entire solid. After quick filtration, this solution was quickly concentrated under reduced pressure at 45°C. The product was crystallized from a mixture of dry ethyl acetate and dry petroleum ether. For further purification the product was recrystallized thrice from dry ethyl acetate and dry petroleum ether mixture. The product that obtained was dried under high vacuum at 50°C and immediately transferred to the glove box. Yield: 4.5 g, (64%)

FT–IR: ν (Cm^{-1}, KBr): N-H (NCA, cbz) 3292; CH_2, 2936; CH_2, 2864; C=O (NCA), 1814 & 1692; C=O (cbz), 1652; N-H (cbz), 1534; C(=O)-O, 1257. ^1H NMR (400 MHz, $CDCl_3$): δ 7.35-7.21 ppm (d, 5H), 5.09 ppm (s, 2H), 4.36-4.31 ppm (t, 1H), 3.28-3.22 ppm (t, 2H), 1.95

ppm (t, 2H), 1.57 ppm (t, 4H). ^{I3}C NMR (100 MHz, $CDCl_3$): δ 170.04, 156.93, 152.65, 128.61, 128.26, 128.04, 66.91, 57.47, 40.15, 30.83, 29.12, 21.35 ppm

2.3.2.1.3 Synthesis of alkyne terminated ε-carbobenzoxy-poly-L-lysine (alkyne-cbz-PLLs) (3)

Various molecular weights of alkyne-cbz-PLL were prepared by using NCA ring opening polymerization. All the reactions and reaction manipulations were done inside the glove box (O_2 > 0.1 ppm and H_2O >1 ppm). For alkyne-cbz-PLL(30), cbz-L-lysine NCA (659 mg, 2.153 mmol) was dissolved in 5 mL of anhydrous DMF into a flame-dried 25mL schlenk flask. The solution was stirred for 10 min after which a solution of N-TMS propargylamine (9.11 mg, 0.072 mmol) in 100 μl of anhydrous DMF was added to it. For alkyne-cbz-PLL(20) and alkyne-cbz-PLL(10), cbz-L-lysine NCA (920 mg, 3 mmol) was dissolved in 9 mL of anhydrous DMF into a flame-dried 50 mL schlenk flask. The solution was stirred for 10 min after which a solution of N-TMS propargylamine (38.22 mg, 0.3 mmol and 19.11 mg, 0.15 mmol for 10 and 20 mer respectively) was added to it. The polymerizations were allowed to proceed inside the glove box for 24 hrs at room temperature. The completions of all the polymerization reactions were monitored by the disappearance of the two CO stretching of NCA at 1851 and 1788 cm^{-1} by FT-IR. The polymer was isolated by repeated precipitation in diethyl ether and was then dried under high vacuum at 60°C. The polymer was characterized by GPC in DMF (0.1 mM LiBr, 60°C) and by ^{1}H NMR. Yield: 547 mg and 763 mg for alkyne-cbz-PLL(30) and alkyne-cbz-PLL(20) respectively (80 – 85%)

2.3.2.1.4 Synthesis of alkyne terminated poly-L-lysine (alkyne-PLL) (4)

To a solution of cbz-poly-L-lysine (1 g) in 25 mL of trifluoroacetic acid was added 33% solution of HBr in acetic acid (1.23 g, 4 equivalents with respect to the cbz groups). The reaction mixture was stirred for one hour at room temperature after which excess of diethyl ether was added into it. The precipitated polymer was centrifuged and the supernatant liquid was decanted. The residue was washed with fresh diethyl ether twice and dried under vacuum at 45°C. Yield: 850 mg (85%)

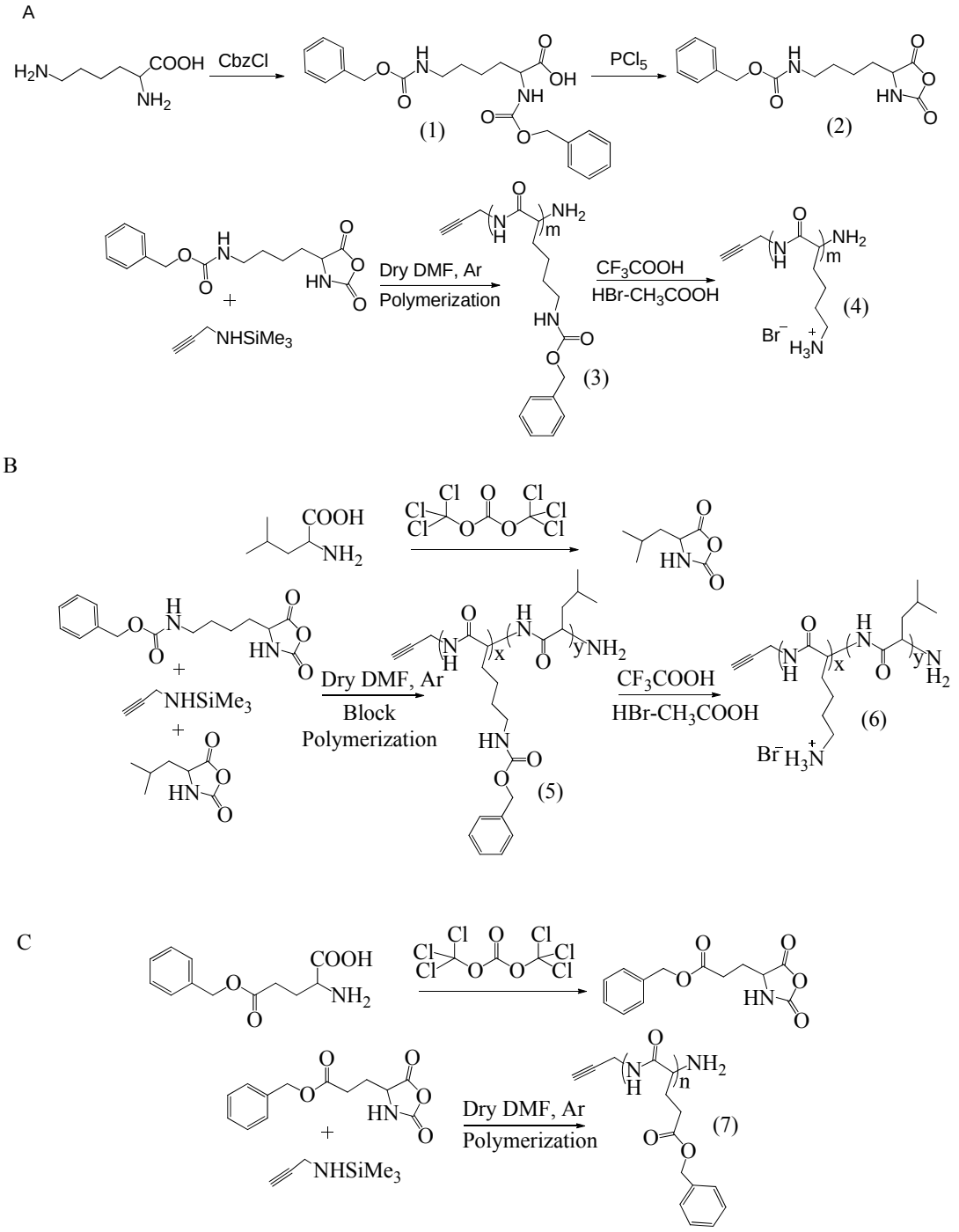

Scheme 2.3: Synthesis of A) alkyne poly-L-lysine, B) alkyne poly-L-lysine-*b*-poly-L-leucine and C) alkyne poly-L-benzyl glutamate

2.3.2.2 Synthesis of alkyne terminated poly-L-lysine-block-poly-L-leucine (alkyne-PLL-b-PLLeu)

2.3.2.2.1 Synthesis of alkyne terminated ε-carbobenzoxy-poly-L-lysine-b-poly-l-leucine block copolymer (alkyne-cbz-PLL-b-PLLeu) (5)

In the glove box, cbz-L-lysine NCA (1.918 g, 6.267 mmol) was dissolved in 19 mL of anhydrous DMF into a flame-dried 50mL schlenk flask. The solution was stirred for 10 min after which a solution of N-TMS propargylamine (31 mg, 0.25 mmol) in 100 µl of anhydrous DMF was added to it. The schlenk flask was then sealed properly and stirred for 14 hrs at room temperature. After 95% of the starting cbz-L-lysine NCA had disappeared as observed by FT-IR, L-leucine NCA (0.393 g, 2.507 mmol) was added into the reaction mixture and stirred for another 12 hrs. The polymer was isolated by repeated precipitation in diethyl ether and was then dried under high vacuum at 45°C. The polymer was characterized by GPC in DMF (0.1 mM LiBr, at 60°C) and by ^{1}H NMR. Yield: 1.58 g (83%)

2.3.2.2.2 Synthesis of alkyne terminated poly-L-lysine-block-poly-L-leucine (alkyne-PLL-b-PLLeu) (6)

To a solution of *alkyne-cbz-PLL-b-PLLeu* (1 g) in 25 mL of trifluoroacetic acid was added 33% solution of HBr in acetic acid (1.23 g, 4 equivalents with respect to the cbz groups). The reaction mixture was stirred for one hour at room temperature after which excess of diethyl ether was added into it. The precipitated polymer was centrifuged and the supernatant liquid was decanted. The residue was washed with fresh diethyl ether twice and dried under vacuum at 45°C. Yield: 870 mg (87%).

2.3.2.3 Synthesis of alkyne terminated poly-L-benzyl glutamate (alkyne-PLBG) (7)

In the glove box, γ-benzyl glutamate NCA (1 g, 3.798 mmol) was dissolved in 10 mL of anhydrous DMF into a flame-dried 25mL schlenk flask. The solution was stirred for 10 min after which a solution of N-TMS propargylamine (16.08 mg, 0.126 mmol) in 100 µl of anhydrous DMF was added to it. The schlenk flask was then sealed properly and was taken outside and stirred for one day (24 hrs) at room temperature. The polymer was isolated by repeated precipitation in diethyl ether and was then dried under high vacuum at 45°C. The polymer was characterized by GPC in DMF (0.1 mM LiBr, 60°C) and by ^{1}H NMR. Yield: 640 mg (64%)

2.3.2.4 Synthesis of alkyne terminated poly-L-Glutamic Acid (alkyne-PLGA)

2.3.2.4.1 Synthesis of phtlaloyl-L-glutamic anhydride (8)

This compound was synthesized according to an earlier report.[10] A suspension of L-glutamic acid (0.22 mol, 10 g**)** and phthalic anhydride (0.22 mol, 10 g) in dry pyridine (36.80 mL) was refluxed for 2 hours. After 2 hrs, the clear reaction mixture was removed under reduced pressure after which acetic anhydride **(**27.60 mL) was added and the resultant solution was boiled for an additional 5 minutes. After completion of the reaction, the solvent was removed under reduced pressure to afford a solid. Anhydrous diethyl ether was then added to this solid and the resultant suspension was kept in ice for 15 mins. The solid was then filtered and washed with additional anhydrous diethyl ether until the orange color disappeared. Finally the resultant white solid was dried under vacuum at 40ºC. Yield: 10.63 g (70%)

FT–IR: ν (Cm^{-1}, KBr): C=O, 1820; C=O, 1780; C=O, 1715. ^{1}H NMR (400 MHz, $CDCl_3$): δ 7.91-7.83 ppm (d, 4H), 5.13 ppm (m, 1H), 3.15-2.89 ppm (m, 3H), 2.23 ppm (m, 2H), 1.66 ppm (s, 0.49H). ^{I3}C NMR (100 MHz, $CDCl_3$): δ 173-170, 166.52, 134, 130, 123, 47, 29, 20 ppm

2.3.2.4.2 Synthesis of phtaloyl-para-methoxybenzyl-L-glutamate (9)

This compound was synthesized according to an earlier report.[10, 11] A mixture of N-phthaloyl-L-glutamic anhydride (1 g, 0.036 mol) and 4-Methoxyphenyl methanol (533 mg, 0.036 mol) in benzene (27 ml) was refluxed for 24 hrs. After completion of the reaction, the solvent was removed under reduced pressure to afford a solid. This solid was recrystallized from ethyl acetate and petroleum ether (boiling point 40-60ºC) twice to afford white crystalline phtaloyl-*p*-methoxybenzyl-L-glutamate. Yield: 0.86 g (58%). (Note: Sometimes a turbid solution is observed at the completion of reaction. In that case, the solution needs to be filtered to remove the undissolved solid prior to removal of benzene)

FT–IR: γ (Cm^{-1}, KBr): C=O, 1772; C=O, 1751; C=O, 1730; C=O, 1700; OH, 3450. ^{1}H NMR (400 MHz, $CDCl_3$): δ 7.70-8 ppm (d,4H), 5.4-5 ppm (m, 1H), 3.25-2.7 ppm (m, 3H), 2.25-1.7 ppm (m, 4H). ^{I3}C NMR (100 MHz, $CDCl_3$): δ 174, 172, 167, 159, 134, 130, 127, 123, 113, 66, 55, 50, 30, 23 ppm

2.3.2.4.3 Synthesis of p-methoxybenzyl-L-glutamate (10)

This compound was synthesized according to an earlier report.[10, 11]A mixture of phtaloyl-*p*-methoxy-L-glutamic acid (2 g, 5.03 mmol), phenyl hydrazine (1.54 mL, 15.10 mmol), and tributylamine (1.24 mL, 5.03 mmol) were added to absolute ethanol (10 mL) and

refluxed for 2 hrs. After 2 hrs, ethyl methyl ketone (10 mL) was added and the resulting mixture was refluxed for another 15 min. After cooling to room temperature, acetic acid (0.3 mL) was added. The resulting crystalline solid was filtered under vacuum and carefully washed with ethyl methyl ketone (130 mL) for several times to afford pure p-methoxybenzyl-L-glutamate. (Note: This compound should be purified carefully in order to make the corresponding NCA with high purity).

Yield: 0.7 g (54%).

FT–IR, ν (cm^{-1}, KBr): (C=O acid), 1680-1540; (C=O), 1730; (OH), 3475-3325. ^{1}H NMR (400 MHz, d6 DMSO): δ 8.24 ppm (s, 3H), 7.31-6.93 ppm (d, 4H), 5.01 ppm (s, 2H), 3.93 ppm (m, 1H), 3.73 ppm (s, 3H), 2.53 ppm (m, 2H), 2.04 ppm (m, 2H). ^{13}C NMR (100 MHz, $CDCl_3$): δ 171.89, 171, 159.18, 158.42, 134, 130, 114.04, 65, 55, 51, 29, 25 ppm

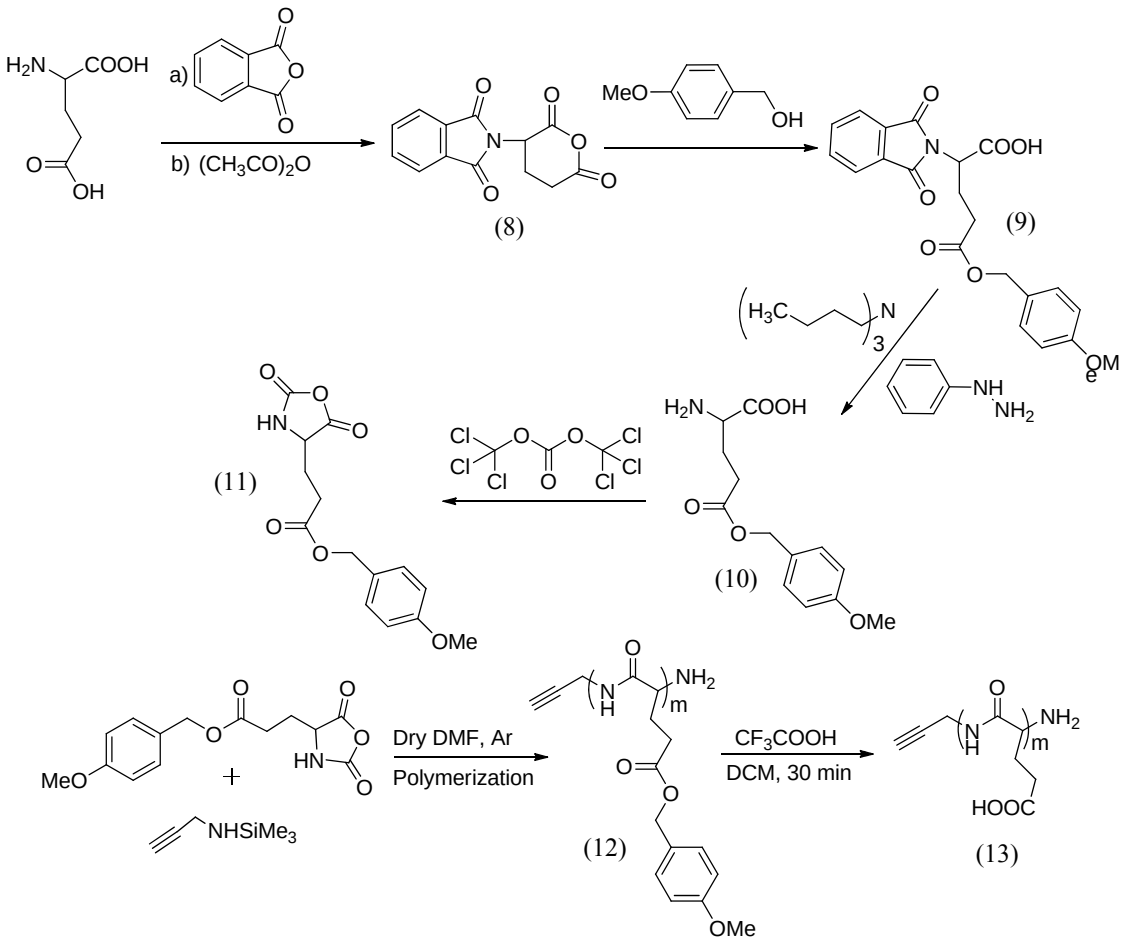

Scheme 2.4: Synthesis of alkyne poly-L-glutamic acid

2.3.2.4.4 Synthesis of p-methoxybenzyl-L- glutamate NCA (11)

This compound was synthesized according to an earlier report with slight modifications.[10, 11] In a flame dried round bottom flask, *p*-methoxybenzyl glutamate (1 g, 1 eq), tri-phosgene (solid, 557 mg, 0.5 eq), and α-pinene (858 µL, 1.5 eq) were added in 30 mL anhydrous ethyl acetate, and stirred for 2 hrs at 70°C in inert atmosphere to obtain a yellow transparent solution. The non-nucleophilic base α-pinene was added to quench HCl that was generated during course of the reaction. After completion of the reaction, this solution was concentrated under reduce pressure and then additional anhydrous ethyl acetate was added twice and evaporated under reduce pressure in order to get rid of excess phosgene. The resultant viscous liquid obtained was then crystallized from anhydrous petroleum ether and ethyl acetate thrice. The NCA compound obtained (white powder) was then dried under vacuum for 30-40 min and transferred immediately into the glove box (O_2<0.1 ppm, H_2O < 0.2 ppm) for polymerization.

Yield: 44%

FT–IR, ν (cm^{-1}, KBr): (C=O), 1730; (C=O), 1790; (C=O), 1860. ^{1}H NMR (400 MHz, $CDCl_3$): δ 7.21-6.83 ppm (d, 4H), 6.58 ppm (s, 1H), 5.00 ppm (s, 2H), 4.30 ppm (s, 2H), 3.74 ppm (s, 3H), 2.49 ppm (t, 2H), 2.18-2.09 ppm (m, 2H). ^{I3}C NMR (100 MHz, $CDCl_3$): δ 172, 169, 159, 151, 130, 127, 114, 67, 57, 55, 30, 27 ppm

2.3.2.4.5 Synthesis of alkyne terminated poly-p-methoxybenzyl-L-glutamate (12)

In the glovebox (O_2 < 0.1ppm,H_2O <0.2 ppm), *p*-methoxy-benzyl-L-glutamate NCA (1 g, 3.798 mmol) was dissolved in 10 mL of anhydrous DMF into a flame-dried 25 mL schlenk flask. The solution was stirred for 10 min, after which a solution of N-TMS propargylamine (16.08 mg, 0.126 mmol) in 100 µL of anhydrous DMF was added. The schlenk flask was then sealed properly and was taken outside and stirred for 1 day (24 hrs) at 0°C. The polymer was precipitated in DI water and washed with DI water several times. A sticky solid was obtained, dried under high vacuum (> 5 mbar) at 60°C and characterized by NMR and GPC. Yield: 756 mg.

2.3.2.4.6 Synthesis of alkyne terminated poly- -L-glutamic acid (alkyne-PLGA) (13)

1 g of poly-*p*-methoxybenzyl-L-glutamic acid was incubated in a 20 ml of 10% trifluoroacetic acid (TFA) in dichloromethane (DCM), stirred for 30 minutes. The polymer was precipitated out with excess anhydrous diethyl ether and washed with diethyl ether for three times. The alkyne-PLGA was characterized by NMR and directly used for next step.

Yield: 552 mg.

2.3.2.5 Synthesis of alkyne terminated poly-L-arginine (alkyne-PLArg)

2.3.2.5.1 Synthesis of sodium tricarbobenzoxylated L-arginine(14)

Sodium tricarbobenzoxylated L-arginine was synthesized by previously reported method.[12] L-arginine HCl (20 gm) was added into 200 ml of 1N NaOH, stirred at 2-3°C for 5 mins , followed by addition of 32 ml of 50% carbobenzoxy chloride in toluene and 240 ml of 2N NaOH solution in alternate portions over a period of 15 min and finally stirred for another 1 hr at 2-3°C. The precipitate formed upon completion of reaction (sodium salt of tricabobenzoxy L-arginine) was filtered under vacuum and subsequently washed with 100 ml 5% cold Na_2CO_3 solution. The precipitate was dissolved in $CHCl_3$ and was washed once with 5% Na_2CO_3 solution, followed by water and brine solution. Subsequently the $CHCl_3$ layer was dried over anhydrous Na_2SO_4 and then concentrated under reduced pressure at 25°C. To the residue was added diethyl ether (400 ml) the resultant solution was stored overnight at -20°C to obtain white crystalline precipitate. The crystalline material obtained was filtered, washed with diethyl ether and dried under vacuum. Yield = 30 g (46%)

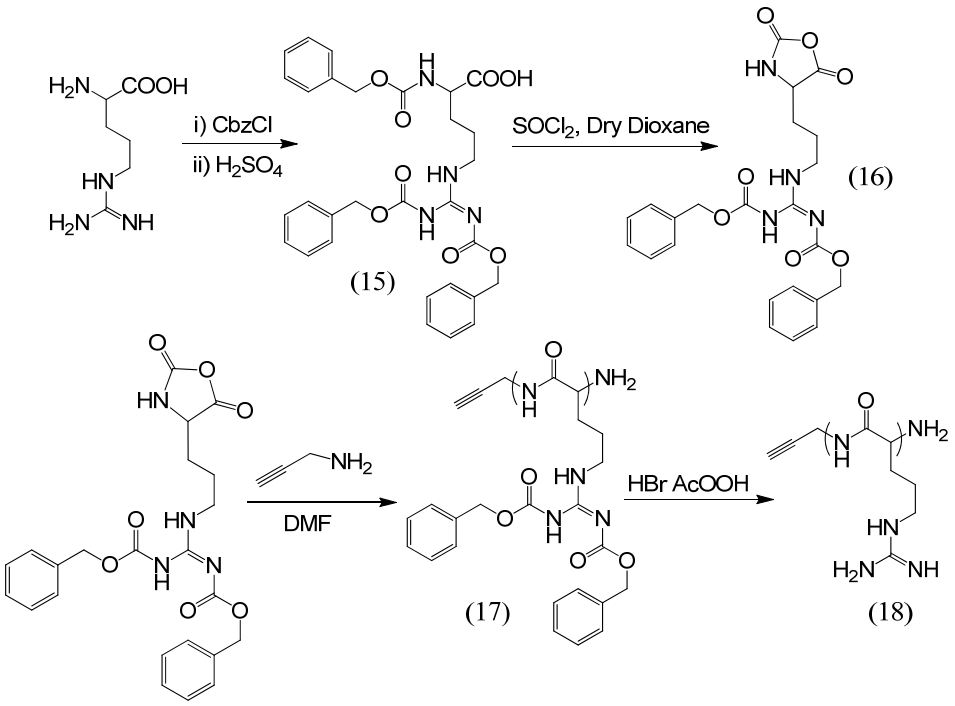

Scheme 2.5: Synthesis of alkyne poly-L-arginine

2.3.2.5.2 Synthesis of tricarbobenzoxylated L-arginine(15)

Sodium tricarbobenzoxylated L-arginine (2 g, recrystallized twice from hot ethanol) was suspended in 100 ml of EtOAc and 25 ml of 2% H_2SO_4 was added dropwise. After the addition of H_2SO_4 was complete, the EtOAc layer was separated washed first with 25 ml 2% H_2SO_4 and twice with water. Finally the EtOAc layer was dried over anhydrous Na_2SO_4 and then concentrated to dryness under reduced pressure.

Yield=1.6 gm

^{1}H NMR (400 MHz, $CDCl_3$): δ 9.40 ppm (s, 1H; NH), 7.30-7.34 ppm (m, 15H; ArH), 5.72-5.68 ppm (d, 1H; NH), 5.20 ppm (s, 2H; CH_2), 5.09 ppm (s, 2H; CH_2), 5.05 ppm (s, 2H; CH_2), 4.36 ppm (dd, 1H; CH), 3.94 ppm (t, 2H; CH_2), 1.68 ppm (m, 4H; CH_2). ^{I3}C NMR (100 MHz, $CDCl_3$): δ 175.73, 163.54, 160.44, 156.25, 155.71, 136.7, 134.54, 128.37, 68.99, 67.06, 53.64, 44.1, 28.59, 24.74 ppm

2.3.2.5.3 Synthesis of dicarbobenzoxy-α-carboxyl-L-arginine anhydride (16)

Di-carbobenzoxy- α -carboxyl-L-Arginine anhydride was synthesized following an earlier report with slight modifications.[12] For a typical reaction, tricarbobenzoxy-L-Arginine (2 g, 3.47 mmol) dissolved in 20 mL of anhydrous dioxane in a 50 ml flame dried schelnk flask was cooled to 0ºC. To this solution was added thionyl chloride (385µl, 5.2 mmol, 1.5 eq.) and the reaction mixture was stirred for 3 hours at room temperature. The resulting yellowish solution was slowly poured into 400ml of anhydrous hexane. The precipitated was collected, washed once with anhydrous hexane and finally dissolved in ice cold chloroform. The chloroform fraction was washed with ice cold water, ice cold 5% sodium bicarbonate solution and with cold brine solution. The solution was subsequently dried over anhydrous Na_2SO_4 and concentrated to dryness under reduced pressure and immediately transferred to the glove box. Yield: 1.05 g, (64%)

FT–IR (DMF): ν = N-H (NCA, cbz) 3539; CH_2, 2926; CH_2, 2861; C=O (NCA)1859, 1794; C=O (cbz), 1683; N-H (cbz), 1508; C(=O)-O, 1257 cm^{-1}; ^{1}H NMR (400 MHz, $CDCl_3$): δ 9.31 ppm (s, 1H; NH), 9.14 ppm (s,1H; NH), 7.76 ppm (s,1H; NH), 7.34-7.13 ppm (m, 10H; ArH), 5.13 ppm (d, J = 8, 2H; CH_2), 5.02 ppm (d, J = 12, 2H; CH_2), ; ^{I3}C NMR (100 MHz, $CDCl_3$): δ 170.45, 162.98, 160.22, 155.3, 151.43, 136.47, 134.28, 128.39, 69.21, 67.06, 56.43, 42.84, 27.36, 23.97 ppm

2.3.2.5.4 Synthesis of alkyne terminated dicarbobenzoxy-poly-L-arginine (alkyne-dicbz-PLArg)(17)

Dicbz-L-arginine NCA (500 mg, 1.067 mmol) was dissolved in 5 mL of anhydrous DMF into a flame-dried 25 mL schlenk flask inside the glove box. The solution was stirred for 5 min after which a solution of propargylamine (2.93 mg, 0.0533 mmol for 20 mer and 5.87 mg, and 0.1067 mmol for 10 mer) in 100 µl of anhydrous DMF was added and stirred for 3 days at RT. The polymer was isolated by repeated precipitation in water and was then dried under high vacuum at 60°C. The polymer was characterized by GPC in DMF (0.1 mM LiBr, 60°C) and by ^{1}H NMR. Yield: 407 mg (82%)

2.3.2.5.5 Synthesis of alkyne terminated poly-L-arginine (alkyne-PLArg)(18)

To a solution of dicbz-poly-L-arginine (0.40 g) in 1 mL of trifluoroacetic acid was added 33% solution of HBr in acetic acid (6.97 ml, 10 equivalents with respect to the cbz groups). The reaction mixture was stirred for one hour at room temperature after which excess of diethyl ether was added. The precipitated polymer was centrifuged and the supernatant liquid was decanted. The residue was washed with fresh diethyl ether thrice and dried under vacuum at 45°C and characterized by ^{1}H NMR. Yield: 0.321mg (80%)

2.3.3 Analytical and characterization methods

2.3.3.1 FT-IR

FT-IR spectra were recorded on Perkin Elmer FT-IR spectrum GX instrument by using both solid and solution sampling. For solution sampling, samples were dissolved in anhydrous DMF, 10 µl of solution is placed in between the NaCl disc and spectra were recorded with 8 number of scan. For solid sampling, samples (3 mg) were mixed with solid KBr (97 mg), transformed to pellet and the spectra were recorded with 8 number of scan.

2.3.3.2 Size exclusion chromatography

Size-exclusion chromatography of all polypeptides were performed using a YoungLin Instrument GPC (Model-CTS30) equipped with refractive index (RI) detector. Separations were effected by 10^5 and 10^3 Å Phenomenex 5µ columns for all ε-cbz-poly-L-lysine, Poly-L-lysine-*b*-poly-L-leucine and Poly-L-benzylglutamate using 0.1 M LiBr in DMF eluent at 60°C. 10^5, 10^3 and 10^2 Å Phenomenex 5µ columns were used to separate Poly-*p*-methoxy-benzyl-L-glutamate and dicarbobenzoxy-poly-L-arginine using 0.1 M LiBr in DMF eluent at 60°C. A constant flow rate of 1 mL/min was maintained and the instrument was calibrated using polystyrene standards.

2.4 Results and discussions

2.4.1 Characterizations of alkyne terminated polypeptides

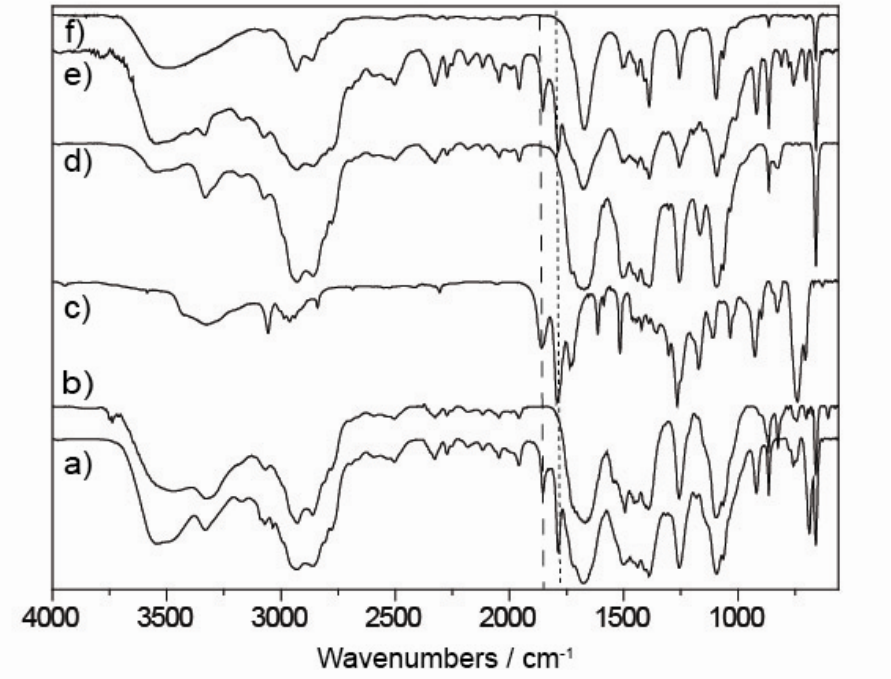

Figure 2.1: FT-IR spectra of a) ε-carbobenzoxy- α -carboxyl-L-Lysine anhydride, b) alkyne-cbz-PLL, c) *p*-Methoxybenzyl-L- glutamate NCA, d) alkyne terminated Poly-*p*-methoxy-benzyl-L-glutamate, e) dicarbobenzoxy-α-carboxyl-L-arginine anhydride and f) alkyne-dicbz-PLArg

2.4.1.1 Synthesis of alkyne terminated poly-L-lysine, poly-L-lysine-b-L-leucine and poly-L-benzylglutamate

The alkyne terminated poly-l-lysine (alkyne-PLL), poly-L-lysine-*b*-L-leucine (alkyne-PLL-*b*-PLLeu) and poly-L-benzyl glutamate (alkyne-PLBG) was obtained by the ring-opening polymerization (ROP) of amino acid N-carboxy anhydrides (NCAs) as shown in Scheme 2.3. Polymerization of the NCA monomer (M) was carried out by using N-TMS propargylamine[8, 13] as the initiator (I) using DMF as the solvent in the dry box. The M/I ratio used were 30, 20 and 10 for the synthesis of alkyne-cbz-poly-L-lysine. The polymerization reactions were monitored by the disappearance of the two CO stretching of NCA at 1851 and 1788 cm^{-1} by FT-IR (Figure 2.1a and b). The polymerization was allowed to proceed for

about 24 hrs after which the alkyne terminated polymers were precipitated by the addition of diethyl ether or water.

The ^{1}H NMR of the resulting polymers obtained in a mixture of $CDCl_3$ with 15% TFA displayed characteristic peaks for the polymer (Figure 2.2). The incorporation of the propargyl group was confirmed by the presence of the terminal proton of the propargyl end group at 2.2 ppm. Its molar mass was estimated from the relative intensity of peak at 3.98 ppm due to the methylenic proton in α-position of the acetylene moiety (-CH_2-C≡CH) with the peak characteristic of methylenic proton of the α proton of alkyne-cbz-PLL at 4.4 ppm as well as the methylenic proton of the cbz moiety at 5.12 ppm. All the other peaks in the proton NMR was in full agreement to the proposed structure. The degree of polymerization, calculated using the ratio of the intensity of the characteristic proton as described above, was determined to be 30, 22 and 11 (for M/I of 30, 20 and 10 respectively). The M_n calculated from ^{1}H NMR displayed a molecular weight of ~ 8000 (actual value 7945) gm/mol, ~ 5800 (actual value 5819) gm/mol and ~ 2900 (actual value 2937) for alkyne-cbz-PLL(30), alkyne-cbz-PLL(20) and alkyne-cbz-PLL(10). A very narrow molecular weight distribution (MWD) was obtained of alkyne-cbz-PLL(30), alkyne-cbz-PLL(20), and alkyne-cbz-PLL(10) from Gel Permeation Chromatography (M_w/M_n = 1.05, 1.07 and 1.04 respectively; note that the GPC molecular weight is with respect to polystyrene standards) (Figure 2.3a).

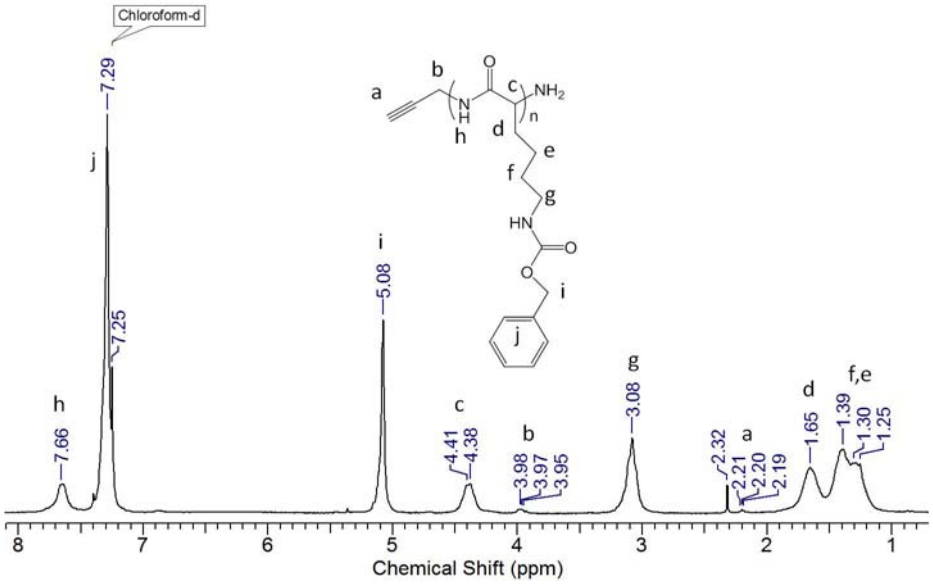

Figure 2.2: ^{1}H NMR of alkyne terminated ε-carbobenzoxy-poly-L-lysine

A similar methodology was adopted for the synthesis of alkyne-cbz-PLL-*b*-PLLeu and alkyne-PLBG (Scheme 2.3B, C). For the synthesis of block co-polymer, the polymerization was initiated with N-TMS propargylamine as the initiator and cbz-L-lysine NCA was the

monomer with an M/I ratio of 25. After >95% of the monomer was consumed (monitored by using FT-IR), 10 eq of L-leucine NCA with respect to the initiator was added as to the polymerization tube and the polymerization was carried out until >99% of the NCA was consumed. From the ^{1}H-NMR, the ratio of cbz-L-lysine to L-leucine in the block co-polymer was estimated to be 25:13 (Figure 2.4). The molecular weight of alkyne-cbz-PLL-*b*-PLLeu and alkyne-PLBG were determined to be ~8000 gm/mol and ~7000 gm/mol respectively. Further, a very narrow molecular weight distribution (MWD) was obtained from Gel Permeation Chromatography (M_w/M_n = 1.1 and 1.06 of alkyne-cbz-PLL-*b*-PLLeu and alkyne-PLBG respectively) (Figure 2.3a).

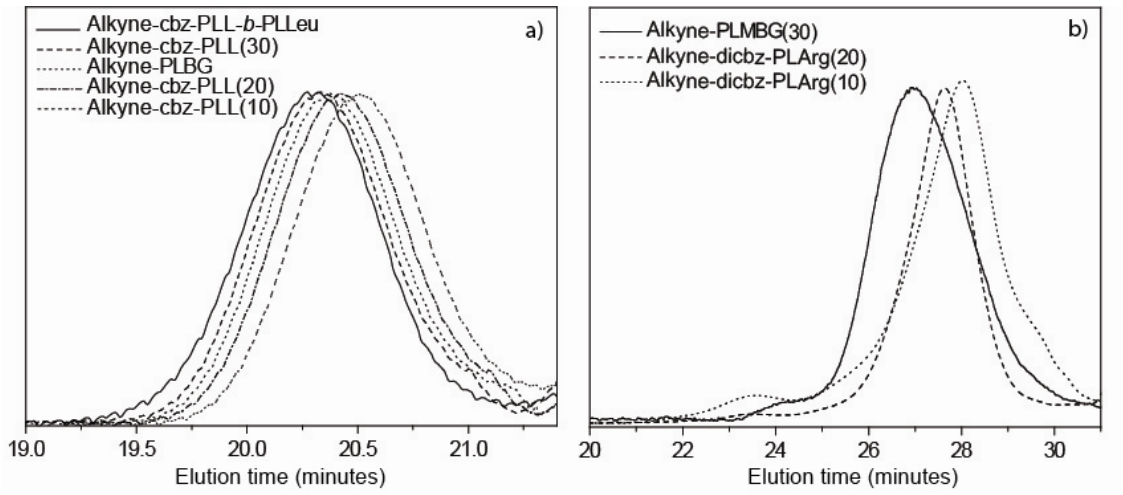

Figure 2.3: GPC spectra of a) alkyne ε-cbz-poly-L-lysine, alkyne poly-L-lysine-*b*-poly-L-leucine and alkyne poly-L-benzylglutamate and b) alkyne poly-*p*-methoxy-benzyl-L-glutamate and alkyne dicarbobenzoxy-poly-L-arginine.

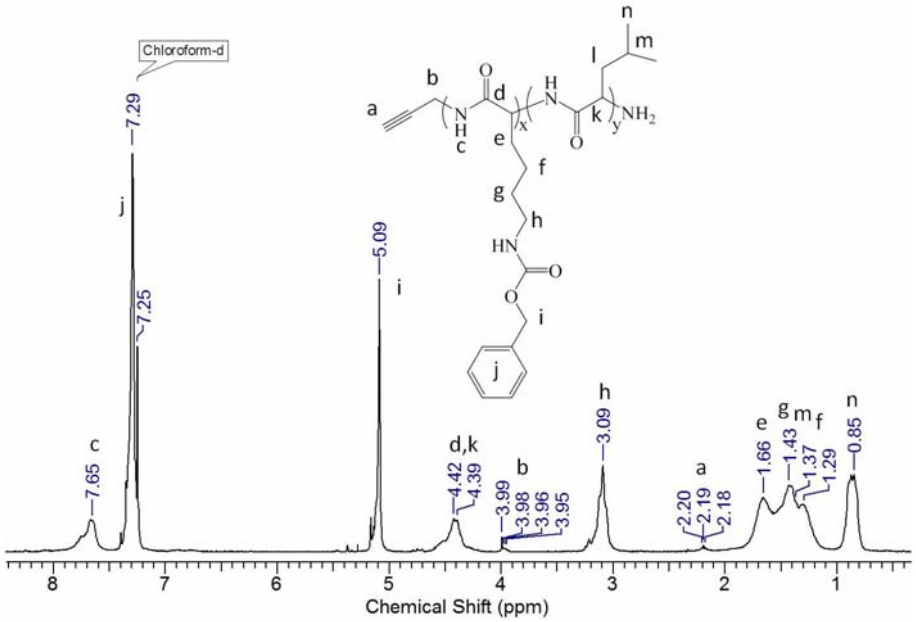

Figure 2.4: ^{1}H NMR of alkyne-cbz-PLL-*b*-PLLeu

The alkyne terminated poly-L-lysine (alkyne-PLL) and alkyne terminated poly-L-lysine-*b*-poly-L-Leucine (alkyne-PLL-*b*-PLLeu) was obtained after deprotection of the cbz group of the alkyne-cbz-PLL and alkyne-cbz-PLL-*b*-PLLeu polymer with HBr in trifluoroacetic acid. The completion of the reaction was monitored by the absence of the 1692 cm^{-1} peak in IR and the absence of benzylic proton in ^{1}H NMR (Figure 2.5). Further, after deprotection of the cbz group, the resultant alkyne-PLL polymer became very soluble in water but alkyne-PLL-*b*-PLLeu was soluble only in DMF-water or toluene/tert-butanol mixture. No further characterization of alkyne-PLL and alkyne-PLL-*b*-PLLeu was performed and it was directly used for next modification.

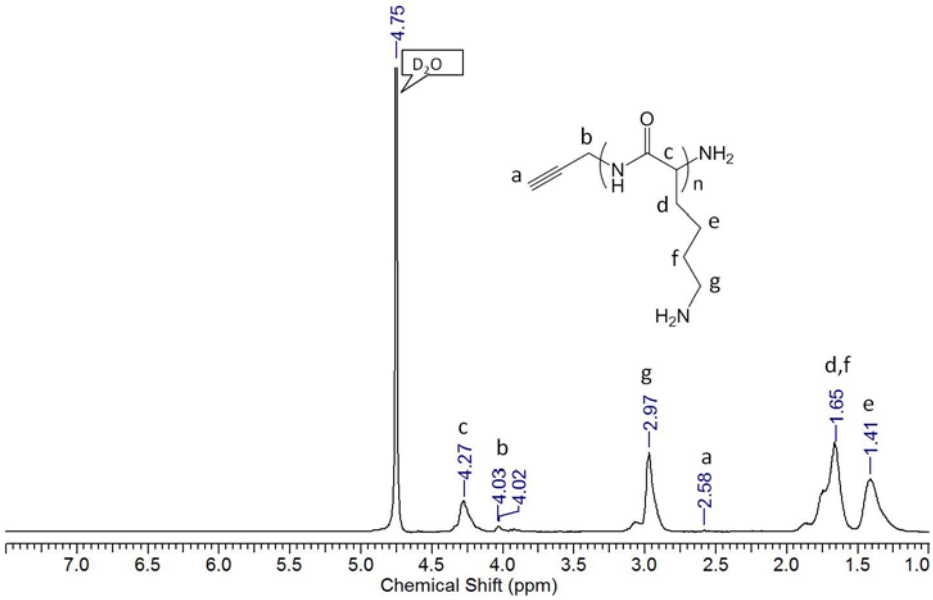

Figure 2.5: ^{1}H NMR of alkyne-PLL

2.4.1.2 Synthesis of alkyne terminated poly-L-glutamic acid (alkyne PLGA)

Alkyne terminated poly-*p*-methoxy-benzyl-L-glutamate were obtained by the ring-opening polymerization (ROP) of amino acid N-carboxy anhydrides (NCAs) as shown in Scheme 2.4. Polymerization of the NCA of *p*-methoxy-benzyl-L-glutamate monomer (M) was carried out by using N-TMS propargylamine as the initiator (I) using anhydrous DMF as the solvent in a glovebox (O_2 < 0.1ppm, H_2O <0.2 ppm). This initiator was chosen because it allows a good control over the molecular weight with a narrow polydispersity.[8, 13] For the synthesis of alkyne-PLGA(30), the M/I ratio used was 30. Polymerization was allowed to proceed for about 24 hrs in ice to control the molecular weight.[14] The polymerization reaction was monitored by FT-IR. The absence of two characteristic stretching vibrations of NCA

(C=O) indicates the formation of alkyne terminated poly-*p*-methoxybenzyl-L-glutamate (alkyne-PLMBG) (Figure 2.1). Subsequently, the poly-*p*-methoxybenzyl-L-glutamate was precipitated by the addition of DI water. A narrow molecular weight distribution (MWD) of alkyne-PLMBG(30) was obtained from Gel Permeation Chromatography (M_w = 9500 g.mol^{-1}; M_w/M_n = 1.08, note that the GPC molecular weight is with respect to polystyrene standards). (Figure 2.3b) Similarly, poly-*p*-methoxybenzyl-L-glutamate(40) was also prepared using the methodology described above.

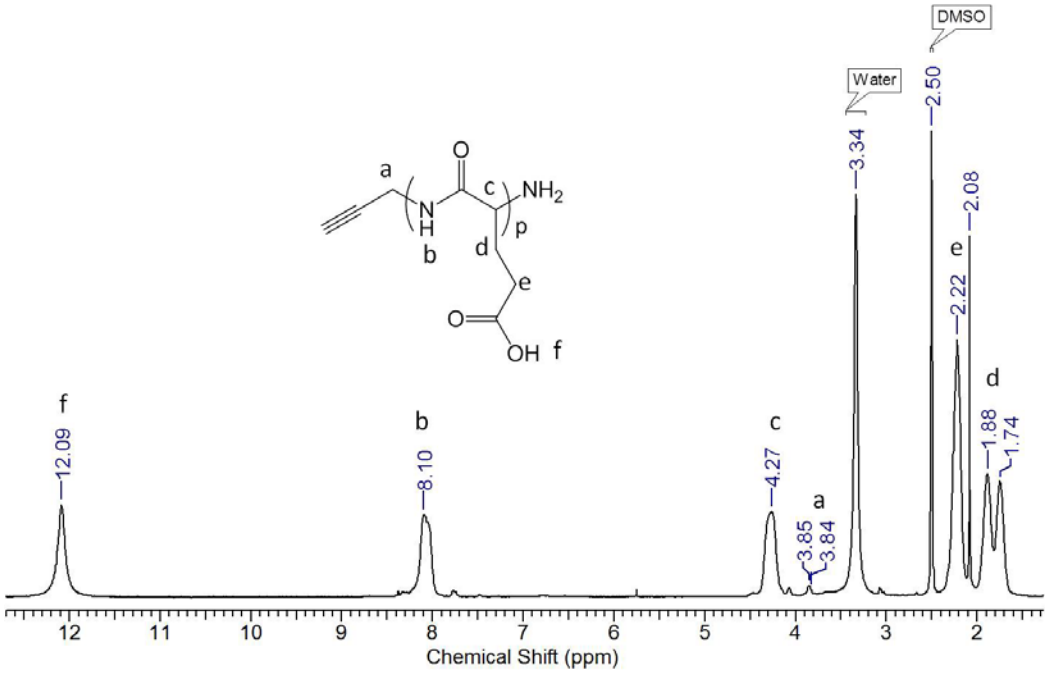

Figure 2.6: ^{1}H NMR of alkyne-PLGA

Alkyne-PLGA(30) was obtained after deprotection of the methoxybenzyl group of the alkyne terminated poly-*p*-methoxybenzyl-L-glutamate with a 10% solution of trifluoroacetic acid in DCM. After completion of the reaction, excess diethyl ether was added to precipitate the alkyne-PLGA(30). The characteristic proton of the p-methoxybenzyl group was absent in ^{1}H NMR indicating complete deprotection of the methoxybenzyl group in the alkyne-PLGA(30) (Figure 2.6). The molar mass of the polymer was estimated from the relative intensity of the peak at 3.85 ppm due to the methylenic proton in the α-position of the acetylene moiety (-CH_2-C≡CH) with the peak characteristic of the methylenic proton of the α proton of alkyne-PLGA at 4.27 ppm. All other peaks in the ^{1}H NMR were in full agreement with the polymer proposed structure. The degree of polymerization calculated using the ratio of the intensity of the characteristic proton as described above, was determined to be 33 corresponding to a molecular weight around 4300 g.mol^{-1}. Similarly, for alkyne-PLGA(40), the degree of polymerization calculated using the ratio of the intensity of the characteristic

proton as described above, was determined to be 39 corresponding to a molecular weight around 5000 g.mol^{-1}. No further characterization of alkyne-PLGA(30) and alkyne-PLGA(40) was performed and they were directly used for CuAAC with azide functionalized silica nanoparticles.

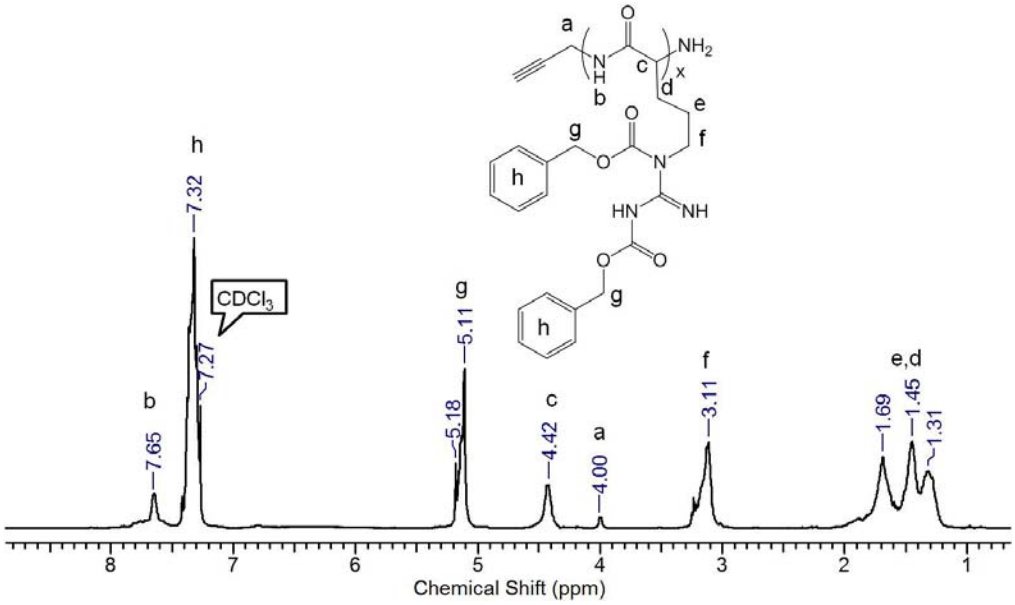

Figure 2.7: ^{1}H NMR of alkyne-dicbz-PLArg

2.4.1.3 Synthesis of alkyne terminated poly-L-arginine (alkyne-PLArg)

The alkyne terminated poly-L-arginine (alkyne-PLArg) was obtained by the ring-opening polymerization (ROP) of amino acid N-carboxy anhydrides (NCAs) as shown in Scheme 2.5. Polymerization of the alkyne terminated dicarbobenzoxy-L-arginine (alkyne-dicbz-PLArg) NCA monomer (M) was carried out by using propargylamine as the initiator (I) using anhydrous DMF as the solvent in the glove box. Since the initiator bears a terminal alkyne group, it was incorporated at the chain end of the poly-L-arginine. Two different M/I ratio of 20 and 10 was used. The polymerization reaction was monitored by IR and was allowed to proceed for 60 hrs. The completion of the polymerization was monitored by the absence of the NCA CO stretching at 1794 and 1859 cm^{-1} (Figure 2.1). After completion of polymerization, the alkyne-dicbz-PLArg was precipitated by the addition of excess water. The ^{1}H NMR of the resulting polymer showed characteristic peaks for the polymer and the propargyl end methylene proton was also observed at 4 ppm (Figure 2.7). Its molar mass was estimated by NMR from the relative intensity of peak at 4 ppm due to the methylenic proton in α-position of the acetylene moiety (-CH_2-C≡CH) with the peak characteristic of methylenic proton of the α proton of alkyne-dicbz-PLArg at 4.42 ppm as well as the

methylenic proton of the cbz moiety at 5.11 ppm. The degree of polymerization, calculated using the ratio of intensity of the characteristic protons as described above, was determined to be 18 and 9 (for M/I of 20 and 10 respectively). The M_n calculated from ^{1}H NMR displayed a molecular weight of ~ 7600 (theoretical value 7687) and ~ 3800 (theoretical value 3871) gm/mol for alkyne-dicbz-PLArg(20) and alkyne-dicbz-PLArg(10). A very narrow molecular weight distribution (MWD) was obtained of alkyne-dicbz-PLArg(20) and alkyne-dicbz-PLArg(10) from Gel Permeation Chromatography (M_w/M_n = 1.06 and 1.11 respectively; note that the GPC molecular weight is with respect to polystyrene standards) (Figure 2.3b).

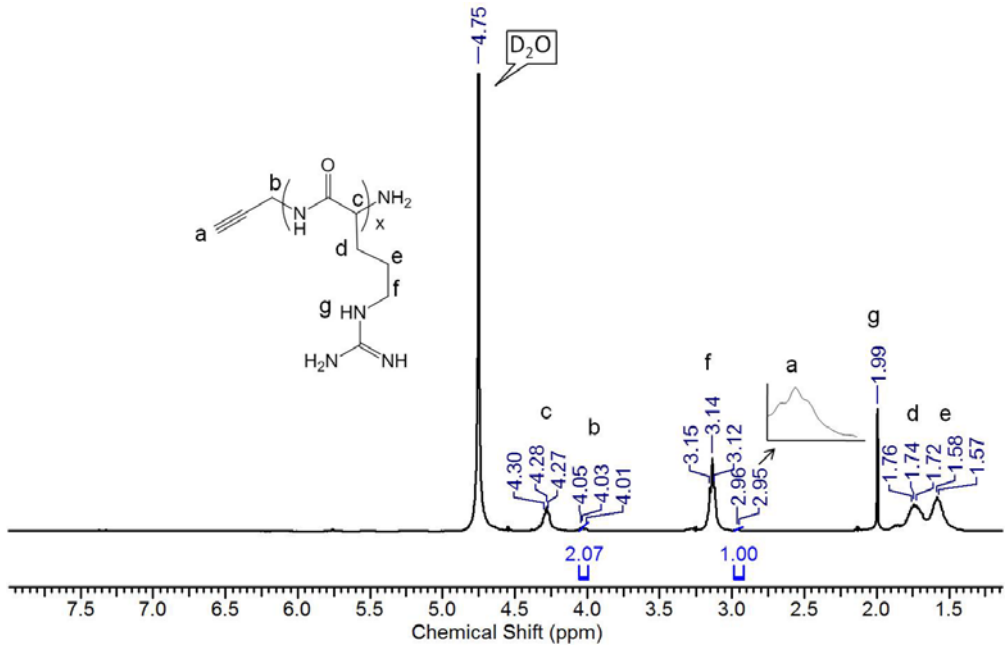

Figure 2.8: ^{1}H NMR of alkyne-PLArg

The alkyne terminated poly-L-arginine, alkyne-PLArg(20) and alkyne-PLArg(10), was obtained after deprotection of the cbz group of the alkyne-dicbz-PLArg polymer. 33% HBr in acetic acid was used to deprotect the cbz groups. The completion of the reaction was monitored by the absence of the 1690 cm^{-1} in IR. The resulting polymers obtained after work-up are highly soluble in water. ^{1}H NMR (Figure 2.8) of polymer was performed to establish the complete deprotection of the cbz groups after which the alkyne-PLArgs were directly used for further applications.

2.5 Conclusion and summary

In summary, all the adapted synthetic methodologies for the preparation of the NCA monomers were high yielding and easy to handle. For the synthesis of alkyne terminated homo- and block co- polypeptides NCA ring opening polymerization were successfully used.

All the NCA polymerization reactions were monitored by FT-IR. For the synthesis of the block co- polypeptides, second monomers were added into the reaction mixture after 95% (determined by FT-IR) of the first NCA monomer was consumed. N-TMS propargyl amine was used as the initiator allows the synthesis of polypeptides with very low polydispersity and precise molecular weights. It also leads to the incorporation of a terminal alkyne at the polymer end which allows it to be further modified using CuAAC. All NCA polymerizations were carried out inside the glove box (O_2 > 0.1 ppm and H_2O >1 ppm) and the synthesized polypeptides were characterized by FT-IR, GPC and NMR.

3.6 References

1. Deming, T. J., Polypeptide Materials: New synthetic methods and applications. *Advanced Materials* **1997,** 9, (4), 299-311.
2. Deming, T.; Klok, H.-A.; Schlaad, H., Polypeptide and Polypeptide Hybrid Copolymer Synthesis via NCA Polymerization
Peptide Hybrid Polymers. In Springer Berlin / Heidelberg: 2006; Vol. 202, pp 1-18.
3. Deming, T. J., Synthetic polypeptides for biomedical applications. *Progress in Polymer Science* **2007,** 32, (89), 858-875.
4. Lu, H.; Wang, J.; Bai, Y.; Lang, J. W.; Liu, S.; Lin, Y.; Cheng, J., Ionic polypeptides with unusual helical stability. *Nat Commun* **2011,** 2, 206.
5. Chen, C.; Wang, Z.; Li, Z., Thermoresponsive Polypeptides from Pegylated Poly-l-glutamates. *Biomacromolecules* **2011,** 12, (8), 2859-2863.
6. Zhang, Z.; Chen, L.; Deng, M.; Bai, Y.; Chen, X.; Jing, X., Biodegradable thermo- and pH-responsive hydrogels for oral drug delivery. *Journal of Polymer Science Part A: Polymer Chemistry* **2011,** 49, (13), 2941-2951.
7. Yang, C.-Y.; Song, B.; Ao, Y.; Nowak, A. P.; Abelowitz, R. B.; Korsak, R. A.; Havton, L. A.; Deming, T. J.; Sofroniew, M. V., Biocompatibility of amphiphilic diblock copolypeptide hydrogels in the central nervous system. *Biomaterials* **2009,** 30, (15), 2881-2898.
8. Lu, H.; Cheng, J., Hexamethyldisilazane-Mediated Controlled Polymerization of a-Amino Acid N-Carboxyanhydrides. *Journal of the American Chemical Society* **2007,** 129, (46), 14114-14115.
9. Bergmann, M.; Zervas, L.; Ross, W. F., ON PROTEOLYTIC ENZYMES. VII. THE SYNTHESIS OF PEPTIDES OF l-LYSINE AND THEIR BEHAVIOR WITH PAPAIN. *J. Biol. Chem.* **1935,** 111, (1), 245-260.
10. Feijen, J.; Sederel, W. L.; de Groot, K.; de Visser, A. C.; Bantjes, A., Synthesis and viscosity behavior of poly(γ-p-biphenylmethyl-L-glutamate) in benzene/dichloroacetic acid mixtures, a comparison with poly(γ-benzyl-L-glutamate). *Die Makromolekulare Chemie* **1974,** 175, (11), 3193-3206.

11. Gandhi, J. V.; Maher, J. V.; Shaffer, K. A.; Chapman, T. M., Capillary Wave Studies of Multiblock Polypeptide Copolymers at the Air/Water Interface. *Langmuir* **1997,** 13, (22), 5933-5940.

12. Hayakawa, T.; Kondo, Y.; Yamamoto, H.; Murakami, Y., The Synthesis of Poly-L-arginine Hydrobromide and Copolymers of L-Arginine and Other Amino Acids. *Bulletin of the Chemical Society of Japan* **1969,** 42, (2), 479-482.

13. Lu, H.; Wang, J.; Lin, Y.; Cheng, J., One-Pot Synthesis of Brush-Like Polymers via Integrated Ring-Opening Metathesis Polymerization and Polymerization of Amino Acid N-Carboxyanhydrides. *Journal of the American Chemical Society* **2009,** 131, (38), 13582-13583.

14. Habraken, G. J. M.; Peeters, M.; Dietz, C. H. J. T.; Koning, C. E.; Heise, A., How controlled and versatile is N-carboxy anhydride (NCA) polymerization at 0°C? Effect of temperature on homo-, block- and graft (co)polymerization. *Polymer Chemistry* 1, (4), 514-524.

Chapter 3

Synthesis of Polypeptide Grafted Silica Nanoparticles and their Application as Biomaterials

This chapter was adapted from

1) Synthesis and Characterization of Poly-L-lysine-Grafted Silica Nanoparticles Synthesized via NCA Polymerization and Click Chemistry

Mrityunjoy Kar, P. S. Vijayakumar, B. L. V. Prasad and Sayam Sen Gupta

Langmuir, **2010**, *26* (8), pp 5772–5781

2) Synthesis of Poly-L-glutamic Acid Grafted Silica Nanoparticles and Their Assembly into Macroporous Structures

Mrityunjoy Kar, Minois Pauline, Kamendra Sharma, Guruswamy Kumaraswamy and Sayam Sen Gupta

Langmuir, **2011**, 27 (19), pp 12124–12133

3.1 Introduction

Surface modification of silica nanoparticles by chemically bound polymers have become a quickly expanding field of research.[1, 2] Polymer coated silica nanoparticles represent organic-inorganic hybrids, where the polymer coating imparts functional surface properties on the rigid inorganic core. The nanoparticulate nature of such hybrids and the ability to vary functionality by choice of polymer coating make such systems highly versatile. Polymer coated silica nanoparticles have found usage in coatings,[3] flame retardants,[4] optical devices,[5] photoresist materials,[6] proton exchange membranes[7] and sensors.[8] Further, these nanoconjugates also have found usage in biomedical applications such as drug delivery, gene delivery,[9, 10] tissue engineering,[11] as antimicrobials,[12-14] in biosensing, separations and in purification of biological molecules.[2, 15, 16] The covalent grafting of polymers onto a silica nanoparticle is typically carried out via a "grafting to" or "grafting from" methodology.[1] Both these techniques have been used to graft various polymers like polystyrene,[17, 18] polyacrylamide[19, 20] and PMMA[17, 21, 22] onto the silica surface. For example, the functionalization of silica particles by PMMA involved the immobilization of the initiator molecule onto the silica surface followed by surface initiated ATRP of methylmethacrylate.[23] Similarly, other controlled radical polymerizations like RAFT,[9, 22, 24-26] NMP,[9, 27] ROP[28, 29] and ROMP[30, 31] have been used successfully to graft polymer brushes onto silica nanoparticles. The surface modification of silica nanoparticles using the "grafting to" technique poses a far greater challenge in achieving high graft density as the attachment of the first polymer chain hinders their subsequent attachment due to steric crowding. Recently, a combination of RAFT and click chemistry was employed to achieve a high density grafting of polymers onto silica nanoparticles by the "grafting to" methodology.[26, 32] However, the grafting density is still lower than those obtained by the corresponding "grafting from" methodology.

Polypeptide polymer grafted silica particles are of considerable interest because the ordered secondary structure of the polypeptide grafts (α-helix or β-sheet) possess a wide range of structural and functional properties.[33] In addition to this, the presence of a wide range of side chains (such as amines, thiols and carboxylic acid) in the polypeptides make them responsive to external stimuli such as pH, temperature, solvent and electrolytes.[34] Therefore, polypeptide grafted silica particles can possibly have various applications in coatings, catalysis, gene delivery, among other things. There have been recent reports in which polypeptides have been grafted onto inorganic surfaces such as quartz planar

surfaces,[35-38] colloidal silica particles,[39, 40] colloidal silica crystals[41] and ordered mesoporous materials.[42] In most of these reports, the polypeptide has been incorporated by surface initiated ring opening polymerization of the N-carboxyanhydrides of their corresponding amino acids onto an inorganic surface functionalized by a primary amine. Schouten *et al.* have very elegantly demonstrated the synthesis of several nanometers thick homogeneous film of poly(γ-benzyl-L-glutamate) onto silicon wafers and quartz slides using this methodology.[37] However, it should be kept in mind that a broad molecular weight distribution of poly-(γ-benzyl-L-glutamate) will probably be expected since all chains will not grow up to the same length.

Synthesis of poly-L-lysine grafted silica nanoparticles would be of considerable interest since the high density of cationic charges on the surface would have many applications including gene delivery[10, 43, 44] and antimicrobial agents.[13, 14] It has been shown that materials with high levels of positive charges are capable of conferring antimicrobial properties, as these cationic species are able to disrupt bacterial membranes.[45] Using this approach, various antimicrobial surfaces have been prepared by covalently anchoring cationic antimicrobials to surfaces.[22, 46] Moreover, poly-L-lysine grafted silica nanoparticles, if prepared, would have multiple cationic attachment point, a property necessary for membrane penetration.[45] Hence, a very high density of low molecular weight poly-L-lysine grafted onto silica particles would be an ideal candidate as antimicrobial. Since unprotected low molecular weight poly-L-lysine graft was required, we developed a "grafting to" methodology that allowed us to covalently attach preformed poly-L-lysine onto silica nanoparticles at a very high grafting density.

Poly-L-glutamic acid (PLGA) is a synthetic poly amino acid that is biodegradable and contains anionic (carboxyl) functional groups which can be further chemically modified to incorporate functional organic and biomolecules. As PLGA is a biocompatible polypeptide, it has been used to prepare scaffolds for drug delivery [47, 48]and tissue engineering applications[49] and, as biodegradable MRI contrast reagents.[22, 50, 51] Interestingly, PLGA is stimuli sensitive and adopts different conformations on varying the pH.[47, 52-54] At pH > 5, the carboxylic acid side chains dissociate and the polypeptide behaves like a polyelectrolyte (and is rendered water soluble). At pH < 4, the carboxylic acid groups do not dissociate and the polypeptide adopts a compact alpha-helical conformation, and becomes progressively more water insoluble. Thus, our target system, PLGA-core-silica-shell nanoparticles represent interesting stimuli sensitive organic-inorganic hybrids, with potential applications as biocompatible building blocks for biomedical scaffolds.

Poly-L-arginine based nanocarriers are widely accepted for gene delivery and drug delivery. In 1965, Ryser & Hancock [55] first demonstrated that homopolymers of cationic amino acids (< 100 kDa) enhance uptake into the *in vitro* cell lines, with this seminal report, a new era has been started to study cellular uptake of various cationic polymers and polypeptides. Mitchell et al. [56] reported poly-L-arginine (from 7 mer to 20 mer) can enter more efficiently than any other cationic homopolymers and Paul et al.[57] reported a comparative study of nonaarginine with tat peptides and demonstrated that poly-arginine (9 mer) is 20 fold more efficient transporter than $tat_{(49-57)}$-peptides. From last decades, poly-arginine has been used as an effective cargo molecule transporter [58-60] and drug delivery [61-63] carriers. Thus, poly-L-arginine grafted silica nanoparticles are very much interesting for enhanced cellular uptake with potential bio-medical applications.

The synthesis of a polypeptide silica nanoparticles hybrids using "grafting to" approach was performed by employing a combination of NCA polymerization[64] and click chemistry.[65, 66] Click chemistry is being increasingly used in polymer and materials chemistry because of its exceptionally high yield, ease and compatibility with a broad repertoire of functional groups that allows fast and simple creation of well defined complex materials.[67] The introduction of an alkyne or azide group on to the polypeptides during its synthesis would give us a handle to attach it efficiently onto its binding partners on the silica surface via an 1,2,3-triazole linkage. Therefore, an alkyne terminated poly-L-lysine, poly-L-glutamic acid and poly-L-arginine were synthesized by using the ring opening polymerization of NCAs with N-TMS propargylamine or propargylamine as the initiator (Chapter 2). All the alkyne terminated polypeptides, formed after deprotection of the protecting functional groups, were then successfully attached to an azide labeled silica nanoparticles by the azide alkyne cycloaddition (CuAAC) "click chemistry" to provide very high grafting densities. All the polypeptide silica conjugates have been very well characterized by multinuclear (^{13}C and ^{29}Si) solid state NMR, TGA, FT-IR and TEM. A similar methodology was adopted to synthesize poly-L-lysine-*b*-poly-L-leucine and poly-L-γ-benzyl glutamte grafted silica nanoparticles to demonstrate that this can be extended to other block and co-polypeptides. This chapter also reports the efficacy of the poly-L-lysine and poly-L-lysine-*b*-poly-L-leucine silica hybrid nanoparticles as antimicrobial agents for both Gram-negative *E. coli* and Gram-positive *bacillus subtilus*. The PLGA grafted silica conjugate particles, although very well dispersed in water, reversibly aggregates on lowering the pH of solution. This is mostly driven by the change in PLGA structure upon changing the pH of the solution. The

preliminary results were shown by the preparation of three dimensional macroporous structures, with oriented pores by ice templating[21, 68-71] of aqueous dispersions of silica-PLGA. The interest in constructing macroporous structures from such nanoparticulate starting blocks is due to their potential use for tissue engineering applications. The PLGA shell on the composite particles renders them biocompatible and, it is possible to independently engineer the mechanical stiffness and toughness of the scaffold, to match those of the host tissue, through control over the PLGA molecular weight relative to the size of the silica particle. Using this method, one can control the pore dimensions, their orientation and geometry when macroporous scaffolds are prepared using methods such as ice templating.[21, 68-71] Silica-PLArgs disperses in water extremely well and have very high surface positive charge. The surface grafted poly-L-arginine displayed enhanced cellular uptake of the silica-PLArg nanoconjugates into various cell lines.

3.2 Experimental section

3.2.1 Materials

Ludox (TM 50), 3-chloropropyltriethoxysilane, tetrabutylammonium bromide, disodium bathophinanthroline sulphate and 6-Fluorescein-5(6)-carboxamido hexanoic acid *N*-hydroxysuccinimide ester were obtained from Aldrich chemicals. Copper sulphate, copper Iodide, sodium azide, sodium ascorbate, trifloro acetic acid, 33% HBr in Acetic acid and all the solvents were obtained from Meark, India. Tris-(hydroxypropyltriazolylmethyl) amine (THPTA) was synthesized according to the earlier reports.[72]

3.2.2 Synthesis

3.2.2.1 Synthesis of 3- Azidopropyl triethoxysilane (AzPTES)

3-chloropropyltriethoxysilane (abbreviated as Cl-PTES; 2 g, 8.3 mmol) was added to a solution of sodium azide (1.08 g, 16.6 mmol) and tetrabutylammonium bromide (0.644 g, 2 mmol) in dry acetonitrile (50 mL), under nitrogen atmosphere. The reaction mixture was stirred under reflux for 18 h. After completion of the reaction, the solvent was removed under reduced pressure. The crude mixture was diluted in n-pentane and the suspension was filtered over celite. Solvent was removed from the resulting filtrate and the crude oil obtained was distilled under reduced pressure of 0.025 mbar at 62°C to give AzPTES (3-azidopropyltriethoxysilane) as a colorless liquid. Yield: 1.52 g, 74%.

FT-IR (NaCl, cm^{-1}): ν 2098 ($-N=N^{+}=N^{-}$, s). ^{1}H NMR (400 MHz, $CDCl_3$): δ 0.66 ppm (t, 2H, J= 8.25 Hz), 1.21 ppm (t, 3H, J= 6.88 Hz), 1.66-1.73 ppm (m, 2H), 3.25 (t, 2H, J = 7.16 Hz), 3.80 ppm (q, 2H, J = 6.88 Hz).^{13}C NMR (100 MHz, $CDCl_3$): δ 58.41, 53.8, 22.64, 18.23, 7.59 ppm.

3.3.2.2 Synthesis of azide grafted silica nanoparticles (silica-N_3)

2.4 g of Ludox sol was diluted with 30 mL DI water-ethanol (1:1) mixture and taken into a Teflon beaker. AzPTES (494 mg, 2 mmol) was added into the homogeneous dispersion. The reaction mixture was stirred for 23 h at room temperature after which the reaction mixture was centrifuged at 12000 rpm for 30 min. The clear supernatant liquid was decanted from the solid deposit. The solid mass obtained was sonicated with ethanol for 20 min and then centrifuged three times. It was then dried at 50°C under high vacuum for 6 hrs. The particles were characterized by FT-IR, CP MAS NMR, SEM, TEM, DLS and elemental analysis. Yield: 0.512 g.

3.3.2.3 Synthesis of Poly-L-lysine grafted silica nanoparticles (silica-PLL)

For CuAAC, the azide functionalized silica nanoparticles were incubated with 2-4 equivalents of the corresponding propargyl alcohol or alkyne-PLL in Tris Buffer (pH 7, 150 mM) containing CuI (0.5 equivalent), disodium bathophenanthroline sulphonate (0.5 equivalent) and sodium ascorbate (4 equivalent). In a typical reaction, azide grafted silica nanoparticles (50 mg, 0.035 mmol of azide) was incubated with alkyne-PLL (464.8 mg, 0.14 mmol, 4 equivalent or 232 mg, 0.07 mmol, 2 equivalent) in 5 mL Tris buffer mixture (pH 7, 100 mM) containing sodium ascorbate (28 mg, 0.14 mmol, 4 equivalent) and copper iodide (3.3 mg, 0.018 mmol, 0.5 equivalent) and disodium sulphonated bathophenanthroline (9.6 mg, 0.018, 0.5 equivalent). The reaction mixture was subjected to three freeze-pump-thaw cycles for rigorous exclusion of dioxygen. The CuAAC was allowed to proceed for 24 hrs with stirring. After completion of the reaction, the mixture was taken into a centrifuge tube and centrifuged for 20 min at 12000 rpm. The supernatant liquid was decanted off and the solid residue was washed with water (2 times), ethanol (2 times), 0.1 M sodium ascorbate (2 times), 0.1 M N,N-diethyldithiocarbamate sodium in ethanol (2 times) and ethanol (2 times). It was finally washed with 0.1 M HCl (2 times) and then stored as a suspension in water. For preparation of samples for NMR and IR, a part of the PLL-silica solution was washed in ethanol and dried under vacuum at 50°C. The product obtained using 4 equivalent of alkyne-

PLL will be referred as Silica-PLL-A and the one obtained by using 2 equivalent of alkyne-PLL will be referred to as Silica-PLL-B. Yield: ~65 mg

The similar protocol was used to 'click' with 4 equivalent of propargyl alcohol to investigate the accessibility of the surface azide on the silica nanoparticle. Yield: ~47 mg

3.2.2.4 Synthesis of poly-L-lysine-block-poly-L-leucine grafted silica nanoparticle (silica-PLL-b-PLLeu)

For CuAAC, azide grafted silica nanoparticles (30 mg, 0.021 mmol of azide) was incubated with alkyne-PLL-*b*-PLLeu (362 mg, 0.063 mmol, 3 equivalent) in 1.5 mL Tris buffer(pH 7, 150 mM) and DMF mixture (1:1) containing sodium ascorbate (16 mg, 0.084 mmol, 4 equivalent) and copper iodide (3.99 mg, 0.021 mmol, 1 equivalent) and disodium sulphonated bathophenanthroline (16 mg, 0.031, 1.5 equivalent). The reaction mixture was subjected to three freeze-pump-thaw cycles for rigorous exclusion of dioxygen. The CuAAC was allowed to proceed for 24 hrs with stirring. After completion of the reaction, the mixture was taken into a centrifuge tube and centrifuged for 20 min at 12000 rpm. The supernatant liquid was decanted off and the solid residue was washed with DMF (2 times), water (2 times), 0.1 M N,N-diethyldithiocarbamate sodium in ethanol (2 times) and acetone (2 times). It was finally washed with ethanol then stored as a suspension in ethanol. For preparation of samples for IR, a part of the silica-PLL-*b*-PLLeu nanoconjugate solution was washed in ethanol and dried under vacuum at 50°C. Yield: 42 mg

3.2.2.5 Synthesis of poly-L-benzylglutamate grafted silica nanoparticle (silica-PLBG)

For CuAAC, azide grafted silica nanoparticles (30 mg, 0.021 mmol of azide) was incubated with alkyne-PLBG (411 mg, 0.063 mmol, 3 equivalent) in 1.5 mL DMF, copper iodide (3.99 mg, 0.021 mmol, 1 equivalent) and bipyridyl (10 mg, 0.063, 3 equivalent). The reaction mixture was subjected to three freeze-pump-thaw cycles for rigorous exclusion of dioxygen. The CuAAC was allowed to proceed for 24 hrs with stirring. After completion of the reaction, the mixture was taken into a centrifuge tube and centrifuged for 20 min at 12000 rpm. The supernatant liquid was decanted off and the solid residue was washed with DMF (2 times), water (2 times), 0.1 M N,N-diethyldithiocarbamate sodium in ethanol (2 times) and acetone (2 times). It was finally washed with ethanol then stored as a suspension in Ethanol. For preparation of samples for IR, a part of the silica-PLBG solution was washed in ethanol and dried under vacuum at 50°C. Yield: 40 mg

3.2.2.6 Synthesis of poly-L-glutamic acid grafted silica nanoparticle (silica-PLGA)

Azide-grafted silica nanoparticles (40 mg, 0.014 mmol of azide) were incubated with alkyne-poly-L-glutamic acid (318.4 mg, 0.040 mmol, 2.8 equivalent) in 2 mL of Tris buffer (pH 7, 100 mM) and a DMF (7:3) mixture containing sodium ascorbate (22.6 mg, 0.057 mmol, 4 equivalent), copper iodide (2.7 mg, 0.0071 mmol, 0.5 equivalent), and disodium sulfonated bathophenanthroline (8 mg, 0.0071 mmol, 0.5 equivalent). The reaction mixture was subjected to three freeze-pump-thaw cycles for rigorous exclusion of dioxygen. CuAAC was allowed to proceed for 40 hrs with stirring at 60°C. After completion of the reaction, the mixture was taken into a centrifuge tube and centrifuged for 20 min at 12000 rpm. The supernatant liquid was decanted off and the solid residue was washed with water (2 times), ethanol (2 times), 0.1 M sodium ascorbate (2 times), 0.1 M N,N-diethyldithiocarbamate sodium in ethanol (2 times) and finally with acetone (2 times) and stored as a suspension in DI water. A part of the silica-PLGA dispersion was washed with acetone and dried under vacuum at 60°C, for IR, NMR and TGA characterization. Yield: ~ 45 mg

3.2.2.7 Synthesis of poly-L-arginine grafted silica nanoparticles (silica-PLArg)

A different and very efficient protocol for CuAAC was adapted to synthesize poly-L-arginine grafted silica nanoparticles established by our group. The azide functionalized silica nanoparticles were incubated with 1equivalent of the corresponding alkyne-PLArg in PBS (pH 7.4, 150 mM) containing $CuSO_4$ (0.25 equivalent), THPTA (1.25 equivalent), aminoguanidine HCl (2.5 equivalent) and sodium ascorbate (2.5 equivalent). In a typical reaction, azide grafted silica nanoparticles (20 mg, 0.016 mmol of azide) were incubated with alkyne-PLArg(20) and alkyne-PLArg(10) (48 mg, 1 equivalent and 32 mg, 1 equivalent, respectively) in 2 mL PBS (pH7.4, 150 mM) containing $CuSO_4$ (0.99 mg) and THPTA (8.68 mg), aminoguanidine HCl (4.42 mg) .The reaction mixture was subjected to three freeze-pump-thaw cycles for rigorous exclusion of dioxygen and then added sodium ascorbate (14.85 mg). The CuAAC was allowed to proceed for 18 hrs with stirring at RT. After completion of the reaction, the mixture was taken into a centrifuge tube and centrifuged for 20 min at 13000 rpm. The supernatant liquid was decanted off and the solid residue was washed with water (2 times), 0.1 M N,N-diethyldithiocarbamate sodium in ethanol (2 times) and ethanol (2 times). It was finally washed with 0.1 M HCl and with ethanol and dried under vacuum at 50°C. Yield: ~ 24 mg.

3.2.2.8 Synthesis of macroporous silica-PLGA scaffold

Ice templating method was used to prepare macroporous scaffolds of silica-PLGA colloidal suspensions in water with directional freezing.[21, 68-70] A colloidal suspension of silica-PLGA (15 wt %; 300 µl) in a glass tube (12 mm diameter) was slowly lowered into liquid nitrogen and the sample was allowed to freeze for 10 min. Frozen samples were then freeze-dried using a Heto power dry LL3000 freeze-dryer to afford macroporous silica-PLGA.

3.2.2.9 EDCI coupling of silica-PLGA and PEI

The Silica-PLGA scaffold was incubated into a solution of PEI (5mg/ml) in anhydrous dichloromethane for 30 minutes. EDCI (30 mg/ml solution in anhydrous dichloromethane) was then added into the reaction mixture. The coupling reaction was allowed to proceed for 8 hrs after which the solvent was pipetted out from the container. Fresh dichloro methane (1 mL) was then added and this process for repeated for five times to remove unreacted EDCI as well as the unreacted PEI. The sample was then dried in vaccum at 50°C for 6 hrs.

3.2.2.10 Synthesis of fluorescein labeled silica-PLArg

A solution of silica-PLArg (1mg/ml) was incubated with 10 µl DMSO solution of 6-[fluorescein-5(6)-carboxamido] hexanoic acid *N*-hydroxysuccinimide ester (stock solution 1mg/ml). The mixture was wrapped with aluminium foil and stirred for 4 hrs at room temperature. After completion of the reaction the mixture was centrifuged at 15000 rpm for 5 min and washed with methanol three times. Finally washed once with DI water and dried the samples in vacuum at 70°C for 12 hrs.

3.2.3 Analytical and characterization methods

3.2.3.1 FT-IR

FT-IR spectra were recorded on Perkin Elmer FT-IR spectrum GX instrument by using solid sampling. For solid sampling, samples (3 mg) are mixed with solid dried KBr (97 mg), transformed to pellet and the spectra were recorded with 8 number of scan.

3.2.3.2 ^{29}Si and ^{13}C solid state CP MAS NMR

^{29}Si and ^{13}C Cross Polarization Magic Angle Spinning (CP MAS) NMR experiments were carried out on a Bruker AVANCE 300 wide bore spectrometer equipped with a

superconducting magnet with a field of 7.1Tesla. The operating frequencies for ^{13}C and ^{29}Si were 300 MHz, 75.4 MHz and 59.6 MHz respectively. The samples were packed into a 4mm zirconia rotor and loaded into a 4mm BL MAS probe and spun about the magic angle (54.74) at 10 KHz using a standard ramp-CP pulse sequence was used for both the experiments. The RF-powers were 50 kHz and 60 kHz for the ^{29}Si and ^{13}C CPMAS experiments. The contact times were 6ms and 3ms for the ^{29}Si and the ^{13}C CPMAS experiments. All the chemical shifts were referenced to TMS. Typically 10,000 to 25,000 scans with a recycle delay of 3s were collected depending on the sensitivity of the sample.

3.2.3.3 Thermogravimetric analysis (TGA)

Thermogravimetric analysis (TGA) of the silica nanoparticles were carried out using a TA Instrument SDT Q600 analyzer between 20 and 800°C in air (flow 50 ml min^{-1}) at a heating rate of 10° min^{-1}. All samples were dried under vacuum at 60°C overnight prior to TGA runs. The graft density of the grafted moiety on the silica surface was determined by thermogravimetric analysis (TGA) using following equation as described before.[27]

$$\text{Graft density (mmol/g)} = \frac{\frac{W_{modified\ silica(60-600)}}{100-W_{modified\ silica(60-600)}}\times 100 - W_{Ludox(60-600)}}{M\times 100}\times 10^{3}$$

$$\text{Graft density (groups/n}^2\text{)} = \frac{\frac{W_{modified\ silica(60-600)}}{100-W_{modified\ silica(60-600)}}\times 100 - W_{Ludox(60-600)}}{M\times S\times 100}\times 6.022\times 10^{23}\times 10^{-18}$$

Where $W_{(60\text{-}600)}$ is the weight loss between 60 and 600 °C corresponding to the decomposition of the grafted silica molecule corrected from the thermal degradation**,** and M is the molecular weight of the grafted silane. *S* represents the specific surface area of the silica nanoparticle (estimated as 140 m^2/g) while W_{Ludox} represents the determined weight loss of silica before grafting. 6.022×10^{23} is the Avogadro number.

3.2.3.4 SEM and HR-TEM

SEM images were obtained on FEI Quanta 200 3D, dual beam ESEM with EDAX microscope. HR-TEM images were taken on a FEI Technai F30 operating at 300 kV with FEG. The samples were prepared by dispersing a 0.1 mg/mL of nanoparticles by sonication, dropping the resulting suspension on a copper grid of 400 mesh for 30 sec and allowing it to dry in air. FT-IR spectra were recorded on Perkin Elmer FT-IR spectrum GX instrument by

making KBr pellets. Pellets were prepared by mixing 3 mg of sample with 97 mg of KBr. Elemental analyses were carried out on Thermo Finnigan FLASH EA 1112 series instrument.

3.2.3.5 Dynamic light scattering and zeta potential

The hydrodynamic diameters of dilute, aqueous solutions of the silica nanoconjugates were determined by dynamic light scattering (DLS) using a Brookhaven Instruments instrument equipped with a He-Ne laser operating at 632 nm. The particle size was calculated using 90Plus particle Sizing Software Ver. 3.94. Sample solutions were made in water and were filtered using a 0.8 μm PTFE filter. Aqueous elelctrophoretic data for the silica nanoconjugates were obtained using a Brookhaven Instruments instrument. For each sample three measurements were taken. Zeta potentials were calculated using PALS Zeta Potential Analyzer Software Ver. 3.54.

3.2.3.6 Antibacterial test

The antibacterial properties of silica-PLL and silica-PLL-*b*-PLLeu hybrids were evaluated and compared with azide functionalized silica (silica-N_3). Standard Luira-Bertani[73] plate method was adapted to evaluate the bactericidal effects. Bacterial cultures were taken with a sterilized loop and were allowed for incubation at 37°C in a shaker at 150 rpm to reach the log phase (0.6 OD at 600 nm). This was diluted to 10^{-4} with 0.9% saline so that the final colony forming units can be easily counted. 200 μL of the above solution was taken and to that desired amount of silica-PLL-A or silica-PLL-*b*-PLLeu sonicated in 800 μL saline was added. This mixture was allowed to incubate at 37°C in a shaker at 150 rpm. The antibacterial kinetics was followed at half, 1, 2, 4, 8 and 16 hrs intervals. From this minimum concentration of our sample that is sufficient for the complete bactericidal activity at half an hour was evaluated.

3.2.3.7 DNA retardation studies using gel electrophoresis

Polyplexes were prepared by addition of 0.2μg of pDNA with increasing ratio of silica-PLArg(20) and silica-PLArg(10) in sterile DI water at room temperature for 30 minutes. Each sample was then electrophoresed on a 0.8% (w/v) agarose gel containing ethidium bromide (EtBr, 0.5 μg/mL) at 110V for 1 h. The gels were analyzed using gel documentation system (Syngene) to show the location of DNA bands.

3.2.3.8 Cell lines and culture

Human cervical cancer cells (HeLa) and human lung carcinoma cells (A549) were grown in DMEM with 10% FBS. Cells were incubated in plastic tissue culture cell-binder flasks (Corning) at 37°C in a 5% CO_2 humidified incubator.

3.2.3.9 Cytotoxicity assay

Cytotoxicity of silica-PLArgs were studied by MTT assay.[74] HeLa and A549 cells were seeded in 96-well tissue culture plates at 6000 cells/well in 90 µL DMEM. All media contained 10% FBS and all cells were incubated overnight (14 to 16 hrs). silica-PLArgs solution (10 µl) at various concentrations were added and cells were incubated for another 48 h. After completion of incubation, the media was removed and 100µl solution of DMEM with filter sterilized MTT (3-(4,5-Dimethylthiazol-2-yl)-2,5-diphenyltetrazolium bromide) solution (0.45 mg/ml) was added into each well. After incubation at 37°C for 4 hrs with MTT, the media was aspirated from the wells and 100 µl DMSO was added to dissolve insoluble formazan crystals formed. The absorbance was measured at 550 nm using a microtitre plate reader (Veroscan, Thermo Scientific) and the cell viability was calculated as a percentage relative to untreated control cells.

3.2.3.10 In vitro transfection study

HeLa and A 549 cells were seeded at $3x10^4$ cells/well in 6-well plates in 2 mL of DMEM containing 10% FBS and incubated at 37°C for a day before transfection. Polyplexes of pDNA and silica-PLArgs were prepared by addition of 0.5 µg of pDNA with different weight ratios of silica-PLArgs in 50 µL sterile DI water and the mixtures were incubated for 30 min at room temperature. 50 µl of optimem was then added to each polyplex solution. Meanwhile, cells were washed with PBS follwed by addition of optimem (900 µl). The cells were then kept inside the incubator at 37°C for 15 min. Polyplex (100 µl) were added to each well containing the cells in optimem and this was further incubated for 4 hrs. After 4 hrs, cells were supplemented with 500 µl of 30% FBS containing DMEM. Transfected cells were visualized for protein expression after 48 h.

3.2.3.11 Fluorescence imaging of cells transfected with DNA-silica-PLArg polyplexes

For imaging cells that expressed mCherry fluorescent protein, cells were grown on glass coverslips and transfected as above. Cells were washed twice in cold PBS and fixed with 4% paraformaldehyde-PBS solution (pH 7.4) for 15 min. Fixative was removed by washing and cells were mounted on glass slides using mounting medium containing DAPI to stain the nuclei. Images were acquired with an epifluorescence microscope (Ziess).

3.3 Results and Discussions

3.3.1 Synthesis and characterization of azide grafted silica nanoparticles

The azide grafted silica nanoparticles (Silica-N_3) were prepared by the post synthetic grafting method in a process similar to that has been described by Menu *et al.*[75] Commercially available silica colloidal solution (Ludox TM 50; 22±2 nm particle size) was condensed with azidopropyltriethoxysilane (AzPTES) in an ethanol water 1:1 solvent mixture (scheme 1). Some parameters like reaction time, solvent volume and AzPTES-to-silica ratio were evaluated to find the optimal grafting condition that would afford monodispersed silica nanoparticles having uniform coverage of the azidopropyl moiety (Table 3.1). It was also observed that Teflon ware is suitable for the AzPTES grafting reaction container than glassware, as the inner glass surface leads to unwanted aggregation mediated by AzPTES. It was determined that 2.4 g of Ludox (50% wt in solution) condensed with 2 mmol AzPTES in 30 mL of ethanol water mixture (1:1) for 24 hrs afforded a grafting ratio of 0.7 mmol of azidopropyl group per gram of silica particle. The grafting ratio was determined by the estimation of nitrogen content by elemental analysis and then confirmed by thermogravimetric analysis (Figure 3.1b). The nitrogen content was found out to be 3.4% while the TGA data displayed a loss of 7.2 % weight. Elemental analysis and TGA shows a grafting ratio of 0.68 and 0.7 mmol of azidopropyl group per gram of silica particle respectively. Assuming a surface area of 140 m^2/gm of silica, the grafting density was determined to be 3 azidopropyl groups/nm^2. For monolayer coverage, it has been estimated that 3-5 silanol sites/nm^2 are available for condensation of organosilane molecules on the silica surface.[75] Therefore, our grafting density of 3 azidopropyl groups/nm^2 is indicative of monolayer coverage of the azidopropyl groups on the silica surface. The azide grafted silica nanoparticle was characterized by FT-IR, multinuclear (^{13}C and ^{29}Si) solid state NMR and TEM.

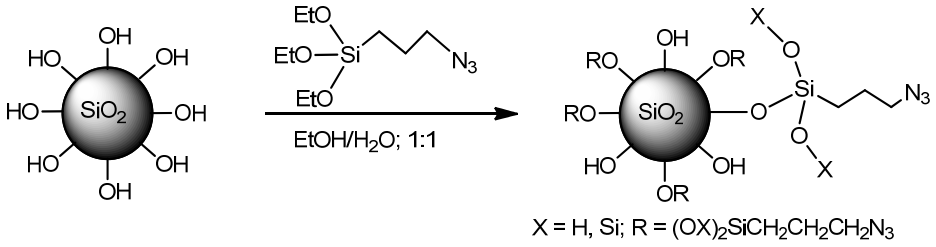

Scheme 3.1: Synthesis of azide grafted silica nanoparticle (silica-N_3)

The FT-IR of the silica-N_3 is presented in the Figure 3.2b. The spectra display an absorbance at ~2100 cm^{-1} which is the characteristic stretching vibration of any organic azide (N_3). The absence of the 2100 cm^{-1} stretch in the starting Ludox particle (Figure 3.2a) indicates that organic azide groups have been successfully incorporated into the silica nanoparticle. Figure 3.3a represents the solid state ^{13}C CP-MAS NMR spectra of the azide grafted silica particle. The three peaks C1 (11 ppm), C2 (24 ppm), C3 (55 ppm) observed in the ^{13}C CP-MAS NMR represent the three C-atoms of the azido-propyl chain in the order as presented. The ^{29}Si CP MAS NMR spectra of N_3-Silica are presented in Figure 3.4a. The spectra display prominent peaks at around -111, -101, -67 and -58 ppm. The peaks at -111 and -101 ppm may be assigned to the different types of the Silica-sites namely Q3 [$(SiO)_3Si(OH)$] and Q4 [$(SiO)_4Si$], that are classified based on the total number of silanol groups (Si-OH) at the Si-centre (i.e. 1, 0 respectively). Two other distinct peaks observed at -58 and -67 ppm may be attributed to the functionalized sites of the Si-framework namely T2 [$R(SiO)_2Si(OH)$] and T3 [$R(SiO)_3Si$] respectively, where R is the azidopropyl group.

Amount of Ludox (g) taken in teflon ware	AzPTES (mmol)	Solvent (1:1 = EtOH : H_2O) (mL)	Time (hrs)	DLS (Mean diameter) (nm)	% of Nitrogen	Yield (mg)
1.2	2	25	72	245±6	6.9	867
1.2	2	25	48	232±6	5.4	612
1.2	2	50	24	29±4	0.86	114
1.2	**2**	**30**	**24**	**27±4**	**3.4**	**512**
Ludox	-	-	-	22±3		-

Table 3.1: Synthesis of azide grafted silica nanoparticle in various different conditions

The dynamic light scattering (DLS) was performed to examine the particle size and size distribution of the azide grafted silica nanoparticles (Table 3.1). All particle size and size distribution curves were obtained by averaging three DLS experiments. Particles with diameters ranging from 23-31 nm, centered on 27 nm (PDI 0.229), were observed for the azide grafted silica particles by DLS (dispersion in ethanol/water) as seen in Figure 3.5b. The increase in the average particle size from the starting Ludox particle (Figure 3.5a), diameter 22±2 nm, PDI 0.183) was consistent with the grafting of the azidopropyl group. The monodisperse nature of the azide grafted silica nanoparticles were further confirmed by TEM

(Figure 3.6a). TEM micrographs show that the very low polydispersity of the azide grafted nanoparticles were conserved after grafting.

Azide grafted silica nanoparticle have been reported before. The synthesis of these nanoparticles involve a two step reaction in which a bromopropyl group is introduced first by reaction of silica with 3-bromopropyltrichorosilane.[32] This is followed by the displacement of the bromide by NaN_3 to yield the azide grafted silica. In contrast, we have employed a one step process in which the monolayer grafting of azidopropyl group has been achieved on the Ludox particle by co-condensation with azidopropyltriethoxysilane. The grafting density of 3 groups/nm^2 in our silica-N_3 is comparable to that of 3.45 groups/nm^2 as has been reported by Brittain *et al.*[32]

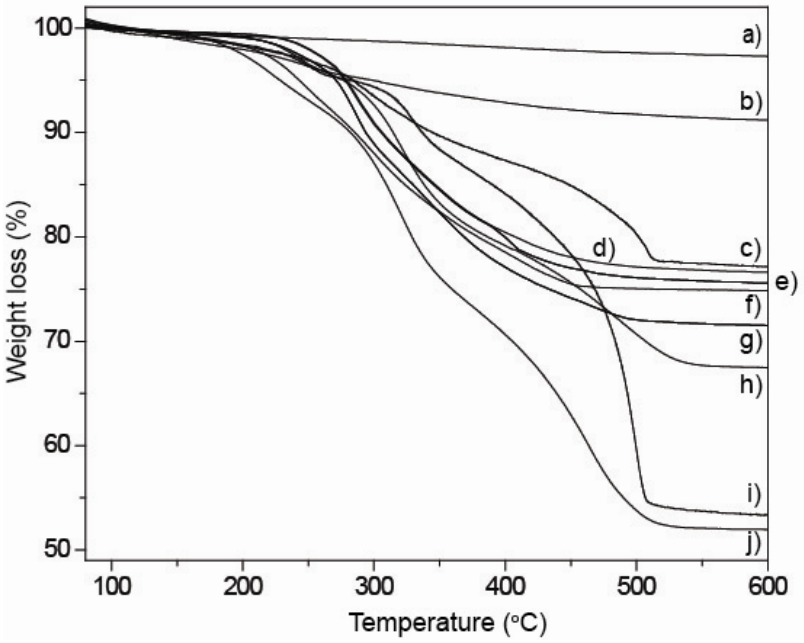

Figure 3.1: TGA of a) Ludox, b) silica-N_3, c) silica-PLArg(10), d) silica-PLBG, e) silica-PLGA(30), f) silica-PLL-B, g) silica-PLGA(40), h) silica-PLL-*b*-PLLeu, i) silica-PLArg(20) and j) silica-PLL-A

3.3.2 Synthesis and characterization of Silica-PLL, silica-PLL-b-PLLeu and silica-PLBG hybrid

The silica-N_3 was subjected to Cu(I) catalyzed azide alkyne cycloaddition reaction (CuAAC). Propargyl alcohol was used as the substrate during the initial experiments to optimize the reaction conditions and to determine the number of azides available for conversion to the corresponding triazole. The CuAAC was attempted using CuI/sulfonated bathophenanthroline in an equimolar mixture of DMF and Tris Buffer (pH 7, 100 mM).

Treatment of N_3-Silica with propargyl alcohol (0.14 mmol, 4-fold molar excess with respect to N_3-Silica) using CuI/sulfonated bathophenanthroline/ascorbate in 1:1 Tris-buffer/DMF for 24 hrs converted >99% of the available azide groups into the corresponding triazole product alcohol-silica. The extent of the reaction was estimated using IR spectroscopy by monitoring the decrease in the integrated intensity of the ν_{as} (N_3) at 2100 cm^{-1} (Figure 3.2c) as has been reported before.[76] Control reactions performed without the usage of CuI showed no conversion of the azide. After the reaction, an extensive washing protocol was followed to remove the Cu(I), ligand, ascorbate and any unreacted propargyl alcohol. One of the key steps in the washing was the usage of dithiocarbamate to remove the Cu(I), as reported earlier.[76]

The reaction conditions optimized above were used to graft alkyne-PLL, alkyne-PLL-*b*-PLLeu and alkyne-PLBG onto the silica-N_3 (Scheme 3.2). Two different concentrations of the alkyne-PLL were used to get silica-PLL with different amount of PLL grafts. It was observed that the reaction of azide grafted silica with 4 equivalent of alkyne-PLL lead to the formation of the corresponding triazole product, Silica-PLL-A. The employment of the sulphonated bathophenanthroline ligand was critical for the successful completion of the CuAAC. The ligand plays a dual role of accelerating the reaction also preventing the binding of Cu(I) to the lysine side chains in PLL. The reaction conditions were slightly altered for the grafting of alkyne-PLL-*b*-PLLeu and alkyne-PLBG for their differing solubility. A mixture of DMF:pH 7 Tris-HCL (1:1) was used as the solvent for grafting alkyne-PLL-*b*-PLLeu while the solvent DMF together with the ligand 2,2′-bipyridyl was used to graft alkyne-PLBG.

The TG-DTA analysis of Silica-PLL-A (Figure 3.1j) indicated a mass loss of 47 % between 100°C and 600°C which corresponds to a loading of 0.23 mmol of PLL/gm of silica. Use of higher amounts of catalyst and longer reaction times did not improve the yield of the reaction. The graft density was estimated to be about 1.01 group/nm^2 (1.68 μmol/m^2). Therefore, approximately 35% of the available azides were converted to the corresponding triazole upon CuAAC with alkyne-PLL. When 2 equivalent of alkyne-PLL as the substrate, only 11 % of the available azides were converted to the corresponding triazole Silica-PLL-B (Figure 3.1d). The graft density of silica-PLL-B was estimated to be 0.3 group/nm^2 (0.07 μmol/m^2) (Table 3.2). Hence, we were able to control the loading of PLL on the silica azide by using different amounts of alkyne-PLL as the substrate. The TG-DTA analysis of silica-PLL-*b*-PLLeu (Figure 3.1h) and silica-PLBG (Figure 3.1d) indicated a mass loss of 30% and 24% respectively between 100°C and 600°C which corresponds to a loading of 0.0627 mmol

of PLL-*b*-PLLeu-silica and 0.034 mmol of PLBG per gm of silica respectively. Therefore, approximately 10% and 5% of the available azides were converted to the corresponding triazole upon CuAAC with alkyne-PLL-*b*-PLLeu and alkyne-PLBG respectively.

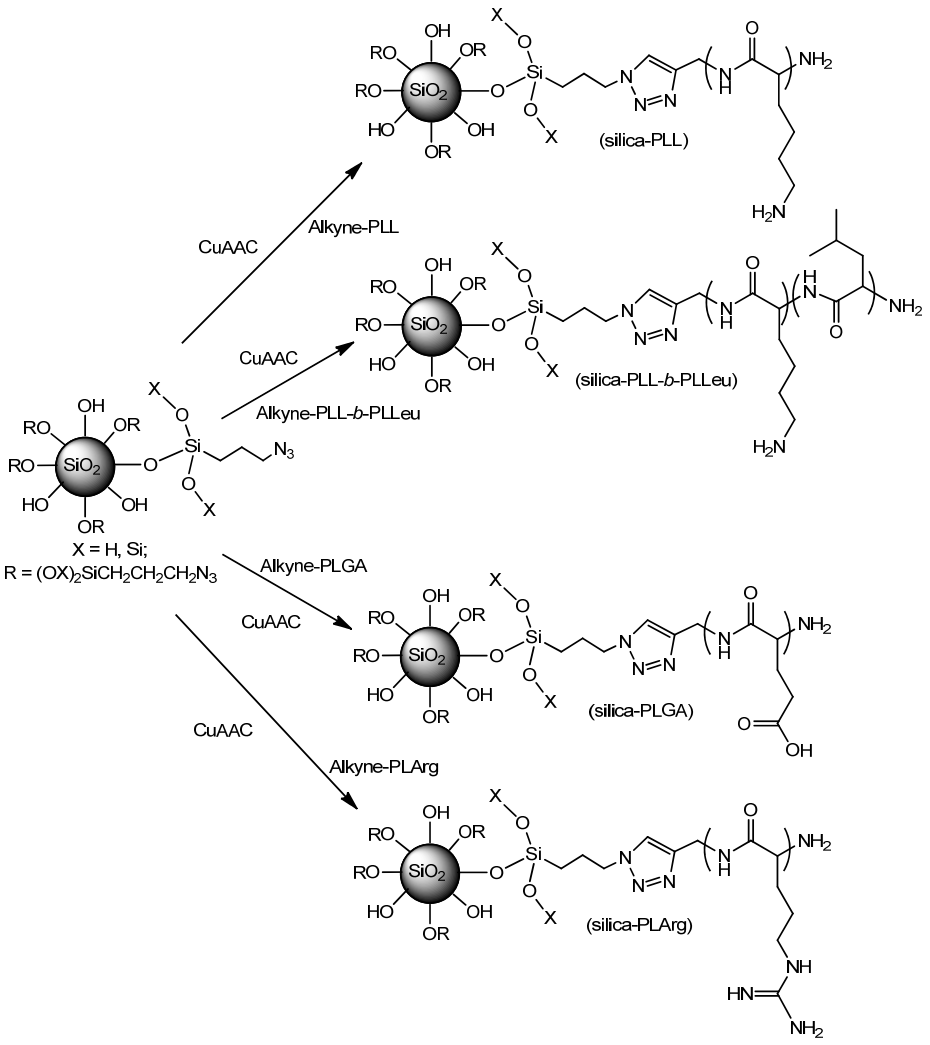

Scheme 3.2: Synthesis of silica polypeptides conjugates using 'click' chemistry

The successful attachment of alkyne-PLL, alkyne-PLL-block-PLLeu, and alkyne-PLBG were also confirmed from the IR spectra. In silica-PLL-A (Figure 3.2d) a concomitant decrease of the $\nu_{as}(N_3)$ at 2100 cm^{-1} was observed with the appearance of the ν(C=O) at 1657 cm^{-1} and ν(N-H) at 1535 cm^{-1}, a region that displayed no peaks for the azide labeled silica. Similar ν(C=O) and ν(N-H) stretches were observed in the other two silica conjugates (Figure 3.2e and f). For Silica-PLL-A, the amide I peak due to C=O stretching is found at 1657 cm^{-1} while the amide II peak resulting from C-N stretching and N-H bending is observed at 1535 cm^{-1}. These values are characteristic of either an alpha helical structure or a random coil structure of PLL. It is expected that the protonated PLL would exist as a random coil

structure in Silica-PLL-A. Recently, some PLL-silica nanocomposites have been synthesized by condensation of TEOS using poly -L-lysine solutions in the α-helix, β-sheet, and random coil conformations as templates. It was observed that poly-L-lysine retains its solution conformation in the nanocomposites when templating from the α-helix and β-sheet conformation, but the random coil conformation was converted to the α-helical form during nanocomposite formation.[38, 77, 78] Similarly, it is possible that in Silica-PLL-A, the interaction between the protonated PLL and the silica surface in the solid state could have resulted in a conformational change. However, the ^{13}C CP-MAS NMR spectra of Silica-PLL-A is consistent with likely an alpha helical structure.

The solid state ^{13}C CP-MAS NMR spectra of PLL-silica-A are shown in Figure 3.3b. The ^{13}C NMR shows extra peaks in addition to the C1, C2 and C3 observed in azide grafted silica. The extra peaks have been identified and labeled in Figure 3.3b. The presence of the extra peaks at 128 ppm and 146 ppm which corresponds to the C4 and C5 atom of the triazole indicates that the PLL have been covalently attached to the silica particle via the triazole ring. The C7 (carbonyl), C8 and C12 observed in the spectra are very characteristic of the PLL moiety that refers the alkyne-PLL was successfully grafted onto the silica surface as well as ^{13}C CP MAS NMR also give the information about the secondary structure of poly-L-lysine onto the silica nanoparticle surface. The chemical shifts of the C7 (176 ppm), C8 (57.6 ppm) and C12 (40.5 ppm) are characteristic of the poly-L-lysine in the α-helical conformation as has been reported recently.[78] The chemical shifts of PLL observed from ^{13}C CP-MAS NMR spectra is known to be sensitive to its secondary structure. The ^{29}Si CP MAS spectrum of the Silica-PLL-A material shows little or no change from the starting aizde grafted silica particles indicating that the Si-sites does not undergo any chemical change during the reaction and its work-up (Figure 3.4b). This is expected since the T1 and T2 Si-sites are that from the azidopropyl modified silica and should not undergo any change during the course of the click reaction.

Based on the data reported above, it can be concluded that PLL has been successfully attached onto azide grafted silica using CuAAC. Using this “grafting to” methodology, a PLL-silica conjugate has been synthesized with a very high PLL content of 50 weight %. “Grafting to” methodologies generally lead to lower grafting densities than their corresponding “grafting from” technique since steric crowding of previously attached polymers inhibits attachment of the newer polymer chains. Synthesis of high density polymer brushes on silica nanoparticles using the “grafting to” approach has been achieved recently

by using a combination of RAFT and click chemistry.[26] The grafting density obtained by the group for polystyrene and polyacrylamide brushes via this "grafting to" approach (0.15 to 0.68 groups/nm^2) is lower than the grafting density of the Silica-PLL-A (1.02 groups/nm^2) hybrid synthesized by us. Silica-poly-ε-carbobenzoxy-L-lysine (cbz protected PLL) conjugate via the "grafting from" approach has been attempted before using surface initiated polymerization of ε-carbobenzoxy-L-lysine NCA and amine grafted colloidal silica particles. It was found out that the grafting thickness was 14 folds lower than expected.[39] The authors attribute this to the parasitic initiation of the NCA monomer by trace impurities and the nucleophilic hydroxyl groups on the silica surface. In another recent report, a 35 nm thick film with a grafting density of 0.68 groups/nm^2 was obtained for poly-L-alanine grafts onto colloidal silica particles.[41] The "grafting to" approach employed by us leads to the facile synthesis of PLL-silica conjugates with much higher grafting density (1.02 groups/nm^2) using a sterically bulky amino acid and also allows us to control the amount of PLL attached. It should also be noted that poly-L-lysine in the α-helical conformation requires around 1.1 nm^2 of space (considering 1.2 nm diameter). Hence a grafting density of 1.02 groups/nm^2 points out to the fact that the maximum amount of poly-L-lysine grafting possible on the nanoparticle surface by steric constraints has been successfully achieved. The grafting density of the PLBG onto silica nanoparticle was significantly lower and that can be attributed to bigger size of the steric bulk of the benzyl protecting group that makes a lot of the azidopropyl groups present inaccessible.

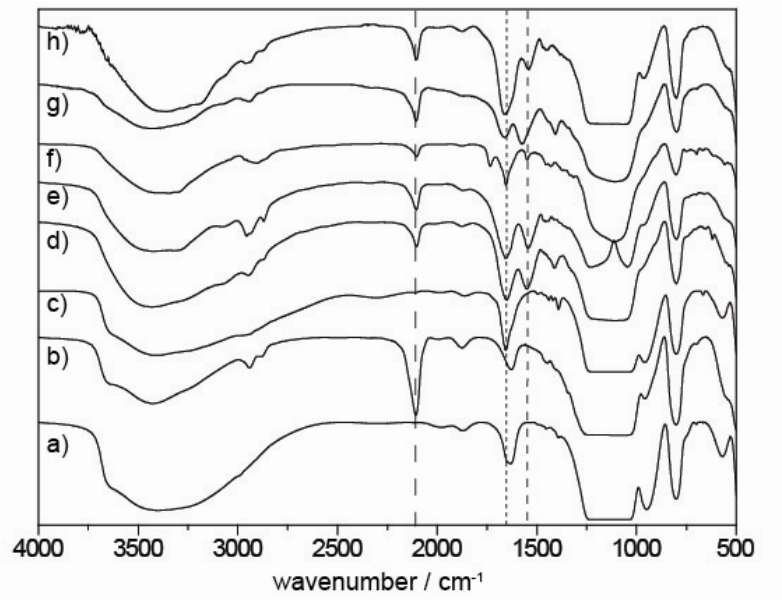

Figure 3.2: FT-IR of a) Ludox, b) silica-N_3, c) silica-N_3 'clicked' with propargyl alcohol, d) silica-PLL, e) silica-PLL-*b*-PLLeu, f) silica-PLBG, g) silica-PLGA and h) silica-PLArg

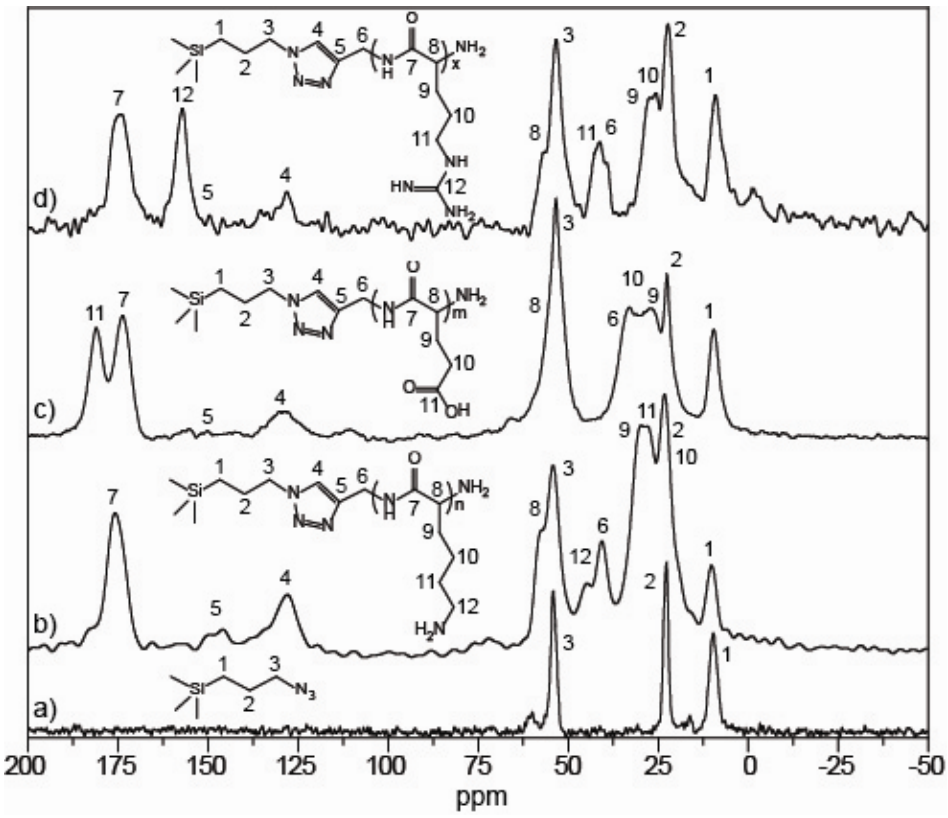

Figure 3.3: ^{13}C CP MAS NMR spectra of a) silica-N_3, b) silica-PLL, c) silica-PLGA and d) silica-PLArg

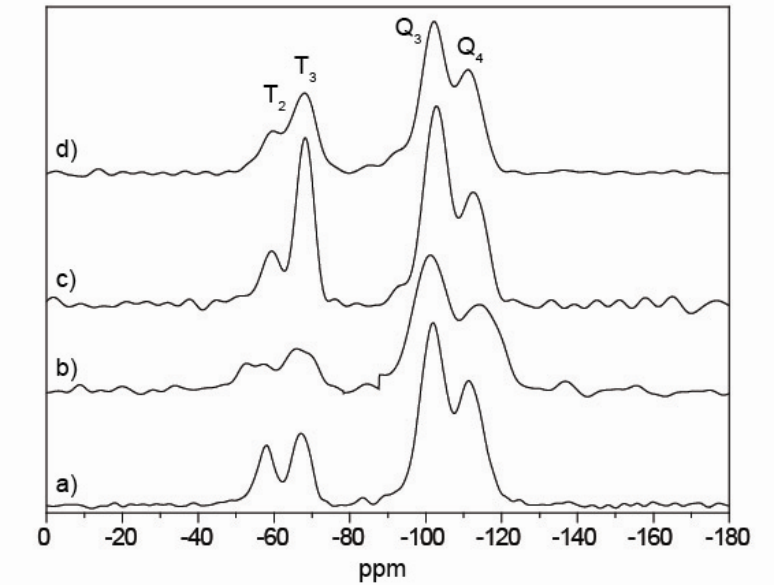

Figure 3.4: ^{29}Si CP MAS NMR spectra of a) silica-N_3, b) silica-PLL, c) silica-PLGA and d) silica-PLArg

Aqueous electrophoresis experiments were performed on the water dispersible silica nanocomposites to estimate the surface charge on the nanoparticles. The zeta potential of the

azide grafted silica nanoparticle was determined to be ±3 mV at pH 7. In contrast, the zeta potential of silica-PLL-A and silica-PLL-B was found to be +51 and +35 mV respectively and this can be attributed to the successful grafting of the cationic poly-L- lysine onto the silica nanoparticle.

	Weight Loss (%)	**Grafting Density (mmol/gm)**	**Grafting Density (groups/nm^2)**	**Zeta potential (mV)**	**DLS (nm)**
Ludox	2	-	-	-22	22±3
N_3-Silica	7.2	0.672	3	±3	27±4
Silica-PLL-A	47.6	0.235	1.013	+51±3	~240
Silica-PLL-B	24	0.07	0.3	+35±3	~230
Silica-PLL-*b*-PLLeu	30.22	0.062	0.27	-	-
Silica-PLBG	23.79	0.037	0.146	-	-
Silica-PLGA(30)	23	0.055	0.257	-70±2	36±8
Silica-PLGA(40)	29	0.06	0.27	-76±3	38±5
Silica-PLArg(20)	47.33	0.27	1.14	+56±4	58±8
Silica-PLArg(10)	23	0.11	0.48	+42±3	43±7

Table 3.2: Various physical characterization and properties of silica nanoconjugates

3.3.3 Synthesis and characterization of silica poly-L-glutamic acid (Silica-PLGA)

Silica-PLGA(30) and silica-PLGA(40) were synthesized by Cu(I)-catalyzed azide alkyne cycloaddition reaction (CuAAC) using silica azide and alkyne-PLGA (Scheme 3.2). CuAAC was attempted using CuI/ sulfonated bathophenanthroline in an equimolar mixture of Tris buffer (pH 7, 100 mM) and DMF (7:3) mixture. The ligand sulphonated bathophenanthroline was critical for the completion of the reaction. After the reaction, an extensive washing protocol was followed to remove the Cu(I) ligand, sodium ascorbate, and unreacted alkyne-PLGA as has been reported earlier.

The TG-DTA analysis of Silica-PLGA(30) (Figure 3.1e) indicated a mass loss of 23% between 100ºC and 600^{o}C that corresponds to a loading of 0.055 mmol of poly-L-glutamic acid/g of silica (Table 1). The grafting density was estimated to be about 0.257 group/nm^2 (0.427 μmol/m^2). For silica-PLGA(40), the loading of poly-L-glutamic acid is 0.06 mmol/ g of silica. The grafting density was estimated to be about 0.27 groups/nm^2 (0.45μmol/m^2). Therefore, approximately 10% of the available azides were converted to the corresponding triazole upon CuAAC with alkyne-PLGA. The lower grafting density of PLGA in

comparison to poly-L-lysine (35%) is probably due to the repulsion between the negatively charged poly-L-glutamic acid chain and the negatively charged silica surface that hinders further attachment of polypeptides. The successful attachment of alkyne-PLGA was also confirmed by the IR spectra. In silica-PLGA(30) (Figure 3.2g), a concomitant decrease in $\nu_{as}(N_3)$ at 2100 cm^{-1} was observed with the appearance of ν(C=O) at 1580-1850 cm^{-1} and ν(N-H) at 1525 cm^{-1}, a region that displayed no peak for the azide-labeled silica (Figure 3.2a).

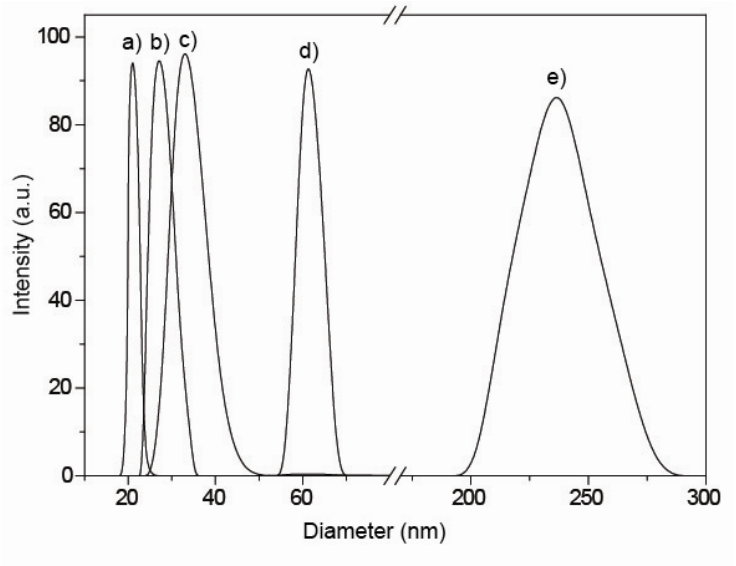

Figure 3.5: DLS of a) Ludox, b) silica-N_3, c) silica-PLGA(30), d) silica-PLArg(20) and e) silica-PLL(30)

The solid state ^{13}C CP-MAS NMR spectrum (Figure 3.3c) of silica-PLGA(30) shows extra peaks in addition to the C1, C2 and C3 observed in azide grafted silica. The extra peaks have been identified and labeled in Figure 3.3c. The presence of the extra peaks at 126 ppm and 143 ppm which corresponds to the C4 and C5 atom of the triazole indicates that the PLGA have been covalently attached to the silica particle via the triazole ring. The C11 (180 ppm) (carboxylic acid), C7 (174 ppm) (carbonyl), C8 (54 ppm), C9 (34 ppm) and C10 (28 ppm) observed in the spectra are characteristic of the PLGA moiety. ^{13}C CP-MAS NMR is very sensitive to investigate the secondary structure of the polypeptides. According to the literature report, ^{13}C CP-MAS chemical shifts of poly-L-glutamic acid are 180 ppm($-COO^-$), 174 ppm (carbonyl), 54 ppm (CH_2), 34 ppm (CH_2) and 28 ppm (CH_2) can be assigned as a α-helix conformation.[79] The literature values are exactly matching with experimental ^{13}C CP MAS values suggest the conformation of the poly-L-glutamic acid onto the silica nanoparticle surface is α-helix. The ^{29}Si CP MAS NMR spectrum of the silica-PLGA material

(Figure 4.4c) shows little or no change from the starting silica-N_3 indicating that the Si-sites do not undergo any chemical change during the reaction and work-up. This is also expected since the T1 and T2 Si-sites are from the azidopropyl modified silica and are not expected to undergo any change during the course of the reaction. Therefore, FT-IR, TG-DTA and NMR show that poly-L-glutamic acid was covalently attached to the silica core to afford core shell silica-PLGA nanoparticles.

Dynamic light scattering (DLS) was performed to examine the particle size and size distribution of azide-grafted silica nanoparticles (silica-N_3) and silica-PLGA(30) (Figure 3.5c). Since the particles used are relatively small, ~ O(30 nm), and monomodal, with only moderate size polydispersity, a single angle (90^o) DLS measurement is adequate to characterize the particle size distribution. For a dispersion of silica-N_3 particles in ethanol/water, the diameter of the particles was found to be 27 ± 4 nm (Figure 3.5b). The increase in the average particle size from the starting Ludox particle (diameter 22 ±2 nm; Figure 3.5a) is probably indicative for the grafting of oligomeric azidopropyl group as has been discussed before. For a dispersion of silica-PLGA-30 nanoparticles in water, an average particle size of 36 nm ± 8 nm was observed. The DLS results are confirmed by TEM that indicates an increase in the size of the PLGA grafted nanoparticles (32±5 nm, Figure 3.6g) relative to the azide grafted silica nanoparticles. Although the PLGA has a very narrow PDI, it was observed that the polydispersity of the PLGA grafted nanoparticles increased upon attachment of the polypeptide. The likely reason for this is that the grafting reaction is dependent on several factors (steric hindrance and charge charge interaction) and hence grafting of the polypeptide will not be uniform on all the silica nanoparticles. This is reflected in the higher size distribution of the PLGA grafted nanoparticle.

3.3.4 Synthesis and characterization of silica-Poly-L-Arginine (Silica-PLArg)

Silica-PLArg(20) and silica-PLArg(10) were synthesized by using modified CuAAC, a different and efficient protocol was developed by our group. Here, the CuAAC was attempted using $CuSO_4$/THPTA/amino guanidine in PBS buffer (pH 7.4, 150 mM). Treatment of N_3-Silica with alkyne-PLArg (1 equivalent molar excess with respect to silica-N_3) using $CuSO_4$/THPTA/ascorbate/amino guanidine (0.25/1.25/2.5/2.5 molar equivalent respect to silica-N_3) in PBS buffer was incubated for 18 h at room temperature. The extent of the reaction was estimated using IR spectroscopy by monitoring the decrease in the integrated intensity of the ν_{as} (N_3) at 2100 cm^{-1} (Figure 3.2b).

The TG-DTA analysis of silica-PLArg(20) (Figure 3.1i) indicated a mass loss of 47.33% between 100°C and 600°C that corresponds to a loading of 0.27 mmol of poly-L-arginine/g of silica (Table 3.2). The grafting density was estimated to be about 1.14 group/nm^2 (1.9 μmol/m^2) (Table 3.2). For silica-PLArg(10), a mass loss of 23% observed between 100°C and 600°C corresponds to a loading of 0.11 mmol/gm with grafting density of 0.48 group/nm^2. The successful attachment of alkyne-PLArg was also confirmed by the FT-IR spectra. In silica-PLArg(20) (Figure 3.2h), a concomitant decrease in $\nu_{as}(N_3)$ at 2100 cm^{-1} was observed with the appearance of ν(C=O) at 1580-1850 cm^{-1} and ν(N-H) at 1525 cm^{-1}, a region that displayed no peak for the azide-labeled silica (Figure 3.2b).

The solid state ^{13}C CP-MAS NMR spectrum of silica-PLArg(20) shows extra peaks in addition to the C1, C2 and C3 observed in silica-N_3 (Figure 3.3b). The presence of the peaks at 128 ppm and 153 ppm which corresponds to the C4 and C5 atom of the triazole indicates that the p(LArg) have been covalently attached to the silica nanoparticle via the triazole ring. The C7(174 ppm) (carbonyl), C12(157 ppm), C11(27 ppm) and C9(25 ppm) observed in the spectra are very characteristic of the poly-L-arginine moiety. The chemical shifts of the C7 (174 ppm), C8 (54 ppm), C9(25 ppm) and C12 (157 ppm) are characteristic of the poly-L-arginine in the random coil conformation as has been reported.[80] The FT-IR spectra also supports this since the observed amide I and amide II peaks at 1656 cm^{-1} and 1543 cm^{-1} are indicative of PLArg in a random coil conformation.

Dynamic light scattering (DLS) was performed to examine the particle size and size distribution of silica-PLArg(20) (Figure 3.5). For a dispersion of silica-PLArg(20) nanoparticles in water, an average particle size of 58±8 nm was observed indicating an increase in size with respect to the starting N_3-silica nanoparticles. The TEM also confirms that the narrow polydispersity in particle size is preserved even after alkyne-PLArg grafting. However, the DLS results show an average particle size of 58 ± 8 nm, which is much more than what was observed in TEM. This probably indicates that the silica-PLArg(20) nanoparticles are partly aggregated in solution. This is not unusual, as another close related silica nanoparticle grafted with a polycationic polypeptide poly-L-lysine (poly-L-lysine grafted silica nanoparticles) have been shown to form large aggregates in solution.[12]

Aqueous electrophoresis experiments were performed on the poly-L-arginine grafted silica nanoparticles (silica-PLArg) to estimate the surface charge on the nanoparticles (Table 3.2). The zeta potential of the silica-N_3 nanoparticle was determined to be -22 mV at pH 7. In contrast, the zeta potential of silica-PLArg(20) and silica-PLArg(10) were found to be

positive, +56±4 mV and +42±3 mV, respectively (Table 3.2), and this can be attributed to the cationic nature of the guanidine side chain moiety. This data also suggest that the poly-L-arginine has been grafted onto the silica nanoparticle surface successfully.

3.3.5 Aggregation behavior of polypeptide grafted silica nanoparticles in solution

The TEM of silica-PLL-A was carried out to obtain information about its size, shape and distribution (Figure 3.6b). TEM of silica-PLL-A shows many particles overlapping each other indicating that they are partially aggregated. This is very unusual as the highly cationic silica-PLL-A particles with a positive zeta potential (+51 mV) would be expected to repel each other thereby preventing aggregation. In contrast, the TEM of silica-PLGA shows well disperse particle throughout the TEM grid without any aggregation (Figure 3.6g), DLS data also supports the same. In silica-PLGA, the PLGA having the same polypeptide back bone than PLL as well as the ^{13}C CP MAS suggested that both have α-helix secondary structure, the only difference is their charges. The side ε-amine of PLL is having pK_a 9.5 where as the δ-carboxylic acid of PLGA is having pKa 4.6. At pH 7, both polypeptides are expected to be positively and negatively charged, which was also reflected in zeta potential measurements (Table 3.2). Instead of having very high surface positive charge silica-PLL showed aggregation where as high negative surface charge containing silica-PLGA did not show aggregation. The fact that they are aggregating probably points to the interactions between the poly-L-lysine chains. It might be noted that the PLL exists as the HBr salt. The presence of Br^- anion might screen the $-NH_3^+$ (or ammonium) charges which would then diminish the electrostatically driven charge repulsion between poly-L-lysine chains between two Silica-PLL-A nanoparticles. It has been shown that poly-L-lysine can aggregate in solution to form higher aggregates in presence of some additives.[81] Such aggregation morphologies have also been observed in other polymer grafted nanoparticles.[51, 82] TEM images from silica-PLBG (Figure 3.6f) exemplify this better where clear individual particles are seen. Individual particles are also seen in the TEM images of the silica-PLL-*b*-PLLeu (Figure 3.6d). It is noteworthy that most of the particles in silica-PLL-*b*-PLLeu, that were drop casted from a dispersion of the nanoparticles in toluene:tert-BuOH (1:1), were present in a monolayer fashion in close proximity. Therefore, the presence of the poly-L-leucine group at the surface of this nanoparticle prevented it from aggregating in more non-polar solvents. In more polar solvents, either they did not disperse well or were forming large aggregates in solution itself. This could be attributed to the fact that the hydrophobic poly-L-leucine present on the surface of nanoparticle drives them to phase separate and form aggregates in the presence of polar

solvents like DMF-H_2O mixture. Silica-PLL-*b*-PLLeu particles are not dispersible in any individual hydrophilic or hydrophobic solvents, but get dispersed in the mixture of both.

The TEM image of silica-PLArg showed also partial aggregation. The DLS of the silica-PLArg also shows a partial aggregation in water solution (~58 nm). The pK_a of the guanidium moiety of PLArg is 12.48. It is expected that the entire guanidium moiety will be as guanidium cation at pH 7. The probable reason of aggregation is due to the presence of the Br^- anion as the guanidium moiety stays as an HBr salts.

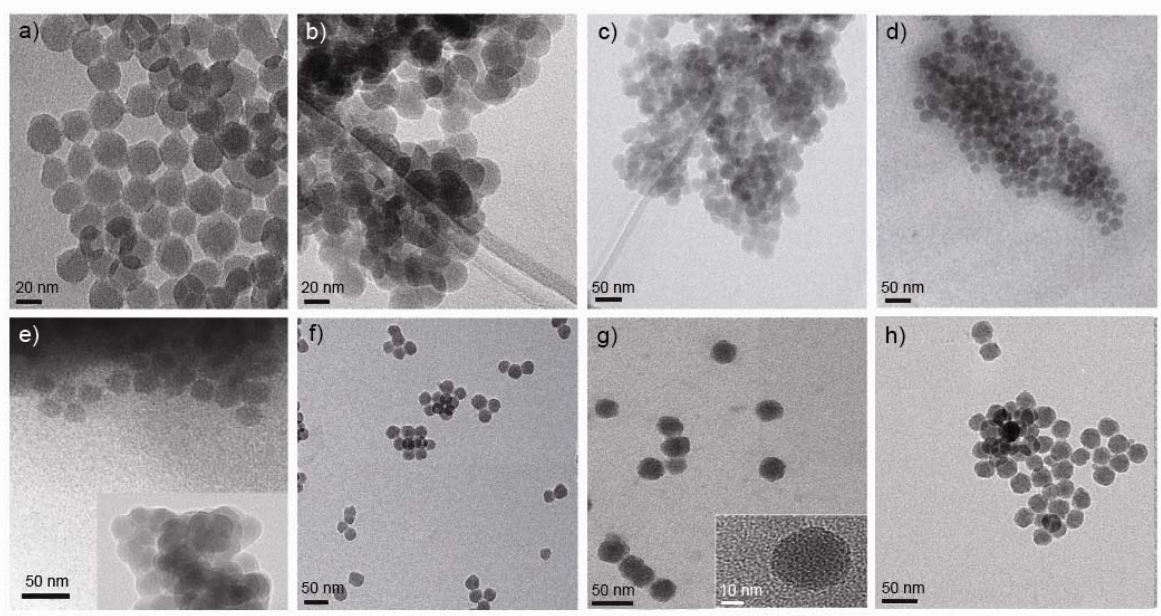

Figure 3.6: TEM of (a) silica-N_3, (b) silica-PLL-A (c) Silica-PLL-B, (d) silica-PLL-*b*-PLLeu (t-butanol-toluene), e) silica-PLBG PLL-*b*-PLLeu (H_2O-DMF), f) silica-PLBG g) silica-PLGA and h) silica-PLArg

3.3.6 pH responsive behavior of silica-PLGA nanoparticles in solution

We have performed electrophoretic mobility measurements of the silica-PLGA(30) particles as a function of pH at different ionic strengths: with no added salt, and on addition of 10^{-4} M, 10^{-3} M and 10^{-2} M sodium chloride (Figure 3.7). Changing the ionic strength of the solution changes the Debye screening length (κ^{-1}), and the width of the electrical double layer around the charged colloidal particles. Therefore, it also changes the value of the zeta potential (ζ) at the slip plane. The zeta potential can be calculated from the measured electrophoretic mobility. For small particles, viz. where $\kappa a << 1$ (where a is the size of the particle), the zeta potential is given by the Hückel equation: $\zeta = 1.5\ \eta\mu/\varepsilon$ (where η is the viscosity and ε is the dielectric permittivity of the solution). For large particles, viz. where

$\kappa a >> 1$, the zeta potential is given by the Helmholtz-Smoluchowski equation: $\zeta = \eta\mu/\varepsilon$. Assuming that the ionic strength of the solution is set only by the added salt (viz. ignoring the effect of the counter-ions from the colloidal particles), we estimate that κ^{-1} is around 30 nm, 9.6 nm and 3 nm for salt concentrations of 10^{-4} M, 10^{-3} M and 10^{-2} M respectively. Thus, for our silica particles (where, $a \sim 30$ nm), $\kappa a \sim 1$ for 10^{-4} M salt while $\kappa a \sim 10$ for 10^{-2} M salt. Thus, the Helmholtz-Smoluchowski equation provides a better estimate of the zeta potential at high ionic strength, while for low ionic strength, or with no added salt, the correct value of the zeta potential is between the values calculated by the Helmholtz-Smoluchowski and Hückel equations. Here, we report the zeta potential calculated using both the Helmholtz-Smoluchowski and Hückel equations (Figure 3.7).

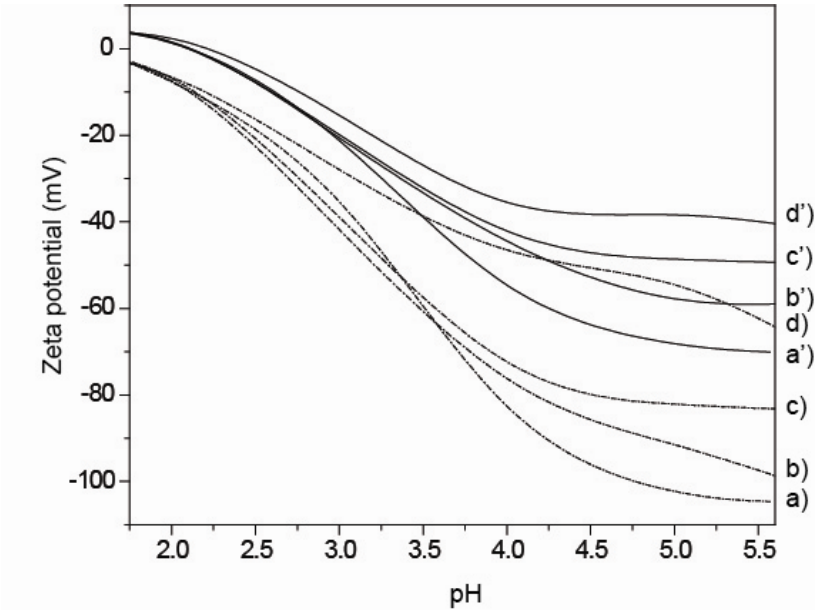

Figure 3.7: Zeta potential versus solution pH of silica-PLGA in a,a') DI water, b,b') 10^{-4} M, c,c') 10^{-3} M, and d,d') 10^{-2} M NaCl solutions using the Huckel and Helmholtz-Smoluchowski equation, respectively

The values of the zeta potential calculated using the Helmholtz-Smoluchowski equation is higher when compared with the values from the Hückel equation. However, we note that, the trends reported for change in zeta potential with pH are robust, and independent of the specifics of the model used to calculate the zeta potential. At pH = 5.5, when no salt is added to the aqueous solution, the zeta potential for the silica-PLGA(30) particles is highly negative (< -65 mV). With decrease in pH, the zeta potential increases and, for pH less than about 2.5, the electophoretic mobility is very low, such that both Huckel and Helmholtz-Smoluchowski equations yield zeta potential values that are close to 0 (Figure 5). Interestingly, we observed

that while silica-PLGA forms a well dispersed, stable solution above pH 5; this solution turns into a milky suspension as the pH is decreased below 5, indicating aggregation of the silica-PLGA(30) nanoparticles. Finally, at pH = 2, we observed complete precipitation of the nanoparticles. Our DLS measurements are in accordance with these observations: at pH above 5, we observed relatively monodisperse particles with an average diameter of 36 nm, while below pH = 4, we observed large aggregates that are larger than 1000 nm in size (Table 3.3).

Our results are in good accord with the literature on the pH dependent chain conformation of poly-L-glutamic acid. Literature reports indicate that PLGA (DP~105) has a pK_a of 4.375, and a transition inflection point (pH_t) about 5.74.[83]. On grafting the PLGA on flat silica substrates, the pH_t is observed to increase to 6.25.[84, 85] We noted that the zeta potentials in our experiments plateau at a large negative value for pH greater than about 5.5, suggesting complete deprotonation of the carboxylic acid side chains. Interestingly, the pH_t for PLGA grafted on silica nanoparticles in our measurements is closer to the value for free PLGA in solution than for PLGA grafted to flat silica surfaces. At high pH (> 5.5), the large electrostatic interparticle repulsion stabilizes the dispersion and prevents particle aggregation. As a result, a stable dispersion was observed. In contrast, the degree of dissociation of the carboxylic acid groups on the silica-PLGA decreases with decrease in pH below 5. Thus, the zeta potentials increase and hydrophobic interactions between peptide chains grafted to the particles result in aggregation.

pH	2	3	4	5	6.54	7
Particle size (nm)	>1000	>1000	>1000	63-66	28-45	28-45

Table 3.3: The particle size of silica-PLGA(30) at different pH

To further probe the structural changes of the PLGA attached to silica nanoparticle with change in pH, the FTIR spectra of the solid silica-PLGA nanoconjugate were recorded after treating with DI water, pH 8 and pH 2 buffers. For the silica-PLGA conjugate at pH 2 (Figure 3.8c), we observed a peak at 1729 cm^{-1} that we attribute to the carboxylic acid side chain. In addition, we observed peaks at 1665 cm^{-1} and 1543 cm^{-1} from the amide I and amide II absorbances. The carboxylic acid peak at 1729 cm^{-1} is absent in the silica-PLGA conjugates dispersed in DI water and at pH 8 (Figure 3.8a and b), indicating dissociation of the carboxylic acid groups; only the amide I and amide II resonances were observed. However,

we were unable to probe the change in secondary structure of the polypeptide on the silica nanoparticle surface with pH by circular dichroism spectroscopy due to the back scattering of the silica nanoparticles.

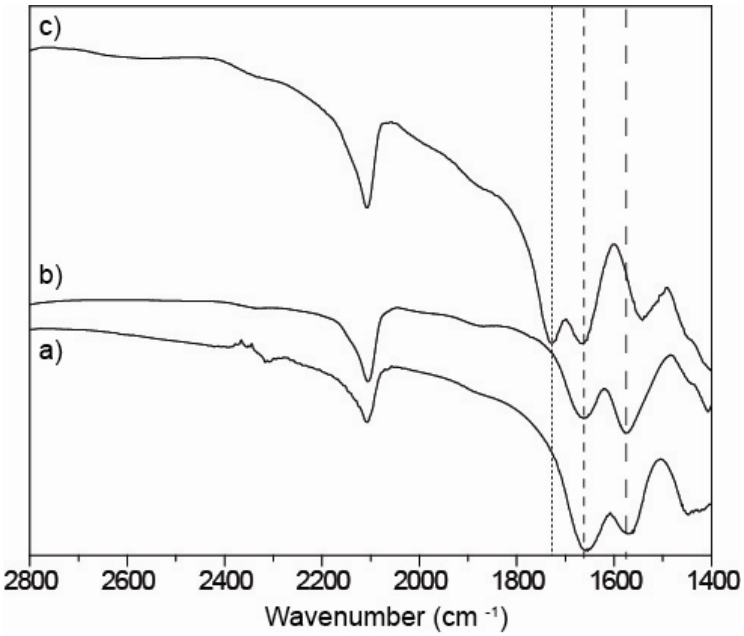

Figure 3.8: IR of a) silica-PLGA (pH 8), b) silica-PLGA (DI water), and c) silica-PLGA (pH 2). All samples were dried after incubation with corresponding water/buffer and the IR of the resulting solids were recorded

3.4 Applications of silica polypeptide nanoconjugates as biomaterials

3.4.1 Antibacterial properties of silica-PLL and silica-PLL-b-PLLeu

The antibacterial property of the silica-PLL and silica-PLL-*b*-PLLeu hybrid is shown in Figure 3.9. 250 μg/mL of silica-PLL-A and 100 μg/mL of silica-PLL-*b*-PLLeu was sufficient for the complete bactericidal activity in both Gram negative and Gram positive bacteria within half an hour. Even at the concentration of 50 μg/mL, considerable reduction (>90%) in the bacterial count was observed for both the nanoparticle conjugates. To confirm that the observed bactericidal effects were purely due to the grafted polypeptides, we tested the antibacterial activity of the precursor, namely azide functionalized silica (silica-N_3). Here, even after treating bacteria with 5 mg/mL of silica-N_3 (more than 100 times of the corresponding silica-PLL-A or silica-PLL-*b*-PLLeu) for 16 hrs, significant bacterial colonies were observed exemplifying the effectiveness of these polypeptides in bactericidal activity.

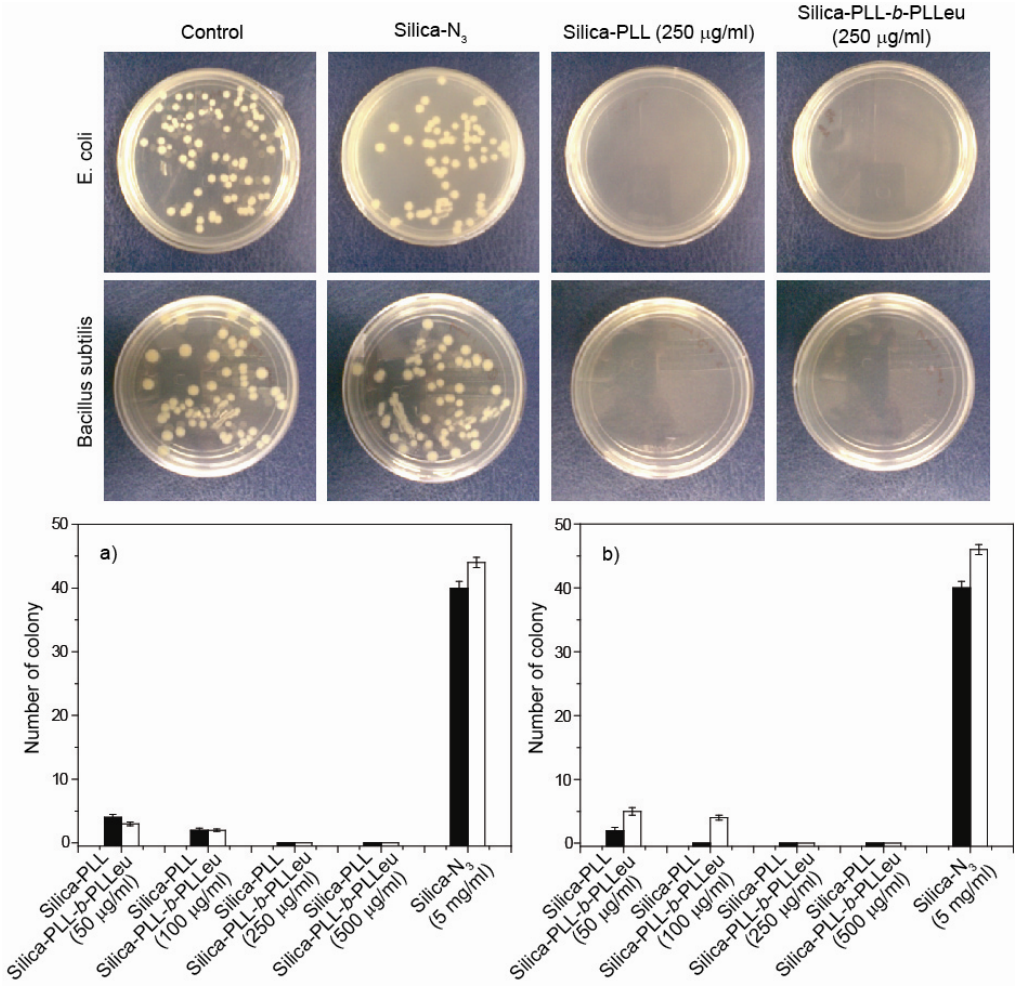

Figure 3.9: Activity of silica-PLL-A and silica-PLL-*b*-PLLeu concentrations at given time (0.5 hours) on a) E. coli and b) Bacillus subtilis bacteria

3.4.2 Assembly of silica-PLGA nanoparticles into 3D macroporous scaffolds and disassembly of these scaffolds

We now describe experiments that employ ice templating with directional freezing of aqueous dispersions of PLGA functionalized silica particles to generate well defined, aligned three dimensional macroporous structures. The PLGA-silica-30 hybrid particles were well dispersed in water at pH > 5. Therefore, we started with a 15% (approx, by weight) dispersion of hybrid particles at pH ≈ 6 in a 12 mm diameter glass vial (viz. sample dimensions are 12 mm diameter and 4 mm height, see supporting information) and directionally freeze it, by dipping the vial into liquid nitrogen. A crude calculation suggests that the interior of the sample freezes within about 3 s (Appendix II). After 10 minutes, the frozen system was freeze-dried to yield a porous monolith. SEM of this composite material indicated an aligned pore structure, as is expected for a unidirectional freezing process

(Figure 1.10a and b). We observed a lamellar structure with ~3-4 μm walls spaced at a periodicity of ~12 μm, and a fishbone-type structure was observed with ~1 μm thick secondary structures that connect the lamellar walls (Figure 3.10a). Such structures form during unidirectional freezing due to instabilities associated with the growth of ice. The primary lamellar spacing is set by the dominant wavelength associated with the highest rate of ice growth,[86] while the finer secondary structure that results in the fishbone architecture is believed to result from secondary instabilities.[68-71, 86] The formation of the primary lamellar structure is well understood.[86] The lamellar ice structures result from a balance between the energy of creating the ice interface and of setting up a concentration gradient of the "solute" particles from the freezing front. The Mullins-Sekerka instability, that results from this balance, yields a length scale that characterizes the primary width of the ice lamellae formed.[87] The formation of the finer secondary structure, such as, for example, the fishbone structure, results from other secondary instabilities that are not yet understood.[71] Interestingly, we observed the lamellar/fishbone structure throughout the sample under the experimental conditions employed, unlike literature reports on different systems[68-70, 86, 88]– however, the lamellar orientation in parts of the sample near the side walls was rotated with respect to that observed near the centre of the sample, in accordance with our intuition of the direction of propagation of the freezing front on immersion of the sample vial in liquid nitrogen (Appendix II). We have prepared large (several mm size) scaffolds using this technique. These PLGA-silica-30 scaffolds have a low bulk density (0.05 gcm^{-3}), and can be easily handled using tweezers.

In a control experiment, when we unidirectionally freeze a 15% aqueous dispersion of silica nanoparticles and PLGA (viz. where the PLGA is not grafted onto the particle surface), we observed qualitatively different morphology with closely spaced serrated walls (Figure 3.10c and d). This is not particularly surprising, since ice crystallization depends on the composition of the solutes, and the influence of PLGA grafted on a nanoparticle surface on the freezing process might be significantly different as compared to that of PLGA in solution. It is worth noting here that PLGA at the experimental pH is anionic, and is expected to stay in solution, rather than adsorbing on the negatively charged surface of the silica colloids.

Thus, ice templating process employed with the PLGA-silica particle dispersions results in the formation of macroporous structures, with aligned lamellar pores. Recently, the ice templating technique has been investigated extensively,[71] and it has been demonstrated

that different pore architectures can be obtained by rational, readily achievable changes in experimental conditions such as concentration of the solutions to be frozen, freezing rates, etc. In the macroporous structure obtained in our work, a biocompatible PLGA functionality is presented by the walls. The porous structure is also amenable to chemical modification, for example, for attachment of growth factors. Thus, ice templating of PLGA-silica dispersions yields surface functionalized macroporous materials with controllable pore geometry that can find use in a variety of applications.

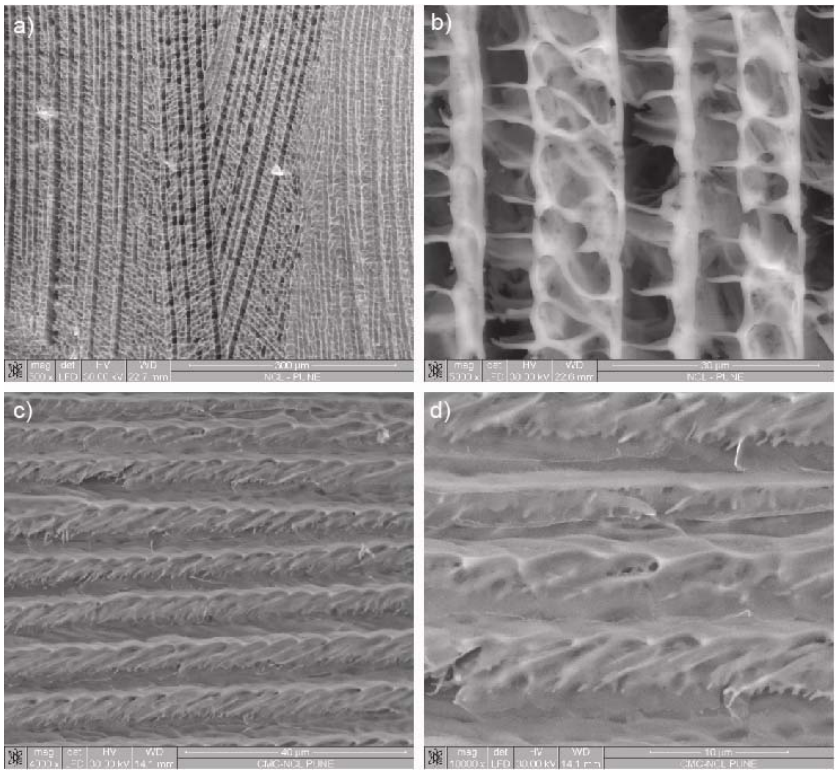

Figure 3.10: SEM of silica-PLGA in a) lower, b) higher resolution; physical mixture of Ludox (TM 50) and PLGA in c) lower resolution and d) higher resolution

Interestingly, we observed that when millimeter-sized pieces of the freeze dried silica-PLGA-30 scaffolds were dispersed in water (at pH ~ 7), they disassembled almost instantly as soon as the samples were dipped into water, and the particles were redispersed in water. DLS measurements of this solution indicated that disassembly of the scaffold was complete and the particle size distribution after disassembly was comparable to the starting PLGA-silica dispersion (Figure 3.11). We believe that this reversible disassembly results from the strong negative charge on the PLGA-silica particles that show a zeta potential of less than -60 mV. If instead, we immerse the scaffolds in acidic water at pH = 2, they fragment into large

aggregates that rapidly settle. Thus, immersion in pH = 2 water yields large aggregates rather than a dispersion of individual PLGA-silica particles.

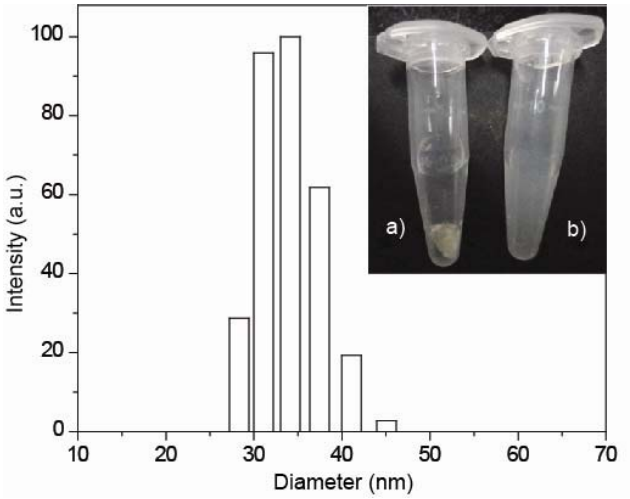

Figure 3.11: DLS of disassembled silica-PLGA scaffold in DI water; a) dispersion of silica-PLGA scaffold grafted with PEI with EDCI in DI water and b) dispersion of only silica-PLGA scaffold in DI water

Note: No scaffold is observed in (b) as it disintegrates instantly to form a well dispersed stable solution.

To stabilize the scaffold against disassembly in water, we have assembled polyethyleneimine (PEI, mol. Wt. 25000) onto the scaffold surface, by immersion of the scaffold into the solution of PEI in an anhydrous dichloromethane. We believe that the assembly of PEI on the Silica-PLGA(30) is driven by hydrogen bonding, as in previous reports of layer-by-layer assembly of polymers from organic solvents.[89, 90] TGA (Figure 3.13) confirmed the PEI grafting on the Silica-PLGA(30) surface and the grafting density is around 0.018 mmol/g. PEI deposition does not alter the structure of the scaffold – however, when PEI coated silica-PLGA scaffolds were dispersed in water at pH = 7, we observed that the scaffolds were stable against disassembly for about 20 min. Thus, while the PEI coated silica-PLGA(30) scaffolds too can be disassembled on immersion in water [91-94], the disassembly proceeds through swelling and disentanglement of the PEI-PLGA, and is therefore slower than for the PLGA-silica systems. Finally, we used EDCI coupling to crosslink the PEI coated PLGA-silica scaffolds to further stabilize the structure against disassembly on immersion in water. We observed that the structure of the macroporous scaffold is preserved after crosslinking (Figure 3.12). However, as anticipated, crosslinking decreases the susceptibility of the scaffold to disassembly and the scaffold is observed to maintain its integrity over several days when immersed in water at pH = 7 (Figure 3.11a).

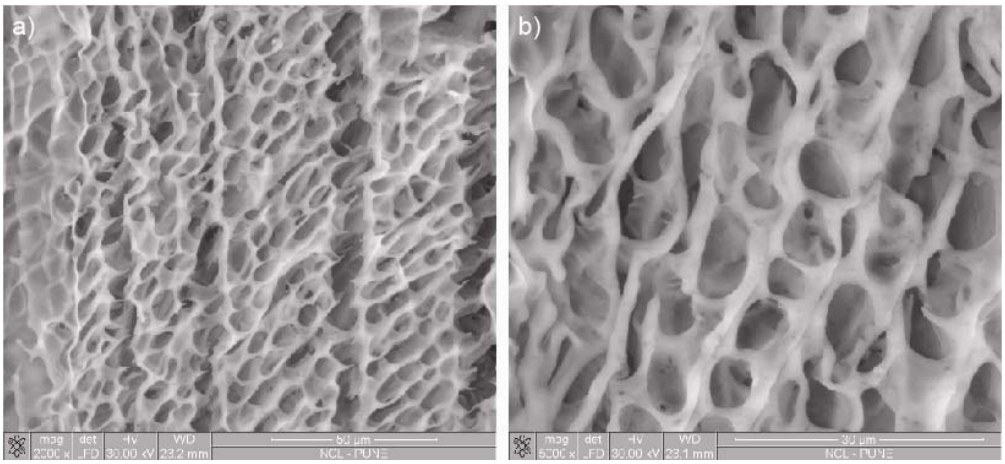

Figure 3.12: SEM Images of Silica-PLGA scaffold cross linked with PEI at a) lower and b) higher resolution

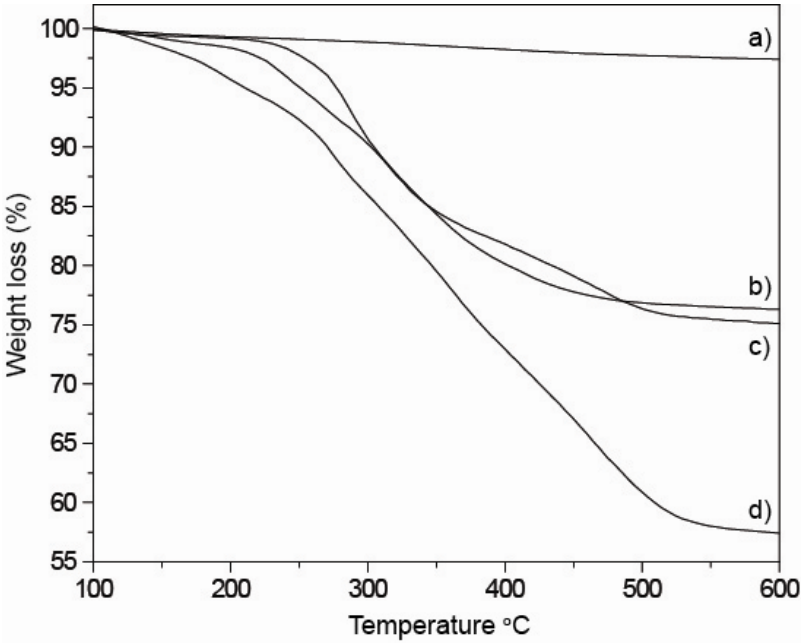

Figure 3.13: TGA of a) Ludox, b) Silica-PLGA, c) physical mixture of Ludox and PLGA, and c) Silica-PLGA-PEI

3.4.3 Cellular uptake and transfection studies with positively charged silica nanoconjugates

The use of gene therapy to treat increasing trends of cancer disease and genetic disorders has drawn major attention.[95-97] However, the progress of such therapy requires successful delivery of specifically designed genetic material such as DNA and SiRNA into the targeted cells or tissues.[10] Although most widely used gene carriers are viruses, their pathogenicity and immunogenicity have limited their application in gene therapy. To overcome these issues, several new synthetic compounds such as amphiphilic cationic lipids and polymers have been developed as non-viral gene vectors to deliver DNA and SiRNA into

cells.[98, 99] Amine grafted silica nanoparticles have been successfully used for DNA transfection.[43] It is known that poly-arginine is efficient transporter into the cells than any synthetic cationic polymers or polypeptides.[56] Here we have synthesized poly-L-arginine grafted silica nanoparticles which may be more efficient for cellular uptake and transfection.

3.4.3.1 Study of plasmid DNA silica-PLL, silica-PLArg(20) and silica-PLArg(10) polyplex formation using agarose gel electrophoresis

Gel retardation assay was performed to study the polyplex formation of the silica-PLL, silica-PLArg(20) and silica-PLArg(10) with plasmid DNA (pDNA). Polyplex formation was obtained by incubating pDNA (0.2 μg) with silica-PLL, silica-PLArg(20) and silica-PLArg(10) at increasing silica:pDNA various weight ratios. After incubation for 30 minutes at room temperature, the polyplex formation was examined by agarose gel electrophoresis. Complete retardation of the pDNA was observed in polyplexes that were formed with pDNA:silica-PLArg(20) ratio of 1:1 and above and for silica-PLArg(10) ratio of 1:2 and above but for pDNA:silica-PLL ratio of 1:30 required for complete retardation (Figure 3.14). The higher ratio required for complete pDNA retardation for silica-PLL was expected as silica-PLL particles are highly prone to aggregate themselves in water solution instead of having higher zeta potential value (+51±3 mV), which shielded their effective positive charge on the surface. Since the zeta potential of silica-PLArg(20) (+56±4 mV) is higher than silica-PLArg(10) (+42±3 mV), the higher positive charge of silica-PLArg(20) allows it to condense pDNA more efficiently than silica-PLArg(10).

3.4.3.2 Cytotoxicity assay of silica-PLArgs

MTT assays[74] were performed to evaluate the cytotoxicity of silica poly-L-arginine nanoconjugates (Figure 3.15). MTT assays of silica-PLArg(20) and silica-PLArg(10) in two mammalian cancerous cell lines HeLa and A549 showed that both the cells retained around 75-80% viability after treatment with up to 100μg of silica-PLArg(20) and silica-PLArg(10). It should be noted that in spite of silica poly-L-arginine nanoconjugates having a very high zeta potential (+56±4 and +42±3 for silica-PLArg(20) and silica-PLArg(10) respectively), they still show very low cytotoxicity at concentrations that would be used for DNA transfection. Although high charge on the surface of silica induces strong interaction with the cell membrane (leading to high cellular uptake), it is also responsible for cell cytotoxicity. As a control experiment, PEI (25 kD) was used for MTT assay. The poly-L-arginine silica nanoconjugates offer a great advantage of having high surface charge and low cytotoxicity.

The poly-L-argnine present on the surface is biodegradable by various cellular proteases enzymes. Hence, the possibility of long term toxicity arising from the polypeptide will be much less.

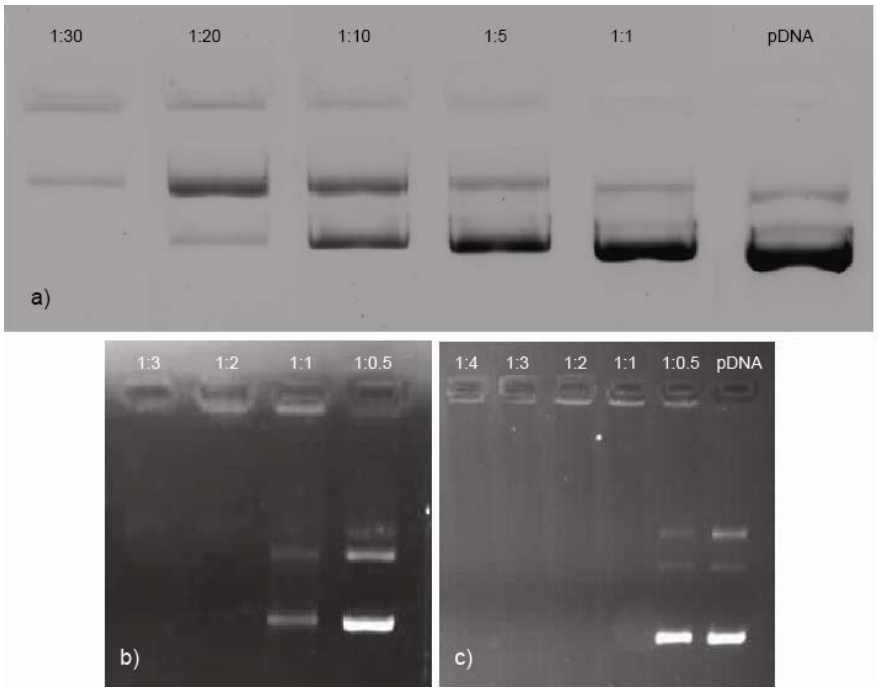

Figure 3.14: Retardation of plasmid DNA by silica-nanoconjugates, a) silica-PLL; from the right DNA and silica-PLL ratio, lane 1 (pDNA), lane 2 (1:1), lane 3 (1:5), lane 4 (1:10), lane 5 (1:20) and lane 6 (1:30), b) silica-PLArg(10); from the right DNA and silica-PLArg(10) ratio, lane 1 (1:0.5), lane 2 (1:1), lane 3 (1:2), lane 4 (1:3) and c) silica-PLArg(20); from the right DNA and silica-PLArg(20) ratio, lane 1 (pDNA), lane 2 (1:0.5), lane 3 (1:1), lane 4 (1:2), lane 5 (1:3) and lane 6 (1:4).

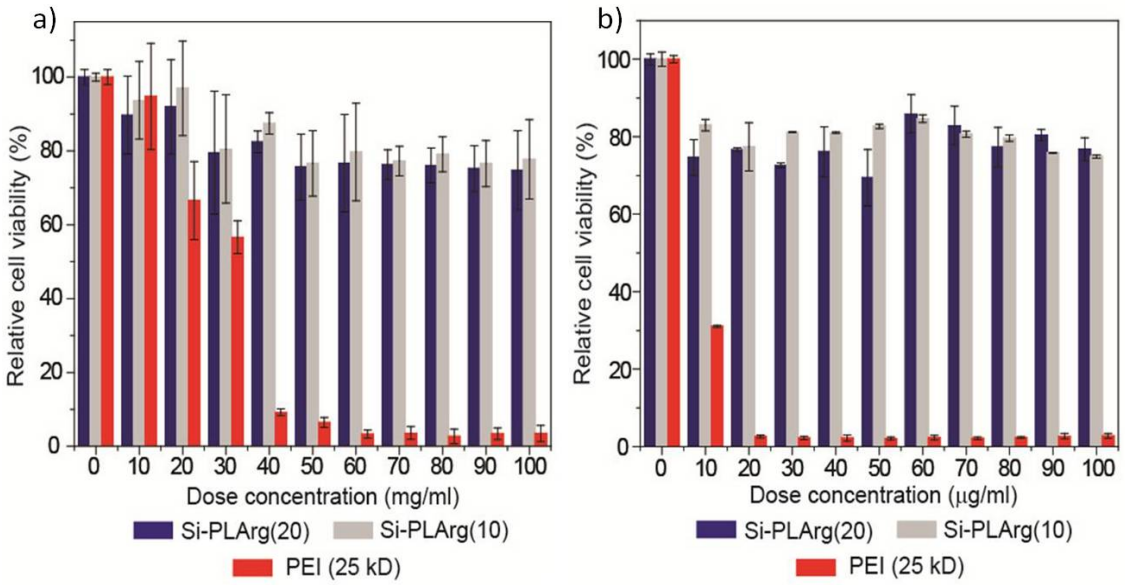

Figure 3.15: Results of MTT assay of silica-PLArg(20) and silica-PLArg(10) in a) HeLa and b) A549 cells

3.4.3.3 Cellular uptake of the silica poly-L-arginine nanoconjugates

The cellular uptake of poly-L-arginine grafted silica nanoparticles were studied in both HeLa and A549 cancer cells. The high zeta potential values of silica-PLArg(20) and silica-PLArg(10) (+56±4 mV and 42±3 mV respectively) indicate that these poly-L-arginine conjugates have the potential to enter cells very effectively. To adequately follow their cellular uptake, silica-PLArg(20) and silica-PLArg(10) were labelled with fluorescein and 2 µg/ml of the fluorescently labeled poly-L-arginine conjugates were added to HeLa and A549 and incubated for 4 hrs. Strong signals from fluorescein were observed in both HeLa and A549 cells indicating that these conjugates were successfully internalized in most of the cells (Figure 3.16 a and c). In control experiment, fluorescein labeled silica azide nanoparticle (2 µg/ml) was added to HeLa and incubated for 24 hours (Figure 3.16e).

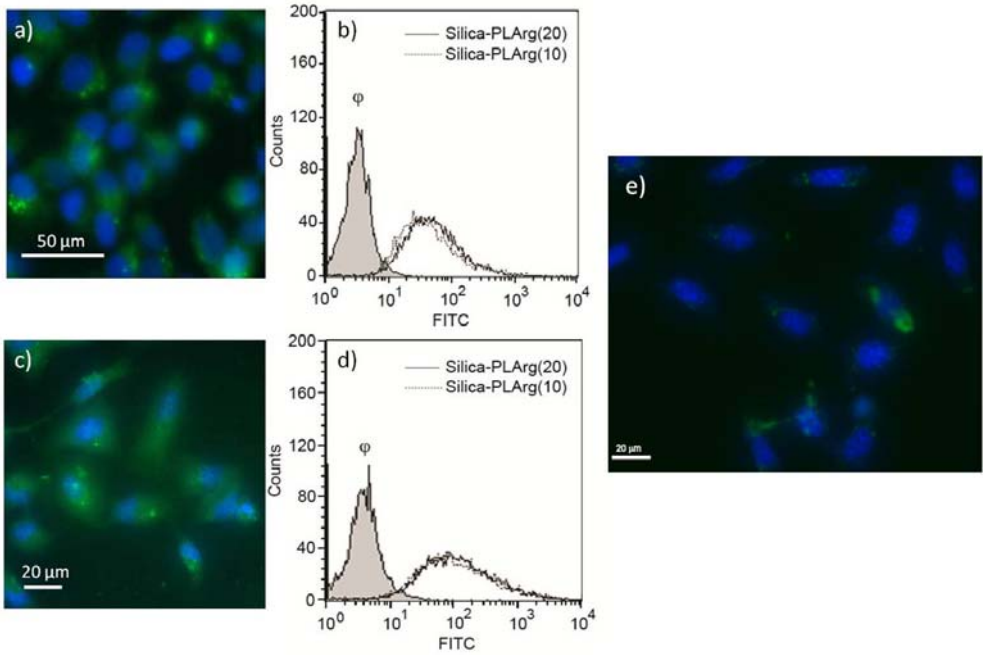

Figure 3.16: a) Epifluorescence image of Hela cells after incubation with fluorescein labeled silica-PLArg(20) for 24 hrs and b) Assessment of cellular uptake of fluorescently labeled silica-PLArg(20) and silica-PLArg(10) onto HeLa cells by flow cytometry analysis c) Epifluorescence image of A549 cells after incubation with fluorescein labeled silica-PLArg(20) for 24 hrs, d) Assessment of cellular uptake of fluorescently labeled silica-PLArg(20) and silica-PLArg(10) onto A549 cells by flow cytometry analysis and e)

Epifluorescence image of HeLa cells after incubation with fluorescein labeled silica azide for 24 hrs.

A very low signals from the HeLa was observed, this is due to the EPR effect. To obtain a quantitative estimation of cellular uptake, fluorescence-activated cell sorting (FACS) was performed on both HeLa and A549 cells that were treated with fluorescently labeled silica-PLArg(20) and silica-PLArg(10). Flow cytometry analysis of all the samples resulted in a clean shift of MFI (mean fluorescent intensity) and the cellular uptake of silica-PLArg(20) and silica-PLArg(10) in both HeLa and A549 cells was estimated to be about 90% and above.(Figure 3.16) This is expected since poly-L-arginine is known to be more efficient cell penetrating polypeptide than poly-L-lysine and hence their presence on the surface of these nanoparticles facilitates its entry into the cells.[100, 101]

3.4.3.4 DNA transfection studies with silica-PLArgs

Silica-PLArg(20) and silica-PLArg(10) were used as carrier to transfect both HeLa and A549 cells with plasmid that expresses mCherry. For transfection study various pDNA:silica-PLArgs ratios (1:6, 1:8 and 1:12) were used. However, almost no expression of mCherry protein was observed by epifluorescence microscopy, although the green fluorescence observed in the cells indicated that the fluorescein labeled nanoparticles entered the cells very efficiently (Figure 3.17). The probable reason for this observation is that the very high positive charge of the silica-PLArg(20) renders very high stability to the polyplex formed with p-DNA and although it enters into the cell very efficiently, the pDNA does not leach out inside the cytoplasm to transfect the protein of interest and the tightly bound pDNA transfect locally mCherry protein. As a control experiment, HeLa cells were treated with 1:4 ratio of pDNA and commercially available lipofectamin and incubated for 48 hrs. The expression of mCherry protein was very intense all over the cells (Figure 3.17). In presence of 100 μM chloroquine on the media, silica-PLArg(20) was able to transfect both the HeLa and A549 cells leading to the expression of the red mCherry protein with very low efficiency (Figure 3.18). The used of chloroquine have been reported for organically modified silica nanoparticles.[43]In these cationic silica nanoparticles, transfection was observed only after addition of 100 μM chloroquine in the media. The chloroquine is expected to interact with polyplex and help to release the pDNA from polyplex to cytoplasm. The poor efficiency of silica-PLArg(20) may be attributed to the high density of poly-L-arginine that is present on the surface of this material. The high positive charge density of these nanoparticles (zeta potential +56±4; size +34±4 nm) results in stronger binding with DNA plasmid which in turn

does not allow its escape from the endosome. Hence normal transfection is not observed and chlorquine is required to effect transfection.

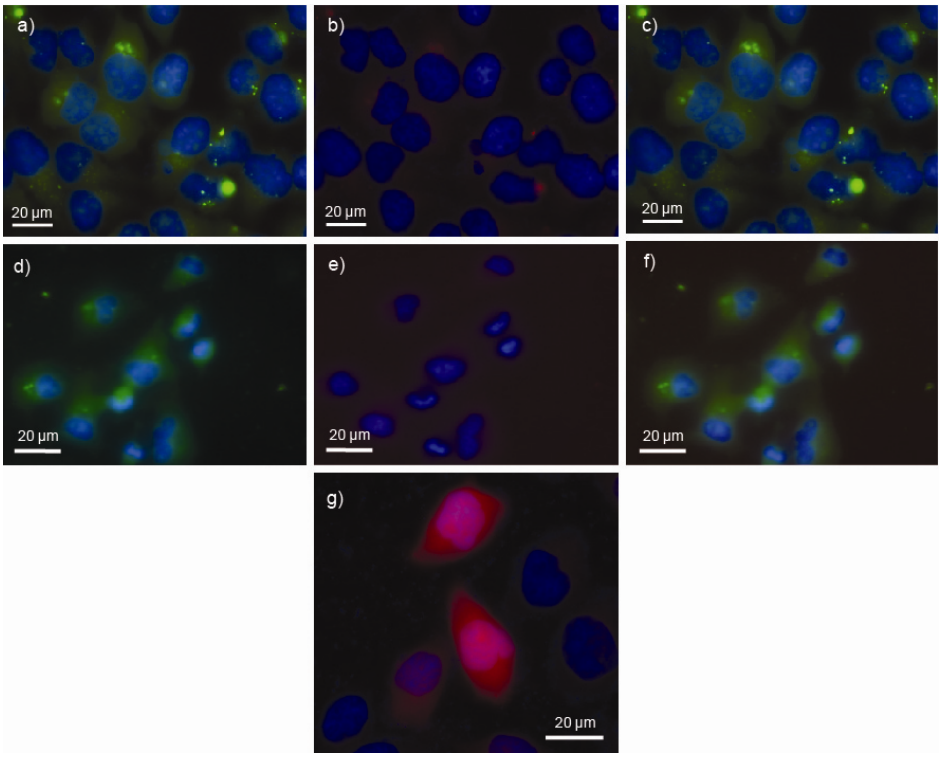

Figure 3.17: Transfection of Hela cells with silica-PLArg(20) and mCherry DNA plasmid: a) The localization of fluorescein labeled silica-PLArg(20) in cells is shown in green with nucleus stained in blue with DAPI, b) The expression of red mCherry protein is absence in the cells with nucleus stained in blue with DAPI c) overlap image of a) and b), and Transfection of A549 cells with silica-PLArg(20) and mCherry DNA plasmid: d) The localization of fluorescein labeled silica-PLArg(20) in cells is shown in green with nucleus stained in blue with DAPI, e) The expression of red mCherry protein is absent in the cells with nucleus stained in blue with DAPI f) overlap image of d) and e), and f) Transfection of HeLa cells with lipofectamin and mcherry DNA plasmid.

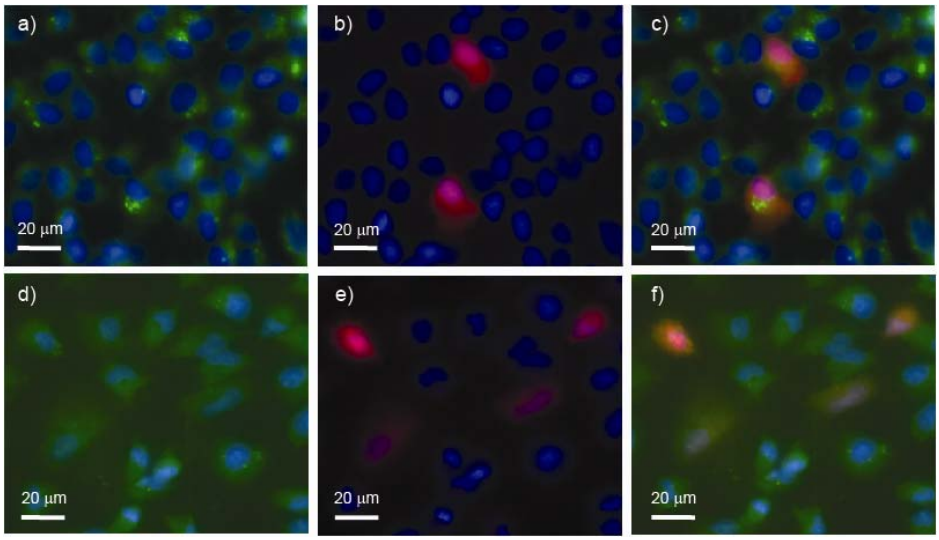

Figure 3.18: Transfection of HeLa cells with silica-PLArg(20) and mCherry DNA plasmid with (100 µm/ml) chloroquine: a) The localization of fluorescein labeled silica-PLArg(20)in cells is shown in green with nucleus stained in blue with DAPI, b) The expression of red mCherry protein is absence in the cells with nucleus stained in blue with DAPI c) overlap image of a) and b) and Transfection of A549 cells with silica-PLArg(20)and mCherry DNA plasmid with (100 µm/ ml) chloroquine: d) The localization of fluorescein labeled silica-PLArg(20) in cells is shown in green with nucleus stained in blue with DAPI, e) The expression of red mCherry protein is absence in the cells with nucleus stained in blue with DAPI f) overlap image of d) and e)

3.5 Conclusions

The synthesis of homo and block co-polypeptides grafted silica nanoconjugates with high grafting density has been successfully achieved by the "grafting to" methodology using a combination of NCA polymerization and click chemistry. Although the grafting to technique is traditionally known to be inefficient, the CuAAC "click chemistry" allows grafting of very high density of unprotected polypeptide onto the silica nanoparticles. This is a general methodology and can be extended to any natural and synthetic polypeptides. For example, uniform poly-L-lysine coated nanoparticles were synthesized using this methodology. Further, the silica-PLL and silica-PLL-*b*-PLLeu displays excellent antimicrobial properties against both Gram positive and Gram negative bacteria. These particles can be therefore used as bactericidal coatings bearing contact bacteria-killing capacity.[102] Their differing solubility also allows us to disperse them in both water and oil-based paints in an effort to make anti-microbial paints.[103] On the other hand, silica-PLGA particles are stable and remain well dispersed in water for long periods. They are also pH

responsive and aggregate into large clusters at pH less than 5. This is driven by a change in the overall charge and conformation of the grafted polypeptide chains with change in pH. This synthetic methodology can also be extended for the synthesis of poly-L-glutamate functionalized porous silica nanomaterials as has been shown before.[104] Such materials can have applications in controlled drug release as has been shown recently with similar poly-acrylic acid functionalized porous silica nanoparticles.[105] Preliminary experiments show that aqueous dispersions of these PLGA functionalized silica nanoparticles can be used to generate well defined, aligned three dimensional macroporous structures using ice templating with directional freezing. Thus, these macroporous materials are comprised of a biocompatible polymer shell covalently attached to rigid inorganic cores. Since the synthetic scheme of the nanoparticle developed by us allows the polymer and inorganic components to be individually tailored, scaffolds having a wide range of physical properties can be synthesized. The poly-L-glutamic acid shell on these scaffolds is biocompatible and is amenable to further functionalization with amine containing molecules. Therefore functional organic moieties like growth factors can be easily incorporated on the surface of these scaffolds to make them amenable for tissue engineering applications. Finally, silica-PLArgs nanoconjugates that have very high surface positive charge and disperse very well in water has been successfully synthesized. The low cytotoxicity coupled with the very high cell-penetrating ability of silica-PLArg's are likely to make them efficient delivery vehicles for nucleic acid. Since silica-PLArgs have very high positive surface charge they bind very efficiently with the nucleic acids. The inherent cell penetrating property of surface poly-L-arginine renders the silica-PLArg nanoconjugates very efficient for entering mamalian cells. Due to the high positive surface charge of this nanoconjugate the pDNA is not able to leach from the polyplex to transfect the protein of interest but transfection can be affected in the presence of 100 μM chloroquine.

3.6 References

1. Radhakrishnan, B.; Ranjan, R.; Brittain, W. J., Surface initiated polymerizations from silica nanoparticles. *Soft Matter* **2006,** 2, (5), 386-396.

2. Zou, H.; Wu, S.; Shen, J., Polymer/Silica Nanocomposites: Preparation, characterization, propertles, and applications. *Chemical Reviews* **2008,** 108, (9), 3893-3957.

3. Chuan Hsiao, S.; Hau-Chun, C.; Raymond Chien-Chao, T.; Ta-Jo, L.; Jeng-Jaw, W., Synthesis of organic-inorganic hybrid polymeric nanocomposites for the hard coat application. *Journal of Applied Polymer Science* **2007,** 103, (6), 3985-3993.

4. Chiang, C.-L.; Ma, C.-C. M.; Wu, D.-L.; Kuan, H.-C., Preparation, characterization, and properties of novolac-type phenolic/SiO2 hybrid organic–inorganic nanocomposite materials by sol–gel method. *Journal of Polymer Science Part A: Polymer Chemistry* **2003,** 41, (7), 905-913.

5. Chang, C.-C.; Chen, W.-C., Synthesis and Optical Properties of Polyimide-Silica Hybrid Thin Films. *Chemistry of Materials* **2002,** 14, (10), 4242-4248.

6. Sondi, I.; Fedynyshyn, T. H.; Sinta, R.; Matijevic, E., Encapsulation of Nanosized Silica by in Situ Polymerization of tert-Butyl Acrylate Monomer. *Langmuir* **2000,** 16, (23), 9031-9034.

7. Saxena, A.; Tripathi, B. P.; Shahi, V. K., Sulfonated Poly(styrene-co-maleic anhydride)-Poly(ethylene glycol)-Silica Nanocomposite Polyelectrolyte Membranes for Fuel Cell Applications. *The Journal of Physical Chemistry B* **2007,** 111, (43), 12454-12461.

8. Jang, J.; Ha, J.; Lim, B., Synthesis and characterization of monodisperse silica-polyaniline core-shell nanoparticles. *Chemical Communications* **2006**, (15), 1622-1624.

9. Bartholome, C.; Beyou, E.; Bourgeat-Lami, E.; Chaumont, P.; Lefebvre, F.; Zydowicz, N., Nitroxide-Mediated Polymerization of Styrene Initiated from the Surface of Silica Nanoparticles. In Situ Generation and Grafting of Alkoxyamine Initiators. *Macromolecules* **2005,** 38, (4), 1099-1106.

10. Bharali, D. J.; Klejbor, I.; Stachowiak, E. K.; Dutta, P.; Roy, I.; Kaur, N.; Bergey, E. J.; Prasad, P. N.; Stachowiak, M. K., Organically modified silica nanoparticles: A nonviral vector for in vivo gene delivery and expression in the brain. *Proceedings of the National Academy of Sciences of the United States of America* **2005,** 102, (32), 11539-11544.

11. Poologasundarampillai, G.; Yu, B.; Tsigkou, O.; Valliant, E.; Yue, S.; Lee, P. D.; Hamilton, R. W.; Stevens, M. M.; Kasuga, T.; Jones, J. R., Bioactive silica-poly([gamma]-glutamic acid) hybrids for bone regeneration: effect of covalent coupling on dissolution and mechanical properties and fabrication of porous scaffolds. *Soft Matter* **2012,** 8, (17), 4822-4832.

12. Kar, M.; Vijayakumar, P. S.; Prasad, B. L. V.; Gupta, S. S., Synthesis and Characterization of Poly-l-lysine-Grafted Silica Nanoparticles Synthesized via NCA Polymerization and Click Chemistry. *Langmuir* **2010,** 26, (8), 5772-5781.

13. Song, J.; Kong, H.; Jang, J., Enhanced antibacterial performance of cationic polymer modified silica nanoparticles. *Chemical Communications* **2009**, (36), 5418-5420.

14. Jang, J.; Kim, Y., Fabrication of monodisperse silica-polymer core-shell nanoparticles with excellent antimicrobial efficacy. *Chemical Communications* **2008**, (34), 4016-4018.

15. Tallury, P.; Payton, K.; Santra, S., Silica-based multimodal/multifunctional nanoparticles for bioimaging and biosensing applications. *Nanomedicine* **2008,** 3, (4), 579-592.

16. Piao, Y.; Burns, A.; Kim, J.; Wiesner, U.; Hyeon, T., Designed Fabrication of Silica-Based Nanostructured Particle Systems for Nanomedicine Applications. *Advanced Functional Materials* **2008,** 18, (23), 3745-3758.

17. Ding, X.; Zhao, J.; Liu, Y.; Zhang, H.; Wang, Z., Silica nanoparticles encapsulated by polystyrene via surface grafting and in situ emulsion polymerization. *Materials Letters* **2004,** 58, (25), 3126-3130.

18. Reculusa, S.; Mingotaud, C.; Bourgeat-Lami, E.; Duguet, E.; Ravaine, S., Synthesis of Daisy-Shaped and Multipod-like Silica/Polystyrene Nanocomposites. *Nano Letters* **2004,** 4, (9), 1677-1682.

19. Jyongsik, J.; Hwanseok, P., Formation and structure of polyacrylamide-silica nanocomposites by sol-gel process. *Journal of Applied Polymer Science* **2002,** 83, (8), 1817-1823.

20. Cheng, W.; Wang, Z.; Ren, C.; Chen, H.; Tang, T., Preparation of silica/polyacrylamide/polyethylene nanocomposite via in situ polymerization. *Materials Letters* **2007,** 61, (14-15), 3193-3196.

21. Li, Z.; Zhu, S.; Gan, K.; Zhang, Q.; Zeng, Z.; Zhou, Y.; Liu, H.; Xiong, W.; Li, X.; Li, G., Poly-L-lysine-Modified Silica Nanoparticles: A Potential Oral Gene Delivery System. *Journal of Nanoscience and Nanotechnology* **2005,** 5, 1199-1203.

22. Bagwe, R. P.; Hilliard, L. R.; Tan, W., Surface Modification of Silica Nanoparticles to Reduce Aggregation and Nonspecific Binding. *Langmuir* **2006,** 22, (9), 4357-4362.

23. von Werne, T.; Patten, T. E., Preparation of Structurally Well-Defined Polymer Nanoparticle Hybrids with Controlled/Living Radical Polymerizations. *Journal of the American Chemical Society* **1999,** 121, (32), 7409-7410.

24. Tsujii, Y.; Ejaz, M.; Sato, K.; Goto, A.; Fukuda, T., Mechanism and Kinetics of RAFT-Mediated Graft Polymerization of Styrene on a Solid Surface. 1. Experimental Evidence of Surface Radical Migration. *Macromolecules* **2001,** 34, (26), 8872-8878.

25. Matsuda, Y.; Kobayashi, M.; Annaka, M.; Ishihara, K.; Takahara, A., Dimensions of a Free Linear Polymer and Polymer Immobilized on Silica Nanoparticles of a Zwitterionic Polymer in Aqueous Solutions with Various Ionic Strengths. *Langmuir* **2008,** 24, (16), 8772-8778.

26. Rajesh, R.; William, J. B., Synthesis of High Density Polymer Brushes on Nanoparticles by Combined RAFT Polymerization and Click Chemistry. *Macromolecular Rapid Communications* **2008,** 29, (12-13), 1104-1110.

27. Bartholome, C.; Beyou, E.; Bourgeat-Lami, E.; Chaumont, P.; Zydowicz, N., Nitroxide-Mediated Polymerizations from Silica Nanoparticle Surfaces: "Graft from" Polymerization of Styrene Using a Triethoxysilyl-Terminated Alkoxyamine Initiator. *Macromolecules* **2003,** 36, (21), 7946-7952.

28. Carrot, G.; Rutot-Houze, D.; Pottier, A.; Degee, P.; Hilborn, J.; Dubois, P., Surface-Initiated Ring-Opening Polymerization: A Versatile Method for Nanoparticle Ordering. *Macromolecules* **2002,** 35, (22), 8400-8404.

29. Mathieu, J.; Christelle, D.; Elodie, B.-L.; Philippe, D., Ring-opening polymerization of e-caprolactone and L-lactide from silica nanoparticles surface. *Journal of Polymer Science Part A: Polymer Chemistry* **2004,** 42, (8), 1976-1984.

30. Mingotaud, A.-F.; Reculusa, S.; Mingotaud, C.; Keller, P.; Sykes, C.; Duguet, E.; Ravaine, S., Ring-opening metathesis polymerization on well defined silica nanoparticles leading to hybrid core-shell particles. *Journal of Materials Chemistry* **2003,** 13, (8), 1920-1925.

31. Jordi, M. A.; Seery, T. A. P., Quantitative Determination of the Chemical Composition of Silica Poly(norbornene) Nanocomposites. *Journal of the American Chemical Society* **2005,** 127, (12), 4416-4422.

32. Rajesh, R.; William, J. B., Tandem RAFT Polymerization and Click Chemistry: An Efficient Approach to Surface Modification. *Macromolecular Rapid Communications* **2007,** 28, (21), 2084-2089.
33. Ulijn, R. V.; Smith, A. M., Designing peptide based nanomaterials. *Chemical Society Reviews* **2008,** 37, (4), 664-675.
34. Mart, R. J.; Osborne, R. D.; Stevens, M. M.; Ulijn, R. V., Peptide-based stimuli-responsive biomaterials. *Soft Matter* **2006,** 2, (10), 822-835.
35. Chang, Y.-C.; Frank, C. W., Grafting of Poly(g-benzyl-l-glutamate) on Chemically Modified Silicon Oxide Surfaces. *Langmuir* **1996,** 12, (24), 5824-5829.
36. Chang, Y.-C.; Frank, C. W., Vapor Deposition Polymerization of a-Amino Acid N-Carboxy Anhydride on the Silicon(100) Native Oxide Surface. *Langmuir* **1998,** 14, (2), 326-334.
37. Wieringa, R. H.; Siesling, E. A.; Geurts, P. F. M.; Werkman, P. J.; Vorenkamp, E. J.; Erb, V.; Stamm, M.; Schouten, A. J., Surface Grafting of Poly(l-glutamates). 1. Synthesis and Characterization. *Langmuir* **2001,** 17, (21), 6477-6484.
38. Lu, Z.-R.; Wang, X.; Parker, D. L.; Goodrich, K. C.; Buswell, H. R., Poly(l-glutamic acid) Gd(III)-DOTA Conjugate with a Degradable Spacer for Magnetic Resonance Imaging. *Bioconjugate Chemistry* **2003,** 14, (4), 715-719.
39. Fong, B.; Russo, P. S., Organophilic Colloidal Particles with a Synthetic Polypeptide Coating. *Langmuir* **1999,** 15, (13), 4421-4426.
40. Fong, B.; Turksen, S.; Russo, P. S.; Stryjewski, W., Colloidal Crystals of Silica Homopolypeptide Composite Particles. *Langmuir* **2004,** 20, (1), 266-269.
41. Abelow, A. E.; Zharov, I., Poly(l-alanine)-modified nanoporous colloidal films. *Soft Matter* **2009,** 5, (2), 457-462.
42. Lunn, J. D.; Shantz, D. F., Peptide Brush Ordered Mesoporous Silica Nanocomposite Materials. *Chemistry of Materials* **2009,** 21, (15), 3638-3648.
43. Kneuer, C.; Sameti, M.; Bakowsky, U.; Schiestel, T.; Schirra, H.; Schmidt, H.; Lehr, C.-M., A Nonviral DNA Delivery System Based on Surface Modified Silica-Nanoparticles Can Efficiently Transfect Cells in Vitro. *Bioconjugate Chemistry* **2000,** 11, (6), 926-932.
44. Putnam, D.; Gentry, C. A.; Pack, D. W.; Langer, R., Polymer-based gene delivery with low cytotoxicity by a unique balance of side-chain termini. *Proceedings of the National Academy of Sciences of the United States of America* **2001,** 98, (3), 1200-1205.
45. Gilbert, P.; Moore, L. E., Cationic antiseptics: diversity of action under a common epithet. *Journal of Applied Microbiology* **2005,** 99, (4), 703-715.
46. Kurt, P.; Wood, L.; Ohman, D. E.; Wynne, K. J., Highly Effective Contact Antimicrobial Surfaces via Polymer Surface Modifiers. *Langmuir* **2007,** 23, (9), 4719-4723.
47. Meng, F.; Zhong, Z.; Feijen, J., Stimuli-Responsive Polymersomes for Programmed Drug Delivery. *Biomacromolecules* **2009,** 10, (2), 197-209.
48. Maeda, H.; Kabanov, A.; Kataoka, K.; Okano, T.; Singer, J. W.; Baker, B.; Vries, P.; Kumar, A.; Shaffer, S.; Vawter, E.; Bolton, M.; Garzone, P., Poly-(L)-Glutamic Acid-Paclitaxel (CT-2103) [XYOTAX™], a Biodegradable Polymeric Drug Conjugate. In *Polymer Drugs in the Clinical Stage*, Springer US: 2004; Vol. 519, pp 81-99.

49. Hsieh, C.-Y.; Tsai, S.-P.; Wang, D.-M.; Chang, Y.-N.; Hsieh, H.-J., Preparation of [gamma]-PGA/chitosan composite tissue engineering matrices. *Biomaterials* **2005,** 26, (28), 5617-5623.

50. Wen, X.; Jackson, E. F.; Price, R. E.; Kim, E. E.; Wu, Q.; Wallace, S.; Charnsangavej, C.; Gelovani, J. G.; Li, C., Synthesis and Characterization of Poly(l-glutamic acid) Gadolinium Chelate: A New Biodegradable MRI Contrast Agent. *Bioconjugate Chemistry* **2004,** 15, (6), 1408-1415.

51. Chen, X.; Randall, D. P.; Perruchot, C.; Watts, J. F.; Patten, T. E.; von Werne, T.; Armes, S. P., Synthesis and aqueous solution properties of polyelectrolyte-grafted silica particles prepared by surface-initiated atom transfer radical polymerization. *Journal of Colloid and Interface Science* **2003,** 257, (1), 56-64.

52. Rodriguez-Hernandez, J.; Lecommandoux, S., Reversible Inside-Out Micellization of pH-responsive and Water-Soluble Vesicles Based on Polypeptide Diblock Copolymers. *Journal of the American Chemical Society* **2005,** 127, (7), 2026-2027.

53. Chécot, F.; Lecommandoux, S.; Gnanou, Y.; Klok, H.-A., Water-Soluble Stimuli-Responsive Vesicles from Peptide-Based Diblock Copolymers. *Angewandte Chemie* **2002,** 114, (8), 1395-1399.

54. Heise, A.; Menzel, H.; Yim, H.; Foster, M. D.; Wieringa, R. H.; Schouten, A. J.; Erb, V.; Stamm, M., Grafting of Polypeptides on Solid Substrates by Initiation of N-Carboxyanhydride Polymerization by Amino-Terminated Self-Assembled Monolayers. *Langmuir* **1997,** 13, (4), 723-728.

55. Ryser, H. J. P.; Hancock, R., Histones and Basic Polyamino Acids Stimulate the Uptake of Albumin by Tumor Cells in Culture. *Science* **1965,** 150, (3695), 501-503.

56. Mitchell, D. J.; Steinman, L.; Kim, D. T.; Fathman, C. G.; Rothbard, J. B., Polyarginine enters cells more efficiently than other polycationic homopolymers. *The Journal of Peptide Research* **2000,** 56, (5), 318-325.

57. Wender, P. A.; Mitchell, D. J.; Pattabiraman, K.; Pelkey, E. T.; Steinman, L.; Rothbard, J. B., The design, synthesis, and evaluation of molecules that enable or enhance cellular uptake: Peptoid molecular transporters. *Proceedings of the National Academy of Sciences* **2000,** 97, (24), 13003-13008.

58. Maiolo, J. R.; Ferrer, M.; Ottinger, E. A., Effects of cargo molecules on the cellular uptake of arginine-rich cell-penetrating peptides. *Biochimica et Biophysica Acta (BBA) - Biomembranes* **2005,** 1712, (2), 161-172.

59. Fonseca, S. B.; Pereira, M. P.; Kelley, S. O., Recent advances in the use of cell-penetrating peptides for medical and biological applications. *Advanced Drug Delivery Reviews* **2009,** 61, (11), 953-964.

60. Bolhassani, A., Potential efficacy of cell-penetrating peptides for nucleic acid and drug delivery in cancer. *Biochimica et Biophysica Acta (BBA) - Reviews on Cancer* **2011,** 1816, (2), 232-246.

61. Temsamani, J.; Vidal, P., The use of cell-penetrating peptides for drug delivery. *Drug Discovery Today* **2004,** 9, (23), 1012-1019.

62. Mae, M.; Langel, U., Cell-penetrating peptides as vectors for peptide, protein and oligonucleotide delivery. *Current Opinion in Pharmacology* **2006,** 6, (5), 509-514.

63. Stewart, K. M.; Horton, K. L.; Kelley, S. O., Cell-penetrating peptides as delivery vehicles for biology and medicine. *Organic & Biomolecular Chemistry* **2008,** 6, (13), 2242-2255.

64. Hadjichristidis, N.; Iatrou, H.; Pitsikalis, M.; Sakellariou, G., Synthesis of Well-Defined Polypeptide-Based Materials via the Ring-Opening Polymerization of a-Amino Acid N-Carboxyanhydrides. *Chemical Reviews* **2009**.

65. Rostovtsev, V. V.; Green, L. G.; Fokin, V. V.; Sharpless, K. B., A Stepwise Huisgen Cycloaddition Process: Copper(I)-Catalyzed Regioselective "Ligatio" of Azides and Terminal Alkynes. *Angewandte Chemie International Edition* **2002,** 41, (14), 2596-2599.

66. Barner-Kowollik, C.; Du Prez, F. E.; Espeel, P.; Hawker, C. J.; Junkers, T.; Schlaad, H.; Van Camp, W., "Clicking" Polymers or Just Efficient Linking: What Is the Difference? *Angewandte Chemie International Edition* **2010,** 50, (1), 60-62.

67. Fournier, D.; Hoogenboom, R.; Schubert, U. S., Clicking polymers: a straightforward approach to novel macromolecular architectures. *Chemical Society Reviews* **2007,** 36, (8), 1369-1380.

68. Deville, S.; Saiz, E.; Tomsia, A. P., Ice-templated porous alumina structures. *Acta Materialia* **2007,** 55, (6), 1965-1974.

69. Deville, S.; Saiz, E.; Nalla, R. K.; Tomsia, A. P., Freezing as a Path to Build Complex Composites. *Science* **2006,** 311, (5760), 515-518.

70. Mukai, S. R.; Nishihara, H.; Tamon, H., Formation of monolithic silica gel microhoneycombs (SMHs) using pseudosteady state growth of microstructural ice crystals. *Chemical Communications* **2004**, (7), 874-875.

71. Gutierrez, M. C.; Ferrer, M. L.; del Monte, F., Ice-Templated Materials: Sophisticated Structures Exhibiting Enhanced Functionalities Obtained after Unidirectional Freezing and Ice-Segregation-Induced Self-Assemblyâ€ *Chemistry of Materials* **2008,** 20, (3), 634-648.

72. Chan, T. R.; Hilgraf, R.; Sharpless, K. B.; Fokin, V. V., Polytriazoles as Copper(I)-Stabilizing Ligands in Catalysis. *Organic Letters* **2004,** 6, (17), 2853-2855.

73. Waksman, S. A.; Fred, E. B., A Tentative Outline of the Plate Method for Determining the Number of Micro-Organisms in the Soil. *Soil Science* **1922,** 14, (1), 27-28.

74. Mosmann, T., Rapid colorimetric assay for cellular growth and survival: application to proliferation and cytotoxicity assays. *Journal of immunological methods* **1983,** 65, (1-2), 55-63.

75. Cousinie, S.; Gressier, M.; Alphonse, P.; Menu, M.-J., Silica-Based Nanohybrids Containing Dipyridine, Urethan, or Urea Derivatives. *Chemistry of Materials* **2007,** 19, (26), 6492-6503.

76. Malvi, B.; Sarkar, B. R.; Pati, D.; Mathew, R.; Ajithkumar, T. G.; Gupta, S. S., "Clickable" SBA-15 mesoporous materials: synthesis, characterization and their reaction with alkynes. *Journal of Materials Chemistry* **2009,** 19, (10), 1409-1416.

77. Tomczak, M. M.; Glawe, D. D.; Drummy, L. F.; Lawrence, C. G.; Stone, M. O.; Perry, C. C.; Pochan, D. J.; Deming, T. J.; Naik, R. R., Polypeptide-Templated Synthesis of Hexagonal Silica Platelets. *Journal of the American Chemical Society* **2005,** 127, (36), 12577-12582.

78. Mirau, P. A.; Serres, J. L.; Lyons, M., The Structure and Dynamics of Poly(l-lysine) in Templated Silica Nanocomposites. *Chemistry of Materials* **2008,** 20, (6), 2218-2223.

79. Pivcova, H.; Saudek, V.; Schmidt, P.; Hlavata, D.; Plestil, J.; Laupretre, F., Conformation of poly(glutamic acid) and of poly(aspartic acid) in the solid state. X-ray diffraction, infra-red and 13C cross-polarization/magic angle spinning nuclear magnetic resonance spectroscopic study. *Polymer* **1987,** 28, (6), 991-997.
80. Saito, H.; Ohki, T.; Kodama, M.; Nagata, C., 13C Nuclear magnetic resonance study of salt induced conformational change of basic polypeptides: Poly (L-lysine), poly (L-arginine), and poly (L-ornithine). *Biopolymers* **1978,** 17, (11), 2587-2599.
81. Bommel, K. J. C. v.; Jung, J. H.; Shinkai, S., Poly(L-lysine) Aggregates as Templates for the Formation of Hollow Silica Spheres. *Advanced Materials* **2001,** 13, (19), 1472-1476.
82. Wang, Y.; Chen, J.; Xiang, J.; Li, H.; Shen, Y.; Gao, X.; Liang, Y., Synthesis and characterization of end-functional polymers on silica nanoparticles via a combination of atom transfer radical polymerization and click chemistry. *Reactive and Functional Polymers* **2009,** 69, (6), 393-399.
83. Nilsson, S.; Zhang, W., Helix-coil transition of a titrating polyelectrolyte analyzed within the Poisson-Boltzmann cell model: effects of pH and salt concentration. *Macromolecules* **1990,** 23, (25), 5234-5239.
84. Zimmermann, R.; Kratzmuller, T.; Erickson, D.; Li, D.; Braun, H.-G.; Werner, C., Ionic Strength-Dependent pK Shift in the Helix-Coil Transition of Grafted Poly(l-glutamic acid) Layers Analyzed by Electrokinetic and Ellipsometric Measurements. *Langmuir* **2004,** 20, (6), 2369-2374.
85. Wang, Y.; Chang, Y. C., Synthesis and Conformational Transition of Surface-Tethered Polypeptide: Poly(l-glutamic acid). *Macromolecules* **2003,** 36, (17), 6503-6510.
86. Zhang, H.; Hussain, I.; Brust, M.; Butler, M. F.; Rannard, S. P.; Cooper, A. I., Aligned two- and three-dimensional structures by directional freezing of polymers and nanoparticles. *Nat Mater* **2005,** 4, (10), 787-793.
87. Butler, M. F., Growth of Solutal Ice Dendrites Studied by Optical Interferometry. *Crystal Growth & Design* **2002,** 2, (1), 59-66.
88. Vickery, J. L.; Patil, A. J.; Mann, S., Fabrication of Graphene–Polymer Nanocomposites With Higher-Order Three-Dimensional Architectures. *Advanced Materials* **2009,** 21, (21), 2180-2184.
89. Quinn, J. F.; Johnston, A. P. R.; Such, G. K.; Zelikin, A. N.; Caruso, F., Next generation, sequentially assembled ultrathin films: beyond electrostatics. *Chemical Society Reviews* **2007,** 36, (5), 707-718.
90. Wang, L.; Wang, Z.; Zhang, X.; Shen, J.; Chi, L.; Fuchs, H., A new approach for the fabrication of an alternating multilayer film of poly(4-vinylpyridine) and poly(acrylic acid) based on hydrogen bonding. *Macromolecular Rapid Communications* **1997,** 18, (6), 509-514.
91. Kovacevic, D.; van der Burgh, S.; de Keizer, A.; Cohen Stuart, M. A., Kinetics of Formation and Dissolution of Weak Polyelectrolyte Multilayers: Role of Salt and Free Polyions. *Langmuir* **2002,** 18, (14), 5607-5612.
92. Lynn, D. M.; Amiji, M. M.; Langer, R., pH-Responsive Polymer Microspheres: Rapid Release of Encapsulated Material within the Range of Intracellular pH. *Angewandte Chemie International Edition* **2001,** 40, (9), 1707-1710.
93. Dubas, S. T.; Schlenoff, J. B., Polyelectrolyte Multilayers Containing a Weak Polyacid: Construction and Deconstruction. *Macromolecules* **2001,** 34, (11), 3736-3740.

94. Sukhishvili, S. A.; Granick, S., Layered, Erasable, Ultrathin Polymer Films. *Journal of the American Chemical Society* **2000,** 122, (39), 9550-9551.
95. Rideout Iii, W. M.; Hochedlinger, K.; Kyba, M.; Daley, G. Q.; Jaenisch, R., Correction of a Genetic Defect by Nuclear Transplantation and Combined Cell and Gene Therapy. *Cell* **2002,** 109, (1), 17-27.
96. Scholl, S. M.; Michaelis, S.; McDermott, R., Gene Therapy Applications to Cancer Treatment. *Journal of Biomedicine and Biotechnology* **2003,** 2003, (1), 35-47.
97. Cross, D.; Burmester, J. K., Gene Therapy for Cancer Treatment: Past, Present and Future. *Clinical Medicine & Research* **2006,** 4, (3), 218-227.
98. Davis, S. S., Biomedical applications of nanotechnology - implications for drug targeting and gene therapy. *Trends in Biotechnology* **1997,** 15, (6), 217-224.
99. Roy, I.; Mitra, S.; Maitra, A.; Mozumdar, S., Calcium phosphate nanoparticles as novel non-viral vectors for targeted gene delivery. *International Journal of Pharmaceutics* **2003,** 250, (1), 25-33.
100. Jones, S. W.; Christison, R.; Bundell, K.; Voyce, C. J.; Brockbank, S. M. V.; Newham, P.; Lindsay, M. A., Characterisation of cell-penetrating peptide-mediated peptide delivery. *British Journal of Pharmacology* **2005,** 145, (8), 1093-1102.
101. Melikov, K.; Chernomordik, L., Arginine-rich cell penetrating peptides: from endosomal uptake to nuclear delivery. *Cellular and Molecular Life Sciences* **2005,** 62, (23), 2739-2749.
102. Li, Z.; Lee, D.; Sheng, X.; Cohen, R. E.; Rubner, M. F., Two-Level Antibacterial Coating with Both Release-Killing and Contact-Killing Capabilities. *Langmuir* **2006,** 22, (24), 9820-9823.
103. Yamashita, R.; Kikuchi, H.; Shirai, K.; Yamauchi, T.; Tsubokawa, N., Preparation of Antibacterial Polymer-grafted Nano-sized Silica and Surface Properties of Silicone Rubber Filled with the Silica. *Polymer Journal* **2006,** 38, (8), 844-851.
104. Kar, M.; Malvi, B.; Das, A.; Panneri, S.; Gupta, S. S., Synthesis and characterization of poly-l-lysine grafted SBA-15 using NCA polymerization and click chemistry. *Journal of Materials Chemistry* **2011**.
105. Yuan, L.; Tang, Q.; Yang, D.; Zhang, J. Z.; Zhang, F.; Hu, J., Preparation of pH-Responsive Mesoporous Silica Nanoparticles and Their Application in Controlled Drug Delivery. *The Journal of Physical Chemistry C* 115, (20), 9926-9932.

Chapter 4

Synthesis of Polypeptide Grafted Silica Mesoporous Materials by "Click Chemistry" and their Application as Biomaterial

This chapter was adapted from

1) Poly-L-Arginine Grafted Silica Mesoporous Nanoparticles for Enhanced Cellular Uptake and their Application in DNA Delivery and Control Drug Release
Mrityunjoy Kar, Neha Tiwari, Mitali Tiwari, Mayurika Lahiri and Sayam Sen Gupta
Particle (accepted manuscript)

3) Synthesis and Characterization of Poly-L-lysine Grafted SBA-15 using NCA Polymerization and Click Chemistry
Mrityunjoy Kar, Bharmana Malvi, Anindita Das, Suyana Panneri and Sayam Sen Gupta
J. Mater. Chem., **2011**, 21, 6690-6697

4.1 Introduction

Ordered mesoporous silicas have recently attracted a great deal of interest as matrices for immobilization of polymers.[1, 2] Mesoporous silica based materials like SBA-15 and MCM-41 are especially useful as efficient matrices for immobilization of polymers including enzymes,[3, 4] due to their controllable pore sizes (2-15 nm), high hydrothermal stability, thick walls and ease of functionalization through simple silanol chemistry that allow easy covalent attachment of these molecules.[5, 6] The resulting nanocomposite materials have very interesting properties that arise from mechanical stability of the inorganic support and the chemical properties of the attached polymer. Since a wide variety of polymers with varying properties such as catalytic or stimuli-responsive can be synthesized, such functional nanocomposite materials have been shown to have applications in diverse fields like adsorption,[7]catalysis[8, 9] and drug delivery.[10] However, synthesis of well defined polymer species onto the surfaces and channels of the mesoporous materials has been a major challenge. One of the first reports was the synthesis of conductive polyaniline inside the pores of mesoporous silica.[11] Recently, surface initiated controlled radical polymerization techniques[12] have been used to graft well defined polymers onto the surfaces of mesoporous materials. ATRP,[8, 13-16] NMP,[17] RAFT[18-20] and ROP[21, 22] polymerization have been successfully used to incorporate polymers like polyacrylonitrile (PAN), poly(N-isopropylacrylamide) (PNIPAAm), polystyrene (PS) and polymethyl methacrylate (PMMA) into mesoporous materials. The general methodology involves covalent attachment of the initiator molecule onto the silica surface and then using controlled radical polymerization as a grafting method to grow the polymer chain from the surface tethered initiator molecule. For example, surface initiated ATRP was used to graft PAN onto SBA-15.[13] This material served as a precursor for the synthesis of mesoporous carbons with potential applications for adsorption and fuel cells.[23] Also, the external surface of MCM-41 has been grafted with the stimuli-responsive PNIPAAm polymer and this hybrid was shown to have potential applications as a drug delivery vehicle.[19]

Ssynthesis of polypeptide grafted mesoporous materials are of considerable interest because the ordered secondary structure of the polypeptide grafts (α-helix, β-sheet and turns) possesses a wide range of structural and functional properties. In addition to this, the presence of a wide range of side chains (such as amines, thiols and carboxylic acid) in the polypeptides makes them responsive to external stimuli such as pH, temperature, solvent and electrolytes. Therefore, polypeptide grafted mesoporous materials can have various applications in chiral

separations, asymmetric synthesis and drug delivery, among other things. Although there have been several reports on grafting inorganic surfaces such as quartz planar surfaces,[24, 25] colloidal silica particles,[26] colloidal silica crystals[27] with polypeptides, not much work has been carried out on the grafting of polypeptides onto ordered mesoporous materials. Recently, a "grafting from" methodology was employed by Shantz *et. al.* to graft poly-L-lysine and poly-L-alanine onto mesoporous silica.[22, 28] In this methodology, APTES grafted onto mesoporous material like SBA-15 and MCM-41 was used as an initiator for the ring opening polymerization of ε-cbz-L-lysine and alanine NCA's. Although the polypeptides were successfully grafted onto the mesoporous material, there was no control over the precise molecular weight and polydispersity of the polymers. For example when ε-cbz-L-lysine was grafted onto SBA-15, the poly-ε-cbz-L-lysine was found to have a wide distribution from 3 to 9 repeating units centred on a 5-mer oligopeptide. It's expected since NCA polymerization is very susceptible to nucleophiles including water and surface silanol groups and this may hinder all the chains from growing to the same length.We envisioned that it would be worthwhile to investigate a 'grafting to' approach for the synthesis of polypeptide-SBA-15 conjugate. The advantage of this methodology stems from the fact that synthesis of homo and block polypeptides with controlled molecular weight and narrow polydispersity is very well developed.[29] Hence, if appropriate end functionalized polypeptide can be synthesized, it can be easily attached to its binding partner that could be installed in the mesoporous silica via simple silanol chemistry.

This chapter reports the synthesis of a poly-L-lysine-SBA-15 hybrid material using a "grafting to" approach by employing click chemistry.[30] Click chemistry is being increasingly used in polymer[31] and materials chemistry because of its exceptionally high yield, ease and compatibility with a broad repertoire of functional groups that allows fast and simple creation of well defined complex materials.[32] We have recently reported the synthesis of an azide grafted "clickable" mesoporous material in which various small organic molecules bearing the alkyne functionality were attached via the Cu(I) catalyzed azide alkyne cycloaddition reaction (CuAAC) with near quantitative yields.[33] Also, polymethacrylate and polyethyleneglycol polymers have been grafted onto alkyne grafted mesoporous silica using click chemistry.[34] The introduction of an alkyne or azide group onto the poly-L-lysine during its synthesis would give us a handle to attach it efficiently onto its binding partners on the silica surface via an 1, 2, 3-triazole linkage. Therefore, an alkyne terminated poly-L-lysine having 10 and 20 repeating units was synthesized using the ring opening NCA

polymerization of cbz-l-lysine NCA with N-TMS propargyl amine as the initiator (Chapter 2).[35] The alkyne terminated poly-L-lysine formed after deprotection of the cbz group was then successfully attached to an azide labeled SBA-15 by the azide alkyne cycloaddition (CuAAC) click chemistry to provide reasonable grafting densities. The poly-L-lysine SBA-15 conjugate was very well characterized by multinuclear (^{13}C, ^{29}Si) solid state NMR, TGA, FT-IR, TEM and BET.

Though SBA-15 polypeptide conjugates have synthesized successfully by using 'grafting to' methodology, it is difficult to use these particles in biomedical application due to its larger size (2-4 μm). In contrast, mesoporous silica nanoparticles (MSN) having diameter <100 nm, are suitable for various *in vitro* and *in vivo* biomedical applications, mainly for gene and drug delivery. The same 'grafting to' methodology can be used to synthesize MSN polypeptide conjugates and applied for various biomedical applications. It is known that poly-L-arginine has better cell penetrating properties than other cationic polypeptides or polymers. Therefore, MSN grafted with poly-L-arginine conjugates could be a potential carrier for gene and drug delivery.

The use of gene therapy to treat increasing trends of cancer disease and genetic disorders has drawn major attention. [36-38] In recent years, novel nanocarriers that are capable of delivering gene and drugs to the organism in an effective and selective way have attracted much attention. Among these nanocarriers, mesoporous silica nanoparticles (MSNs) offer distinct advantages over other nanomaterials. The large surface area, controllable particle size and morphology, highly ordered porosity with tuneable pore sizes, chemical stability, potential biocompatibility[43, 44] and low cytotoxicity have made MSNs highly attractive for a wide variety of nano biotechnological applications such as gene transfection [2, 45-48] and drug delivery.[1, 49, 50] Chemically modified silica nanoparticles that bear positive charge around their surfaces allows to condense and protect negatively charged plasmid DNA. The polyplex then interact with the negatively charged plasma membrane for cell entry.[51] Porous silica nanoparticles (MSNs) have several advantages over their non-porous analogues because it has the ability to selectively bind biomolecules both on the surface and/or within the pores. This allows delivery of higher amounts of the biomolecules to the target cells with the possibility of co-delivery. The ability to selectively put targeting ligands on the surface of MSNs and drugs inside the pores has also made these nanoparticles very promising candidates for drug delivery. It has been demonstrated that these encapsulated drug molecules inside mesoporous nanoparticles can also be released "on demand" using various stimuli such as redox [15], pH [35, 46, 52, 53] and light.[54]

However, the successful application of MSNs for delivery of plasmid DNA or drugs requires surface modification of the silica in order to generate sufficient binding affinity for the negatively charged nucleic acids and to help it penetrate through the cell membrane. To achieve this, positively charged functional groups have been grafted on the surface of silica materials either through noncovalent interactions or by covalent bonding. These include amino-silanes and a host of synthetic polycationic polymer such as PAMAM [45] and PEI. [46] Synthetic polymers like PEI and PAMAM are not very desirable as their long term toxicities are unknown. Recently, poly-L-lysine polypeptide has been attached to mesoporous nanoparticles and the conjugate was used for delivery of SiRNA.[48] Since polypeptides like PLL are composed of naturally occurring amino acids, they have the distinct advantage of being more biocompatible than most synthetic non-natural polymers like PEI. Among all known polypeptides, low molecular weight poly-L-arginine (from 7 mer to 20 mer) is most efficient towards cell entry.[55] For example, it has been reported that poly-L-arginine (9 mer) is 20 fold more efficient transporter of cargo than the naturally occurring cell penetrating $tat_{(49-57)}$-peptides.[56] This property has been utilized for the design of polymer based carriers for gene delivery [57-60] and drug delivery. [61-64] There are two familiar classes of cationic polypeptides that are known to enter most of the mammalian cells very effectively through plasma membrane. These are the "protein transduction domain" (PTD) and "cell penetrating peptides" (CPPs), both of which are consists of positively charged amino acids (< 20 amino acids).[114, 115] The earliest report on synthetic polypeptides for biomedical was focused on the easy synthesis of water soluble homo polypeptides which can be used as a drug delivery vehicle.[116]

The hybrid materials based on poly-L-arginine modified mesoporous silica nanoparticle can give supplementary advantages since they would combine both the structural attributes of MSN and functional attributes of poly-L-arginine. Such hybrid materials can be very efficient carriers for both drug delivery and gene delivery. This chapter also demonstrates a very facile synthesis of poly-L-arginine grafted MSN and also studies their efficacy as a carrier for delivery of DNA plasmid. The poly-L-arginine MSN conjugates are very attractive as they are synthesized by a very simple and high yielding methodology, developed in our group, in which alkyne end-group functionalized poly-L-arginine synthesized by NCA polymerization is attached to organoazide functionalized MSN nanoparticles using Cu(I) catalyzed azide alkyne click chemistry (CuAAC). In a recent report, poly-L-lysine was grafted onto epoxy-functionalized MSN via the ring-opening reaction of epoxy group by the side chain amino group of lysine.[48] Since all the amino groups in the aminobutyl moiety in each unit of poly-L-

lysine have similar reactivity with the epoxide, this methodology offers no control over the orientation and conformation of the polymer on the MSN surface. In contrast, our methodology allows the polypeptide to be attached from one end of the chain, thus allowing much more control over the orientation and conformation of the polypeptide. The poly-L-arginine on the MSN surface could have dual functionality: (i) it imparts positive charge onto the surface of MSN to condense negatively charged DNA plasmid and also uses its cell penetrating ability to deliver the MSN nanoparticles inside the cells (ii) the ability to modify the inside and outside surface of MSN independently allows us to attach poly-L-arginine outside the MSN surface and cargo or small molecules on the inside of the MSN nanoparticles. The influence of poly-L-arginine polymer present onto the MSNs on DNA adsorption,[60] cell uptake, [55] cytotoxicity [65] and its biological activity is reported.

4.2 Experimental section

4.2.1 Materials

Tetraethylorthosilicate (TEOS), chloropropyltrimethoxysilane (99%), t-butylammonium chloride, disodium bathophenanthrolinesulphonate, Poly(ethylene glycol) methyl ether (mol. Wt. 1000), propargyl bromide(80% solution in toluene), 5(6)-Carboxyfluorescein N-hydroxysuccinimide ester, copper iodide were obtained from Sigma Aldrich and used as received. All other chemicals used were obtained from Merck, India.

4.2.2 Synthesis

4.2.2.1 Synthesis of 3-azidopropyltrimethoxysilane (AzPTMS)

3-chloropropyltrimethoxysilane (abbreviated as Cl-PTMS; 2 g, 8.3 mmol) was added to a solution of sodium azide (1.08 g, 16.6 mmol) and tetrabutylammonium bromide (0.644 g, 2 mmol) in dry acetonitrile (50 mL), under nitrogen atmosphere. The reaction mixture was stirred under reflux for 18 h. After completion of the reaction, the solvent was removed under reduced pressure. The crude mixture was diluted in n-pentane and the suspension was filtered through Celite bed. Solvent was removed from the resulting filtrate and the crude oil obtained was distilled under reduced pressure of 0.025 mbar at 62°C to give AzPTMS (3-azidopropyl trimethoxysilane) as a colorless liquid. Yield: 1.52 g, 74%.

FT-IR (NaCl, cm^{-1}): 2098 ($-N=N^{+}=N^{-}$, s). ^{1}H NMR (500 MHz, $CDCl_3$): δ 0.68 ppm (t, 2H, J= 8.25 Hz), 1.69 ppm (t, 2H, J= 6.88 Hz), 3.25 ppm (t, 2H, J = 7.16 Hz), 3.56 ppm (s, 9H). ^{13}C NMR (50 MHz, $CDCl_3$): δ 59.67, 53.52, 30.85, 7.38 ppm.

4.2.2.2 Synthesis of alkyne terminated poly(ethylene glycol) methyl ether (mol. Wt. 1000 and 2000)

Poly (ethylene glycol) methyl ether (2 mmol) was added to an ice cold anhydrous THF solution of sodium hydride (0.072 g, 3 mmol) under nitrogen atmosphere. The reaction mixture was stirred for 20 minutes under ice followed by drop wise addition of 80% toluene solution of propargyl bromide (0.218 ml, 2.2 mmol). The reaction mixture was stirred for another 3 hrs under nitrogen atmosphere at room temperature. After completion of the reaction, the solvent was removed under reduced pressure. The crude mixture was crystallized thrice from hexane/ethyl acetate. The resulting filtrate was dried under reduced pressure at 60°C to give alkyne terminated poly (ethylene glycol) methyl ether as a colorless liquid. Yield: 84%.

4.2.2.3 Synthesis of SBA-15(CAL-SBA-15)

SBA-15 material was synthesized using previously reported procedure with slight modifications.[66] In a typical batch synthesis, 9.6 g of the nonionic block copolymer Pluronic P123 and 0.108 g NH_4F were dissolved in 336 mL of 1.3 M aqueous HCl solution at room temperature. Then the temperature of the mixture was reduced to 23°C and mixture was stirred thoroughly for 1 hr. Then a mixture of 22 mL TEOS and 4.8 mL TIPB was added. The solution was allowed to stir for 24 hrs while maintaining the temperature at 23°C. The synthesized gel was then loaded in a 500 mL polypropylene bottle, sealed air tight and kept at 100°C for 48 hrs under static condition. The contents were then filtered and the residue was washed with copious amount of water until the pH of the water became neutral. The white solid was dried at 60ºC in vacuum oven. Calcination of the as-synthesized solid material was then done at 550ºC for 5 hrs, using a heating ramp of 2 degree per minute. The sample was preserved under argon atmosphere for further use. (Yield: ~ 4.9 g) This material will be represented as CAL-SBA-15.

4.2.2.4 Synthesis of azide grafted SBA-15 (N_3-SBA-15)

Azide grafted SBA-15 was synthesized by a method described in an earlier report of our group.[33] To a suspension of 500 mg of CAL-SBA-15 in 25 mL of toluene, 1 mL

AzPTMS were added, and the mixture was stirred for 16 hrs at 80°C under nitrogen atmosphere. After the completion of reaction, the contents were cooled, filtered and washed with toluene until it became free from AzPTMS. The sample was then dried at 80°C for 8 hrs in a vacuum oven and preserved under argon atmosphere for further use. This material was characterized by FT-IR, NMR, TGTDA and nitrogen adsorption desorption experiments. Yield: ~600 mg. This material will be referred as N_3-SBA-15.

4.2.2.5 Synthesis of Mesoporous silica nanoparticles (MSN)

MSN was synthesized by method that has been previously reported. 1 gm of cetyltrimethylammonium bromide (CTAB) was added to 480 ml of water followed by addition of NaOH solution (3.5 ml, 2 M). The mixture was stirred vigorously at 80°C and followed by addition of 5ml of tetraethylorthosilicate (TEOS). The mixture was stirred (at ~600 rpm) for another 2 hrs at 80°C. The resulting precipitate was collected by filtration and washed with copious amounts of water and dried under vacuum. This material was used directly for further reactions. Yield = 1.8 g

4.2.2.6 Outside surface functionalization of MSN with AzPTES

As synthesized MSN without template removal (1.2 g) was added to 80 ml anhydrous toluene followed by addition with 98 µl of 3-azidopropyltriethoxysilane (0.8 mmol/gm grafting density) in presence of catalytic amount of Et_3N. The reaction mixture was refluxed for 18 hrs under argon atmosphere. After completion of the reaction, the material was then filtered, washed with toluene and with ethanol. Finally, the template (CTAB) was removed by refluxing the material with acidic methanol solution overnight. The material was the filtered, washed with methanol and dried under vacuum. This material will be referred to as MSN-N_3.

4.2.2.7 Synthesis of SBA-15 poly-L-lysine (SBA-PLL) conjugates using CuAAC

In a typical CuAAC, the azide grafted SBA-15 (50 mg, 0.09 mmol of azide) was incubated with alkyne-PLL (378 mg, 0.27 mmol, 3 equivalent and 756 mg and 0.27 mmol, 3 equivalent for 10 and 20 mer respectively) in 3 ml DMF:Tris buffer(pH 7, 100 mM) mixture (3:7) containing sodium ascorbate (53.46 mg, 0.27 mmol, 3 equivalent) and disodium sulphonated bathophenanthroline (24.12 mg, 0.045 mmol, 0.5 equivalent). The reaction mixture was subjected to three freeze-pump-thaw cycles for rigorous exclusion of dioxygen. Copper iodide (8.55 mg, 0.045 mmol, 0.5 equivalent) was then added and the reaction was

allowed to proceed for 36 hrs with stirring at 60°C. After completion of the reaction, the mixture was taken into a centrifuge tube and centrifuged for 15 min at 12000 rpm. The supernatant liquid was decanted off and the solid residue was washed with water (2 times) to wash off the unreacted alkyne-PLL, 0.1 M solution of sodium N, N-diethyldithiocarbamate in ethanol (2 times) and acetone (2 times). Finally, the faint brownish white powder obtained was dried at 60°C in vacuum oven for 6-8 hrs and characterized by IR, NMR, TGDTA and nitrogen adsorption desorption studies. These materials will be referred as SBA-PLL-10 and SBA-PLL-20. Yield: 58 and 56 mg of SBA-PLL-10 and SBA-PLL-20 respectively.

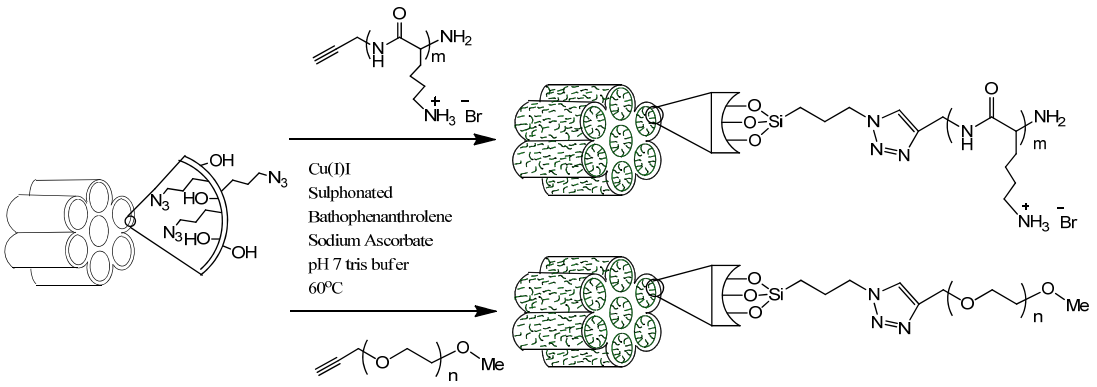

Scheme 4.1: Synthesis of poly-L-lysine silica mesoporous conjugate (SBA-PLL) and poly ethylene glycol silica mesoporous conjugate (SBA-PEG)

4.2.2.8 Synthesis of SBA-15 polyethylene glycol (SBA-PEG) conjugates using CuAAC

For a typical CuAAC reaction, azide grafted SBA-15 (100 mg, 0.18 mmol of azide) was incubated with alkyne-PEG (554 mg, 0.54 mmol, 3 equivalent and 1.008 g, 0.54 mmol, 3 equivalent for Mol. Wt. 1000 and Mol. Wt. 2000 respectively) in 5 ml DMF: DI water mixture (1:4) containing sodium ascorbate (71.28 mg, 0.36 mmol, 2 equivalent), copper iodide (17 mg, 0.09 mmol, 0.5 equivalent) and disodium sulphonated bathophenanthroline (48.24 mg, 0.09 mmol, 0.5 equivalent). The reaction mixture was subjected to three freeze-pump-thaw cycles for rigorous exclusion of dioxygen. The CuAAC was allowed to proceed for 36 hrs with stirring at 60°C. After completion of the reaction, the mixture was taken into a centrifuge tube and centrifuged for 15 min at 12000 rpm. The supernatant liquid was decanted off and the solid residue was washed with water (2 times) to wash off the unreacted alkyne-PEG, 0.1 M solution of sodium N, N-diethyldithiocarbamate in ethanol (2 times) and acetone (4 times). Finally, the faint brownish white powder obtained was dried at 60°C in vacuum oven for 6-8 hrs and characterized by FT-IR, NMR, TGDTA and nitrogen

adsorption. These materials will be referred as SBA-PEG-1000 and SBA-PEG-2000. Yield: ~120 mg

4.2.2.9 Synthesis of mesoporous silica nanoparticle-poly-L-arginine (MSN-PLArg) conjugates using CuAAC

The CuAAC procedure was modified by our group, the azide functionalized silica nanoparticles were incubated with 1equivalent of the corresponding alkyne-PLArg in PBS (pH 7.4, 150 mM) containing $CuSO_4$ (0.25 equivalent), THPTA (1.25 eq), aminoguanidine HCl (2.5 equivalent) and sodium ascorbate (2.5 equivalent). In a typical reaction, azide grafted silica nanoparticles (20 mg, 0.016 mmol of azide) were incubated with alkyne-PLArg(20) and alkyne-PLArg(10) (48 mg, 1 equivalent and 32 mg, 1 equivalent respectively) in 2 mL PBS (pH 7.4, 150 mM) containing $CuSO_4$ (0.99 mg) and THPTA (8.68 mg), aminoguanidine HCl (4.42 mg). The reaction mixture was subjected to three freeze-pump-thaw cycles for rigorous exclusion of dioxygen and then added sodium ascorbate (14.85 mg). The CuAAC was allowed to proceed for 18 hrs with stirring at RT. After completion of the reaction, the mixture was taken into a centrifuge tube and centrifuged for 20 mins at 13000 rpm. The supernatant liquid was decanted off and the solid residue was washed with water (2 times), 0.1 M solution of sodium N, N-diethyldithiocarbamate in ethanol (2 times) and ethanol (2 times). It was finally washed with 0.1 M HCl and ethanol. The sample was dried under vacuum at 50°C. These materials will be referred as MSN-PLarg(20) and MSN-PLArg(10). Yield: ~ 22 mg.

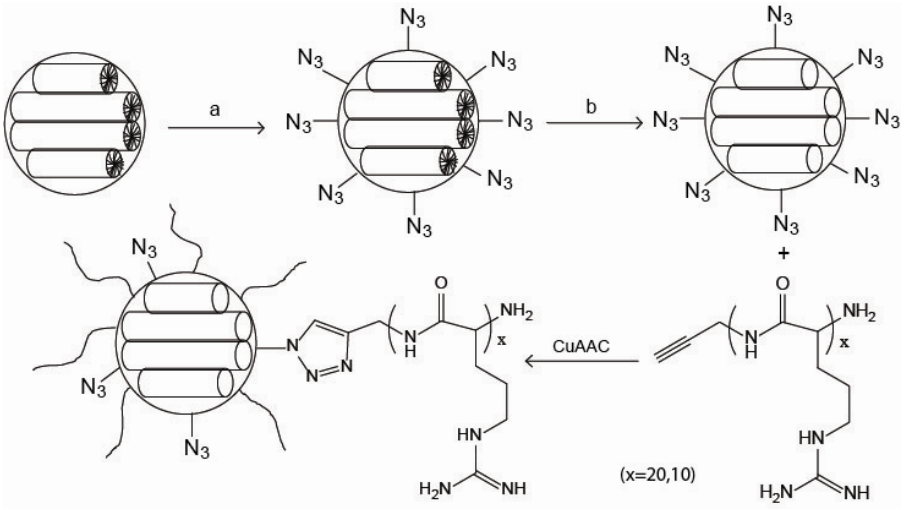

Scheme 4.2: Synthesis of poly-L-arginine grafted MSN (a) azidopropyltriethoxysilane in toluene (b) methanol/HCl for surfactant removal

4.2.2.10 Synthesis of fluorescein labeled MSN-PLArg

A solution of MSN-PLArg (1mg/ml) was incubated with 10 µl DMSO solution of 6-[fluorescein-5(6)-carboxamido] hexanoic acid *N*-hydroxysuccinimide ester (stock solution 1mg/ml). The mixture was wrapped with aluminium foil and stirred for 4 hrs at room temperature. After completion of the reaction the mixture was centrifuged at 15000 rpm for 5 min and washed with methanol three times. Finally washed one time with DI water and dried the samples in vacuum at 70°C for 12 hrs.

4.2.3 Characterizations and methods

4.2.3.1 FT-IR

FT-IR spectra were recorded on Perkin Elmer FT-IR spectrum GX instrument by making KBr pellets. Pellets were prepared by mixing 3 mg of sample with 97 mg of KBr.

4.2.3.2 ^{29}Si and ^{13}C solid state CP MAS NMR

^{29}Si and ^{13}C Cross Polarization Magic Angle Spinning (CP MAS) NMR experiments were carried out on a Bruker AVANCE 300 wide bore spectrometer equipped with a superconducting magnet with a field of 7.1Tesla. The operating frequencies for ^{13}C and ^{29}Si were 300 MHz, 75.4 MHz and 59.6 MHz respectively. The samples were packed into a 4 mm zirconia rotor and loaded into a 4 mm BL MAS probe and spun about the magic angle (54.74) at 10 KHz using a standard ramp-CP pulse sequence was used for both the experiments. The RF-powers were 50 kHz and 60 kHz for the ^{29}Si and ^{13}C CP MAS experiments. The contact times were 6ms and 3ms for the ^{29}Si and the ^{13}C CP MAS experiments. All the chemical shifts were referenced to TMS. Typically 10,000 to 25,000 scans with a recycle delay of 3 s were collected depending on the sensitivity of the sample.

4.2.3.3 Thermogravimetric analysis (TGA)

Thermogravimetric analysis (TGA) of the silica nanoparticles were carried out using a TA Instrument SDT Q600 analyzer between 20 and 800°C in air (flow 50 ml min^{-1}) at a heating rate of 10° min^{-1}. All samples were dried under vacuum at 60°C overnight prior to TGA runs. The graft density of the grafted moiety on the silica surface was determined by thermogravimetric analysis (TGA) using following equation as described before.[67]

$$\text{Graft density (mmol/g)} = \frac{\frac{W_{modified\ silica(60-600)}}{100-W_{modified\ silica(60-600)}}\times 100 - W_{silica(60-600)}}{M\times 100}\times 10^3$$

Where $W_{(60\text{-}600)}$ is the weight loss between 60 and 600°C corresponding to the decomposition of the grafted silica molecule corrected from the thermal degradation**,** and M is the molecular weight of the grafted silane. W_{silica} represents the determined weight loss of silica before grafting.

4.2.3.4 SEM and HR-TEM

SEM images were obtained on FEI Quanta 200 3D, dual beam ESEM with EDAX microscope. HR-TEM images were taken on a FEI Technai F30 operating at 300 kV with FEG. The samples were prepared by dispersing a 0.1 mg/mL of nanoparticles by sonication, dropping the resulting suspension on a copper grid of 400 mesh for 30 sec and allowing it to dry in air. FT-IR spectra were recorded on Perkin Elmer FT-IR spectrum GX instrument by making KBr pellets. Pellets were prepared by mixing 3 mg of sample with 97 mg of KBr. Elemental analyses were carried out on Thermo Finnigan FLASH EA 1112 series instrument.

4.2.3.5 Dynamic light scattering and zeta potential

The hydrodynamic diameters of dilute, aqueous solutions of the polypeptide grafted silica mesoporous paericles were determined by dynamic light scattering (DLS) using a Brookhaven Instruments instrument equipped with a He-Ne laser operating at 632 nm. The particle size was calculated using 90 Plus particle Sizing Software Ver. 3.94. Sample solutions were made in water and were filtered using a 0.8 μm PTFE filter. Aqueous elelctrophoretic data for the polypeptide silica mesoporous conjugates were obtained using a Brookhaven Instruments instrument. For each sample three measurements were taken. Zeta potentials were calculated using PALS Zeta Potential Analyzer Software Ver. 3.54.

Zeta potential of different ratios of MSN-poly-L-arginine /plasmid DNA complexes particles were determined by using a Brookhaven Instruments instrument equipped with PALS Zeta Potential Analyzer Software Ver. 3.54. About 2 μL of polyplex solutions at various weight ratios was prepared to a final concentration of 2 μg/mL plasmid DNA in distilled water. The polyplex solution (at a fixed weight ratio) was kept in a 37°C incubator. At the indicated time points, the potentials of the polyplex were measured.

4.2.3.6 Nitrogen adsorption and desorption

Nitrogen adsorption and desorption studies at -196°C were carried out using Quadrasorb *SI* instrument. Before the nitrogen adsorption measurement, the samples were

degassed overnight under vacuum using FloVac Degasser at 100°C (for modified silicas). Multi point BET surface area was obtained from the nitrogen adsorption isotherm in the relative pressure range from 0.1 to 0.3. Pore sizes were calculated using the BJH method from adsorption branch of the isotherm in the relative pressure range from 0.3 to 0.99 and total pore volume was calculated at P/P_o of 0.99.

4.2.3.7 DNA Retardation studies using gel electrophoresis

Polyplexes were prepared by addition of 0.2 μg of pDNA with increasing ratio of MSN-PLArg(20) and MSN-PLArg(10) in sterile DI water at room temperature for 30 minutes. Each sample was then electrophoresed on a 0.8% (w/v) agarose gel containing ethidium bromide (EtBr, 0.5 μg/mL) at 110V for 1 hr. The gels were analyzed using gel documentation system (Syngene) to show the location of DNA bands.

4.2.3.8 Cell lines and culture

Human cervical cancer cells (HeLa) and human lung carcinoma cells (A549) were grown in DMEM with 10% FBS. Cells were incubated in plastic tissue culture cell-binder flasks (Corning) at 37°C in a 5% CO_2 humidified incubator.

4.2.3.9 Cytotoxicity assay

Cytotoxicity of MSN-PLArgs were studied by MTT assay.[68] HeLa and A549 cells were seeded in 96-well tissue culture plates at 6000 cells/well in 90 μL DMEM. All media contained 10% FBS and all cells were incubated overnight (14 to 16 hrs). MSN-PLArgs solution (10 μl) at various concentrations was added and cells were incubated for another 48 hrs. After completion of incubation, the media was removed and 100 μl solution of DMEM with filter sterilized MTT (3-(4,5-Dimethylthiazol-2-yl)-2,5-diphenyltetrazolium bromide) solution (0.45 mg/ml) was added into each well. After incubation at 37°C for 4 hrs with MTT, the media was aspirated from the wells and 100 μl DMSO was added to dissolve insoluble formazan crystals formed. The absorbance was measured at 550 nm using a microtitre plate reader (Veroscan, Thermo Scientific) and the cell viability was calculated as a percentage relative to untreated control cells.

4.2.3.10 In vitro transfection

HeLa and A549 cells were seeded at $3x10^4$ cells/well in 6-well plates in 2 mL of DMEM containing 10% FBS and incubated at 37°C for a day before transfection. Polyplexes

of pDNA and MSN-PLArgs were prepared by addition of 0.5 µg of pDNA with different weight ratios of MSN-PLArgs in 50 µL sterile DI water and the mixtures were incubated for 30 min at room temperature. 50 µl of optimem was then added to each polyplex solution. Meanwhile, cells were washed with PBS followed by addition of optimem (900 µl). The cells were then kept inside the incubator at 37 °C for 15 min. Polyplex (100 µl) were added to each well containing the cells in optimem and this was further incubated for 4h. After 4 hours, cells were supplemented with 500 µl of 30% FBS containing DMEM. Transfected cells were visualized for protein expression after 48 hrs.

4.2.3.11 Fluorescence imaging of cells transfected with DNA-MSN-PLArg polyplexes

For imaging cells that expressed mCherry fluorescent protein, cells were grown on glass coverslips and transfected as above. Cells were washed twice in cold PBS and fixed with 4% paraformaldehyde-PBS solution (pH 7.4) for 15 min. Fixative was removed by washing and cells were mounted on glass slides using mounting medium containing DAPI to stain the nulclei. Images were acquired with an epifluorescence microscope (Ziess).

4.2.3.12 Determination/ quantification of transfection efficiency of polyplexes

Transfection efficiency of MSN-PLArg was determined by counting transfected versus total number of cells per field under at 20X magnification while acquiring microscopic images. In addition, quantification was verified by direct flow cytometic analysis of cells.
In brief, cells tranfected with mCherry-Plasmid using MSN-PLArg or a commercial transfection reagent- Lipofectamine, were trypsinised and suspended in PBS and analyzed by FACS (BD FACS Aria). Untransfected cells were taken as control and cells incubated with only MSN-PLArg polyplexes were analyzed to show the efficiency of particle uptake by cells.

4.3 Results and discussion

4.3.1 Synthesis and characterization of azide functionalized SBA-15(N_3-SBA-15)

Since we envisioned grafting large polypeptides polymers onto SBA-15, we attempted the synthesis of SBA-15 having pore sizes which were greater than 10 nm. SBA-15 material was synthesized following the procedure reported by Kruk *et. al.* with slight modifications.[66] The powder XRD pattern of calcined SBA-15 (Cal-SBA-15) displayed characteristic high intensity 100 peak near the 2θ value of 0.75°. Presence of higher order peaks 110 and 200

near the 2θ values of 1.33° and 1.53° respectively indicates formation of long range ordered mesoporous material (Figure 4.1a). The SEM image displayed wormlike external morphology with about 1μ particle size while the TEM micrographs showed the hexagonal pore arrangement with thick walls of the calcined SBA-15 (Cal-SBA-15) mesoporous material (Figure 4.4). Nitrogen adsorption and desorption experiments show type IV isotherm with steep increase in adsorption at P/P_o = 0.72-0.83 due to capillary condensation of the nitrogen in the mesopores (Figure 4.7). The BJH pore-size distribution (PSD) analysis shows very narrow PSD in the range 9-14 nm (Table 4.1). These values are consistent with the data reported in the literature.[66] The azide grafting was performed by following procedure that has been reported before.[33]

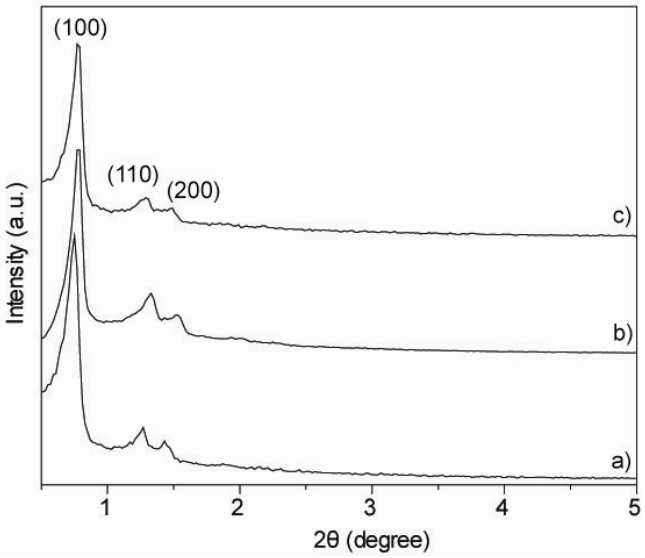

Figure 4.1: Powder XRD patterns of a) Cal-SBA-15, b) N3-SBA-15 and c) SBA-PLL-10

The FT-IR of the N_3-SBA-15 is presented in the Figure 4.3b. The spectra display an absorbance at ~2100 cm^{-1} which is the characteristic stretching vibration of organic azide (N_3). The absence of the 2100 cm^{-1} stretch in the starting Cal-SBA-15 particle (Figure 4.3a) indicates that organic azide groups have been successfully incorporated into the SBA-15 materials. Figure 4.5a represents the solid state ^{13}C CP-MAS NMR spectra of the azide grafted SBA-15 particles. The three peaks C1 (11 ppm), C2 (24 ppm), C3 (55 ppm) observed in the ^{13}C CP-MAS NMR represent the three C-atoms of the azidopropyl chain in the order as presented. The ^{29}Si CP MAS NMR spectra of N_3-SBA-15 are presented in Figure 4.6a. The spectra display prominent peaks at around -111, -101, -67 and -58 ppm. The peaks at -111 and -101 ppm may be assigned to the different types of the Silica-sites namely Q3 [$(SiO)_3Si(OH)$] and Q4 [$(SiO)_4Si$], that are classified based on the total number of silanol

groups (Si-OH) at the Si-centre (i.e. 1, 0 respectively). Two other distinct peaks observed at -58 and -67 ppm may be attributed to the functionalized sites of the Si-framework namely T2 [$R(SiO)_2Si(OH)$] and T3 [$R(SiO)_3Si$] respectively, where R is the azidopropyl group.

Nitrogen adsorption and desorption experiments also showed a type IV isotherm and the BET surface area and average pore size (BJH method) were determined to be 407 m^2/g and 9.93 nm respectively (Figure 4.7). The decrease in the pore size and surface area was commensurate with the grafting of the azidopropyl group onto Cal-SBA-15. The amount of azidopropyl groups incorporated was determined to be ~1.83 mmol/gm by TGA (Figure 4.2c).

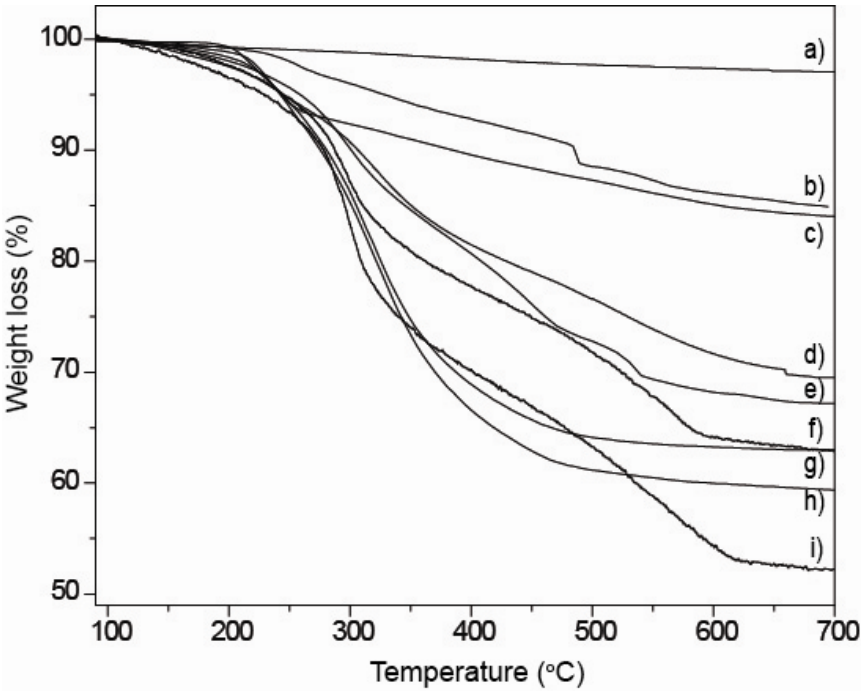

Figure 4.2: Thermogravimetric analysis of a) Cal-SBA-15, b) MSN-N_3, c) N_3-SBA-15, d) SBA-PLL-10, e) SBA-PLL-20, f) MSN-PLArg(10), g) SBA-PEG-2000, h) SBA-PEG-1000 and i) MSN-PLArg(20)

4.3.2 Synthesis and characterization of SBA-PLL hybrid

The N_3-SBA-15was subjected to Cu(I) catalyzed azide alkyne cycloaddition reaction (CuAAC) with 3eq of alkyne-PLL as the substrate. The employment of the sulphonated bathophenanthroline ligand was critical for the successful completion of the CuAAC. The ligand plays a dual role of accelerating the reaction and also preventing the binding of Cu(I) to the lysine side chains in PLL. The successful attachment of alkyne-PLL-10 was also

confirmed from the IR spectra of SBA-PLL-10 (Figure 4.3c) in which concomitant decrease of the $\nu_{as}(N_3)$ at 2105 cm^{-1} was observed with the appearance of the ν(C=O) at 1657 cm^{-1} and ν(N-H) at 1541 cm^{-1}, a region that displayed no peaks for the azide labeled SBA-15. Similar ν(C=O) and ν(N-H) stretches was observed in alkyne-PLL. After the reaction, an extensive washing protocol was followed to remove the Cu(I), ligand, ascorbate and any unreacted alkyne-PLL. One of the key steps in the washing was the usage of dithiocarbamate to remove the Cu(I), as reported earlier. [33, 69] Use of higher amounts of catalyst and longer reaction times did not improve the yield of the reaction. The XRD of the resultant material SBA-PLL-10 displayed characteristic high intensity 100 peak near the 2θ value of 0.77º together with peaks corresponding to 110 and 200 diffractions indicating that the material remained intact upon grafting alkyne-PLL (Figure 4.1c). The TG-DTA analysis of SBA-PLL-10 indicated a mass loss of 32.85% between 100ºC and 700ºC which corresponds to a loading of 0.23 mmol of PLL/gm of SBA-15 (Figure 4.2d). Recently, PMMA and PEG have been grafted onto alkyne labeled SBA-15 using CuAAC.[34] The grafting density obtained with alkyne-PLL-10 by us is similar to the low molecular weight PMMA that was grafted onto SBA-15. Similar reaction conditions were employed to graft alkyne-PLL-20. In SBA-PLL-20 mass loss 30.45% corresponds to a loading of 0.1mmol PLL-20 per gram of SBA-15(Figure 4.2e).

Sample Name	**Wt% of groups**	**Density (mmol/g of silica)**	**Pore Diameter (nm)**	**M_{BET} (m^2/g)**	**Pore Volume (cm^3/g)**	**Zeta Potential (mV)**
Cal-SBA-15A	-	-	11.39	637	1.3	-32±1
N_3-SBA-15B	15.86	1.83	9.93	407	0.97	±2
SBA-PLL-10	16.99	0.23	8.96	200	0.511	+22±2
SBA-PLL-20	14.59	0.1	8.09	248	0.699	+18±1
SBA-PEG-1000	24.96	0.516	8.07	174	0.51	-
SBA-PEG-2000	22.14	0.206	8.04	150	0.44	-

Table 4.1: Physical properties of various SBA-15 materials

The solid state ^{13}C CP-MAS NMR spectrum of SBA-PLL-20 shows extra peaks in addition to the C1, C2 and C3 observed in azide grafted silica. The extra peaks have been identified and labeled in Figure 4b. The presence of the extra peaks at 126 ppm and 143 ppm which corresponds to the C4 and C5 atom of the triazole indicates that the PLL have been covalently attached to the silica particle via the triazole ring. The C7 (carbonyl), C12, C10 and C9 observed in the spectra are very characteristic of the PLL moiety. The chemical shifts

of the C7 (173.1 ppm), C8 (54 ppm) and C12 (39.5 ppm) are characteristic of the poly-L-lysine in the random coil conformation as has been reported recently.[70] The FT-IR spectra also supports this since the observed amide I and amide II peaks at 1657 cm^{-1} and 1541 cm^{-1} are indicative of PLL in a random coil conformation. This is expected since PLL is known to adopt a random coil conformation at neutral pH. The ^{29}Si CP MAS spectrum of the SBA-PLL-20 material shows little or no change from the starting N_3-SBA-15 indicating that the Si-sites do not undergo any chemical change during the reaction and its work-up (Figure 4.6b). This is also expected since the T1 and T2 Si-sites are those that are from the azidopropyl modified silica and should not undergo any change during the course of the click reaction.

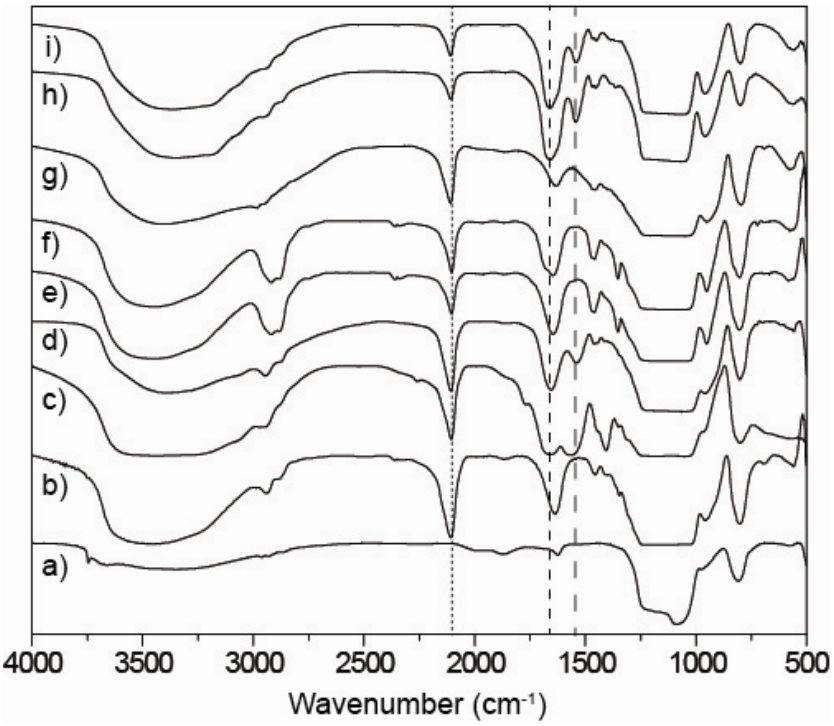

Figure 4.3: Infrared spectra of a) Cal-SBA-15, b) N_3-SBA-15, c) SBA-PLL-10, d) SBA-PLL-20, e) SBA-PEG-1000, f) SBA-PEG-2000, g) MSN-N_3, h) MSN-PLArg(20) and i) MSN-PLArg(10)

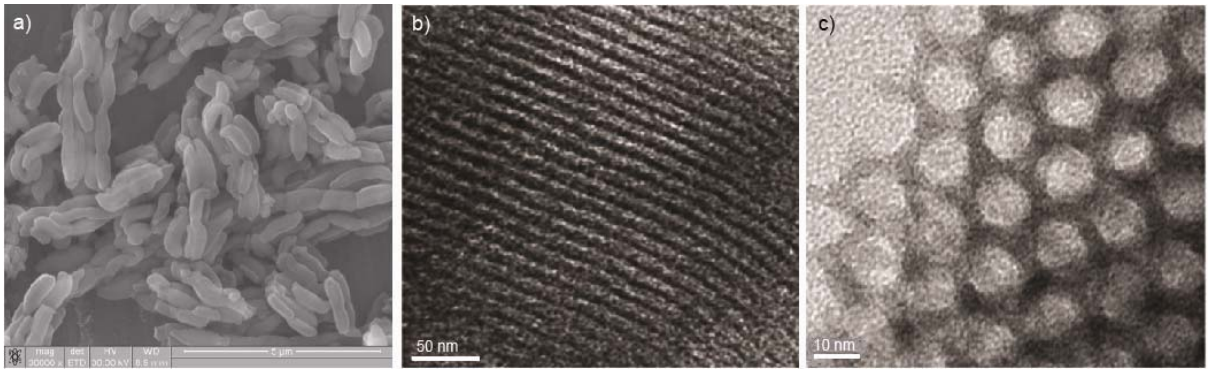

Figure 4.4: a) SEM of Cal. SBA-15, TEM of Cal-SBA-15; b) channels and c) pores

Nitrogen adsorption and desorption experiments for both SBA-PLL-10 and SBA-PLL-20 display type IV isotherms (Figure 4.7).The average pore size of SBA-PLL-10 decreased to 8.96 nm which was around 1 nm lower than the starting N_3-SBA-15. The specific surface area and pore volume was estimated to be 248 m^2/g and 0.699 cm^3/g (Figure 7a, Table 4.1).For SBA-PLL-20, the pore size decreased further to 8.09 nm and is consistent with the increased chain length of PLL-20 (Figure 4.7b).The retention of narrow pore size distribution after attachment of PLL is indicative of an uniform polymer layer across the surface of the material. The thickness of the polymer film for SBA-PLL-20 was estimated to be 1 nm from the decrease of the pore radius after "click" grafting.

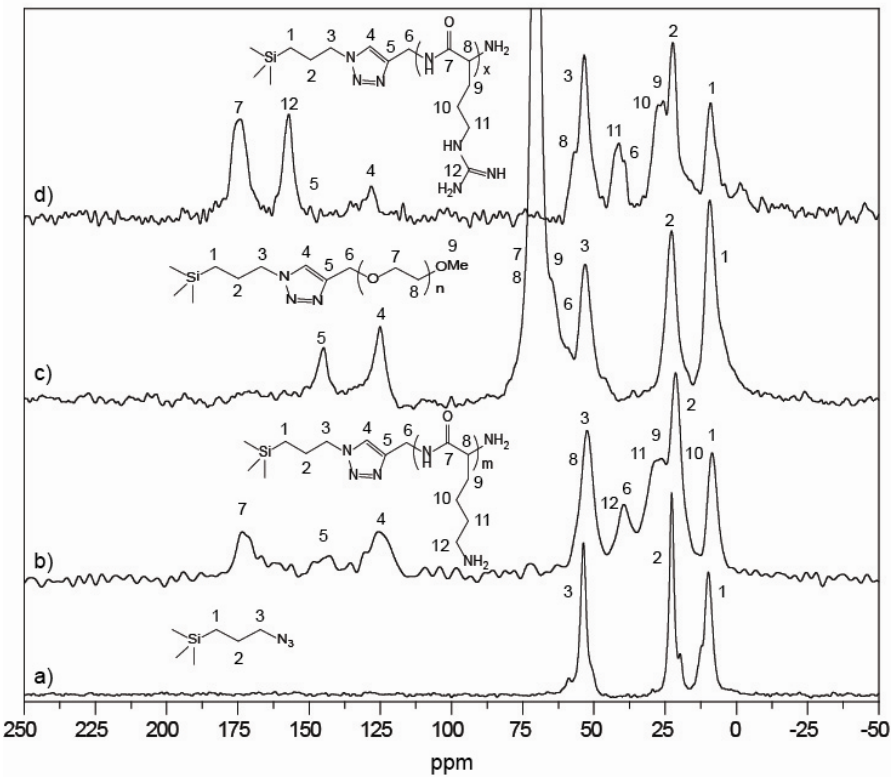

Figure 4.5: ^{13}C NMR spectra of a) N3-SBA-15 and MSN-N3, b) SBA-PLL-20, c) SBA-PEG-1000 and c) MSN-PLArg(20)

To probe further if the nitrogen adsorption desorption data was consistent with a grafting of PLL across the whole SBA-15 material and was not limited to the external surface, we compared this data to that of polyethyelene glycol (PEG-1000 and PEG-2000) grafted SBA-15 (SBA-PEG-1000 and SBA-PEG-2000). SBA-PEG-1000 and SBA-PEG-2000 hybrid was prepared by the CuAAC of N_3-SBA-15 with alkyne-PEG-1000 and alkyne-

PEG-2000, respectively. The successful grafting of PEG was confirmed by FT-IR and ^{13}C CP-MAS NMR spectrum (Figure 4.3e and Figure 4.5c). The grafting density was estimated to be 0.516 mmol and 0.206 mmol of PEG-1000 and 2000 respectively per gm of SBA-15 by TG-DTA. Nitrogen adsorption and desorption experiments for both SBA-PEG-1000 and SBA-PEG-2000 shows type IV isotherm (Figure 4.8).The average pore size of SBA-PEG-1000 decreases to 8.04 nm which is around 2 nm lower than the starting N_3-SBA-15. The high grafting of PEG-1000 onto SBA-15 and the nitrogen adsorption and desorption experiments indicate that PEG-1000 has been grafted throughout the material. Both PEG-1000 and PLL-20 have around 20 repeating units and are expected to have similar polymer thickness when grafted onto SBA-15 surface. SBA-PLL-20 and SBA-PEG-1000 have average pore size of 8.09 and 8.07 nm. This indicated that although the grafting density of PLL-20 was lower than PEG-1000 (mainly due to sterics and ionic interaction of the cationic side chain of PLL with the silica surface), they were both grafted across the whole material and not limited to the external surface. Aqueous electrophoresis experiments were performed on all the SBA-15 based materials that were synthesized. The zeta potential of these materials has been listed in Table 4.1. It can be observed that the zeta potential changed from -1for Cal-SBA-15 to +22 for SBA-PLL-10(Table 4.1). The change in zeta potential also confirms that PLL has been successfully grafted onto SBA-15.

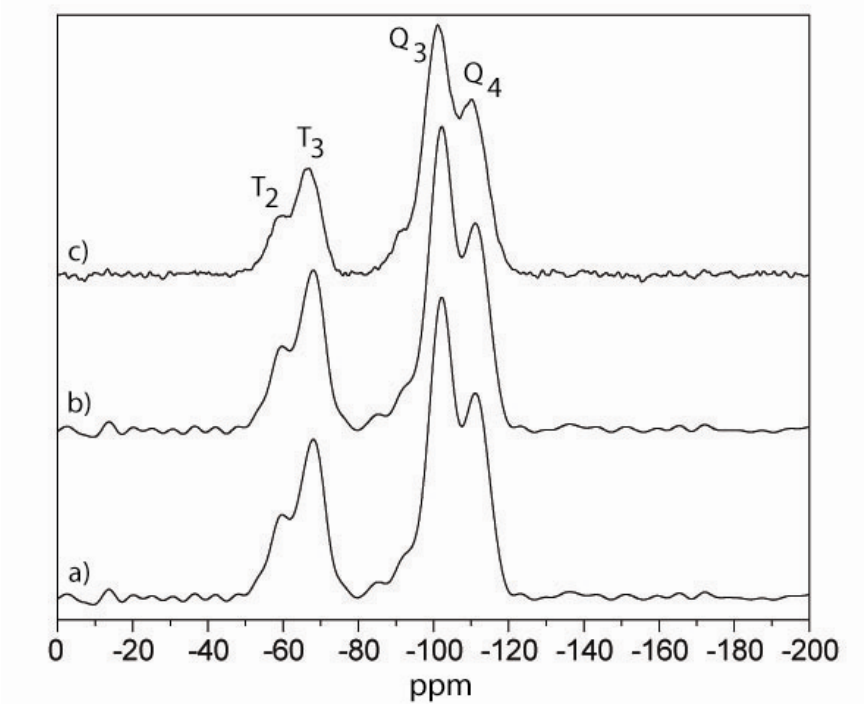

Figure 4.6: ^{29}Si CP-MAS NMR of (a) N_3-SBA-15, (b) SBA-PLL-20 and (c) SBA-PEG-1000

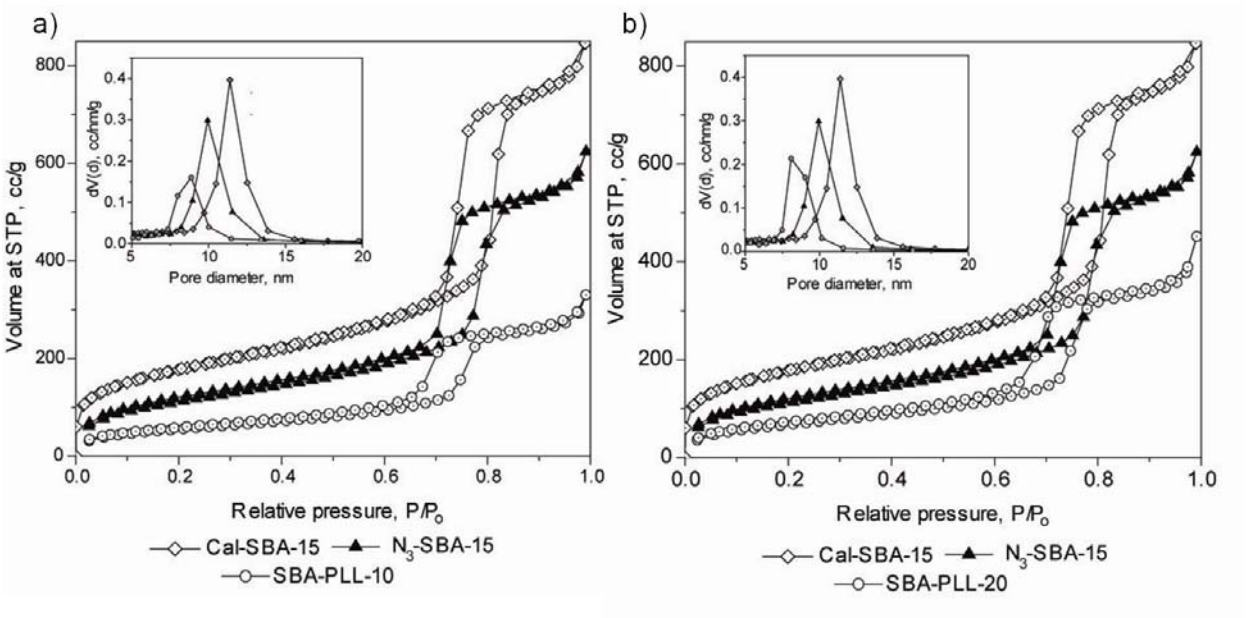

Figure 4.7: a) Nitrogen adsorption isotherms for unmodified SBA-15 (Cal-SBA-15), SBA-15 modified with azide (N3-SBA-15) and PLL-10 (SBA-PLL-10), and b) Nitrogen adsorption isotherms for unmodified SBA-15 (Cal-SBA-15), SBA-15 modified with azide (N3-SBA-15) and PLL-20 (SBA-PLL-20)

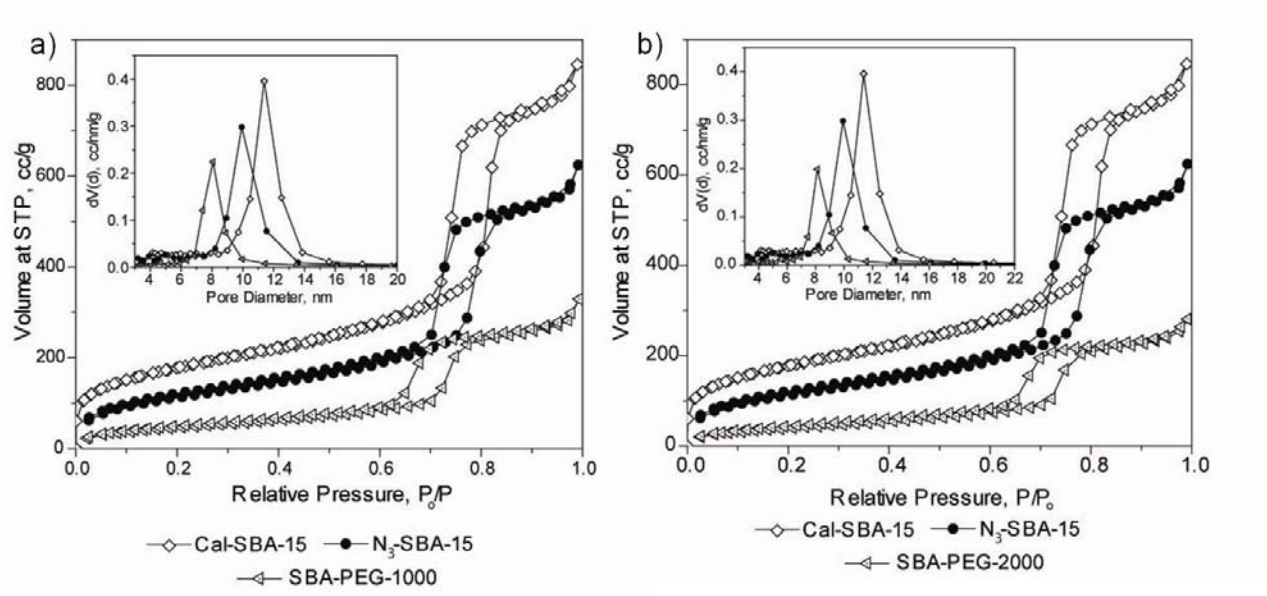

Figure 4.8: a) Nitrogen adsorption isotherms for unmodified SBA-15 (Cal-SBA-15), SBA-15 modified with azide (N3-SBA-15) and PEG-1000 (SBA-PEG-1000), and b) Nitrogen adsorption isotherms for unmodified SBA-15 (Cal-SBA-15), SBA-15 modified with azide (N3-SBA-15) and PEG-2000 (SBA-PEG-2000)

4.3.3 Synthesis and characterization of MSN-poly-L-arginine (MSN-PLArg)

Mesoporous silica nanoparticle was synthesized by using previously reported methodology. MSN having organoazide groups grafted on the external surface (MSN-N_3) was synthesized by methodology developed by our group earlier.[71] The powder XRD pattern of azide grafted MSN (MSN-N_3) displayed characteristic high intensity 100 peak near the 2θ value of 0.75°. Presence of higher order peaks 110 and 200 near the 2θ values of 1.33°and 1.53° respectively indicates formation of long range ordered mesoporous material (Figure 4.9b). Nitrogen adsorption and desorption experiments show type IV isotherm with steep increase in adsorption at P/P_0 due to capillary condensation of the nitrogen in the mesopores (Figure 4.9c). The BJH pore-size distribution (PSD) analysis shows very narrow PSD in the range 2.5-2.9 nm (Figure 4.9c).

Alkyne containing poly-L-arginine (20 and 10 mer) was grafted onto MSN-N_3 by CuAAC as using methodology reported before with slight modifications to yield MSN-PLArg(20) and MSN-PLArg(10) respectively.[72] The successful attachment of alkyne-PLArg(20) and alkyne-PLArg(10) was also confirmed from the IR spectra of MSN-PLArg(20) and MSN-PLArg(10) (Figure 4.3h and i) in which concomitant decrease of the $\nu_{as}(N_3)$ at 2103 cm^{-1} was observed with the appearance of the ν(C=O) at 1656 cm^{-1} and ν(N-H) at 1543 cm^{-1}, a region that displayed no peaks for the azide labeled MSN (MSN-N_3). Similar ν(C=O) and ν(N-H) stretches was observed in alkyne-PLArg. After the reaction, an extensive washing protocol was followed to remove the Cu(I), ligand, ascorbate and any unreacted alkyne-PLArg. One of the key steps in the washing was the use of dithiocarbamate to remove the Cu(I), as reported earlier. [71, 73] The TG-DTA (Figure 4.3i and f) analysis of MSN-PLArg(20) and MSN-PLArg(10) indicated a mass loss of 47.56% and 37.1% respectively between 100°C and 700°C which corresponds to a loading of 0.251 mmol (755 mg) and 0.219 mmol (438 mg) of PLArg per gm of MSN (Table 4.2).

The solid state ^{13}C CP-MAS NMR spectrum of MSN-PLArg(20) shows extra peaks in addition to the C1, C2 and C3 observed in azide grafted MSN(MSN-N_3) (Figure 4.5d). The presence of the peaks at 128 ppm and 153 ppm corresponds to the C4 and C5 atom of the triazole indicates that the PLArg have been covalently attached to the MSN particle via the triazole ring. The C7(174 ppm) (carbonyl), C12(157 ppm), C11(27 ppm) and C9 (25 ppm) observed in the spectra are very characteristic of the PLArg moiety. The chemical shifts of the C7 (174 ppm), C8 (54 ppm), C9(25 ppm) and C12 (157 ppm) are characteristic of the poly-L-arginine in the random coil conformation as has been reported.[74] The FT-IR spectra

also supports this since the observed amide I and amide II peaks at 1656 cm^{-1} and 1543 cm^{-1} are indicative of PLArg in a random coil conformation.

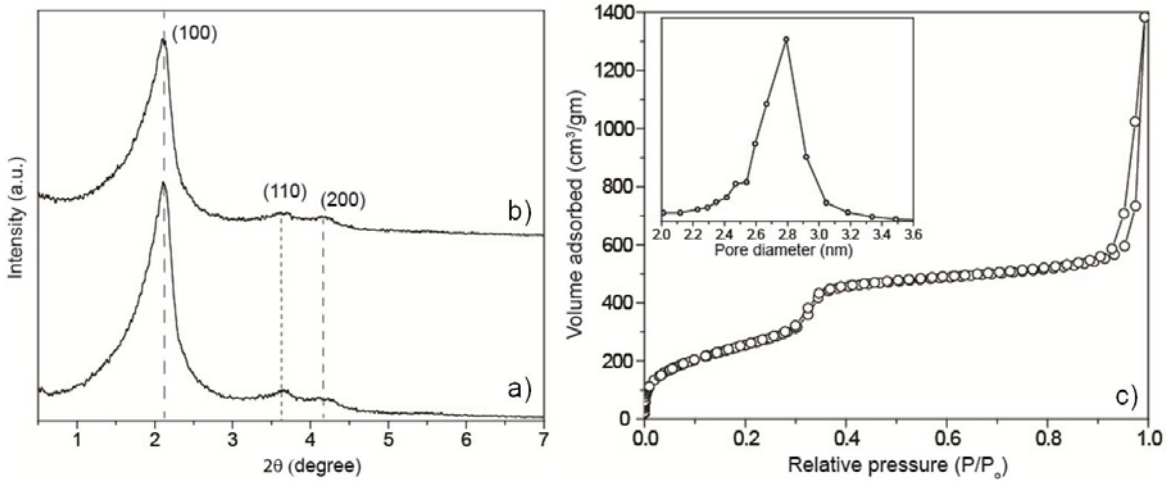

Figure 4.9: ^{13}C CPMAS NMR of a) MSN as synthesized, b) MSN-N_3, and c) Nitrogen adsorption isotherms for MSN-N_3

Aqueous electrophoresis experiments were performed on the MSN-PLArg(10) and MSN-PLArg(20) to determine their zeta potential.(Table 4.2) It was observed that the zeta potential in water increased considerably from -47±2 (MSN-N_3) to +32±4 and +20±2 for MSN-PLArg(20) and MSN-PLArg(10) respectively (Table 4.2). The change in zeta potential also confirms that the cationic PLArg has been successfully grafted onto MSN. The SEM and TEM image of MSN-PLArg(20) shows the particles were discrete and having average diameter around 70 nm (Figure 4.10a and b). The average hydrodynamic diameter of the particle was calculated to be around 80 nm using Dynamic Light Scattering (DLS)(Figure 4.10c). Similarly, the TEM and SEM image of MSN-PLArg(10) particles were discrete and the average diameter was found to be around 76 nm (Table 4.2).

Sample name	**Weight loss (%)**	**Grafting density of PLArg (mmol/gm)**	**Mean zeta potential (mV)**	**DLS (nm)**
MSN-N_3	11.1	1.1	-47±2	-
MSN-PLArg(20)	47.56	0.25	+32±4	80
MSN-PLArg(10)	37.12	0.21	+20±2	76

Table 4.2: Physical properties of various MSNs and silica

4.3.4 Study of plasmid DNA MSN-PLArgs polyplex formation using agarose gel electrophoresis

Gel retardation assay was performed to study the polyplex formation of the MSN-PLArgs with plasmid DNA (pDNA). Polyplex formation was obtained by incubating pDNA (0.2 μg) with MSN-PLArg(20), MSN-PLArg(10) at increasing MSN:pDNA weight ratios (from 1:0.5 to 1:4). After incubation for 30 minutes at room temperature, the polyplex formation was examined by agarose gel electrophoresis. Complete retardation of the pDNA was observed in polyplexes that were formed with pDNA:MSN-PLArg(20) ratio of 1:2 and above and for MSN-PLArg(10) ratio of 1:4 and above (Figure 4.11a and b). Since the zeta potential of MSN-PLArg(20) is higher than MSN-PLArg(10) (+32±4 and +20±2 respectively), the higher positive charge of MSN-PLArg(20) allows it to condense pDNA more efficiently than MSN-PLArg(10).

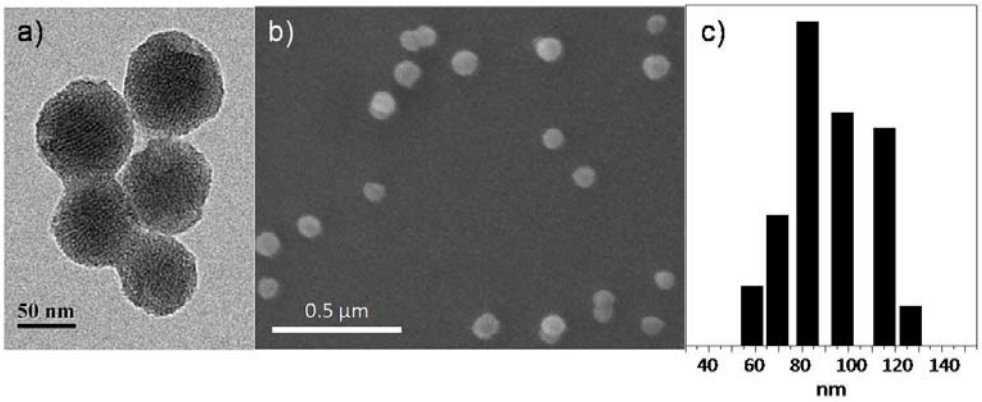

Figure 4.10: a) TEM Image, b) SEM Image and c) DLS of MSN-PLArg(20)

Zeta potential for the polyplexes formed by condensation of pDNA and MSN-PLArgs at various ratios was measured to understand the change of the overall zeta potential of the polyplexes with various pDNA and poly-L-arginine conjugates ratios (Figure 4.11c). The zeta potential for the polyplex formed with pDNA:MSN-PLArg ratio of 1:2 for MSN-PLArg(20) and 1:4 for MSN-PLArg(10) was determined to be nearly zero and increases with increasing concentration of poly-L-arginine conjugates. However, an overall positive zeta potential is required for the polyplex to efficiently enter the cell and undergo efficient transfection. Hence, for transfection studies a minimum pDNA-nanoparticle ratio of 1:6 and 1:8 was used for MSN-PLArg(20) and MSN-PLArg(10) respectively.

4.3.5 Cytotoxicity assay of MSN-PLArg nanoconjugates

MTT assays[68] were performed to evaluate the cytotoxicity of poly-L-arginine MSN conjugates, although cytotoxicity studies of both poly-L-arginine and MSN nanoparticles

individually have shown them to be non-toxic. MTT assays of MSN-PLArg(20) and MSN-PLArg(10) in two mammalian cancerous cell lines HeLa and A549 showed that both the cells retained around 80-85% viability after treatment with up to 100µg of MSN-PLArg(20) and MSN-PLArg(10) (Figure 4.12). It should be noted that in spite of poly-L-arginine MSN conjugates having a very high zeta potential (+32±2 and +20±2 for MSN-PLArg(20) and MSN-PLArg(10) respectively), they still show very low cytotoxicity at concentrations that would be used for DNA transfection. Although high charge on the surface of MSN induces strong interaction with the cell membrane (leading to high cellular uptake), it is also responsible for cell cytotoxicity. The poly-L-arginine MSN conjugates offer a great advantage of having high surface charge and low cytotoxicity. The poly-L-argnine present on the surface is biodegradable by various cellular proteases enzymes. Hence, the possibility of long term toxicity arising from the polypeptide will be much less. This would be in contrast MSN conjugated synthetic polymers like PEI which are known to be cytotoxic (IC_{50} of MSN-PEI_{25kD} is 35 µg/mL) due to damage to the surface membrane, lysosomes, and mitochondria.[75-77]

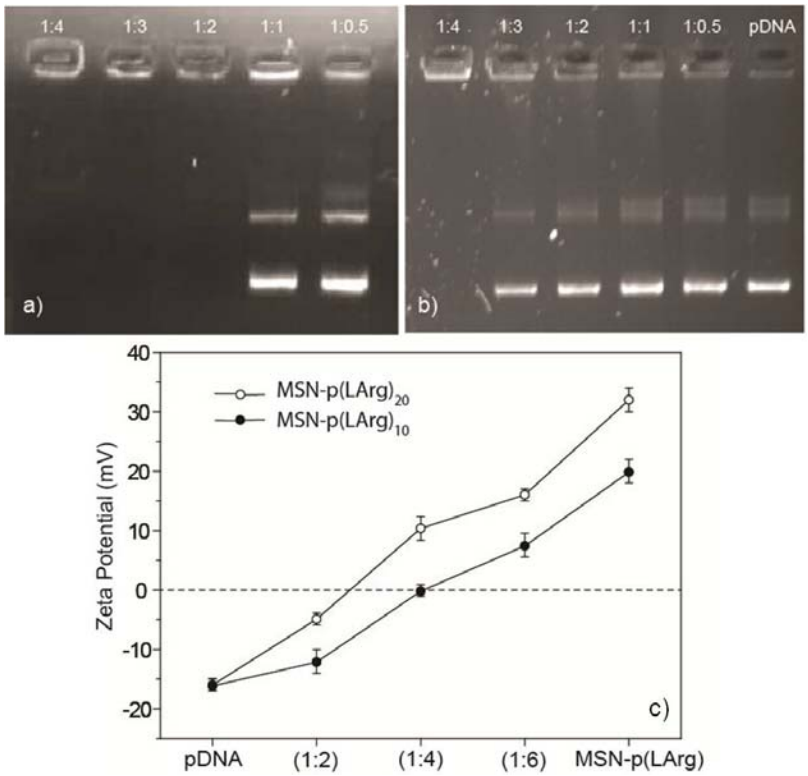

Figure 4.11: Retardation of plasmid DNA by MSN-PLArg. a) MSN-PLArg(20); from the right DNA and MSN-PLArg(20) ratio, lane 1 (1:0.5), lane 2 (1:1), lane 3 (1:2), lane 4 (1:3) and lane 5 (1:4), b) MSN-PLArg(10); from the right DNA and MSN-PLArg(10) ratio, lane 1

(1:0.5), lane 2 (1:1), lane 3 (1:2), lane 4 (1:3) and lane 5 (1:4) and lane 6 (1:5) and c) Zeta potentials for various ratio of DNA: MSN-PLArgs.

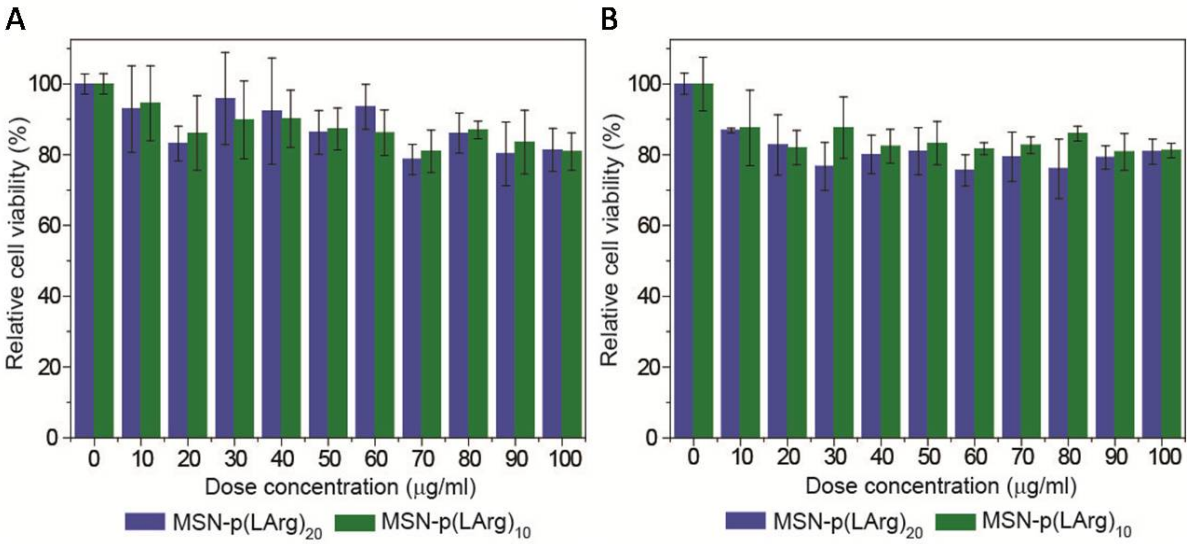

Figure 4.12: Results of MTT assay of MSN-PLArg(20) and MSN-PLArg(10) in A) HeLa and B) A549 cells

4.3.6 Cellular uptake of the MSN-PLArg nanoconjugates

The cellular uptake of poly-L-arginine grafted MSNs were studied in both HeLa and A549 cancer cells. The high zeta potential values of MSN-PLArg(20) and MSN-PLArg(10) (+20±2 and +56±4 respectively) indicate that these poly-L-arginine conjugates have the potential to enter cells very effectively. To adequately follow their cellular uptake, MSN-PLArg(20) and MSN-PLArg(10) were labeled with fluorescein and 2 μg/ml of the fluorescently labeled poly-L-arginine conjugates were added to HeLa and A549 and incubated for 24 hours. The results from the cell uptake study are illustrated in Figure 4.13 .Strong signals from fluorescein were observed in both HeLa and A549 cells indicating that these conjugates were successfully internalized in most of the cells. Control experiments with fluorescently labeled MSN-N_3 showed very low fluorescence in HeLa (Figure 4.13 e). To obtain a quantitative estimation of cellular uptake, fluorescence-activated cell sorting (FACS) was performed on both HeLa and A549 cells that were treated with fluorescently labeled MSN-PLArg(20) and MSN-PLArg(10). Flow cytometry analysis of all the four samples resulted in a clean shift of MFI (mean fluorescent intensity) and the cellular uptake of MSN-PLArg(20) and MSN-PLArg(10) in both HeLa and A549 cells was estimated to be about 90% and above.(Figure 4.13b and d) Recently, the efficiency of cellular uptake for poly-L-lysine grafted MSN conjugates (100 – 200 nm diameter) has been studied and found

to be about 68%. [48] Therefore, poly-L-arginine conjugated MSNs and silica are more efficient in entering cells than their corresponding poly-L-lysine conjugated particles that were recently reported. This is expected since poly-L-arginine is known to be more efficient cell penetrating polypeptide than poly-L-lysine and hence their presence on the surface of these nanoparticles facilitates its entry into the cells.[78, 79]

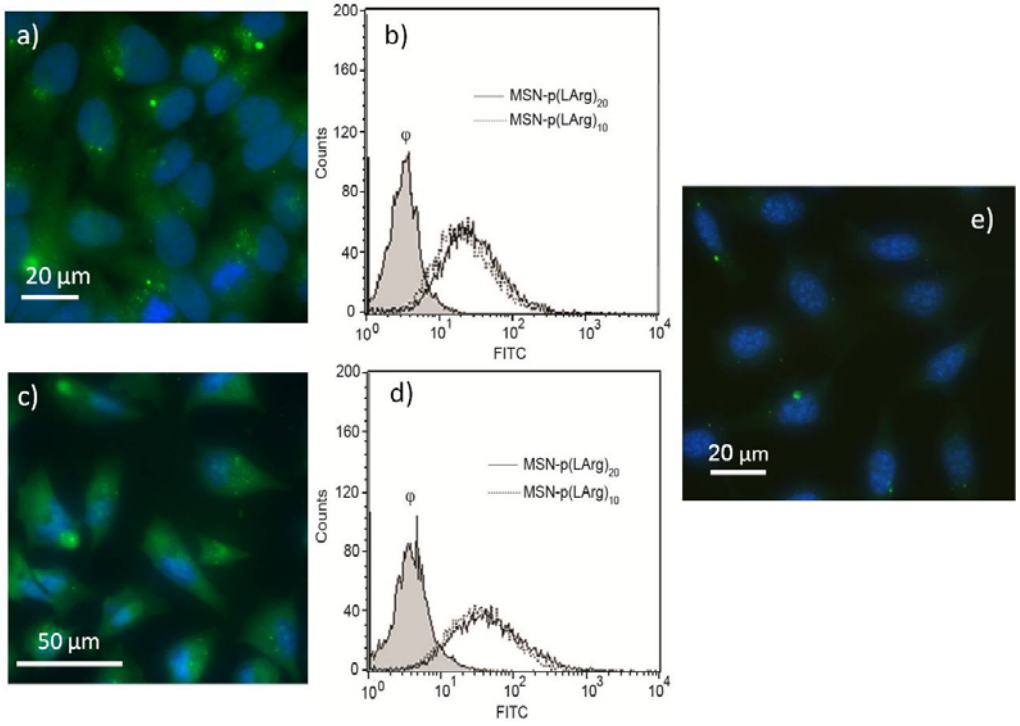

Figure 4.13: a) Epifluorescence image of Hela cells after incubation with fluorecien labeled MSN-PLArg(20) for 24 hrs and b) Assessment of cellular uptake of fluorescently labeled MSN-PLArg(10) and MSN-PLArg(20) onto HeLa cells by flow cytometry analysis c) Epifluorescence image of A549 cells after incubation with FITC labeled MSN-PLArg(20) for 24 hrs and d) Assessment of cellular uptake of fluorescently labeled MSN-PLArg(10) and MSN-PLArg(20) onto A549 cells by flow cytometry analysis and e) Epifluorescence image of Hela cells after incubation with fluorescein labeled MSN-N_3 for 24 hrs.

4.3.7 Transfection studies of the MSN –PLArg nanoconjugates

The efficacy of poly-L-arginine coated MSNs in terms of DNA plasmid delivery was studied by transfecting mCherry DNA plasmid into HeLa and A549 cells using MSN-PLArg(20) and MSN-PLArg(10) as the carrier. For transfection studies using MSN-PLArgs, pDNA: MSN-PLArg ratios of 1:6 to 1:14 was used to optimize the efficiency. Zeta potential study of the polyplexes shows that only at ratios of pDNA:nanoparticle of 1:6 and above the

polyplexes had a positive charge. Hence, a pDNA:nanoparticle ratio of 1:6 and above was used.

The results of the *in vitro* transfection experiments show that the best efficiency was observed at pDNA:MSN ratios of 1:12 and 1:14 for MSN-PLArg(20) and MSN-PLArg(10) respectively. The higher amounts of MSN-PLArgs are required since a high overall positive charge of the polyplex is essential to strongly interact with the negatively charged cell membrane to undergo effective cellular uptake. [80] This is supported by earlier reports that the *in vitro* transfection efficiency is enhanced by increasing the positive charge of the polyplex. [81-84] However, it should be noted that for the efficient transfection of pDNA, not only the polyplex charge and stability is important but also the efficiency in which the pDNA leaches inside the cytoplasm (endosomal escape) to transfect the protein of interest. To study both the cell entry of the polyplexes and the subsequent transfection of the protein of interest, both MSN-PLArg(20) and MSN-PLArg(10) were labeled with fluorescein and a plasmid DNA that expressed the red mcherry fluorescent protein was used. This would allow us to follow both the processes by epifluorescence microscopy in which visualization of nanoparticle uptake would be seen by green excitation at 488 nm and the expression of mCherry protein demonstrating efficient transfection can be visualized by red excitation at 610 nm. In a standard experiment, 0.5 μg of pDNA complexed with MSN-PLArgs were incubated with the cells for 48 hours. It was observed that the transfection efficiency of MSN-PLArg(20) particles were higher than that of MSN-PLArg(10). Microscopic images of transfected cells with mcherry protein by pDNA and MSN-PLArg(20) (1:12) showed around 50% of Hela and around 60% of A549 cells expressed the red mcherry fluorescent protein (Figure 4.14). These results were confirmed by FACS analysis. FACS analysis showed transfection efficiencies for Hela cell lines of 48±2% and 21±2% for MSN-PLArg(20) and MSN-PLArg(10) respectively. For A549 cell lines, transfection efficiencies of 60±2% (MSN-PLArg(20)) and 18±2% (MSN-PLArg(10)) were observed. This was comparable to the transfection efficiency of commercially available transfection agent, lipofectamine (38±2 % for HeLa and 15±3% A549).

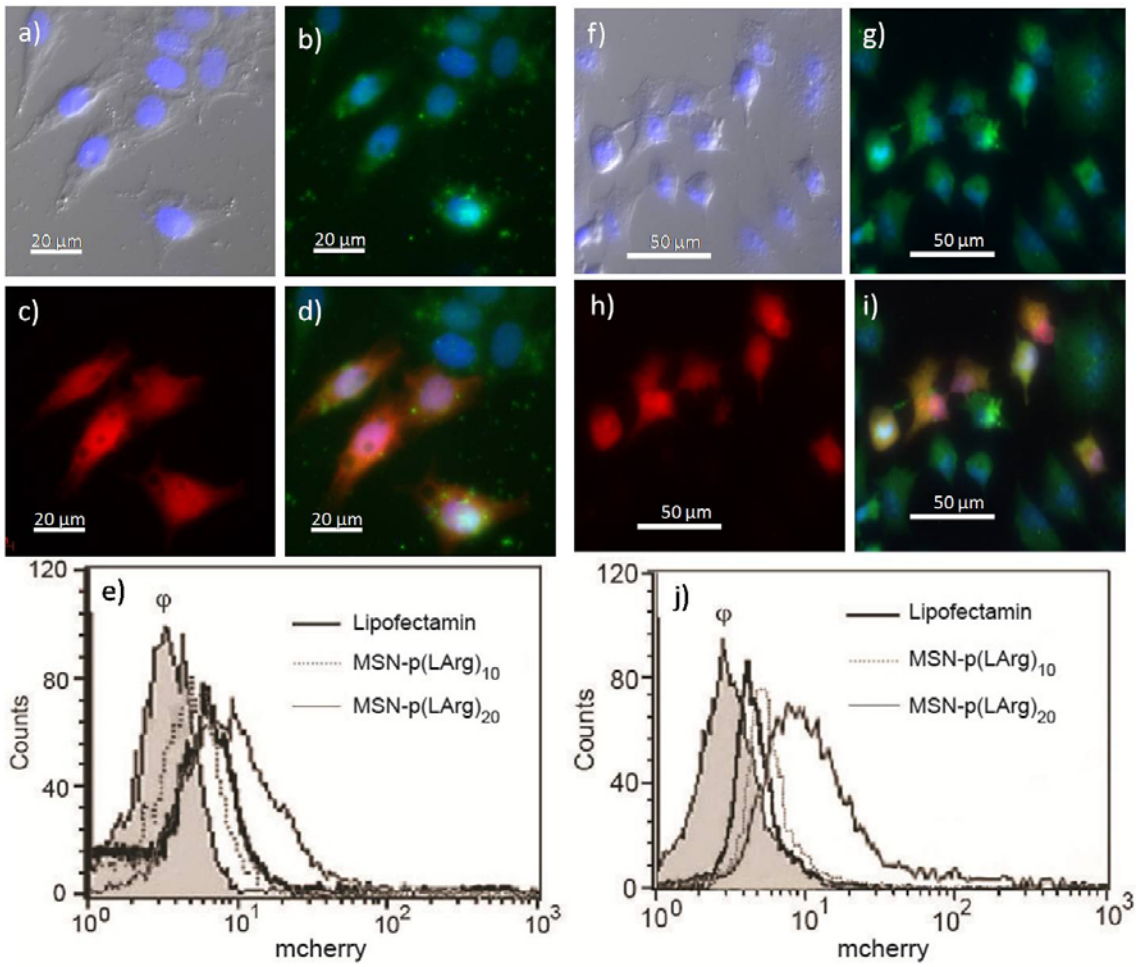

Figure 4.14: Transfection of Hela cells with MSN-PLArg(20) and mCherry DNA plasmid : a) DIC of cells with nucleus stained in blue with DAPI b) The localization of fluorescein labeled MSN-PLArg(20) in cells is shown in green c) The expression of red mCherry protein is observed in the cells d) overlap image of b) and c) showing co-localization of MSN and expressed mCherry protein e) Assessment of red mCherry protein expressed by flow cytometry analysis using MSN-PLArg(20) and lipofectamine; φ represents unstained cells Transfection of A549 cells with MSN-PLArg(20) and mCherry DNA plasmid : f) DIC of cells with nucleus stained in blue with DAPI, g) The localization of fluorescein labeled MSN-PLArg(20) in cells is shown in green h) The expression of red mCherry protein is observed in the cells i) overlap image of g) and h) showing co-localization of MSN and expressed mCherry protein j) Assessment of red mCherry protein expressed by flow cytometry analysis using MSN-PLArg(20) and lipofectamine; φ represents unstained cells

4.4 Conclusions

The synthesis of poly-L-lysine grafted SBA-15 with reasonable grafting density has been successfully achieved by the "grafting to" methodology using a combination of NCA polymerization and click chemistry. This "grafting to" methodology reported here offers several advantages and is complementary to the "grafting from" methodology developed by Shantz*et.al*. PLL with much higher molecular weights with very low polydispersity can be attached to SBA-15 than that has been reported by the "grafting from" methodology. Further, our materials retain their porosity after conjugation with PLL and this is in contrast to the lack of porosity observed in the SBA-PLL-conjugate material synthesized by the "grafting from" method. Also the use of corrosive reagents like HBr used for deprotection of cbz on the mesoporous material can be eliminated. We believe that successful attachment of high molecular weight homo polypeptides, block polypeptides and co-polypeptides to the SBA-15 with controlled molecular weights and high grafting density would be possible by this methodology.

The above methodology was modified to graft poly-L-arginine specifically onto the surface of the mesoporous silica thus keeping the pores empty. Synthesis of well defined poly-L-arginine grafted silica mesoporous nanoparticles (MSN-PLArg) with high grafting density has been successfully achieved by using same established "grafting to" methodology using click chemistry. The low cytotoxicity of these nanoparticles together with very high ability to penetrate cancer cells like HeLa and A549 make them excellent delivery vehicles for nucleic acid. The poly-L-arginine grafted MSNs can be used effectively to deliver mCherry DNA plasmid into cells leading to expression of the protein mCherry inside the cells. The huge unused inner surface area can be used to load and deliver therapeutic drug like, doxorubicin, cis-platin and actinomycin inside the cancer cells very effectively due to its high cellular uptake efficiency. Various pore size MSN can be easily be synthesized using our methodology. These parameters can be easily controlled by our synthetic methodology. The biocompatibility of poly-L-arginine and its cell penetrating ability will make these MSN conjugates more exciting over synthetic cationic polymer like PEI whose long term toxicity is unknown. We also believe that our methodology can also be used to deliver high amounts of SiRNA into cancer cells which can be very important for gene therapy.

4.5 References

1. Slowing, I. I.; Trewyn, B. G.; Giri, S.; Lin, V. S. Y., Mesoporous Silica Nanoparticles for Drug Delivery and Biosensing Applications. *Advanced Functional Materials* **2007,** 17, (8), 1225-1236.
2. Torney, F.; Trewyn, B. G.; Lin, V. S. Y.; Wang, K., Mesoporous silica nanoparticles deliver DNA and chemicals into plants. *Nat Nano* **2007,** 2, (5), 295-300.
3. Sarah, H.; Jakki, C.; Edmond, M., Proteins in Mesoporous Silicates. *Angewandte Chemie International Edition* **2008,** 47, (45), 8582-8594.
4. Schlossbauer, A.; Schaffert, D.; Kecht, J.; Wagner, E.; Bein, T., Click Chemistry for High-Density Biofunctionalization of Mesoporous Silica. *Journal of the American Chemical Society* **2008,** 130, (38), 12558-12559.
5. Zhao, D.; Feng, J.; Huo, Q.; Melosh, N.; Fredrickson, G. H.; Chmelka, B. F.; Stucky, G. D., Triblock Copolymer Syntheses of Mesoporous Silica with Periodic 50 to 300 Angstrom Pores. *Science* **1998,** 279, (5350), 548-552.
6. Nakazawa, J.; Stack, T. D. P., Controlled Loadings in a Mesoporous Material: Click-on Silica. *Journal of the American Chemical Society* **2008,** 130, (44), 14360-14361.
7. Hicks, J. C.; Drese, J. H.; Fauth, D. J.; Gray, M. L.; Qi, G.; Jones, C. W., Designing Adsorbents for CO2 Capture from Flue Gas-Hyperbranched Aminosilicas Capable of Capturing CO2 Reversibly. *Journal of the American Chemical Society* **2008,** 130, (10), 2902-2903.
8. Choi, M.; Kleitz, F.; Liu, D.; Lee, H. Y.; Ahn, W.-S.; Ryoo, R., Controlled Polymerization in Mesoporous Silica toward the Design of Organicâ˜'Inorganic Composite Nanoporous Materials. *Journal of the American Chemical Society* **2005,** 127, (6), 1924-1932.
9. Abelow, A. E.; Zharov, I., Poly(l-alanine)-modified nanoporous colloidal films. *Soft Matter* **2009,** 5, (2), 457-462.
10. Zhou, Z.; Zhu, S.; Zhang, D., Grafting of thermo-responsive polymer inside mesoporous silica with large pore size using ATRP and investigation of its use in drug release. *Journal of Materials Chemistry* **2007,** 17, (23), 2428-2433.
11. Wu, C.-G.; Bein, T., Polyaniline Wires in Oxidant-Containing Mesoporous Channel Hosts. *Chemistry of Materials* **1994,** 6, (8), 1109-1112.
12. Edmondson, S.; Osborne, V. L.; Huck, W. T. S., Polymer brushes via surface-initiated polymerizations. *Chemical Society Reviews* **2004,** 33, (1), 14-22.
13. Kruk, M.; Dufour, B.; Celer, E. B.; Kowalewski, T.; Jaroniec, M.; Matyjaszewski, K., Grafting Monodisperse Polymer Chains from Concave Surfaces of Ordered Mesoporous Silicas. *Macromolecules* **2008,** 41, (22), 8584-8591.
14. Moreno, J.; Sherrington, D. C., Well-Defined Mesostructured Organicâ˜'Inorganic Hybrid Materials via Atom Transfer Radical Grafting of Oligomethacrylates onto SBA-15 Pore Surfaces. *Chemistry of Materials* **2008,** 20, (13), 4468-4474.
15. Hsiao, J.-K.; Tsai, C.-P.; Chung, T.-H.; Hung, Y.; Yao, M.; Liu, H.-M.; Mou, C.-Y.; Yang, C.-S.; Chen, Y.-C.; Huang, D.-M., Mesoporous Silica Nanoparticles as a Delivery System of Gadolinium for Effective Human Stem Cell Tracking. *Small* **2008,** 4, (9), 1445-1452.

16. Pasetto, P.; Blas, H. l. n.; Audouin, F.; BoissieÌ€re, C. d.; Sanchez, C. m.; Save, M.; Charleux, B., Mechanistic Insight into Surface-Initiated Polymerization of Methyl Methacrylate and Styrene via ATRP from Ordered Mesoporous Silica Particles. *Macromolecules* **2009,** 42, (16), 5983-5995.

17. Lenarda, M.; Chessa, G.; Moretti, E.; Polizzi, S.; Storaro, L.; Talon, A., Toward the preparation of a nanocomposite material through surface initiated controlled/"living" radical polymerization of styrene inside the channels of MCM-41 silica. *Journal of Materials Science* **2006,** 41, (19), 6305-6312.

18. Hong, C.-Y.; Li, X.; Pan, C.-Y., Smart Core Shell Nanostructure with a Mesoporous Core and a Stimuli-Responsive Nanoshell Synthesized via Surface Reversible Addition Fragmentation Chain Transfer Polymerization. *The Journal of Physical Chemistry C* **2008,** 112, (39), 15320-15324.

19. Po-Wen, C.; Rajeev, K.; Marek, P.; Victor, S. Y. L., Temperature Responsive Solution Partition of Organic-Inorganic Hybrid Poly(N-isopropylacrylamide)-Coated Mesoporous Silica Nanospheres. *Advanced Functional Materials* **2008,** 18, (9), 1390-1398.

20. Bonoiu, A. C.; Mahajan, S. D.; Ding, H.; Roy, I.; Yong, K.-T.; Kumar, R.; Hu, R.; Bergey, E. J.; Schwartz, S. A.; Prasad, P. N., Nanotechnology approach for drug addiction therapy: Gene silencing using delivery of gold nanorod-siRNA nanoplex in dopaminergic neurons. *Proceedings of the National Academy of Sciences* **2009,** 106, (14), 5546-5550.

21. Jin-Ho, M.; Ramaraj, B.; Soo Min, L.; Kuk Ro, Y., Direct grafting of e-caprolactone on solid core/mesoporous shell silica spheres by surface-initiated ring-opening polymerization. *Journal of Applied Polymer Science* **2008,** 107, (4), 2689-2694.

22. Lunn, J. D.; Shantz, D. F., Peptide Brush Ordered Mesoporous Silica Nanocomposite Materials. *Chemistry of Materials* **2009,** 21, (15), 3638-3648.

23. Kruk, M.; Dufour, B.; Celer, E. B.; Kowalewski, T.; Jaroniec, M.; Matyjaszewski, K., Synthesis of Mesoporous Carbons Using Ordered and Disordered Mesoporous Silica Templates and Polyacrylonitrile as Carbon Precursor. *Journal of Physical Chemistry B* **2005,** 109, (19), 9216-9225.

24. Chang, Y.-C.; Frank, C. W., Vapor Deposition Polymerization of a-Amino Acid N-Carboxy Anhydride on the Silicon(100) Native Oxide Surface. *Langmuir* **1998,** 14, (2), 326-334.

25. Muhammad, F.; Guo, M.; Qi, W.; Sun, F.; Wang, A.; Guo, Y.; Zhu, G., pH-Triggered Controlled Drug Release from Mesoporous Silica Nanoparticles via Intracelluar Dissolution of ZnO Nanolids. *Journal of the American Chemical Society* **2011,** 133, (23), 8778-8781.

26. Fong, B.; Russo, P. S., Organophilic Colloidal Particles with a Synthetic Polypeptide Coating. *Langmuir* **1999,** 15, (13), 4421-4426.

27. Fong, B.; Turksen, S.; Russo, P. S.; Stryjewski, W., Colloidal Crystals of Silica Homopolypeptide Composite Particles. *Langmuir* **2004,** 20, (1), 266-269.

28. Lunn, J. D.; Shantz, D. F., Novel polypeptide/thiol-SBA-15 hybrid materials synthesized via surface selective grafting. *Chemical Communications* **2010,** 46, (17), 2926-2928.

29. Hadjichristidis, N.; Iatrou, H.; Pitsikalis, M.; Sakellariou, G., Synthesis of Well-Defined Polypeptide-Based Materials via the Ring-Opening Polymerization of Î±-Amino Acid N-Carboxyanhydrides. *Chemical Reviews* **2009**.

30. Rostovtsev, V. V.; Green, L. G.; Fokin, V. V.; Sharpless, K. B., A Stepwise Huisgen Cycloaddition Process: Copper(I)-Catalyzed Regioselective ldquoLigationrdquo of Azides and Terminal Alkynes13. *Angewandte Chemie International Edition* **2002,** 41, (14), 2596-2599.

31. Nurmi, L.; Lindqvist, J.; Randev, R.; Syrett, J.; Haddleton, D. M., Glycopolymers via catalytic chain transfer polymerisation (CCTP), Huisgens cycloaddition and thiol-ene double click reactions. *Chemical Communications* **2009**, (19), 2727-2729.

32. Fournier, D.; Hoogenboom, R.; Schubert, U. S., Clicking polymers: a straightforward approach to novel macromolecular architectures. *Chemical Society Reviews* **2007,** 36, (8), 1369-1380.

33. Malvi, B.; Sarkar, B. R.; Pati, D.; Mathew, R.; Ajithkumar, T. G.; Gupta, S. S., "Clickable" SBA-15 mesoporous materials: synthesis, characterization and their reaction with alkynes. *Journal of Materials Chemistry* **2009,** 19, (10), 1409-1416.

34. Huang, L.; Dolai, S.; Raja, K.; Kruk, M., "Click" Grafting of High Loading of Polymers and Monosaccharides on Surface of Ordered Mesoporous Silica. *Langmuir* **2009**.

35. Casasus, R.; Climent, E.; Marcos, M. D.; Martinez-Manez, R.; Sancenon, F.; Soto, J.; Amoros, P.; Cano, J.; Ruiz, E., Dual Aperture Control on pH- and Anion-Driven Supramolecular Nanoscopic Hybrid Gate-like Ensembles. *Journal of the American Chemical Society* **2008,** 130, (6), 1903-1917.

36. Scholl, S. M.; Michaelis, S.; McDermott, R., Gene Therapy Applications to Cancer Treatment. *Journal of Biomedicine and Biotechnology* **2003,** 2003, (1), 35-47.

37. Cross, D.; Burmester, J. K., Gene Therapy for Cancer Treatment: Past, Present and Future. *Clinical Medicine & Research* **2006,** 4, (3), 218-227.

38. Rideout Iii, W. M.; Hochedlinger, K.; Kyba, M.; Daley, G. Q.; Jaenisch, R., Correction of a Genetic Defect by Nuclear Transplantation and Combined Cell and Gene Therapy. *Cell* **2002,** 109, (1), 17-27.

39. Bharali, D. J.; Klejbor, I.; Stachowiak, E. K.; Dutta, P.; Roy, I.; Kaur, N.; Bergey, E. J.; Prasad, P. N.; Stachowiak, M. K., Organically modified silica nanoparticles: A nonviral vector for in vivo gene delivery and expression in the brain. *Proceedings of the National Academy of Sciences of the United States of America* **2005,** 102, (32), 11539-11544.

40. Davis, S. S., Biomedical applications of nanotechnology - implications for drug targeting and gene therapy. *Trends in Biotechnology* **1997,** 15, (6), 217-224.

41. Roy, I.; Mitra, S.; Maitra, A.; Mozumdar, S., Calcium phosphate nanoparticles as novel non-viral vectors for targeted gene delivery. *International Journal of Pharmaceutics* **2003,** 250, (1), 25-33.

42. McAllister, K.; Sazani, P.; Adam, M.; Cho, M. J.; Rubinstein, M.; Samulski, R. J.; DeSimone, J. M., Polymeric Nanogels Produced via Inverse Microemulsion Polymerization as Potential Gene and Antisense Delivery Agents. *Journal of the American Chemical Society* **2002,** 124, (51), 15198-15207.

43. Borm, P.; Klaessig, F. C.; Landry, T. D.; Moudgil, B.; Pauluhn, J. r.; Thomas, K.; Trottier, R.; Wood, S., Research Strategies for Safety Evaluation of Nanomaterials, Part V: Role of Dissolution in Biological Fate and Effects of Nanoscale Particles. *Toxicological Sciences* **2006,** 90, (1), 23-32.

44. Finnie, K.; Waller, D.; Perret, F.; Krause-Heuer, A.; Lin, H.; Hanna, J.; Barbé, C., Biodegradability of sol–gel silica microparticles for drug delivery. *Journal of Sol-Gel Science and Technology* **2009,** 49, (1), 12-18.

45. Radu, D. R.; Lai, C.-Y.; Jeftinija, K.; Rowe, E. W.; Jeftinija, S.; Lin, V. S. Y., A Polyamidoamine Dendrimer-Capped Mesoporous Silica Nanosphere-Based Gene Transfection Reagent. *Journal of the American Chemical Society* **2004,** 126, (41), 13216-13217.

46. Gao, Q.; Xu, Y.; Wu, D.; Sun, Y.; Li, X., pH-Responsive Drug Release from Polymer-Coated Mesoporous Silica Spheres. *The Journal of Physical Chemistry C* **2009,** 113, (29), 12753-12758.

47. Qin, F.; Zhou, Y.; Shi, J.; Zhang, Y., A DNA transporter based on mesoporous silica nanospheres mediated with polycation poly(allylamine hydrochloride) coating on mesopore surface. *Journal of Biomedical Materials Research Part A* **2008,** 90A, (2), 333-338.

48. Hartono, S. B.; Gu, W.; Kleitz, F.; Liu, J.; He, L.; Middelberg, A. P. J.; Yu, C.; Lu, G. Q.; Qiao, S. Z., Poly-l-lysine Functionalized Large Pore Cubic Mesostructured Silica Nanoparticles as Biocompatible Carriers for Gene Delivery. *ACS Nano* **2012,** 6, (3), 2104-2117.

49. Giri, S.; Trewyn, B. G.; Stellmaker, M. P.; Lin, V. S. Y., Stimuli-Responsive Controlled-Release Delivery System Based on Mesoporous Silica Nanorods Capped with Magnetic Nanoparticles. *Angewandte Chemie International Edition* **2005,** 44, (32), 5038-5044.

50. Hu, S.-H.; Liu, T.-Y.; Huang, H.-Y.; Liu, D.-M.; Chen, S.-Y., Magnetic-Sensitive Silica Nanospheres for Controlled Drug Release. *Langmuir* **2007,** 24, (1), 239-244.

51. Brigger, I. n.; Dubernet, C.; Couvreur, P., Nanoparticles in cancer therapy and diagnosis. *Advanced Drug Delivery Reviews* **2002,** 54, (5), 631-651.

52. Gao, W.; Chan, J. M.; Farokhzad, O. C., pH-Responsive Nanoparticles for Drug Delivery. *Molecular Pharmaceutics* **2010,** 7, (6), 1913-1920.

53. Sun, J.; Zhang, H.; Ma, D.; Chen, Y.; Bao, X.; Klein-Hoffmann, A.; Pfander, N.; Su, D. S., Alkanes-assisted low temperature formation of highly ordered SBA-15 with large cylindrical mesopores. *Chemical Communications* **2005**, (42), 5343-5345.

54. Cauda, V.; Argyo, C.; Schlossbauer, A.; Bein, T., Controlling the delivery kinetics from colloidal mesoporous silica nanoparticles with pH-sensitive gates. *Journal of Materials Chemistry* **2010,** 20, (21), 4305-4311.

55. Mitchell, D. J.; Steinman, L.; Kim, D. T.; Fathman, C. G.; Rothbard, J. B., Polyarginine enters cells more efficiently than other polycationic homopolymers. *The Journal of Peptide Research* **2000,** 56, (5), 318-325.

56. Wender, P. A.; Mitchell, D. J.; Pattabiraman, K.; Pelkey, E. T.; Steinman, L.; Rothbard, J. B., The design, synthesis, and evaluation of molecules that enable or enhance cellular uptake: Peptoid molecular transporters. *Proceedings of the National Academy of Sciences* **2000,** 97, (24), 13003-13008.

57. Maiolo, J. R.; Ferrer, M.; Ottinger, E. A., Effects of cargo molecules on the cellular uptake of arginine-rich cell-penetrating peptides. *Biochimica et Biophysica Acta (BBA) - Biomembranes* **2005,** 1712, (2), 161-172.

58. Fonseca, S. B.; Pereira, M. P.; Kelley, S. O., Recent advances in the use of cell-penetrating peptides for medical and biological applications. *Advanced Drug Delivery Reviews* **2009,** 61, (11), 953-964.
59. Bolhassani, A., Potential efficacy of cell-penetrating peptides for nucleic acid and drug delivery in cancer. *Biochimica et Biophysica Acta (BBA) - Reviews on Cancer* **2011,** 1816, (2), 232-246.
60. Emi, N.; Kidoaki, S.; Yoshikawa, K.; Saito, H., Gene Transfer Mediated by Polyarginine Requires a Formation of Big Carrier-Complex of DNA Aggregate. *Biochemical and Biophysical Research Communications* **1997,** 231, (2), 421-424.
61. Temsamani, J.; Vidal, P., The use of cell-penetrating peptides for drug delivery. *Drug Discovery Today* **2004,** 9, (23), 1012-1019.
62. Mae, M.; Langel, U., Cell-penetrating peptides as vectors for peptide, protein and oligonucleotide delivery. *Current Opinion in Pharmacology* **2006,** 6, (5), 509-514.
63. Stewart, K. M.; Horton, K. L.; Kelley, S. O., Cell-penetrating peptides as delivery vehicles for biology and medicine. *Organic & Biomolecular Chemistry* **2008,** 6, (13), 2242-2255.
64. Slowing, I. I.; Vivero-Escoto, J. L.; Wu, C.-W.; Lin, V. S. Y., Mesoporous silica nanoparticles as controlled release drug delivery and gene transfection carriers. *Advanced Drug Delivery Reviews* **2008,** 60, (11), 1278-1288.
65. Koo, H.; Kang, H.; Lee, Y., Analysis of the Relationship between the Molecular Weight and Transfection Efficiency/Cytotoxicity of Poly-L-arginine on a Mammalian Cell Line. *Bulletin of the Korean Chemical Society* **2009,** 30, (4), 927-930.
66. Cao, L.; Man, T.; Kruk, M., Synthesis of Ultra-Large-Pore SBA-15 Silica with Two-Dimensional Hexagonal Structure Using Triisopropylbenzene As Micelle Expander. *Chemistry of Materials* **2009,** 21, (6), 1144-1153.
67. Bartholome, C.; Beyou, E.; Bourgeat-Lami, E.; Chaumont, P.; Zydowicz, N., Nitroxide-Mediated Polymerizations from Silica Nanoparticle Surfaces: "Graft from" Polymerization of Styrene Using a Triethoxysilyl-Terminated Alkoxyamine Initiator. *Macromolecules* **2003,** 36, (21), 7946-7952.
68. Mosmann, T., Rapid colorimetric assay for cellular growth and survival: application to proliferation and cytotoxicity assays. *Journal of immunological methods* **1983,** 65, (1-2), 55-63.
69. Kar, M.; Vijayakumar, P. S.; Prasad, B. L. V.; Gupta, S. S., Synthesis and Characterization of Poly-l-lysine-Grafted Silica Nanoparticles Synthesized via NCA Polymerization and Click Chemistry. *Langmuir* **2010,** 26, (8), 5772-5781.
70. Mirau, P. A.; Serres, J. L.; Lyons, M., The Structure and Dynamics of Poly(l-lysine) in Templated Silica Nanocomposites. *Chemistry of Materials* **2008,** 20, (6), 2218-2223.
71. Kar, M.; Malvi, B.; Das, A.; Panneri, S.; Gupta, S. S., Synthesis and characterization of poly-l-lysine grafted SBA-15 using NCA polymerization and click chemistry. *Journal of Materials Chemistry* **2011,** 21, (18), 6690-6697.
72. Hong, V.; Presolski, S. I.; Ma, C.; Finn, M. G., Analysis and Optimization of Copper-Catalyzed Azide–Alkyne Cycloaddition for Bioconjugation. *Angewandte Chemie International Edition* **2009,** 48, (52), 9879-9883.

73. Kar, M.; Pauline, M.; Sharma, K.; Kumaraswamy, G.; Sen Gupta, S., Synthesis of Poly-l-glutamic Acid Grafted Silica Nanoparticles and Their Assembly into Macroporous Structures. *Langmuir* **2011,** 27, (19), 12124-12133.

74. Saito, H.; Ohki, T.; Kodama, M.; Nagata, C., 13C Nuclear magnetic resonance study of salt induced conformational change of basic polypeptides: Poly (L-lysine), poly (L-arginine), and poly (L-ornithine). *Biopolymers* **1978,** 17, (11), 2587-2599.

75. Boussif, O.; Lezoualc'h, F.; Zanta, M. A.; Mergny, M. D.; Scherman, D.; Demeneix, B.; Behr, J. P., A versatile vector for gene and oligonucleotide transfer into cells in culture and in vivo: polyethylenimine. *Proceedings of the National Academy of Sciences* **1995,** 92, (16), 7297-7301.

76. Xia, T.; Kovochich, M.; Liong, M.; Zink, J. I.; Nel, A. E., Cationic Polystyrene Nanosphere Toxicity Depends on Cell-Specific Endocytic and Mitochondrial Injury Pathways. *ACS Nano* **2007,** 2, (1), 85-96.

77. Xia, T.; Kovochich, M.; Liong, M.; Meng, H.; Kabehie, S.; George, S.; Zink, J. I.; Nel, A. E., Polyethyleneimine Coating Enhances the Cellular Uptake of Mesoporous Silica Nanoparticles and Allows Safe Delivery of siRNA and DNA Constructs. *ACS Nano* **2009,** 3, (10), 3273-3286.

78. Melikov, K.; Chernomordik, L., Arginine-rich cell penetrating peptides: from endosomal uptake to nuclear delivery. *Cellular and Molecular Life Sciences* **2005,** 62, (23), 2739-2749.

79. Jones, S. W.; Christison, R.; Bundell, K.; Voyce, C. J.; Brockbank, S. M. V.; Newham, P.; Lindsay, M. A., Characterisation of cell-penetrating peptide-mediated peptide delivery. *British Journal of Pharmacology* **2005,** 145, (8), 1093-1102.

80. Rosenholm, J. M.; Meinander, A.; Peuhu, E.; Niemi, R.; Eriksson, J. E.; Sahlgren, C.; LindeÌ n, M., Targeting of Porous Hybrid Silica Nanoparticles to Cancer Cells. *ACS Nano* **2008,** 3, (1), 197-206.

81. Pouton, C. W.; Lucas, P.; Thomas, B. J.; Uduehi, A. N.; Milroy, D. A.; Moss, S. H., Polycation-DNA complexes for gene delivery: a comparison of the biopharmaceutical properties of cationic polypeptides and cationic lipids. *Journal of Controlled Release* **1998,** 53, (13), 289-299.

82. Tang, M. X.; Szoka, F. C., The influence of polymer structure on the interactions of cationic polymers with DNA and morphology of the resulting complexes. *Gene therapy* **1997,** 4, (8), 823-32.

83. Duguid, J. G.; Li, C.; Shi, M.; Logan, M. J.; Alila, H.; Rolland, A.; Tomlinson, E.; Sparrow, J. T.; Smith, L. C., A Physicochemical Approach for Predicting the Effectiveness of Peptide-Based Gene Delivery Systems for Use in Plasmid-Based Gene Therapy. *Biophysical Journal* **1998,** 74, (6), 2802-2814.

84. De Smedt, S. C.; Demeester, J.; Hennink, W. E., Cationic Polymer Based Gene Delivery Systems. *Pharmaceutical Research* **2000,** 17, (2), 113-126.

Chapter 5

Conclusions and Future Directions

5.1 Summary and conclusions

This dissertation describes the synthesis and characterization of various homo- and block co- polypeptides that had an alkyne group at its chain end. These alkyne end functionalized polypeptides were grafted onto various silica materials (silica nanoparticles and mesoporous silica nanoparticles) by using Cu(I) catalyzed azide alkyne cycloaddition reaction. These polypeptide silica nanoconjugates were characterized by using various analytical techniques. The application of these polypeptide silica nanoconjugates as antimicrobial agent, gene transfection agent and as building blocks of 3-D macroporous scaffolds is also reported. This chapter presents the summaries and conclusions of all the previous chapters. It also discusses the future scope based on the work reported in this thesis.

Chapter 1 provides a brief review on the synthesis of amino acid NCA's and their ring opening polymerization for the synthesis of polypeptides. This chapter also discusses the importance of the surface modification of various conventional materials in biological context as well as the synthesis, surface modification and application of organic-inorganic hybrid nanomaterials. A brief introduction to Cu(I) catalyzed azide-alkyne click chemistry (CuAAC) is discussed. Finally, the motivation for the development of polypeptide grafted core-shell silica nanoparticles that would combine the biological property of polypeptides and the structural properties of silica nanoparticles is discussed.

Chapter 2 describes the synthesis of alkyne terminated various homo and block co-polypeptides. All the synthetic methodologies developed for the preparation of the various amino acid NCA monomers were high yielding and easy to handle. NCA ring opening polymerization was used to synthesis alkyne terminated homo- and block co- polypeptides using N-TMS propargylamine as the initiator. The progress of the NCA polymerization reactions was monitored by disappearance of the FT-IR resonances at 1855±5 cm^{-1} and 1780±5 cm^{-1} that are considered to be characteristic of the stretching modes of the two carbonyl groups in the NCA ring. For the synthesis of the block co- polypeptides, second monomers were added into the reaction mixture after 95% (determined by FT-IR) of the first NCA monomer was consumed. Use of N-TMS propargylamine as the initiator allows the synthesis of polypeptides with very low polydispersity and precise molecular weights. It also leads to the incorporation of a C- terminal alkyne at the polypeptide end which can be further modified by using Cu(I) catalyzed azide alkyne cycloaddiction reaction. All NCA

polymerizations were carried out inside the glove box (O2 > 0.1 ppm and H_2O >1 ppm) and the synthesized polypeptides were characterized by FT-IR, GPC and NMR.

Chapter 3 describes the synthesis of homo and block co-polypeptides grafted silica nanoconjugates and their application as biomaterials. "Grafting to" methodology was used for the synthesis of all the silica polypeptide nanoconjugates via CuAAC. Although 'grafting to' technique is traditionally known to be inefficient due to the steric reasons, the efficiency of "click chemistry" compensated for the unfavorable sterics and allowed grafting of a very high density of the unprotected polypeptide onto the silica nanoparticles. The progression of 'click' reaction was monitored by monitoring the decrease of the characteristic organoazide peak at 2100 cm^{-1} using FT-IR. This methodology developed by us is general and can be extended for grafting any natural and unnatural polypeptide. For example, uniform poly-L-lysine (PLL), poly-L-glutamic acid (PLGA) and poly-L-arginine (PLArg) coated silica nanoparticles were synthesized using this methodology. The grafting density was characterized by using thermogravimetric analysis (TGA). Solid state CP MAS NMR was used to structurally characterize the silica polypeptide nanoconjugates and to investigate the secondary conformations of the polypeptides that were grafted onto the surface of the silica nanoparticles. The silica polypeptide nanoconjugates exhibited interesting aggregation properties. For example, although silica-poly-L-lysine (silica-PLL) nanoconjugates containing very high grafting density of charged poly-L-lysine onto the silica surface was highly cationic, yet the nanoconjugates are very prone to aggregation in water. On the other hand, positively charged silica-poly-L-arginine (silica-PLArg) showed much less partial aggregation in water while negatively charged silica-poly-L-glutamic acid (silica-PLGA) showed no aggregation in water. Application of all these synthesized polypeptide silica nanoconjugates was explored. Silica-PLL and silica-PLL-*b*-PLLeu conjugates displayed excellent antimicrobial properties against both Gram positive and Gram negative bacteria. A minimum of 250 μg/mL concentration was sufficient to kill all the bacteria. These particles can be therefore used as bactericidal coatings bearing contact bacteria-killing capacity.[1] Their differing solubility also allows us to disperse them in both water and oil-based paints in an effort to make anti-microbial paints.[2] Silica-PLGA particles containing high surface negative charge is very stable and remain well dispersed in water for longer periods. They are also pH responsive and aggregate into large clusters at pH less than 5. This is driven by a change in the overall charge and conformation of the grafted polypeptide chains with change in pH. Preliminary experiments show that aqueous dispersions of these PLGA functionalized silica

nanoparticles can be used to generate well defined, aligned three dimensional macroporous structures using ice templating with directional freezing. Thus, these macroporous materials are comprised of a biocompatible polymer shell covalently attached to rigid inorganic cores. Since the synthetic scheme of the nanoparticles developed by us allows the polymer and inorganic components to be individually tailored, scaffolds having a wide range of physical properties can be synthesized. Finally, highly water dispersible silica-PLArg nanoconjugate having very high surface positive charge has been successfully synthesized. The low cytotoxicity and the very high cell-penetrating ability of silica-PLArg's are likely to make them efficient delivery vehicles for nucleic acid. Since silica-PLArgs have very high positive surface charge they bind very efficiently with the nucleic acids. The inherent cell penetrating property of surface poly-L-arginine renders the silica-PLArg nanoconjugates very efficient for entering mammalian cells. From FACS analysis, 90% cellular uptake efficiency was observed. However, these nanoparticles were not efficient as a carrier for the transfection of protein of interest. The primary reason for this could be that the high positive surface charge of this nanoconjugate binds very strongly to the pDNA and the pDNA is unable to effectively leach out of the polyplex to transfect the protein of interest. However, the transfection can be affected in presence of 100 μM chloroquine. Chloroquine is known to compete with nucleic acids to bind with positively charged carriers and this helps the nucleic acid to leach from the polyplex and transfect the protein of interest.

Chapter 4 describes the synthesis of poly-L-lysine grafted SBA-15 with reasonable grafting density by using CuAAC via the "grafting to" methodology. Alkyne terminated poly-L-lysine containing both 20 and 10 repeating units was successfully grafted onto azide grafted SBA-15 material. The high hydrodynamic volume of the 20 mer poly-L-lysine prevents it to enter inside the 10 nm pores of the azide grafted SBA-15 materials. Hence only the surface of the SBA-15 material gets grafted leading to a very low grafting density of 0.1 mmol/gm. When low molecular weight poly-L-lysine (10 mer) was used a significantly higher grafting of 0.23 mmol/gm was observed. Further, the materials retain their porosity after conjugation with PLL and this is in contrast to the lack of porosity observed in the SBA-PLL-conjugate material synthesized by the "grafting from" method. This methodology can be implemented for the successful attachment of high molecular weight homo polypeptides, block polypeptides and co-polypeptides to the SBA-15 with controlled molecular weights and high grafting density. The above methodology was modified to graft poly-L-arginine specifically onto the surface of the mesoporous silica thus keeping the pores empty. Synthesis

of well defined poly-L-arginine grafted silica mesoporous nanoparticles (MSN-PLArg) with high grafting density has been successfully achieved by using same established "grafting to" methodology using click chemistry. MSN-PLArg nanoconjugates posses' low cytotoxicity and the viability of cancer cells like HeLa and A549 cells was found to be around 85% at 100 μg/mL concentration. The presence of poly-L-arginine on the MSN surface enhances the cellular uptake efficiency to greater than 90 %. The low cytotoxicity together with the very high ability to penetrate cancer cells like HeLa and A549 make MSN-PLArg excellent delivery vehicles for nucleic acid. The poly-L-arginine grafted MSNs were used effectively to deliver mCherry DNA plasmid into cells leading to expression of the protein mCherry inside the cells. The observed transfection efficiencies with MSN-PLArg were 48% and 60% for HeLa and A549 cells respectively. The huge unused inner surface area of the MSN can be used to load and deliver therapeutic drugs like doxorubicin, cis-platin and actinomycin inside cancer cells very effectively. The biocompatibility of poly-L-arginine and its cell penetrating ability will make these MSN conjugates more exciting over synthetic cationic polymer like PEI whose long term toxicity is unknown. We also believe that our methodology can also be used to deliver high amounts of SiRNA into cancer cells which can be very important for gene therapy.

5.2 Scope of future work

The work described in the dissertation opens up several new opportunities. Some of them are listed below.

1) Tissue engineering scaffold

In the dissertation, silica-PLGA was used to make scaffold by using ice templating methods. The silica core of these nanoconjugates can provide the mechanical strength while the soft biocompatible PLGA on the surface can be utilized to interact with cells leading to their binding and proliferation. The poly-L-glutamic acid on the silica surface can also be functionalized with integrin binding motifs like RGD or growth factors by simple acid amine coupling chemistry.[3] By using the ice templating methodology, the pore size of the scaffold can be varied from 10s to 100s of microns. Synthesis of scaffolds with porosity higher than 100 μm can make them suitable for use in tissue engineering. For application of these materials in tissue engineering, the cytotoxicity, cell proliferation rates and degradability of these scaffolds have to be studied in details.

For tissue engineering application, development of bioactive hydrogels as synthetic scaffolds that mimic the extracellular matrix of cells is extremely critical.[4] It is well known that the phenotype of the cells depends on the mechanical properties of the synthetic scaffold.[5] Most of the polymer based scaffold does not satisfy the mechanical properties required for them to function as scaffolds for bone and cartilage regeneration. However, by physically mixing the water dispersion of silica poly-L-glutamic acid or poly-L-arginine nanoconjugates as nanofillers with biocompatible polymeric gels, the mechanical properties of the gel can be varied to a great extent. The huge surface area of nanoparticle will provide a large volume fraction interface interaction between polymer gel and nanoconjugates and this would lead to its high mechanical strength. Further, the surface polypeptides also can play other biological roles. For example, gel embedded poly-arginine surface of silica nanoconjugates can provide better surface interaction with the harvested cells since it mimics the ECM. Poly-L-glutamic acid based scaffolds have been recently used for tissue engineering.[6, 7]

In last decades, several methodologies have been developed to prepare porous scaffold from inorganic and polymer materials.[8] The pore size and the mechanical properties of the scaffold can be easily varied according to the requirements of the particular tissue engineering application. But most of these porous scaffolds are not biologically compatible since the lack of surface functionality and poor surface properties inhibits the proper binding and proliferation of cells on their surfaces. The grafting of various synthetic biologically active polypeptides onto the inorganic and polymeric scaffold by using 'grafting to' methodologies would make these materials much more biocompatible for attachment and proliferation of cells which is the first step in tissue regeneration.

1) SiRNA delivery vehicle

In the chapter 4, the high efficient cellular uptake of the MSN-PLArg (>90%) has been reported. Plasmid DNA was subsequently condensed onto the surface of the positively charged surface of the MSN-PLArgs and this polyplex was used to efficiently transfect a protein of interest in mammalian cells Recently, the delivery of SiRNA become as a gene therapeutic medicine has received a lot of atention.[9, 10] Using our methodology, SiRNA's can be loaded inside the MSN[11] and the outer surface can be grafted by poly-L-arginine with a acid/enzyme cleavable linker. The bulky poly-L-arginine grafted on the surface of the mesoporous nanoparticle will both prevent leaching of SiRNA from its pores and also

efficiently delivers the MSN inside the cells. Once these SiRNA loaded poly-L-arginine grafted MSN's enter the cell, the linker attaching the MSN to poly-L-arginine would get cleaved in the presence of acid or enzymes. This would then selectively deliver SiRNA into the cells efficiently.

5.3 References

1. Li, Z.; Lee, D.; Sheng, X.; Cohen, R. E.; Rubner, M. F., Two-Level Antibacterial Coating with Both Release-Killing and Contact-Killing Capabilities. *Langmuir* **2006,** 22, (24), 9820-9823.
2. Yamashita, R.; Kikuchi, H.; Shirai, K.; Yamauchi, T.; Tsubokawa, N., Preparation of Antibacterial Polymer-grafted Nano-sized Silica and Surface Properties of Silicone Rubber Filled with the Silica. *Polymer Journal* **2006,** 38, (8), 844-851.
3. Gentilini, C.; Dong, Y.; May, J. R.; Goldoni, S.; Clarke, D. E.; Lee, B.-H.; Pashuck, E. T.; Stevens, M. M., Functionalized Poly(γ-Glutamic Acid) Fibrous Scaffolds for Tissue Engineering. *Advanced Healthcare Materials* **2012,** 1, (3), 308-315.
4. O'Brien, F. J., Biomaterials & scaffolds for tissue engineering. *Materials Today* **2011,** 14, (3), 88-95.
5. Place, E. S.; Evans, N. D.; Stevens, M. M., Complexity in biomaterials for tissue engineering. *Nat Mater* **2009,** 8, (6), 457-470.
6. Poologasundarampillai, G.; Yu, B.; Tsigkou, O.; Valliant, E.; Yue, S.; Lee, P. D.; Hamilton, R. W.; Stevens, M. M.; Kasuga, T.; Jones, J. R., Bioactive silica-poly([gamma]-glutamic acid) hybrids for bone regeneration: effect of covalent coupling on dissolution and mechanical properties and fabrication of porous scaffolds. *Soft Matter* **2012,** 8, (17), 4822-4832.
7. Poologasundarampillai, G.; Ionescu, C.; Tsigkou, O.; Murugesan, M.; Hill, R. G.; Stevens, M. M.; Hanna, J. V.; Smith, M. E.; Jones, J. R., Synthesis of bioactive class II poly([gamma]-glutamic acid)/silica hybrids for bone regeneration. *Journal of Materials Chemistry* **2010,** 20, (40), 8952-8961.
8. Rezwan, K.; Chen, Q. Z.; Blaker, J. J.; Boccaccini, A. R., Biodegradable and bioactive porous polymer/inorganic composite scaffolds for bone tissue engineering. *Biomaterials* **2006,** 27, (18), 3413-3431.
9. Ryther, R. C. C.; Flynt, A. S.; Phillips, J. A.; Patton, J. G., siRNA therapeutics: Big potential from small RNAs. *Gene Therapy* **2005,** 12, (1), 5-11.
10. Wang, J.; Lu, Z.; Wientjes, M. G.; Au, J. S., Delivery of siRNA Therapeutics: Barriers and Carriers. *The AAPS Journal* **2010,** 12, (4), 492-503.
11. Hartono, S. B.; Gu, W.; Kleitz, F.; Liu, J.; He, L.; Middelberg, A. P. J.; Yu, C.; Lu, G. Q.; Qiao, S. Z., Poly-l-lysine Functionalized Large Pore Cubic Mesostructured Silica Nanoparticles as Biocompatible Carriers for Gene Delivery. *ACS Nano* **2012,** 6, (3), 2104-2117.

Appendix I

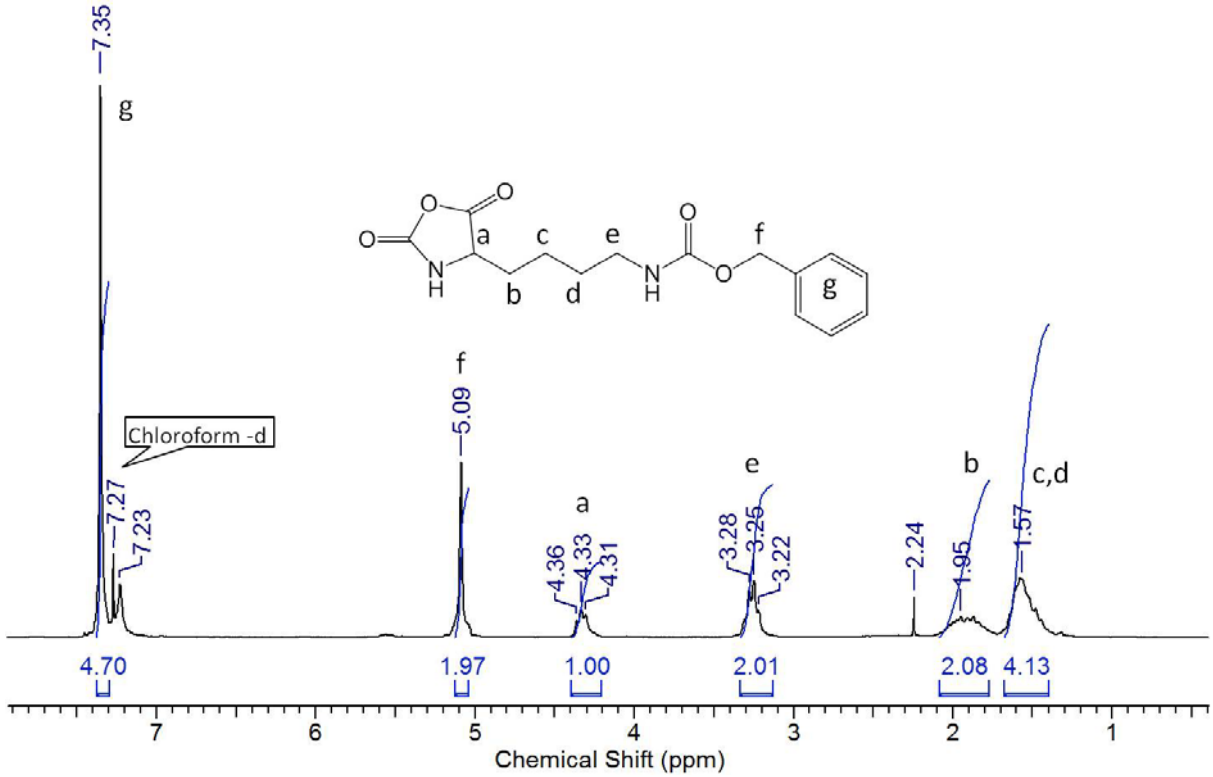

Figure 1: ^{1}H NMR of ε-carbobenzoxy-α-carboxyl-L-lysine anhydride

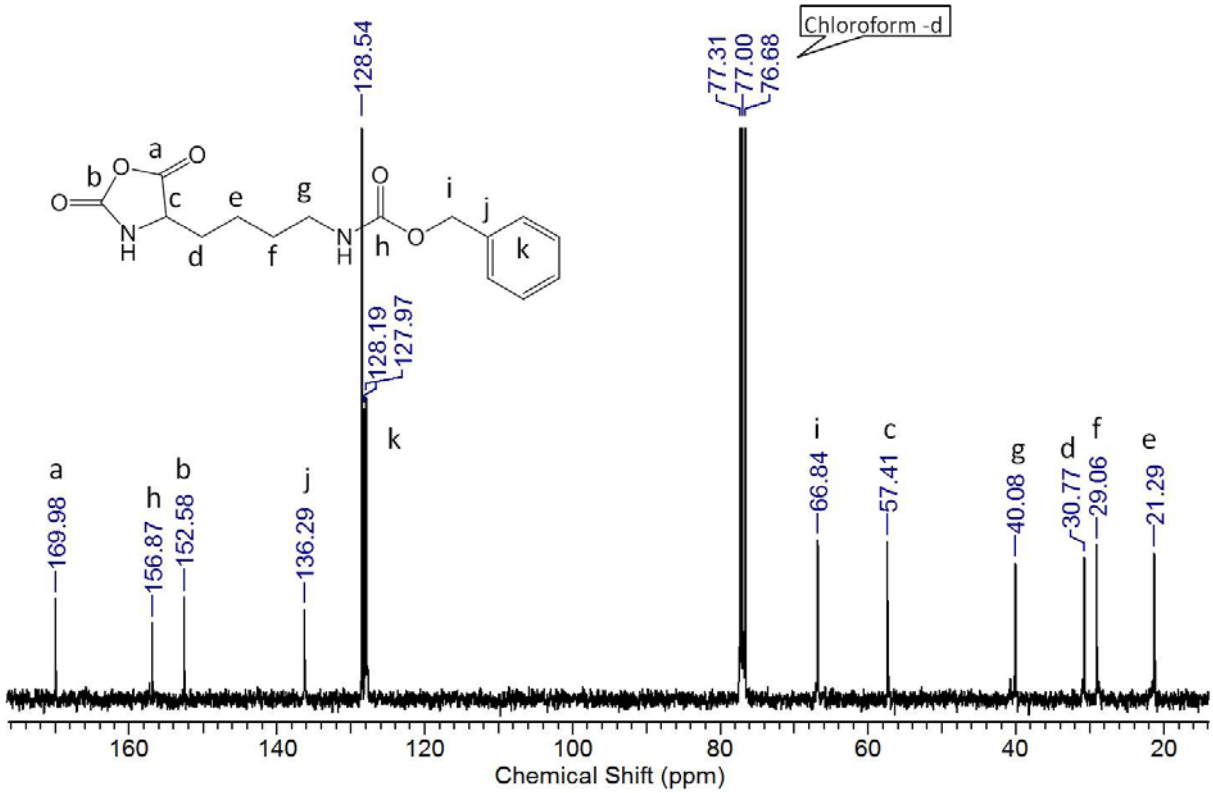

Figure 2: ^{13}C NMR of ε-carbobenzoxy-α-carboxyl-L-lysine anhydride

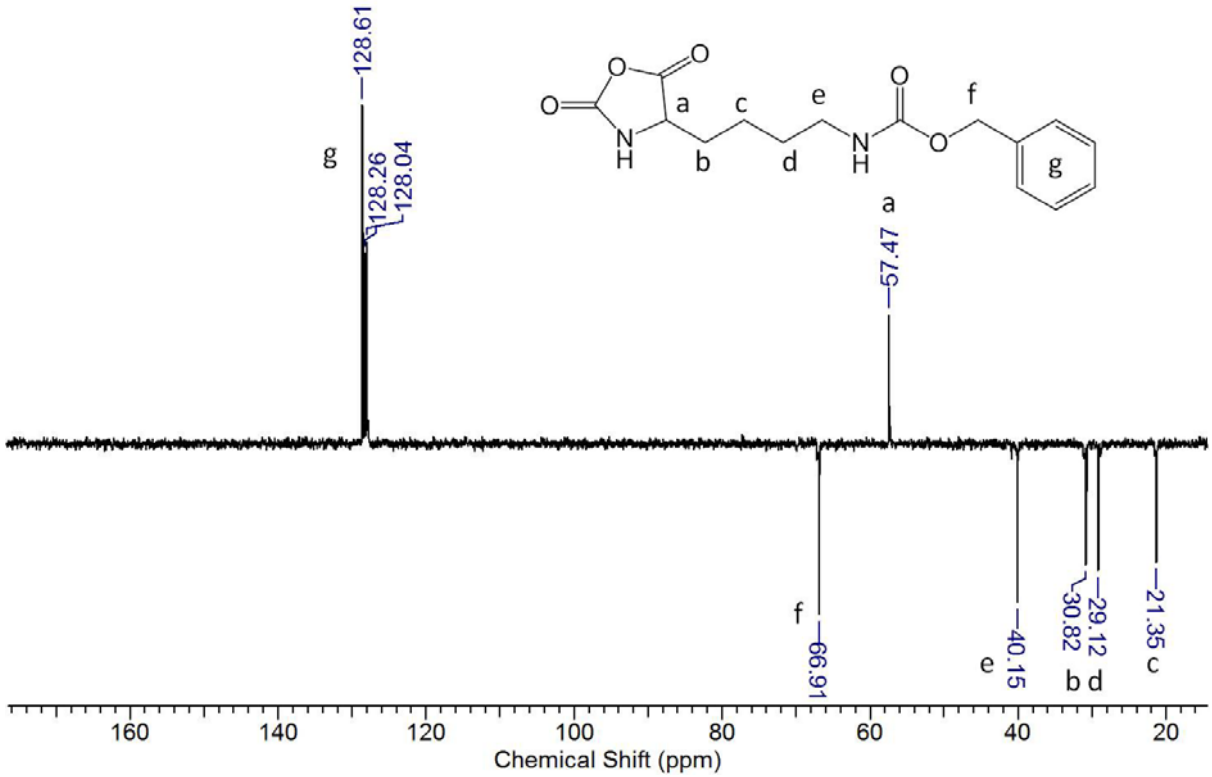

Figure 3: ^{13}C DEPT NMR of ε-carbobenzoxy-α-carboxyl-L-lysine anhydride

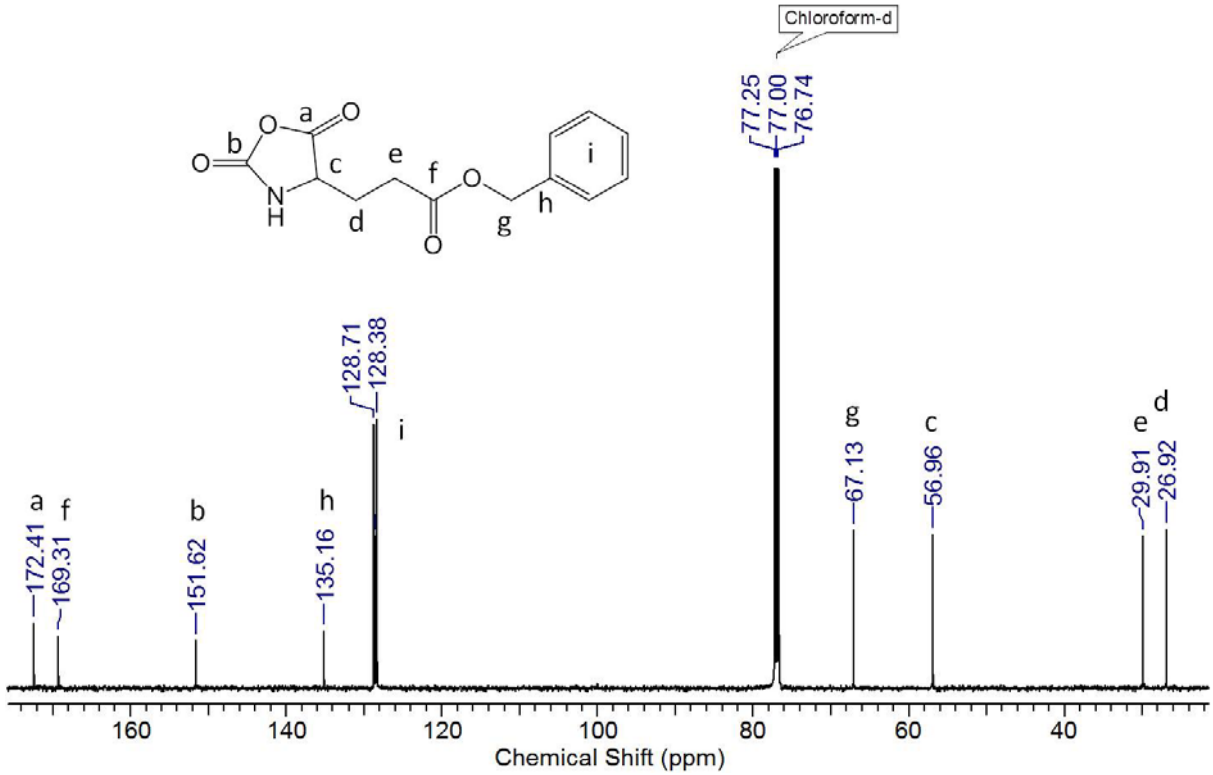

Figure 4: ^{13}C NMR of L-benzylglutamate-α-carboxyl anhydride

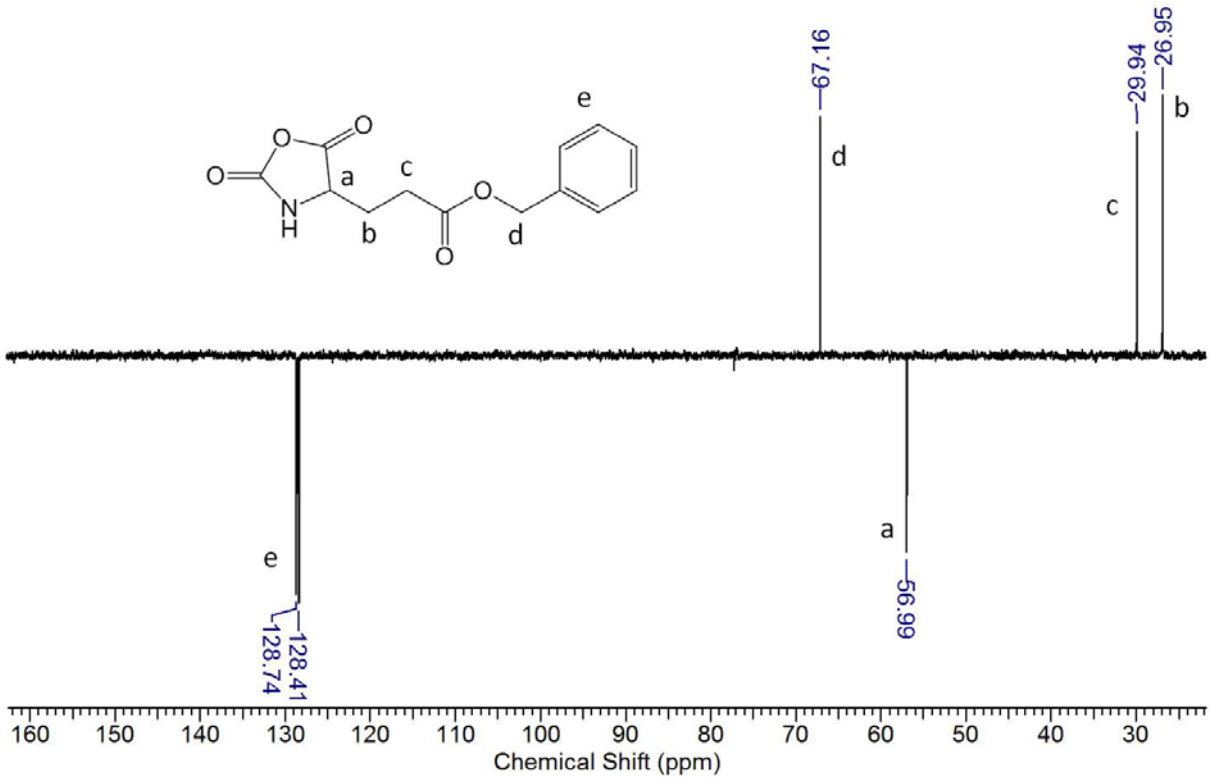

Figure 5: ^{13}C DEPT NMR of L-benzylglutamate-α-carboxyl anhydride

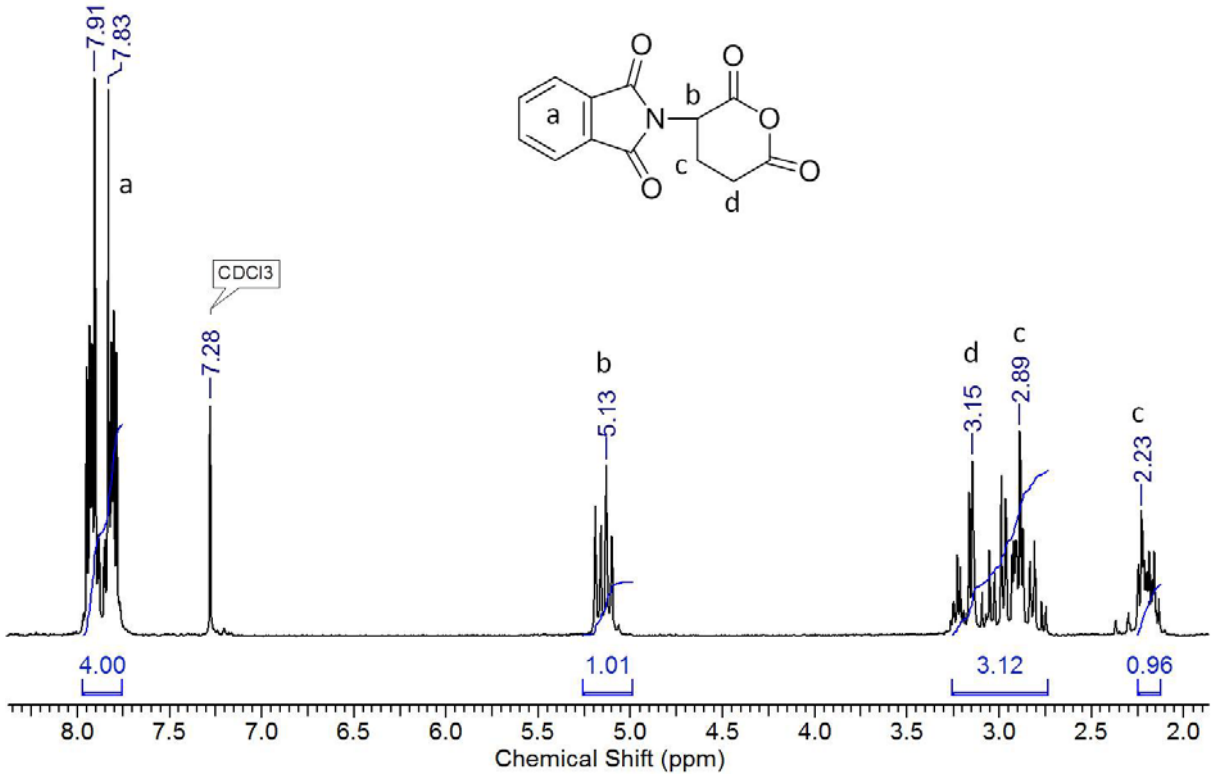

Figure 6: ^{1}H NMR of phtlalozl-L-glutamic anhydride

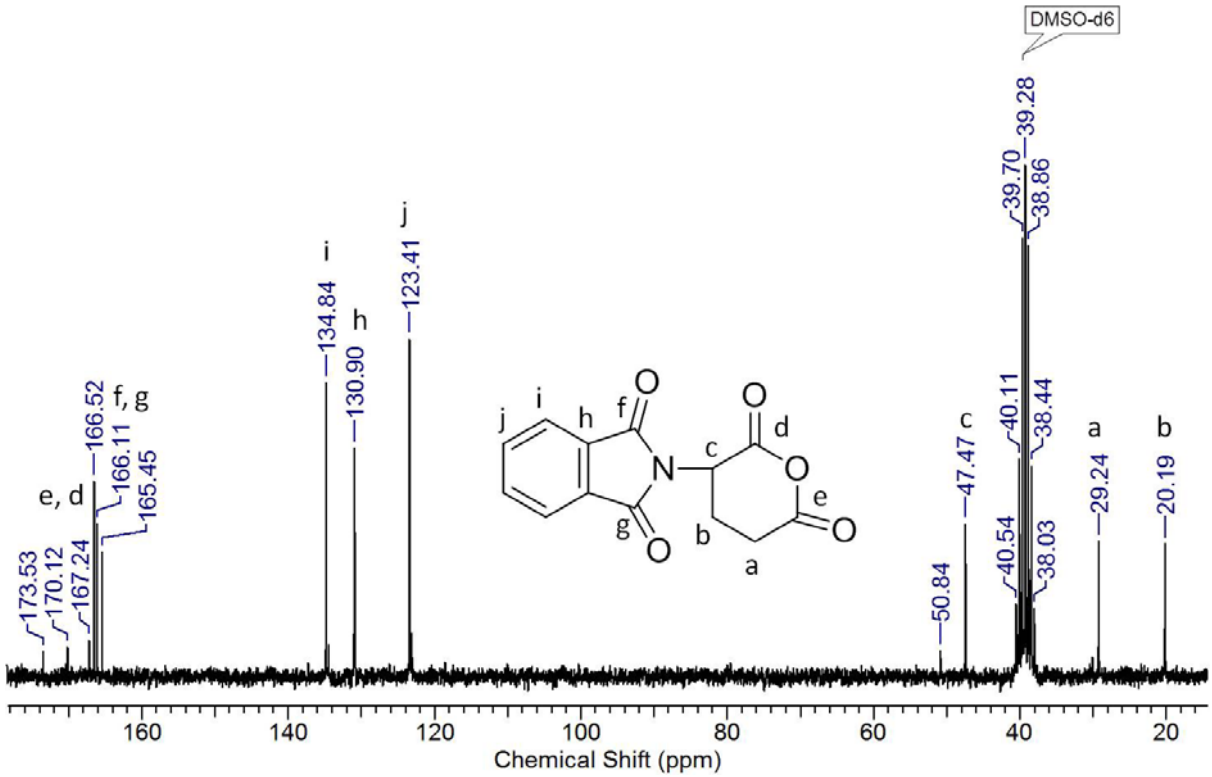

Figure 7: ^{13}C NMR of phtlalozl-L-glutamic anhydride

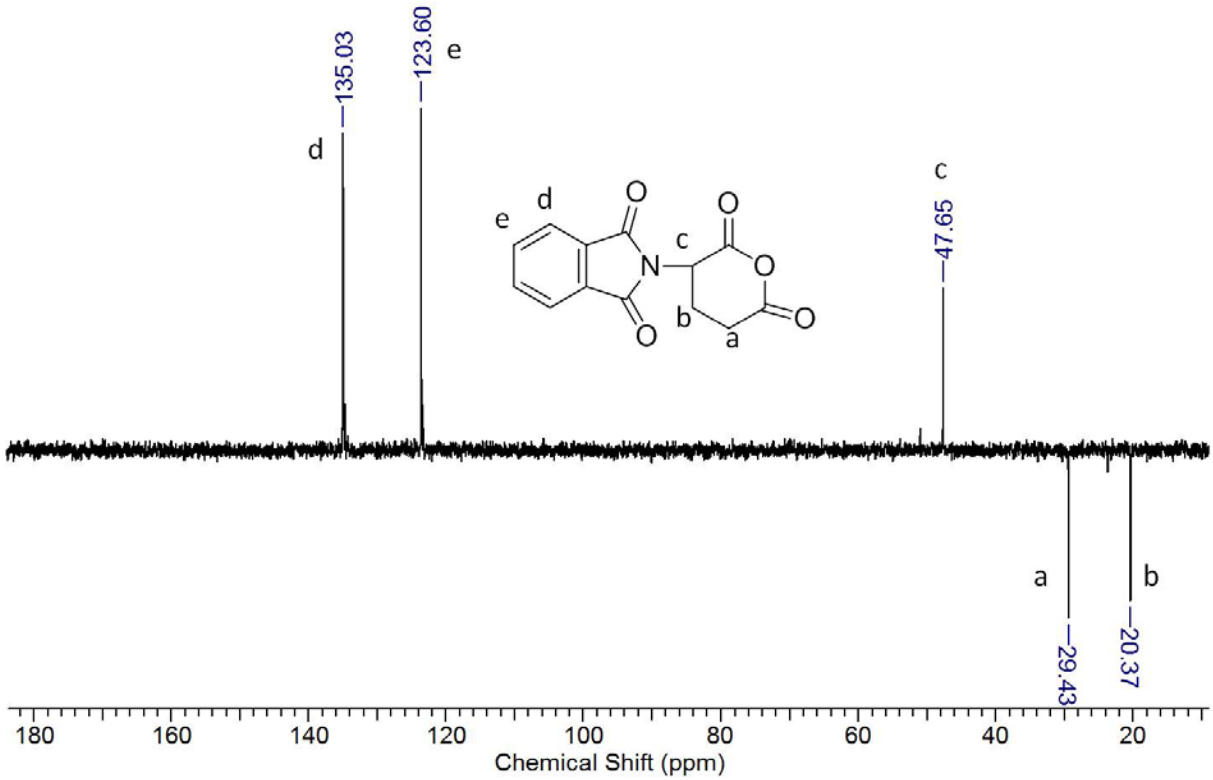

Figure 8: ^{13}C DEPT NMR of phtlalozl-L-glutamic anhydride

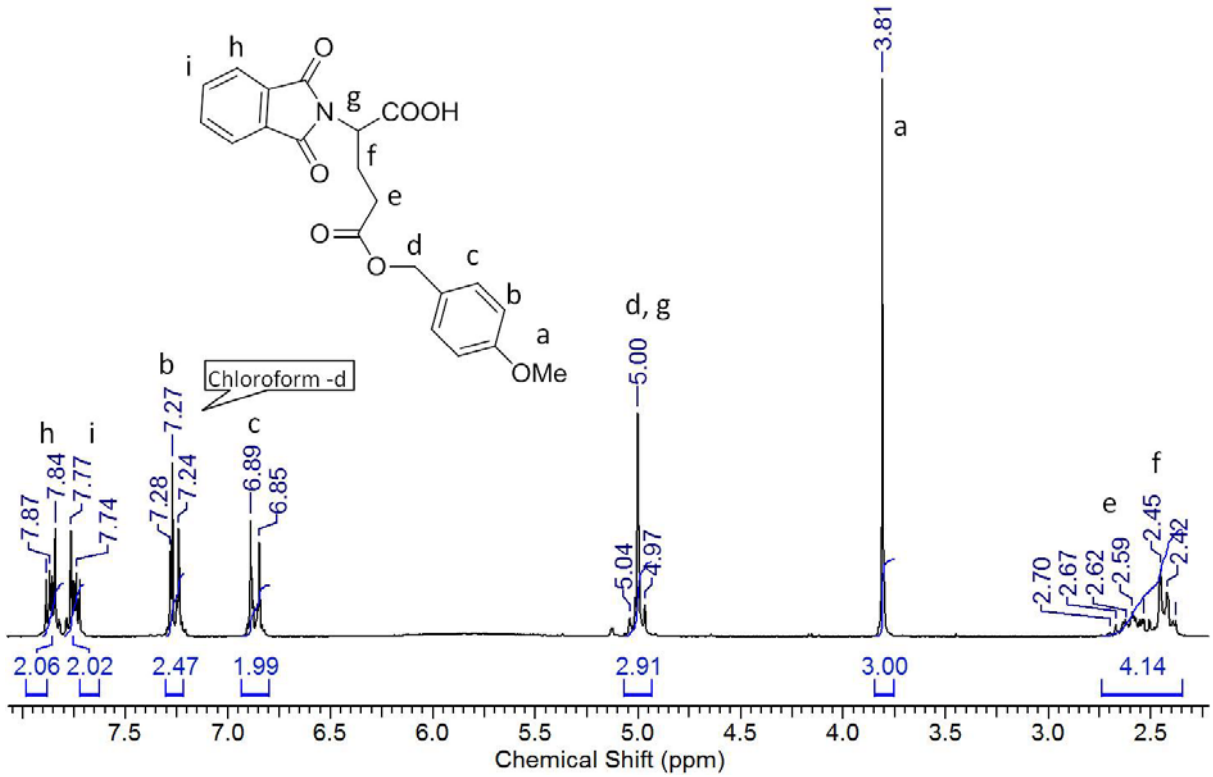

Figure 9: ^{1}H NMR of phtlaoyl-*para* methoxybenzyl-L-glutamate

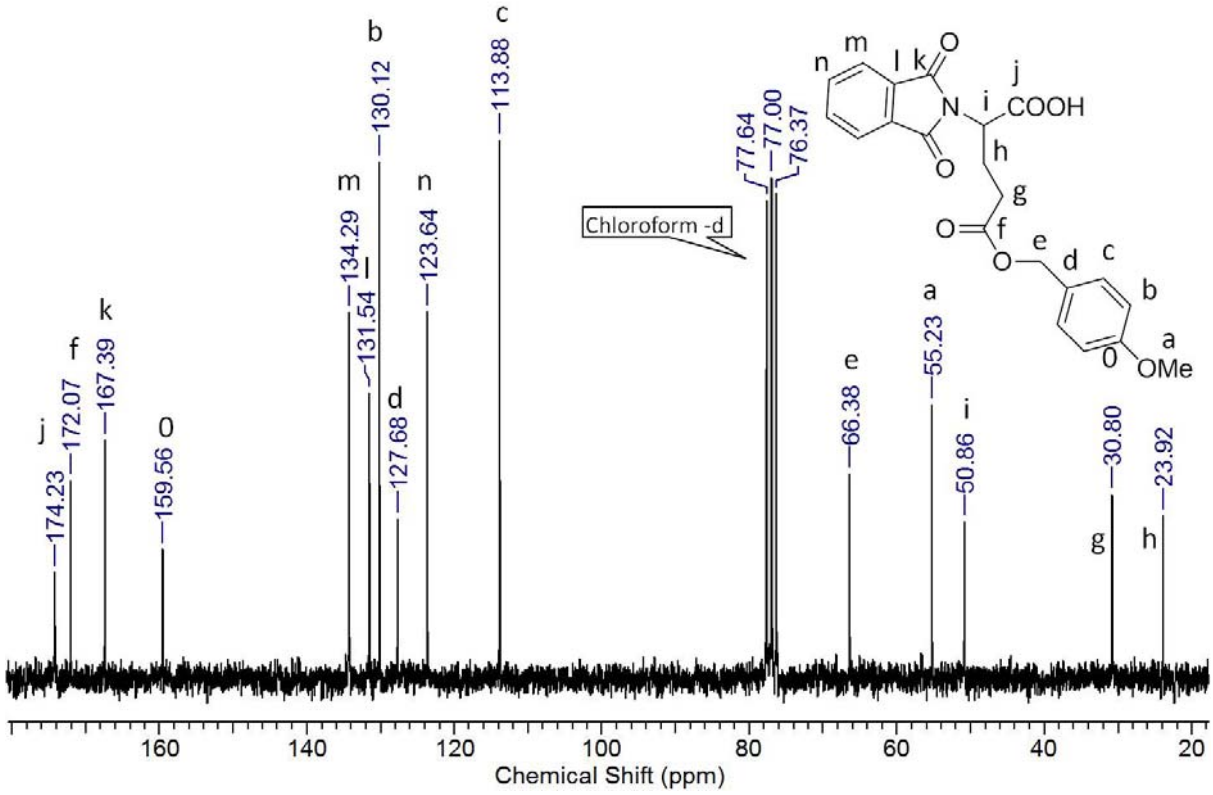

Figure 10: ^{13}C NMR of phtlaoyl-*para* methoxybenzyl-L-glutamate

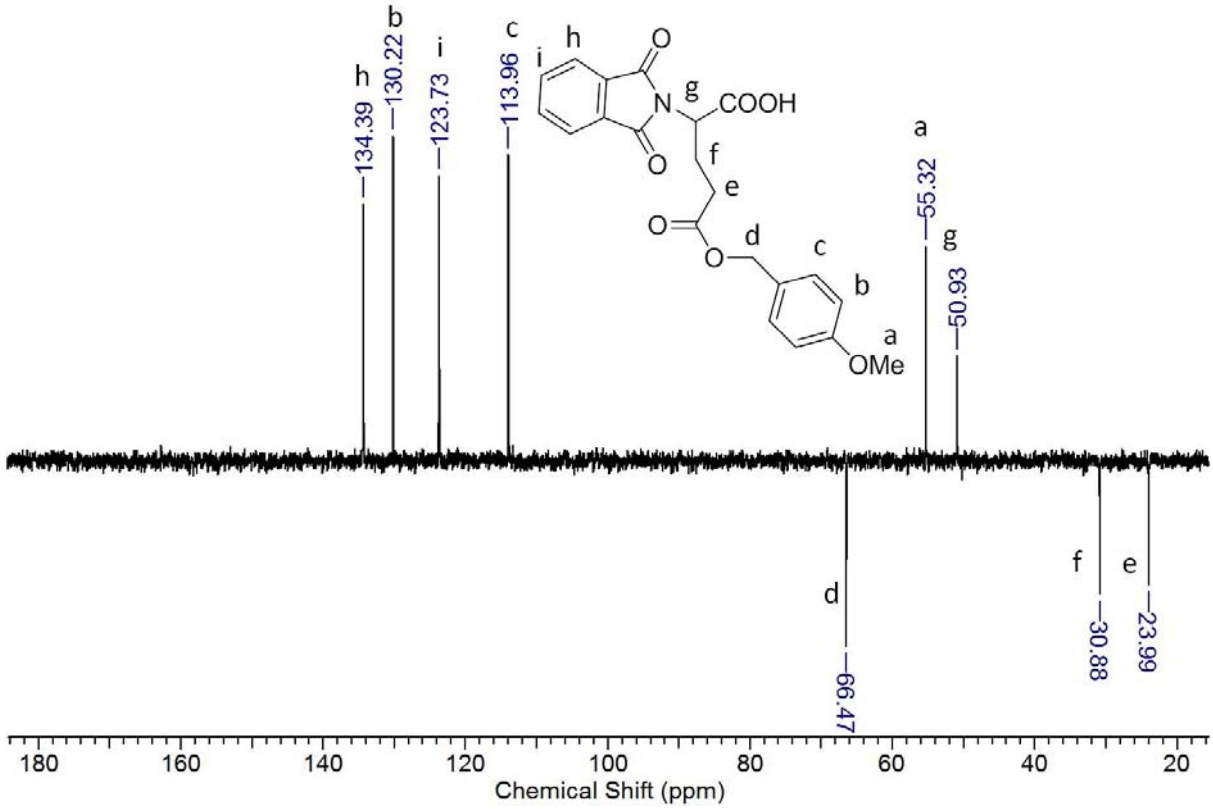

Figure 11: ^{13}C DEPT NMR of phtlaoyl-*para* methoxybenzyl-L-glutamate

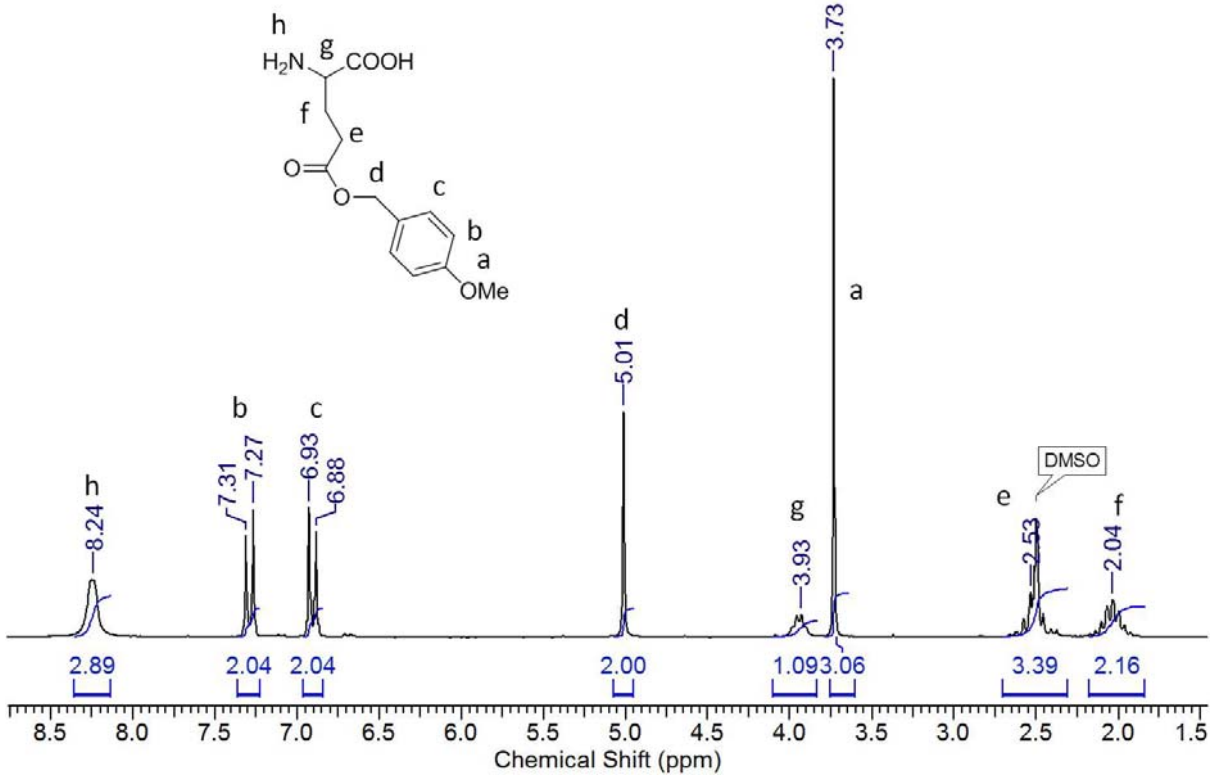

Figure 12: ^{1}H NMR of *para*-methoxybenzyl-L-glutamate

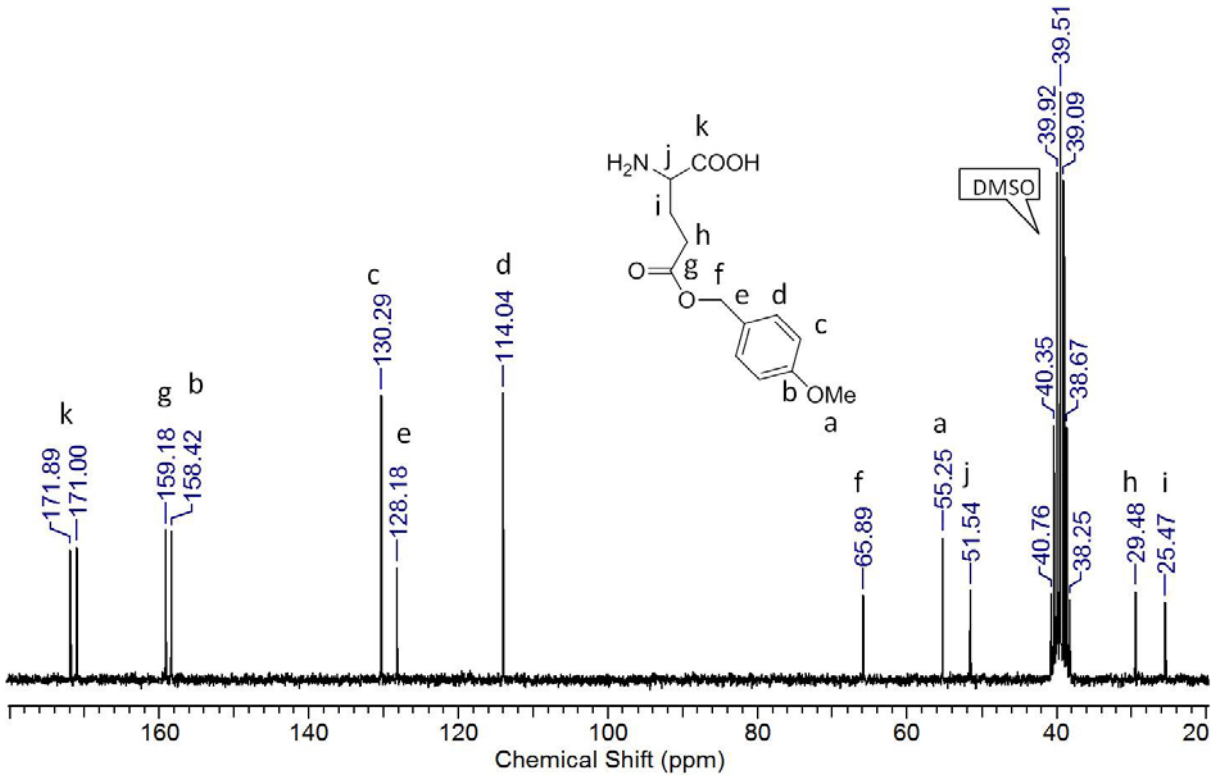

Figure 13: ^{13}C NMR of *para*-methoxybenzyl-L-glutamate

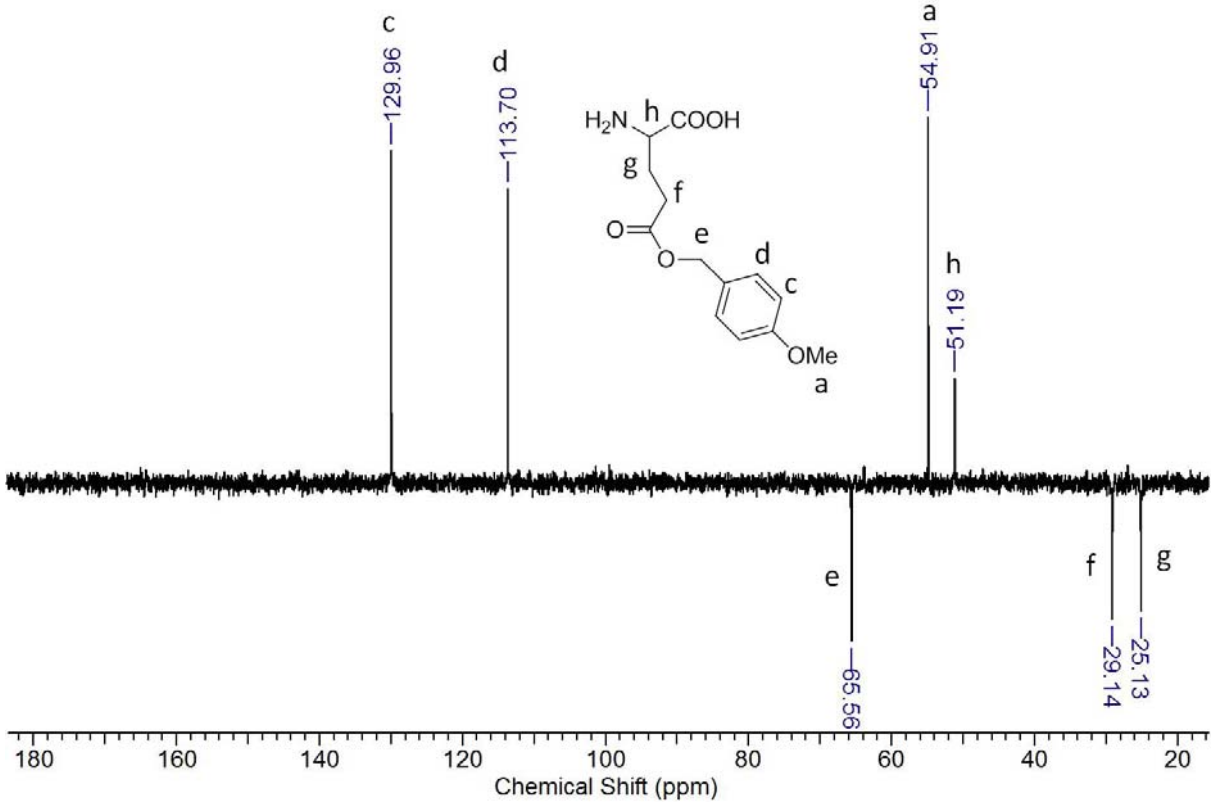

Figure 14: ^{13}C DEPT NMR of *para*-methoxybenzyl-L-glutamate

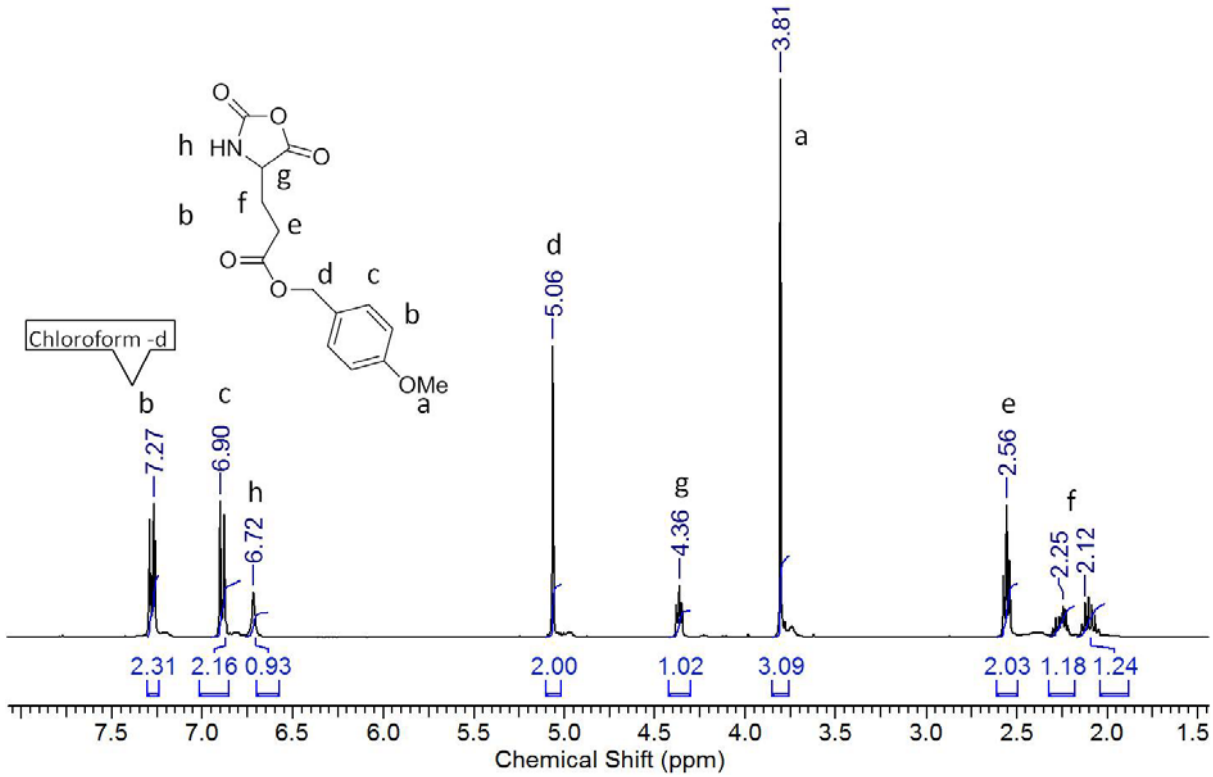

Figure 15: ^{1}H NMR of *p*-methoxybenzyl-L-glutamate NCA

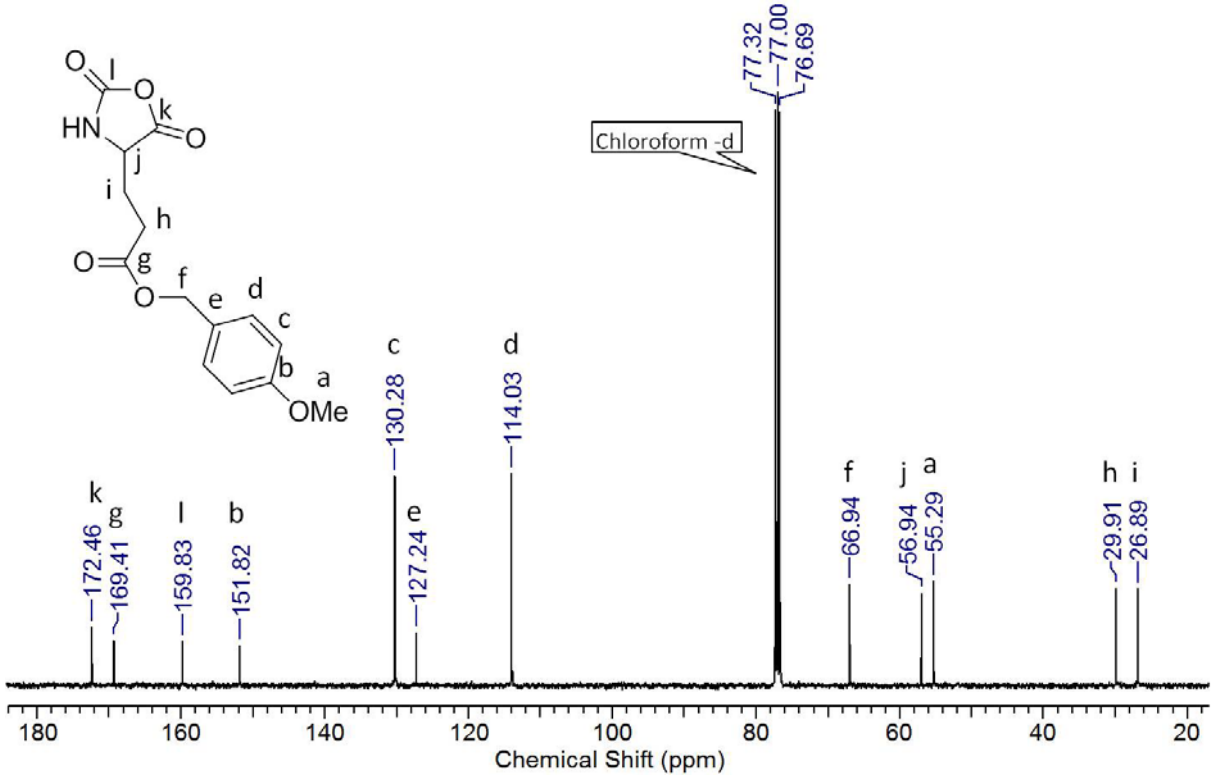

Figure 16: ^{13}C NMR of *p*-methoxybenzyl-L-glutamate NCA

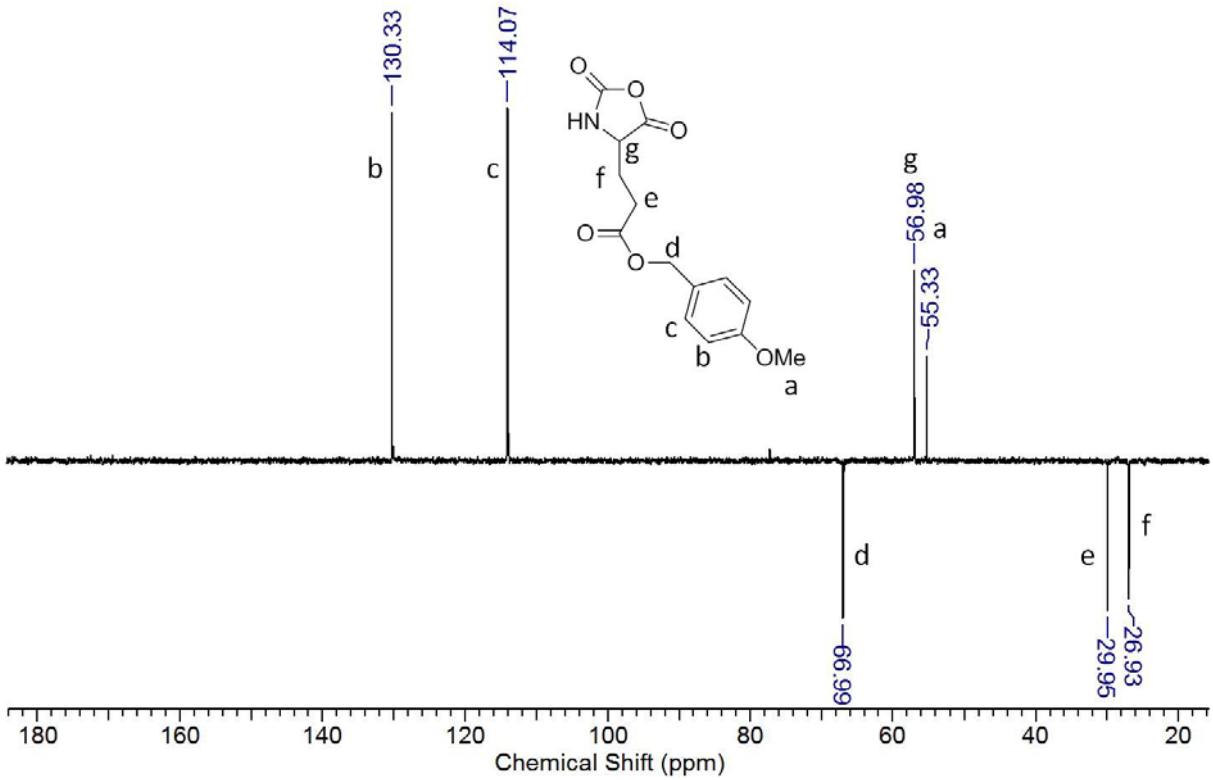

Figure 17: ^{13}C DEPT NMR of *p*-methoxybenzyl-L-glutamate NCA

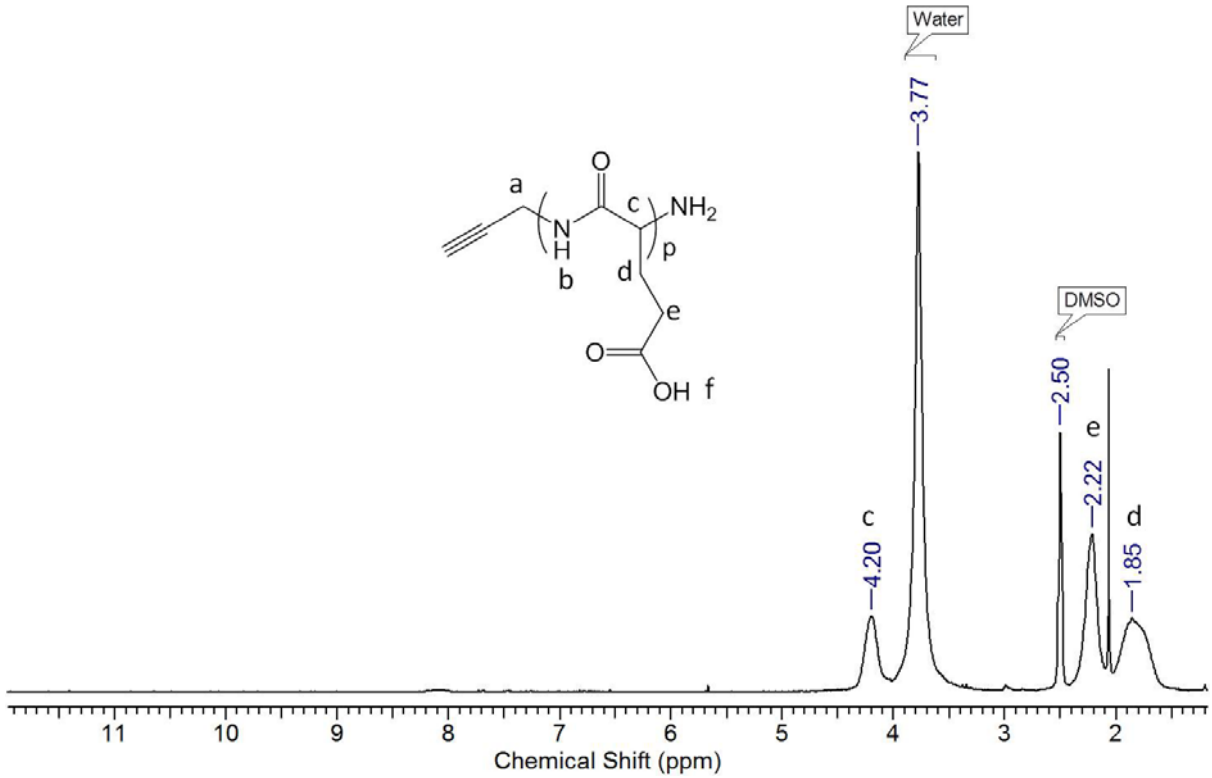

Figure 18: ^{1}H NMR of poly-L-glutamic acid after D_2O exchange

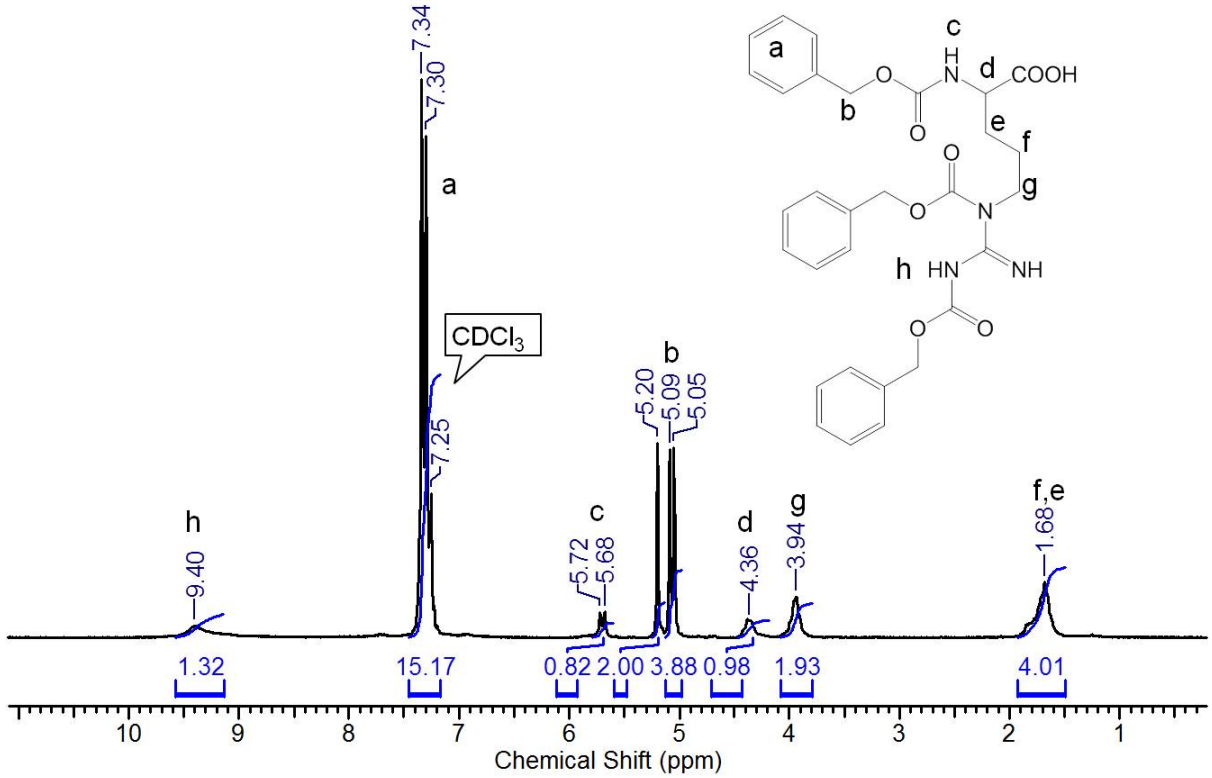

Figure 19: ^{1}H NMR of tricarbobenzoxylated L-arginine

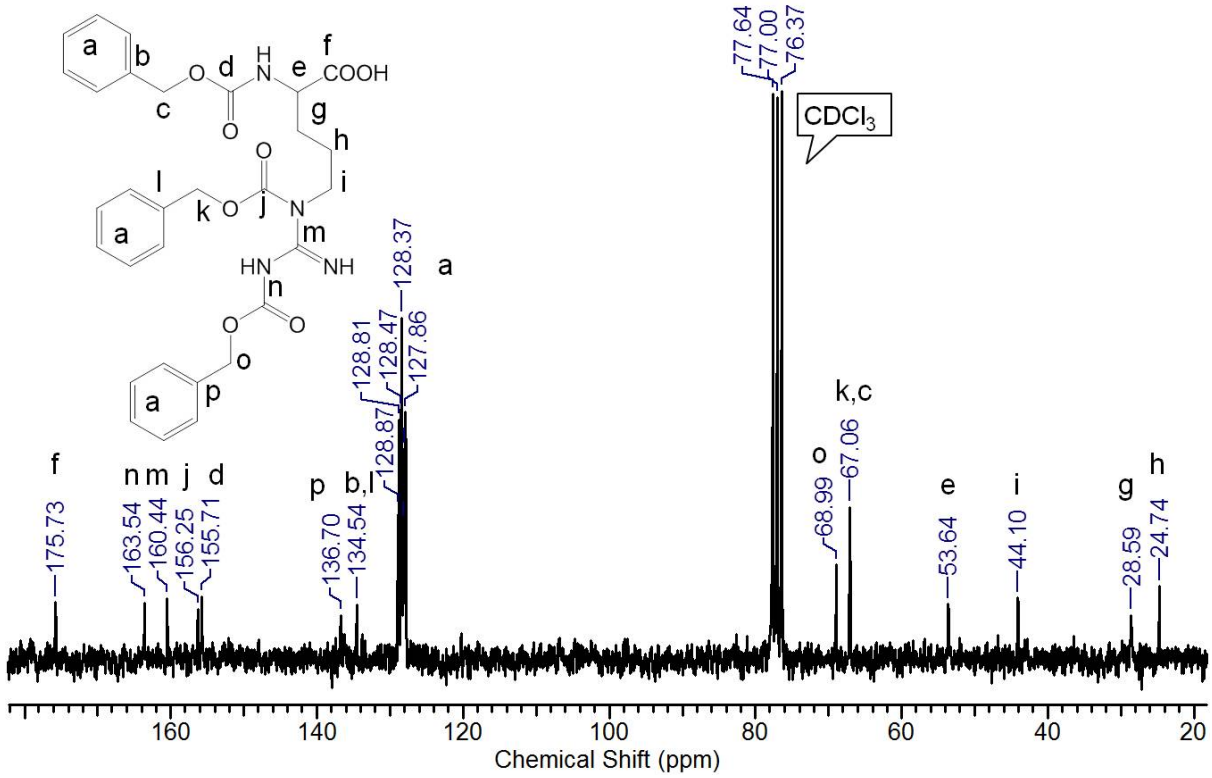

Figure 20: ^{13}C NMR of tricarbobenzoxylated L-arginine

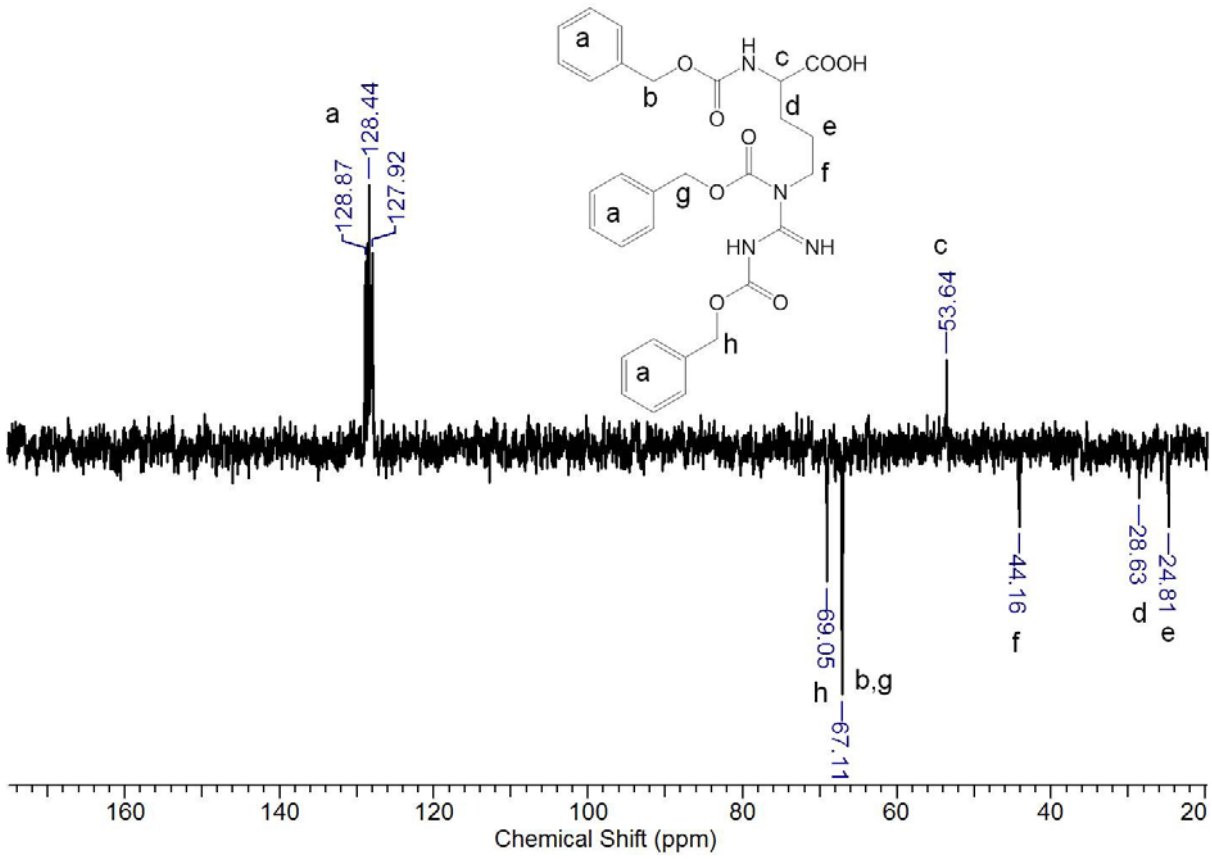

Figure 21: ^{13}C DEPT NMR of tricarbobenzoxylated L-arginine

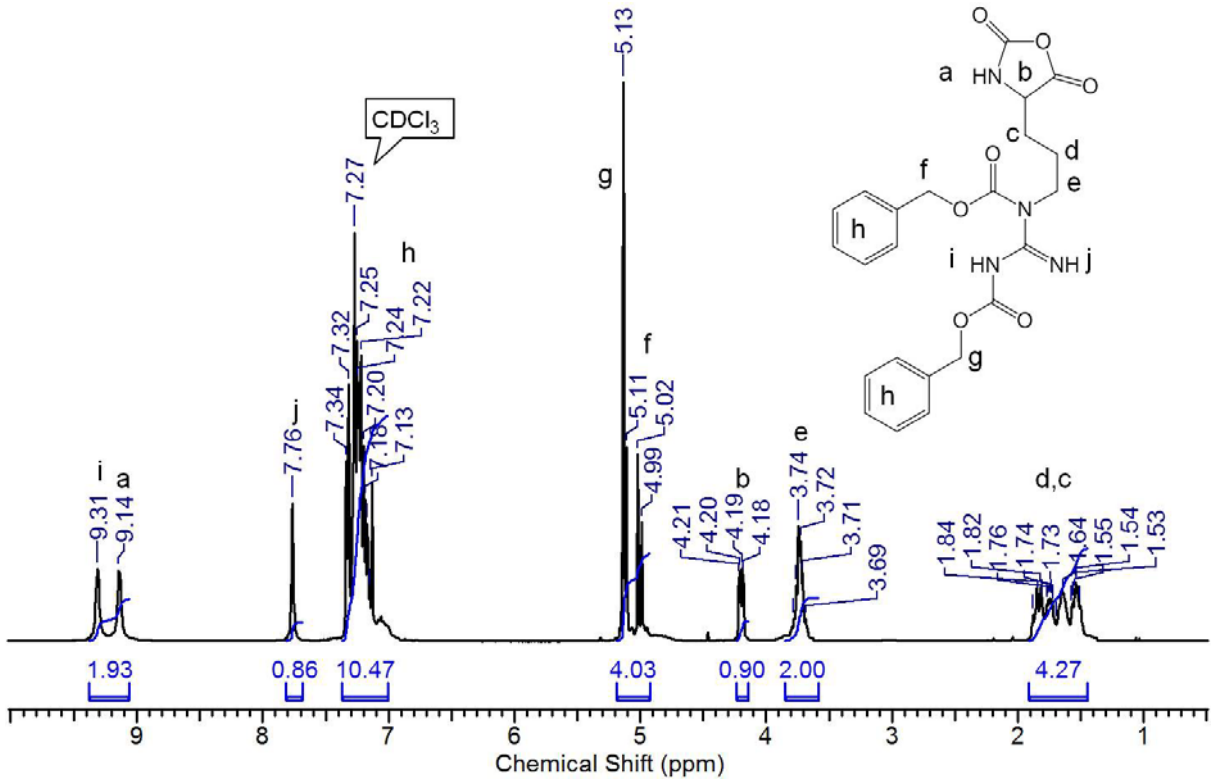

Figure 22: ^{1}H NMR of di-carbobenzoxy-α-carboxyl-L-arginine

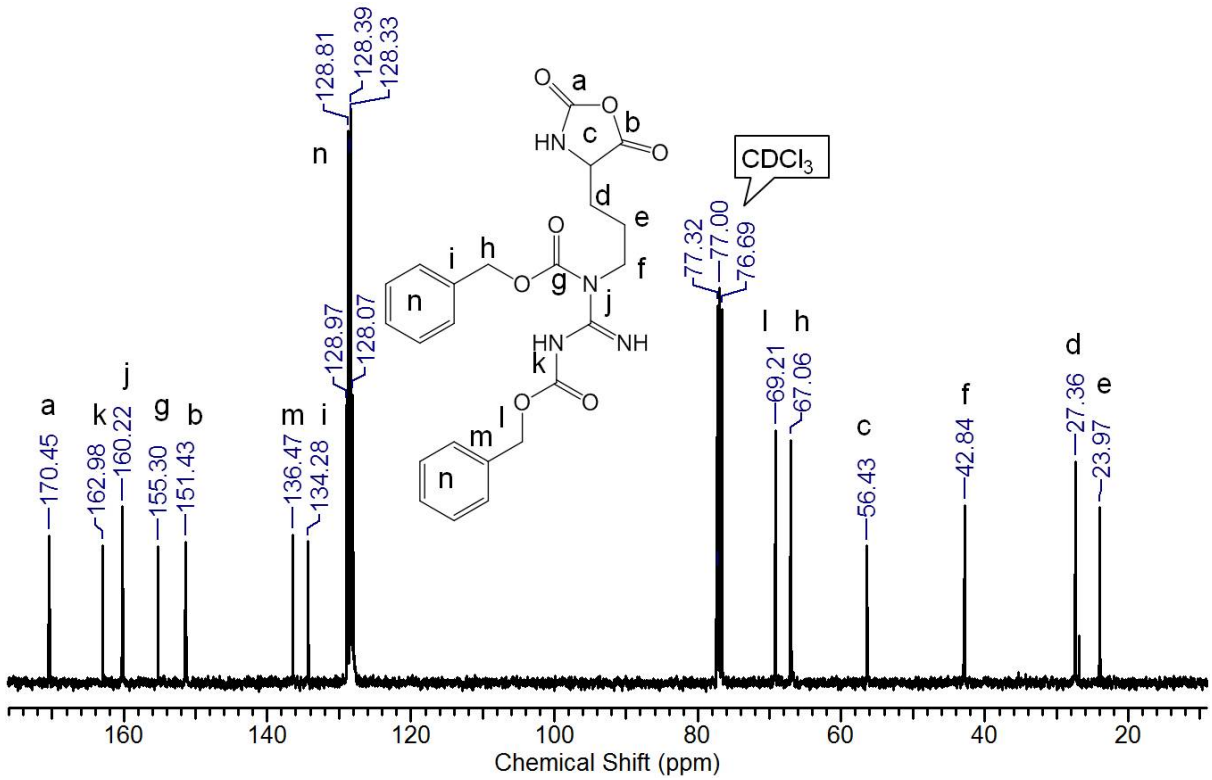

Figure 23: ^{13}C NMR of di-carbobenzoxy-α-carboxyl-L-arginine

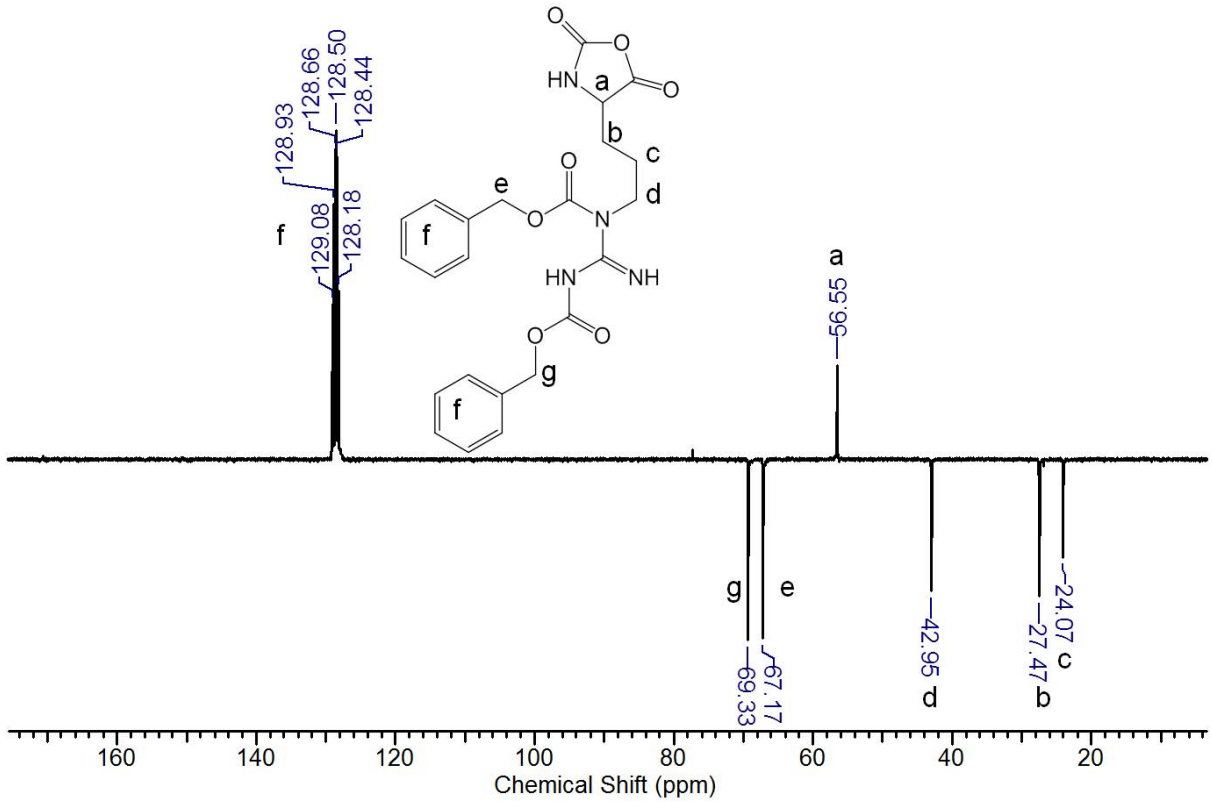

Figure 24: ^{13}C DEPT NMR of di-carbobenzoxy-α-carboxyl-L-arginine

Appendex II

Crude calculation for freezing of the dispersion, when a vial containing it is dipped into liquid nitrogen:

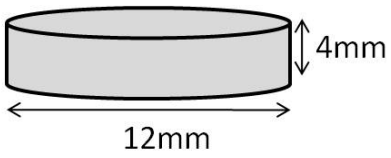

Parameters: Thermal conductivity, k = 0.58 W/mK; density, ρ = 1000 kg.m^{-3}; specific heat, C_p = 4187 J/kgK. $k/\rho C_p = 1.38524 \times 10^{-7}$ m^2.s^{-1}

Assumptions: We assume that the vial wall temperature is 77 K on plunging into liquid nitrogen and that the freezing front propagates from the wall, and calculate the temperature in the dispersion. For a location in the center of the sample, we assume that the heat removal is primarily by conduction and approximate this as a 1D heat transfer problem, with a sample of 4 mm thickness with walls held at 77 K. Under these assumptions, and assuming no phase change, the temperature in a point 2 mm (thickness (T)) from the top/bottom of the sample is given by above cartoon. This crude calculation is used to get a rough estimate of the time for the sample to freeze, (viz. for the temperature to get to 273 K).

$\tau = T^2/(k/\rho C_p)$ s = 28.87 s. Temperature = 77+(300-77)x10$^{(\,-\,\text{time(s)}/\tau)}$ K

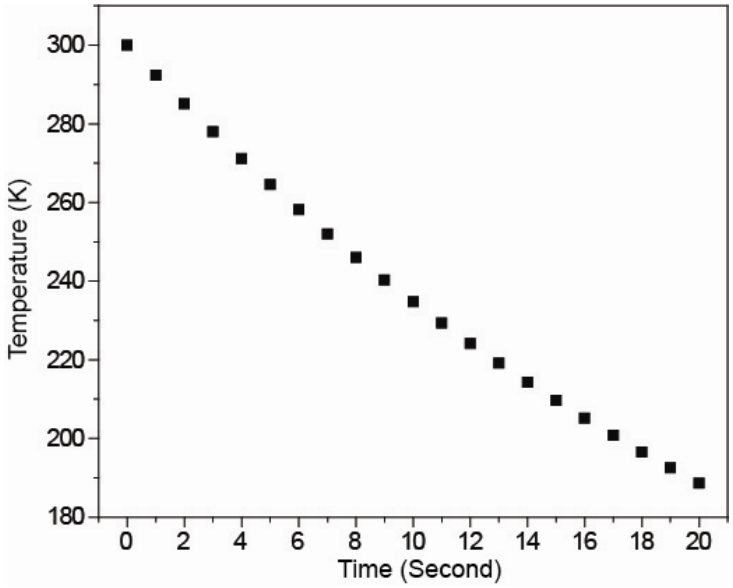

Figure 4.1: Time dependent temperature profile at a point in the center of the sample.

For a location within the sample close to the side walls, the assumption of 1D heat transfer is clearly wrong. It is easy to see that for a point in the sample close to the side walls, but distant from the top/bottom, the conductive heat flux is primarily from the side walls. Thus, it is easy to imagine that the macroporous morphology obtained will be rotated through 90^o, as observed in Figure S5.

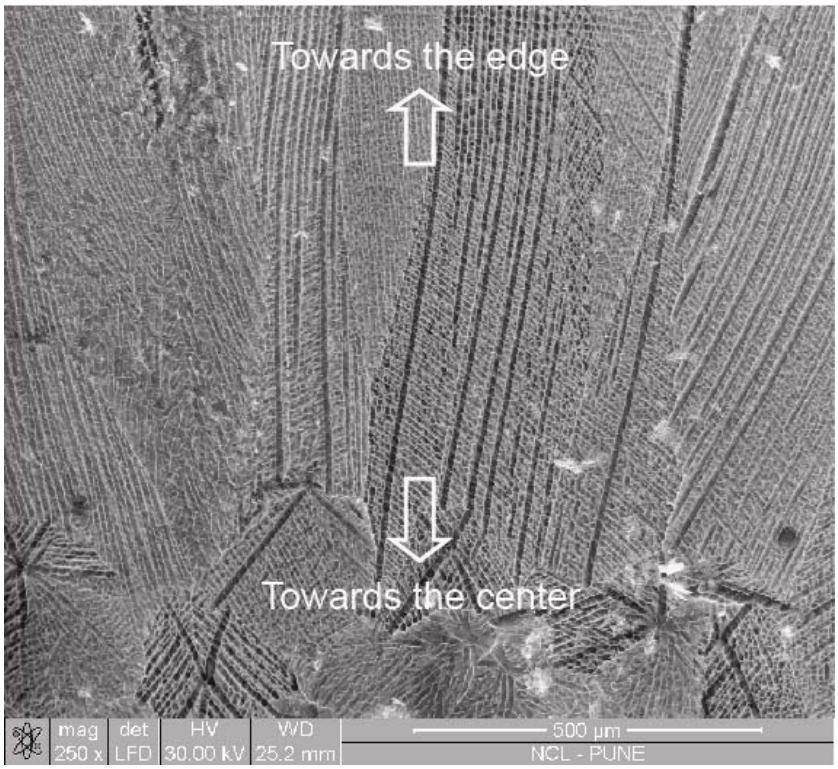

Figure 1: SEM of silica-PLGA scaffold.

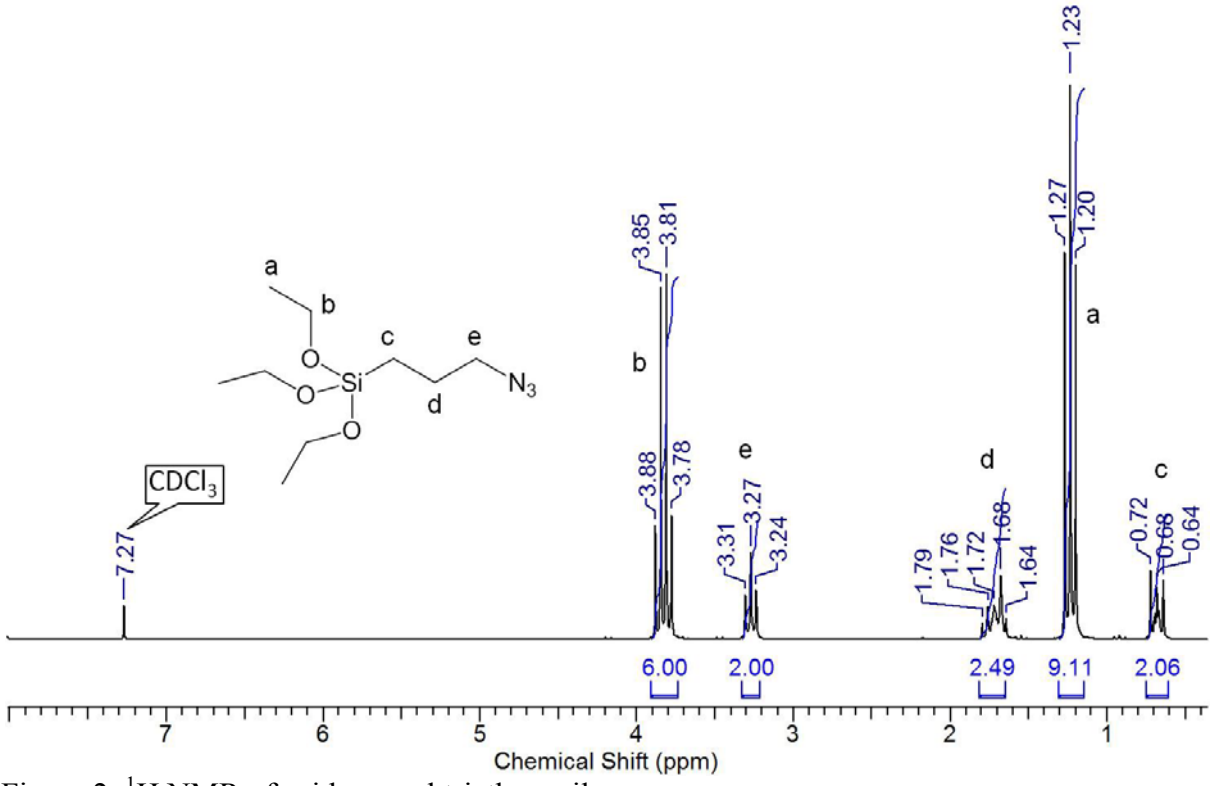

Figure 2: ^{1}H NMR of azidopropyl triethoxysilane

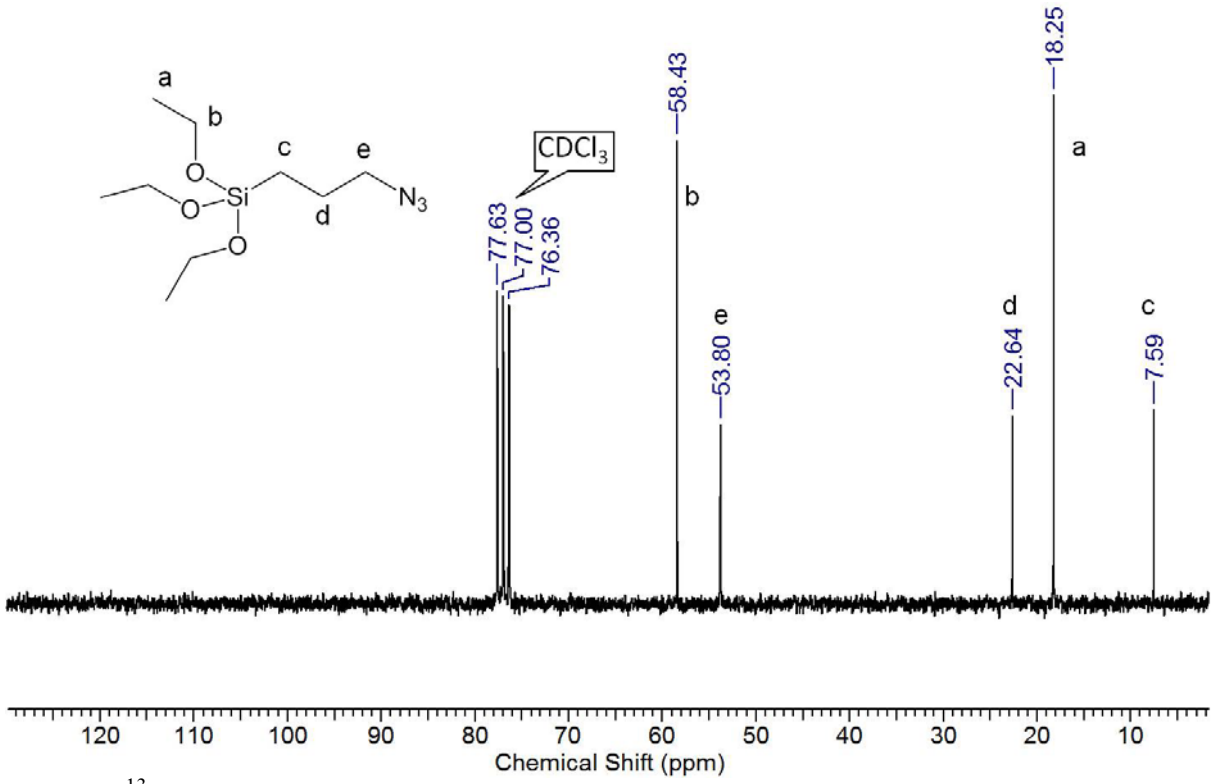

Figure 3: ^{13}C NMR of azidopropyl triethoxysilane

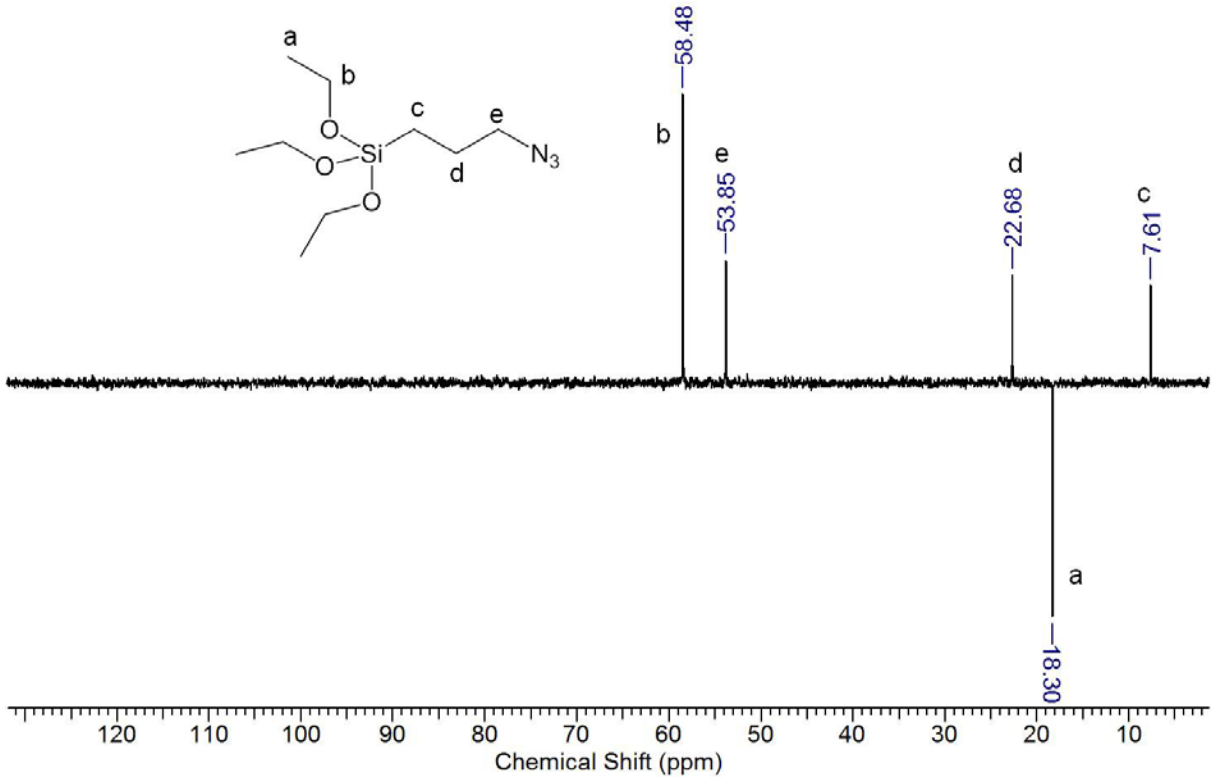

Figure 4: ^{13}C DEPT NMR of azidopropyl triethoxysilane

Appendix III

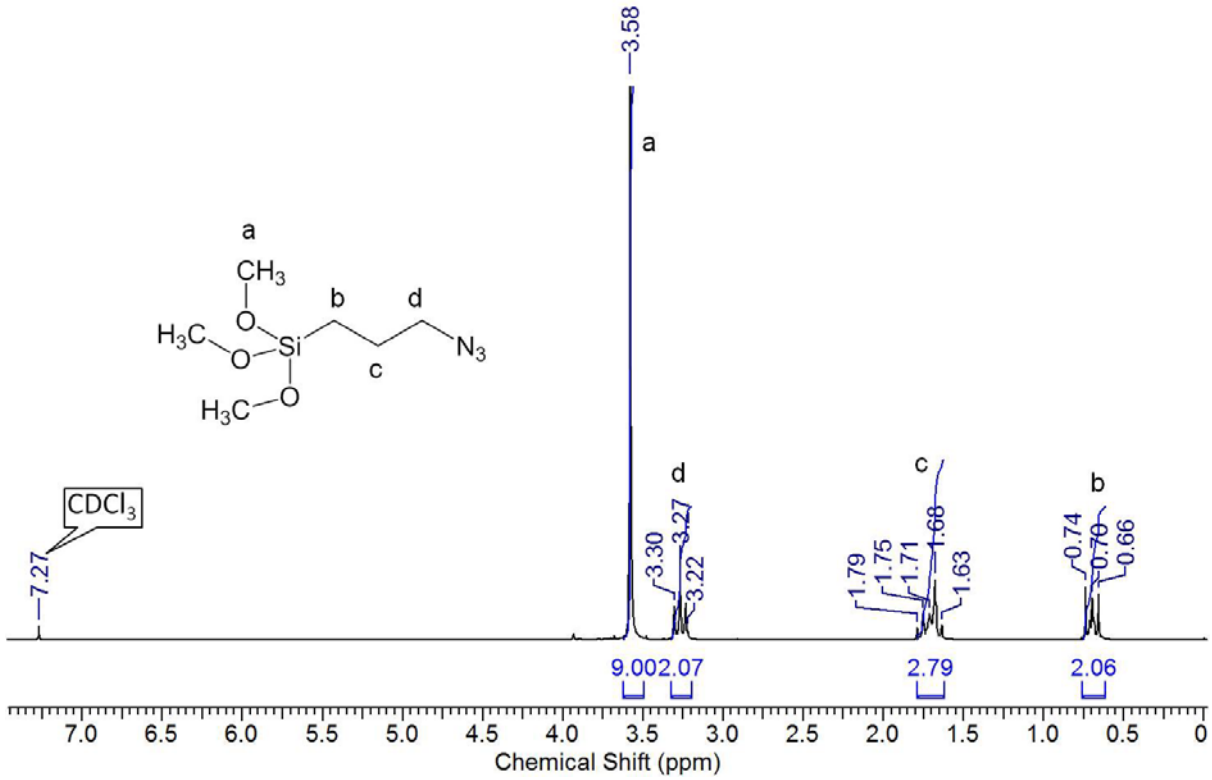

Figure1: 1H NMR of azidopropyl trimethoxy silane

Curriculum Vitae

Mrityunjoy Kar

Objective: Aspire to engage in research activities with the focus on chemistry and chemical biology for sustainable future.

Education

Degree	Subject/Area	University/Institute/Board	Year of passing
M. Sc.	Organic Chemistry	Vidyasagar University, Purba Medinipur, WB, India	2007
B. Sc.	Chemistry	Vidyasagar University, Purba Medinipur, WB, India	2005

Selected Publications

1) Poly-L-Arginine Grafted Silica Mesoporous Nanoparticles for Enhanced Cellular Uptake and their application in DNA Delivery and control drug release
Mrityunjoy Kar, Neha Tiwari, Mitali Tiwari, Mayurika Lahiri and Sayam Sen Gupta.
Particle, 2013 (accepted for publication)

2) Synthesis of Poly-L-glutamic Acid Grafted Silica Nanoparticles and Their Assembly into Macroporous Structures
Mrityunjoy Kar, Minois Pauline, Kamendra Sharma, Guruswamy Kumaraswamy, and Sayam Sen Gupta.
Langmuir, 2011, *27*, 12124

3) Synthesis and characterization of poly-L-lysine grafted SBA-15 using NCA polymerization and click chemistry
Mrityunjoy Kar, Bharmana Malvi, Anindita Das, Suyana Panneri and Sayam Sen Gupta.
J. Mater. Chem., 2011, 21, 6690-6697

4) Synthesis and Characterization of Poly-L-lysine-Grafted Silica Nanoparticles Synthesized via NCA Polymerization and Click Chemistry
Mrityunjoy Kar, P. S. Vijayakumar, B. L. V. Prasad and Sayam Sen Gupta
Langmuir, **2010,** *26* (8), pp 5772–5781

5) Gold catalyzed glycosidations for the synthesis of sugar acrylate/acrylamide hybrids and their utility.
Shivaji A. Thadke, Mritunjoy Kar, Sayam Sen Gupta, Srinivas Hotha
Carbohydrate research, 2011, 346(12), 1511

Conferences/symposia/workshops attended

- 11th CRSI National Symposium in Chemistry 2009, National Chemical Laboratory, Pune, India.
- 3rd CRSI-RSC Symposium 2009, National Chemical Laboratory, Pune, India.
- RSC West India Ph.D.Students Symposium, September 2010, University of Goa. Goa, Inida.
- International Conference on Nanomaterials & Nanotechnology 2011, Delhi University, Delhi, Inida.
- 99th Indian Science Congress meeting 2012, Bhubaneswar, Orissa, India.
- 76th Prague meeting on Macromolecules: Polymers in Medicine 2012, Prague, Czech Republic.

Personal Information

Father's Name	:	Madhusudan Kar
Mother's Name	:	Priety Rani Kar
Date of Birth	:	8th April 1984
Gender	:	Male
Marital Status	:	Single
Nationality	:	Indian
Languages Known	:	Bengali, English, Hindi.
Permanent Address	:	Vill-Jagannath Pur, Post-Bakulda, Dist-Purba Medinipur, West Bengal, India - 721139
Residential Address	:	Room-123, G J Hostel, National Chemical Laboratory, Pune, India 411008
E-mail	:	mrityunjoykar1@gmail.com

References

Dr. Sayam Sen Gupta
Scientist
Chemical engineering and Process development Division,
National Chemical Laboratry,
Dr. Homi Bhabha Road,
Pune-411008
India
E-mail: ss.sengupta@ncl.res.in

Dr. B. L. V. Prasad
Scientist
Physical and Materials Chemisrty Division, National Chemical Laboratry,
Dr. Homi Bhabha Road,
Pune-411008
India
E-mail: pl.bhagavatula@ncl.res.in

Dr. Guruswamy Kumaraswamy
Scientist
Polymer Science and Engineering Division,
National Chemical Laboratory,
Dr. Homi Bhabha Road,
Pune - 411008
India
Email: g.kumaraswamy@ncl.res.in

Dr. Ashish Lele
Scientist
Polymer science and Engineering Division,
National Chemical Laboratory,
Dr. Homi Bhabha Road,
Pune - 411008
India
Email: ak.lele@ncl.res.in

Declaration:

I hereby declare, that the above information and details provided by me are correct to the best of my knowledge.

Yours Sincerely

Place: NCL, Pune

(Mrityunjoy Kar)